THE ROYAL INSTITUTE OF TECHNOLOGY
STOCKHOLM
SWEDEN

DEPARTMENT OF
NUMERICAL ANALYSIS
AND COMPUTING SCIENCE

[redacted]

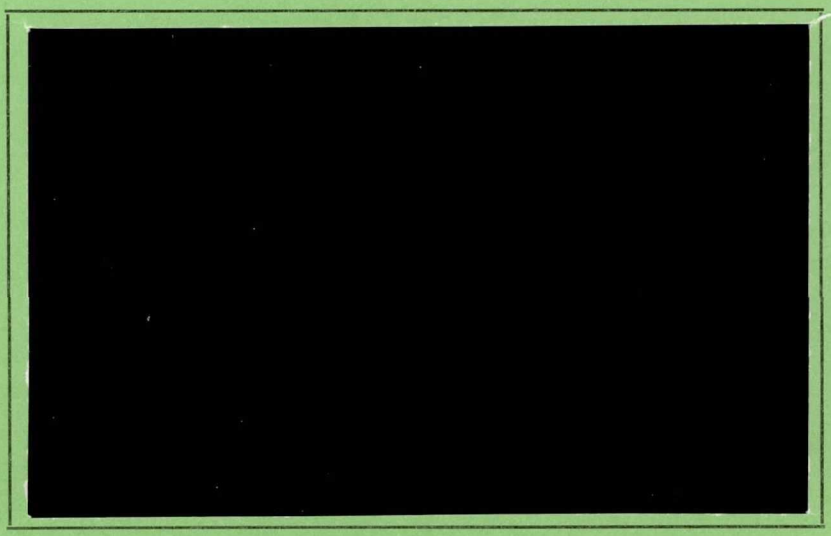

NASA Conference Publication 2186

Capacitor Technologies, Applications and Reliability

Proceedings of a symposium sponsored by
NASA Marshall Space Flight Center and IEEE Components,
Hybrids and Manufacturing Technology Society
and held at Marshall Space Flight Center
February 24-25, 1981

NASA
National Aeronautics
and Space Administration

**Scientific and Technical
Information Branch**

1981

1. REPORT NO.	2. GOVERNMENT ACCESSION NO.	3. RECIPIENT'S CATALOG NO.
NASA CP-2186		

4. TITLE AND SUBTITLE	5. REPORT DATE
Capacitor Technologies, Applications and Reliability	June 1981
	6. PERFORMING ORGANIZATION CODE
7. AUTHOR(S)	8. PERFORMING ORGANIZATION REPORT #
9. PERFORMING ORGANIZATION NAME AND ADDRESS George C. Marshall Space Flight Center Marshall Space Flight Center, Alabama 35812	10. WORK UNIT NO. M-351
	11. CONTRACT OR GRANT NO. RTOP No. 397-00-00
	13. TYPE OF REPORT & PERIOD COVERED Conference Publication
12. SPONSORING AGENCY NAME AND ADDRESS National Aeronautics and Space Administration Washington, DC 20546	14. SPONSORING AGENCY CODE

15. SUPPLEMENTARY NOTES

16. ABSTRACT

Capacitors continue to be a cause of problems in both space and conventional electronic equipment. The NASA-Marshall Space Flight Center, in cooperation with the Components, Hybrids and Manufacturing Technology Society of IEE, organized a seminar to highlight and focus attention on today's capacitor technologies, applications and reliability. Twenty-one papers were presented, which covered ceramic, metallized polycarbonate, PVF_2, and electrolytic (wet and dry) capacitors. These papers addressed the causes of failures, accelerated testing, screening tests, destructive physical analysis, application techniques, and improvements in capacitor capabilities.

17. KEY WORDS	18. DISTRIBUTION STATEMENT
Capacitor technologies Capacitor applications Capacitor Test, Analysis, and Reliability	Unclassified - Unlimited Subject Category 33

19. SECURITY CLASSIF. (of this report)	20. SECURITY CLASSIF. (of this page)	21. NO. OF PAGES	22. PRICE
Unclassified	Unclassified	[illegible]	A09

For sale by National Technical Information Service, Springfield, Virginia 22161

SYMPOSIUM ON CAPACITOR TECHNOLOGIES, APPLICATIONS AND RELIABILITY

PROGRAM COMMITTEE

CHAIRMAN

Leon Hamiter
NASA/Marshall Space Flight Center
EC43
Huntsville, AL 35812
(205) 453-4562

MEMBERS

John Moynihan, Sprague Electric Company
Dr. A. M. Holladay, NASA/Marshall Space Flight Center
Prof. Henry Domingos, Clarkson College
John K. Morris, NASA/Marshall Space Flight Center

TABLE OF CONTENTS

SESSION A. CAPACITOR TECHNOLOGIES
Chairman: John Moynihan, Sprague Electric Company

SESSION B. CAPACITOR APPLICATIONS
Chairman: Dr. A. M. Holladay, NASA/Marshall Space Flight Center

SESSION C. CAPACITOR TEST, ANALYSIS & RELIABILITY - I
Chairman: Prof. Henry Domingos, Clarkson College

SESSION D. CAPACITOR TEST, ANALYSIS & RELIABILITY - II
Chairman: Sherman Cohen, Aerospace Corporation

RADIATION RESPONSE AND ELECTRICAL PROPERTIES OF POLYMER ENERGY STORAGE CAPACITORS: PVF_2, POLYSULFONE, AND MYLAR*

L. R. Edwards
Division 2153
Sandia National Laboratories
Albuquerque, NM 87185
(505) 844-7058

SUMMARY

Sandia National Laboratories is currently interested in the development of a polymer film capacitor that is tolerant to radiation. The capacitors are to be utilized in a high voltage-pulse discharge application.

Radiation response data at high dose/dose rate levels are presented for polyvinylidene fluoride (PVF_2), polysulfone, and Mylar.† The results show that PVF_2 is the most radiation tolerant while Mylar is the least tolerant. The data also show that the radiation response is quite dependent on operating electric stress.

Although PVF_2 has good radiation tolerance and a dielectric constant which is a factor of three larger than Mylar and polysulfone, PVF_2 has properties which complicate its use as a capacitor dielectric. Electrical properties of these materials will be presented and discussed.

INTRODUCTION

The motivation for this work is the development of pulse discharge, energy storage capacitors which are tolerant to high dose rate and high dose radiation environments where a recharge option is not available. The capacitance and voltage ranges of interest are, respectively, 0.1-3 μF and 2.5-6 kV. In general, the effect of radiation on a capacitor is a charge or voltage loss. This charge loss is the result of radiation-induced conductivity in the capacitor dielectric.[1] The absorption of radiation in a dielectric results in the creation of electron-hole pairs in conduction states. (The number of charge carriers created is dependent on the atomic cross sections of the dielectric.) The excited carriers will travel toward the electrodes because of the electric field and effectively reduce the charge on the electrodes. The mechanism which impedes the charged carrier displacement in a solid dielectric is the interaction of the carriers with traps. In a given radiation environment, a dielectric which has a high trap density will exhibit less charge loss than one with a low trap density. The radiation-induced conductivity is very material dependent. It is a function of composition, impurities, and structural defects. For a solid dielectric, a theoretical prediction of the magnitude of the radiation response is not tractable; the response is best determined by experiment.

For the past 10 years, Sandia National Laboratories has been active in developing the technology for utilizing polymer films as the dielectric in pulse discharge, energy storage capacitors. The primary focus has been on developing Mylar both in dry and wet[2] configurations. Mylar is an excellent dielectric; however, in a high dose rate, high dose radiation environment [10^{12} Rad(Si)/sec, 10^5 Rad(Si)], Mylar exhibits a high radiation-induced conductivity. A part of the current effort on polymer dielectrics is to examine other commercially available plastic films which may have better radiation tolerance.

The liquid-impregnated, plastic film (wet) capacitor technology that has been successful in dramatically improving the energy density[2] unfortunately, cannot be used in a high dose radiation environment. A liquid dielectric generally exhibits a large radiation-induced conductivity because a liquid, as opposed to a solid dielectric, does not have carrier traps to impede charge carrier displacement. A dry design capacitor, at the outset, will have a better radiation tolerance.

---

*This work was supported by the U.S. Department of Energy.

†Mylar is a trade name of the DuPont Company for polyethylene terephthalate.

Preliminary low dose radiation studies on polymer films have shown that both polysulfone and polyvinylidene fluoride (PVF_2) are superior to Mylar.[3] The data presented here extend these results to the high dose [10^5 Rad(Si)] regime. PVF_2 is also attractive because of its high dielectric constant of 10 as compared to 3 for Mylar and polysulfone. On the other hand, PVF_2 has been shown to exhibit ferroelectricity,[4] which may have a detrimental effect on high electric field applications. Obviously, there are trade-offs that must be considered in the development of specialized capacitors.

The data presented in this paper will focus on the radiation response and electrical properties of PVF_2. Some data on polysulfone and Mylar will also be given for comparison.

CAPACITOR DESIGN

The dielectrics used were commercially available, capacitor-grade films.* For the present studies, either 2-12 μm or 1-25 μm layers were employed for the dielectric pad. The capacitor design is a dry, foil-wound, tapewrapped, epoxy end encapsulation construction and is shown in Figure 1. The end margins were varied between 0.250 and 0.50 in. The capacitor rolls were wound on a precision, tension-controlled winder,[2] with polysulfone being the most difficult to wind.

The processing consists of a drying cycle followed by end sealing. The capacitor rolls are dried (in dry nitrogen) at 71°C for 24 hours and then at 80-100°C for another 24 hours. The rolls are cooled to 71°C and maintained at this temperature during the end sealing process. The end seals are made with mica-loaded epoxy.

RADIATION PROPERTIES

The radiation response data were obtained on a high-intensity-flash x-ray machine.[5] This machine is capable of producing up to 10^5 Rad(Si) at a rate of 10^{12} Rad(Si)/sec with a photon energy spectrum between 60 keV and 10 MeV. The radiation pulse width is 50 nsec. The

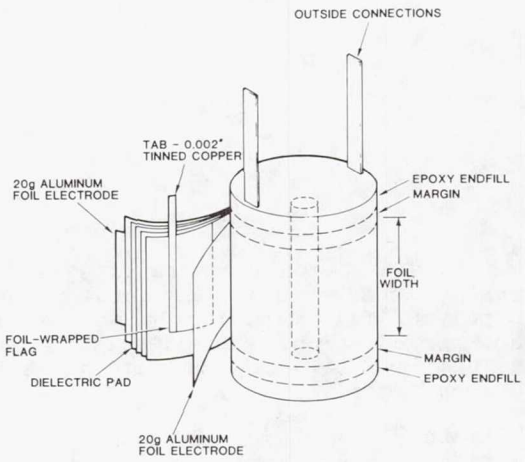

Figure 1. Capacitor design used in this study.

quantity of interest is the fraction of voltage loss on the capacitor at a given dose. The fraction of voltage loss is defined as the ratio of the actual voltage loss to the initial applied voltage. (Hereafter, the term voltage loss will be synonymous with fraction of voltage loss.) The voltage-loss data presented reflects both the prompt and delayed radiation-induced conductivity components. All data were recorded at 20° to 25°C, and no dose memory effects were observed.

The radiation response as a function of dose for the three polymer dielectrics is shown in Figure 2. As is expected, the voltage loss in all cases increases with increasing dose. It is observed that PVF_2 has the best radiation tolerance, Mylar is the poorest, and polysulfone is intermediate. For PVF_2 and polysulfone, the radiation response is represented by families of curves. This shows that the voltage loss is electric stress dependent. The electric stress dependence is shown more clearly in Figure 3 where the voltage loss is plotted as a function of the electric stress at a constant dose of 100 KRad(Si). Similar plots can be made at say 10 or 50 KRad(Si), but these plots will show essentially the same behavior except that the voltage loss will be scaled down proportionately. This type of data representation exemplifies the relative ranking of the dielectrics.

*Polysulfone is marketed by Kimberly-Clark Corp. under the trademark of Kimfone. Polyvinylidene flouride (PVF_2) is marketed by Kureha Chemical Industry Co. under the name of KF film.

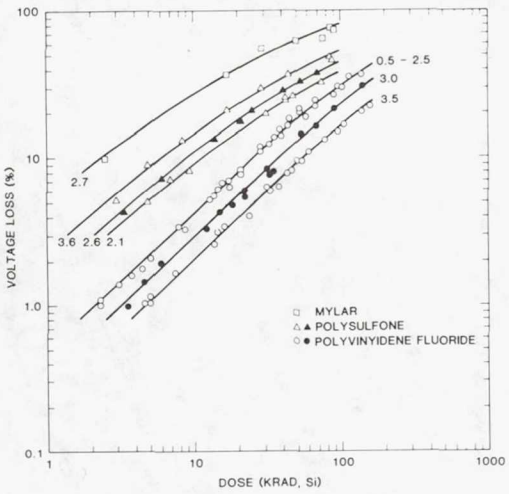

Figure 2. The basic radiation response data. The numbers associated with each of the curves are the electric stresses in kV/mil.

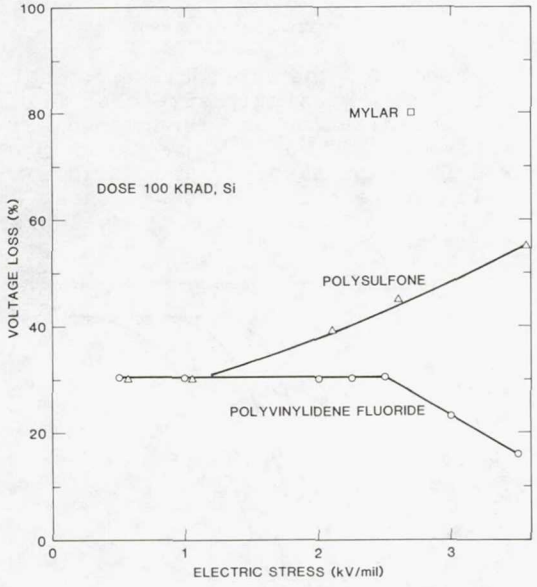

Figure 3. The electric stress dependence of the radiation response.

In the case of polysulfone, the voltage loss is observed to increase with increasing electric field. Low dose data on Mylar also show the same electric stress dependence.[3] The electric stress dependence for PVF_2 is rather unique. The voltage loss is observed to be independent of the electric stress up to 2.5 kV/mil and then decreases rather dramatically at higher stresses.

The radiation response of a polymer-film dielectric depends on the number of free carriers generated per unit dose and the free carrier mobility-lifetime product. The electric stress dependence is usually observed to be in the above factors. All of the films in this study have similar densities and are all composed of low atomic number elements. This implies that the photon absorption cross section should be similar for all of the films. (Calculations bear this out.) Thus the number of carrier pairs created per unit dose should be nearly equal for these films. The number of free carriers that will participate in conduction, however, will be less than the number of carriers initially created by the radiation. This is due to geminate recombination effects. Initially, it takes time for the electric stress to disperse (or penetrate) the space charge clouds; and it is during this time that recombination takes place. This process is electric stress dependent. The number of free carriers available for conduction is a strong function of electric stress, increasing with the stress.[1] Therefore, it is expected that the voltage loss at a given dose should increase with increasing electric stress. This effect is observed in both Mylar and polysulfone; however, in PVF_2 there must be another competing mechanism. This will be discussed at the end of this section.

The second factor which affects the radiation response is the carrier mobility-lifetime product. This product is electric stress dependent; however, it has been shown that most of the stress dependence is in the number of free carriers generated.[1] The carrier lifetime is dependent on the trap structure and trap density of a given film. A film which, for example, has a high trap density will probably have a short lifetime. Thus a film with a high trap density should exhibit a lower voltage loss at a given dose than a film with a low trap density. It is felt that the difference in the relative radiation responses of these films is due to differences in the trap structure and trap density.[3] Both the mobility and lifetime are difficult quantities to determine in polymer films.

As is observed in Figure 3, the electric stress dependence of the voltage loss in PVF_2 is quite different than in Mylar and polysulfone. It is possible that this behavior is related to the ferroelectric/structural properties of PVF_2. The biaxially stretched PVF_2 film is approximately half amorphous and half crystalline in structure. It has been reported that the crystalline structure of the biaxially oriented film contains both a polar and an antipolar phase, and there is a field-induced phase transition for electric stresses above 2.5 kV/mil.[6] It is possible that this field-induced phase transition could result in an increase in trap density.[7] This, in turn, would result in a decrease in the voltage loss. The plausibility of this explanation is being pursued further.

ELECTRICAL PROPERTIES

Both Mylar and polysulfone are linear dielectrics up to high voltages (i.e., the relation, Q = CV, is valid). PVF_2, by virtue of the ferroelectric behavior, is a nonlinear dielectric, especially at high electric stresses. The ferroelectric data were obtained by standard looping techniques. The results are shown in Figure 4. At 25°C, the polarization is fairly linear up to 1.5 kV/mil, and above 2.5 kV/mil, the polarization increases very rapidly with electric stress. The loops below 1.5 kV/mil were observed to be quite narrow. At -55°C, there is a dramatic decrease in the polarization. This behavior will influence or limit capacitor design and application.

The temperature and frequency dependence of the small signal dielectric properties of PVF_2 are shown in Figures 5 and 6. In Figure 5, it is observed that the capacitance (or dielectric constant) is very temperature and frequency dependent, especially at low temperatures. This is consistent with the low temperature ferroelectric data. The dissipation factor is also very temperature and frequency dependent. It should be noted that the dissipation factor becomes very significant (19 percent) at 100 kHz and 0°C. The observed low temperature behavior in PVF_2 is associated with the glass transition. Mylar and polysulfone, in contrast, exhibit a much subdued temperature and frequency dependence. Also, the magnitude of the dissipation factor is much less for these materials. For example, over a frequency range of 1 to 100 kHz and a temperature range of -55° to 70°C, the dissipation factor of Mylar varies only from 0.2 to 4.5 percent.

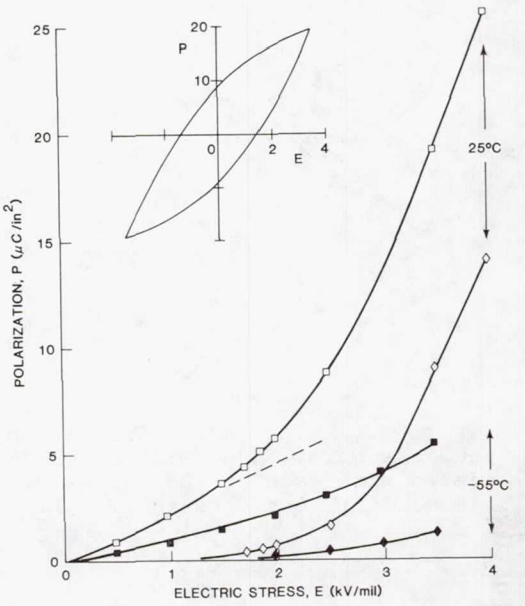

Figure 4. The ferroelectric data for PVF_2, biaxially stretched film. The polarization and remnant polarization at 25°C are represented by □ and ◊, respectively. The solid symbols represent the same data at -55°C. The inset is a typical hysteresis loop at 25°C.

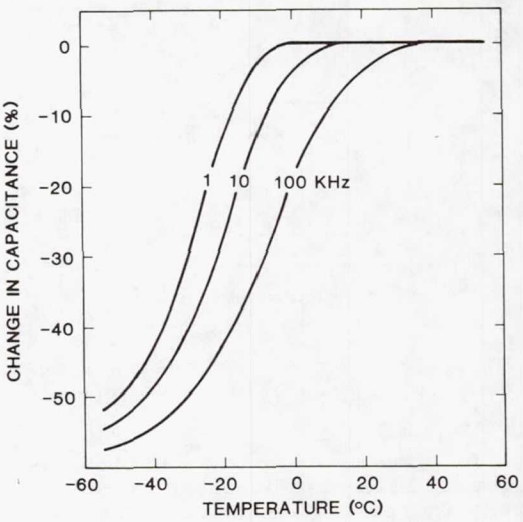

Figure 5. The temperature and frequency dependence of the capacitance (or dielectric constant) for PVF_2.

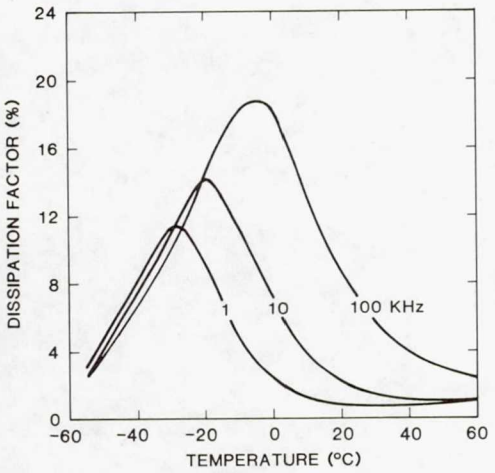

Figure 6. The temperature and frequency dependence of the dissipation factor for PVF_2.

The short-term dielectric breakdown of PVF_2 at 20° to 25°C is similar to that observed for Mylar in the same capacitor design configuration. For end margins greater than or equal to 0.375 in, average breakdown stress was 8 kV/mil with a standard deviation of 1 kV/mil. Additional data are needed at low and high temperatures.

The ambient temperature insulation resistance of PVF_2, polysulfone, and Mylar are, respectively, 823; 13,300; and 266,000 MΩ-μF. The value for PVF_2 is adequate for pulse discharge application; however, there is evidence that the insulation resistance decreases with increasing temperature. We have observed, for a 1 μF capacitor at 3 kV/mil, thermal runaway at 80°C.

CONCLUSIONS

The radiation tolerance and high dielectric constant of PVF_2 make it an attractive candidate for our current applications. However, PVF_2 has some interesting properties which complicate its use as a capacitor dielectric. The ferroelectric behavior will probably limit the design stress to ~ 2.5 kV/mil. The dielectric constant and dissipation factor will influence low-temperature usage while the insulation resistance will govern the high-temperature limit. Further research is still necessary to better define the limits of this film.

ACKNOWLEDGMENTS

The author would like to thank R. G. Kepler, R. C. Hughes, and S. Kurtz of Sandia National Laboratories for very useful technical discussions on PVF_2. The author also acknowledges the continuing support and assistance of C. B. McCampbell, D. H. Weingarten, R. V. Baron, and L. A. Washington of Sandia National Laboratories, and W. E. Packer and N. A. Sidnell of the General Electric Neutron Devices Department.

REFERENCES

1. R. C. Hughes, "Charge Transport by Photocarriers in Polymer Films," Second International Conference on Electrophotography, 1974.

2. G. H. Mauldin, "The Application of Perfluorocarbons as Impregnants for Plastic Film Capacitors," in this Proceedings.

3. R. C. Hughes, Sandia National Laboratories private communication. The low dose [1 Rad(Si)] data was obtained with a Febetron pulse x-ray machine on small, single-layer films. The sample electrodes were evaporated aluminum.

4. R. G. Kepler, "Saturation Remnant Polarization of Polyvinylidene Fluoride," Organic Coatings and Plastics Chemistry, Vol. 38, p. 278, 1978.

5. The Hermes II facility at Sandia National Laboratories.

6. G. T. Davis, et al., "Electric-Field-Induced Phase Changes in Polyvinylidene Flouride," J. Appl. Phys., Vol. 49, p. 4998, 1978.

7. S. Kurtz, Sandia National Laboratories, private communication.

POLYVINYLIDENE FLUORIDE FILM AS A CAPACITOR DIELECTRIC

Henrique V. DeMatos
Union Carbide Corporation
Components Department
P. O. Box 5928
Greenville SC 29606
(803) 963-6300

SUMMARY

Thin strips of polyvinylidene fluoride film (PVDF) with vacuum-deposited electrodes were made into capacitors by conventional winding and fabrication techniques. These devices were used to identify and evaluate the performance characteristics offered by the PVDF in metallized film capacitors. Variations in capacitor parameters with temperature and frequency are presented, compared with other dielectric films, and their impact on capacitor applications discussed. Typically, capacitors using metallized PVDF film can be used over the temperature range from -55°C to +100°C. Dielectric constant is approximately 10.5 at 1 KHz and dissipation factor less than 1.5% at the same frequency. Insulation resistance is 10,000 megohm-μF at room temperature, decreasing to 200 megohm-μF at 100°C. High frequency ripple current testing at frequencies to 10 KHz, with as much as 2.5 amperes applied, shows excellent performance in high frequency alternating current applications. Thermal stability was reached with a maximum of 15°C heat rise above ambient. Capacitors made using PVDF film offer performance characteristics comparable to those of the more recognized dielectric films in most applications, while providing a threefold increase in volumetric efficiency. Its use in high performance, ultra stable, or low loss, applications is not recommended without careful examination of the parameters involved.

INTRODUCTION

Many films made from synthetic organic polymers have been used in electrical and electronic devices for insulation. Some, because of their unique combination of properties, enjoy success as capacitor dielectrics. The applications for film dielectric capacitors have grown steadily, because they offer performance features equal or superior to impregnated paper capacitors and, also, are smaller in size.

Most dielectric films exhibit dielectric constant values between 2 and 3. Although this is lower than impregnated paper, the ability to use single layer insulating systems with plastic films generally results in smaller sizes. Volumetric efficiency gains of five to 10 times were accomplished over paper capacitors, resulting in capacitance/volume ratio of 2.5 to 5 μF/cm^3 (50 to 100 μF/in.^{3}) for films such as polyester and polycarbonate.

A new film, polyvinylidene fluoride, (referred to as PVDF), has a dielectric constant of approximately 10.5 and offers the potential to increase the efficiency to 7.5 to 15 μF/cm^3 (150 to 300 μF/in.^{3}). This paper will report on the properties of PVDF film and the performance of capacitors using this material as a dielectric.

FILM PROPERTIES

The general properties of PVDF film have been reported by the manufacturer[1] and are shown in Table I. These values represent the intrinsic properties of the dielectric and are used by capacitor designers to establish preliminary design parameters. Optimum design and performance characteristics are obtained empirically.

TABLE I

General Properties of PVDF Film

Property		Unit	Value	Test method
Density		gr/cc	1.80	ASTM D 1505
Tensile strength	(MD)	kg/mm²	15~ 20	ASTM D 882
" "	(TD)	"	20~ 25	"
Elongation	(MD)	%	150~200	ASTM D 882
"	(TD)	"	100~150	"
Modulus of elasticity		kg/mm²	150	ASTM D 882
Gas permeability	(25°C)	cc·cm/cm²·sec·cmHg		
	O_2		$5\sim8\times10^{-12}$	ASTM D 1434
	N_2		$4\sim7\times10^{-12}$	"
	CO_2		$20\sim30\times^{-12}$	"
Water vapor transmission	(25°C)	g/m²/24hr/mm	0.8	ASTM E 96—66
Water absorption	(40°C 90 %RH)	%	<0.03	ASTM D 570
Melting point		°C	180	
Flammability			Self extinguish	
Heat Shrinkage	100°C	%	<1.0	
	150°C	"	<5.0	
Breakdown strength		KV/mm, 25μ	160	ASTM D 149—64
Volume resistivity		Ω·cm	10^{15}	ASTM D 257—61
Dielectric constant	22°C 60Hz		11.0	ASTM D 150—64T
	10^3Hz		10.7	"
	10^6Hz		7.0	"
Dissipation Factor	22°C 60Hz		0.012	ASTM D 150—64T
	10^3Hz		0.015	"
	10^6Hz		0.22	"

Material used in the evaluations was capacitor grade, biaxially oriented, PVDF film with aluminum, metallized, electrodes in 6 μm(0.00024") and 9 μm (0.00036") thicknesses. No significant differences, other than device rated voltage, were noted between the thicknesses.

MATERIAL EVALUATIONS

The electrical properties of PVDF film were determined by measuring parallel plate capacitors formed by metallizing strips of film on both sides. The resulting capacitor had a nominal value of 15 ηF, with a plate area approximately 12.9 cm^2 (2 $in.^2$). The dielectric thickness was determined using the weight density method; the dielectric constant by the capacitance-area-thickness measurements on the samples. The values obtained are listed in Table II.

TABLE II

Electrical Properties of PVDF Film With Aluminum Metallized Electrodes

Property	Value
Dielectric Constant	10.95 at 1 KHz
Dissipation Factor	0.012 at 1 Khz
Volume Resistivity	1.5X10" Ω-cm at 25°C
Dielectric Strength	215 V/μm (∿5500 V/Mil) at 25°C

Curves showing the variation of dielectric constant and dissipation factor with temperature and frequency are shown in Figures 1 and 2. Figure 3 shows the variation in volume resistivity with temperature. Slight differences between the data and published values, particularly for dielectric strength and volume resistivity, are attributed to the large surface area of the parallel plate capacitors used in the evaluation.

Mechanical properties are important in identifying potential problem areas in the winding and processing of the wound capacitor elements. Specific properties of interest were — tensile strength, elongation and shrinkage. Standard methods per ASTM were used to measure the properties which are listed in Table III.

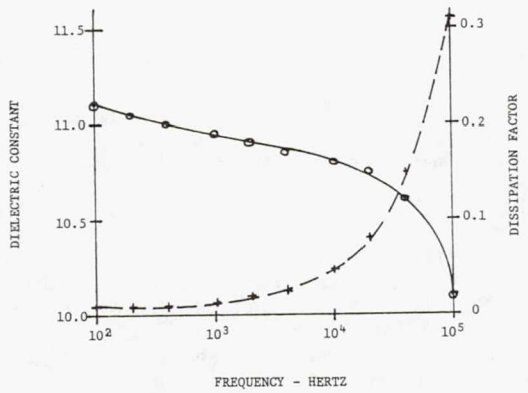

FIGURE 1: DIELECTRIC CONSTANT AND DISSIPATION FACTOR VS. FREQUENCY

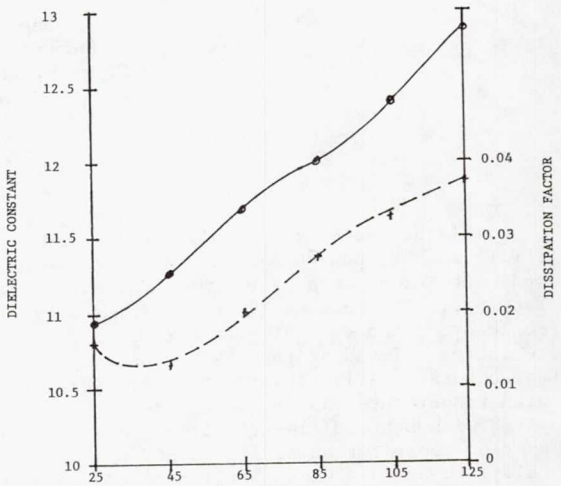

FIGURE 2. DIELECTRIC CONSTANT AND DISSIPATION FACTOR VS. TEMPERATURE

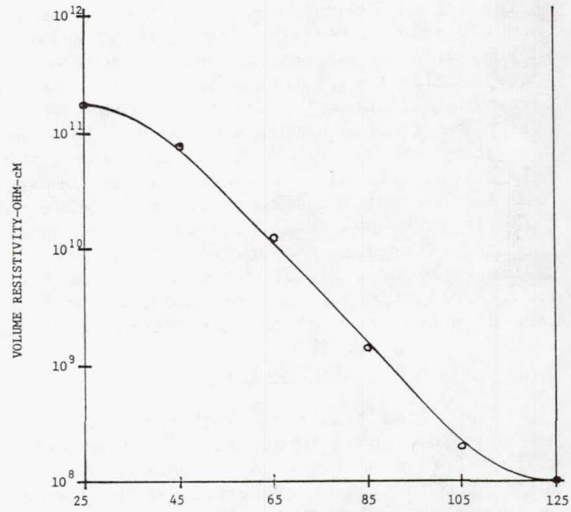

FIGURE 3. VOLUME RESISTIVITY VS. TEMPERATURE

TABLE III

Mechanical Properties of PVDF Film

Property	Value
Tensile Strength	110 N/M^2 (16,000 PSI)
Elongation	65%
Shrinkage (4 hrs. at 100°C)	0.25%
Shrinkage (4 hrs. at 125°C)	3.5 %

The electrical and mechanical film properties obtained are reasonably consistent with published data and are comparable with the properties of the more commonly used film dielectrics such as polycarbonate and polyester.

CAPACITOR FABRICATION

A hermetically sealed, wound, metallized film capacitor design was selected to evaluate the performance of PVDF film in capacitors. Film strips with aluminum metallized electrodes were obtained in two base film thicknesses, 6μm (∿0.00024") and 9 μm (∿0.00036"). Film properties were found to be in close agreement with the materials evaluation data reported earlier. Electrode resistivity was between 2.5 and 3.5 ohms per square.

Two capacitance values, one in each voltage rating, were designed. The values selected represent units currently in general use in the industry. Large capacitance values were selected in order to measure the impact of large surface areas, with the increased potential for fault sites, on the voltage life performance. Electrode surface area in the test capacitors was approximately 1 to 1.5M^2 (1500 to 2500 $in.^2$).

Capacitor windings were rolled on winding machines commonly used in the industry. Particular attention was given to the winding qualities of the film. Observations revealed the winding properties of PVDF to be excellent. Firm, wrinkle-free windings were produced; the slip coefficient of the film precluded "blocking" with subsequent trapped air pockets, and the static charges generated during winding were not excessive. Winding tension levels were consistent with standard practice for films with similar tensile and elongation properties.

After winding, the elements were assembled, using conventional methods, including heat aging to relieve winding stresses, contacting the aluminum metallized electrodes with sprayed metal end terminations and vacuum drying of assemblies prior to final sealing to preclude moisture from the assembly. No unusual problems were encountered during the processing and assembly of the capacitors for test.

Prior to the start of performance testing, the capacitors were screened in accordance with the requirements of MIL-C-83421. The test capacitor voltage ratings were selected so as to produce a stress on the dielectrics of approximately 40 V/μm (1000 V/Mil).

CAPACITOR EVALUATIONS

Following the screening tests, capacitors were subjected to the performance evaluation tests of Table IV. These tests were selected to show the variation of capacitor performance under normal use environments.

TABLE IV

Performance Tests and Sequence

TEST	CONDITIONS
Capacitance vs. Temperature	-55°C to +100°C at 1 KHz
Dissipation Factor vs. Temperature	-55°C to +100°C at 1 KHz
Insulation Resistance vs. Temperature	25°C to +100°C at Rated Voltage
Dielectric Absorption	25°C at 100 VDC
Effective Series Resistance	25°C at 100 KHz
Impedance vs. Frequency	25°C (100 Hz to 10 MHz
Heat Rise	25°C (1 KHz, 4 KHz, 10 KHz)
High Frequency A.C. Life Test	25°C at 4 KHz
D.C. Voltage Life Test	100°C at Rated Voltage

The variation of electrical characteristics with temperature are shown in Figures 4 and 5.

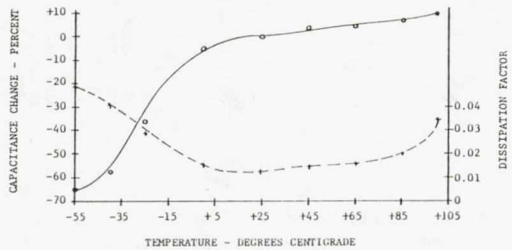

FIGURE 4. VARIATION OF CAPACITANCE AND DISSIPATION FACTOR WITH TEMPERATURE

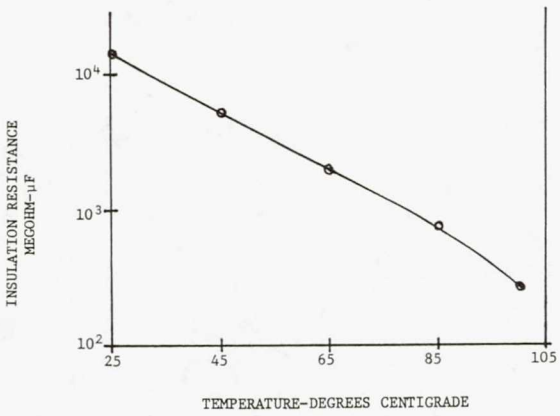

FIGURE 5. INSULATION RESISTANCE VS. TEMPERATURE

The capacitance change with temperature is to be particularly noted in that it shows a sharp roll-off in capacitance, beginning at approximately 0°C and reaching a minimum of ∿35% of the 25°C value at -55°C. This is obviously a property of the film and applications where the low temperature capacitance value is of significant importance must consider this factor in the circuit design. The insulation resistance varies directly with temperature and follows the classical behavior pattern exhibited by commonly used dielectrics.

The dielectric absorption and effective series resistance (ESR) of the test capacitors are summarized in Table V and average 3.5% and

TABLE V

DIELECTRIC ABSORPTION AND ESR OF PVDF FILM CAPACITORS

	DIELECTRIC ABSORPTION-PERCENT AT 25°C; 100 VDC APPLIED*			EFFECTIVE SERIES RESISTANCE-OHMS AT 25°C; 100 KHz	
S/N	15 uF	30 uF	S/N	15 uF	30 uF
1	2.55	2.98	1	0.035	0.038
2	2.75	3.23	2	0.035	0.041
3	2.70	3.03	3	0.036	0.037
4	2.58	2.90	4	0.035	0.037
5	2.62	3.30	5	0.034	0.040
6	2.60	3.05	6	0.033	0.038
7	2.55	3.00	7	0.034	0.039
8	2.70	3.20	8	0.035	0.041
9	2.65	2.95	9	0.035	0.040
10	2.80	3.10	10	0.035	0.036

* Test per MIL-C-83421

0.035 to 0.040 ohms, respectively. The dielectric absorption is important for linearity in timing circuits, and the ESR is a major consideration in filtering and bypass applications.

The impedance of the capacitor over a wide range of frequencies is shown in Figure 6 and shows a smooth transition through, and a low value at, resonance.

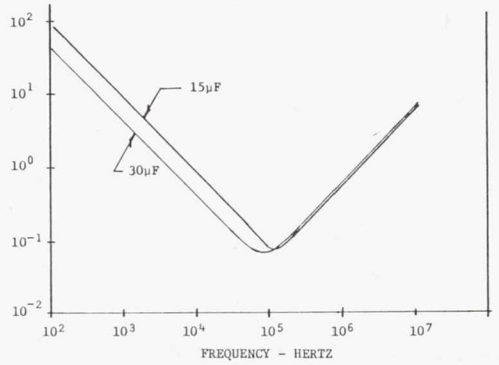

FIGURE 6. IMPEDANCE VS. FREQUENCY CURVES FOR PVDF FILM CAPACITORS

The effects of high frequency alternating currents applied to the capacitor are shown in Figure 7. Case temperature was recorded using

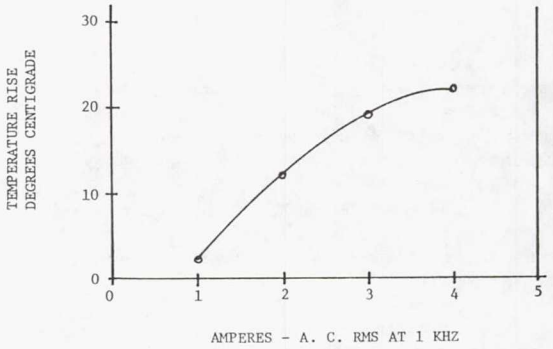

FIGURE 7. TEMPERATURE RISE VS. A. C. CURRENT

thermocouples attached to the case wall. The temperature of the lead wires, at the point of egress from the case, was monitored also. The temperature rise is proportional to the applied current and follows a curve of approximately 20°C per watt dissipated. Lead wire temperatures were approximately 1.2 to 1.5 times the case wall temperature and indicated the end termination to be the area where the losses concentrated.

Capacitors were exposed to a 4 KHz A.C. voltage sufficient to generate a 2.5 ampere RMS current in the capacitor. The test was conducted at 25°C for 250 hours. No significant changes, except for a slight increase in dissipation factor, were noted, as shown in Table VI. (See top of page 5.)

The voltage life of the capacitor was evaluated by testing at 100°C with device rated voltage applied for 1000 hours. Post test measurements are shown in Table VI and indicate satisfactory life performance at the dielectric stress used. Of significant interest is the marked increase in the dissipation factor at the conclusion of life test. Normally, there is little change in this parameter as a result of exposure to the test. Military specifications, such as MIL-C-83421, allow only modest increases in dissipation factor and, usually, 30% decreases in insulation resistance limits.

The unique performance of the PVDF film capacitor, in this regard, has been attributed to the conversion of aluminum in the metallized electrode to non-conducting aluminum fluoride[2] at the positively charged capacitor electrode plate, due to the presence of free fluoride ions in the film. This causes significant increase

in the electrode resistivity and increases the loss factor.

TABLE VI

LIFE TEST PERFORMANCE OF PVDF FILM CAPACITORS

D.C. LIFE TEST:

15 uF; 400 Volt

	INITIAL MEASUREMENTS			POST TEST MEASUREMENTS		
S/N	Cap-uF% 1 KHz	D.F.% 1KHz	I.R.-MEGS 400VDC	Cap-uF 1 KHz	D.F.% 1KHz	I.R.-MEGS 400VDC
1	17.74	1.20	500	17.64	2.14	750
2	17.96	1.26	500	17.75	2.18	600
3	17.70	1.23	500	17.60	2.17	800
4	17.70	1.20	450	17.48	2.18	550
5	17.84	1.27	450	17.66	2.18	650
6	17.55	1.25	500	17.46	2.21	575
7	17.72	1.24	600	17.64	2.21	700
8	17.82	1.24	550	17.49	2.15	600
9	17.61	1.26	450	17.46	2.17	550
10	17.55	1.27	500	17.33	2.19	750

30 uF; 200 Volt

	INITIAL MEASUREMENTS			POST TEST MEASUREMENTS		
S/N	Cap-uF 1 KHz	D.F.% 1KHz	I.R.-MEGS 200VDC	Cap-uF 1 KHz	D.F.% 1KHz	I.R.-MEGS 200VDC
1	35.65	1.47	350	35.88	2.28	450
2	35.26	1.47	400	36.13	2.16	500
3	35.40	1.39	350	36.23	2.20	400
4	35.74	1.49	350	36.16	2.31	400
5	36.06	1.53	375	36.46	2.33	400
6	35.48	1.40	400	36.12	2.15	500
7	35.84	1.45	400	36.21	2.18	500
8	35.48	1.40	400	36.34	2.21	550
9	36.04	1.48	350	36.26	2.30	400
10	35.82	1.42	350	36.11	2.15	400

A.C. LIFE TEST:

15 uF; 400 Volt

	INITIAL MEASUREMENTS			POST TEST MEASUREMENTS		
S/N	Cap-uF% 1 KHz	D.F.% 1KHz	I.R.-MEGS 400VDC	Cap-uF 1 KHz	D.F.% 1KHz	I.R.-MEGS 400VDC
1	17.50	1.22	550	17.46	1.45	550
2	17.53	1.29	550	17.45	1.50	550
3	17.50	1.22	600	17.47	1.47	550
4	17.70	1.20	650	17.66	1.44	700
5	17.55	1.25	500	17.44	1.48	650
6	17.53	1.25	500	17.43	1.44	500

30 uF; 200 Volt

	INITIAL MEASUREMENTS			POST TEST MEASUREMENT		
S/N	Cap-uF 1 KHz	D.F.% 1KHz	I.R.-MEGS 200VDC	Cap-uF 1 KHz	D.F.% 1KHz	I.R.-MEGS 200VDC
1	34.80	1.35	350	35.31	1.57	352
2	34.99	1.34	350	35.67	1.53	352
3	35.24	1.35	350	35.83	1.56	352
4	34.78	1.35	450	35.50	1.57	350
5	34.94	1.34	400	35.57	1.55	350
6	35.17	1.35	350	35.79	1.53	350

The performance of PVDF film capacitors is compared to that of commonly used film dielectrics in Table VII.

TABLE VII

COMPARISON OF COMMON CAPACITOR CHARACTERISTICS FOR PVDF AND OTHER FILM DIELECTRIC MATERIALS

CHARACTERISTIC	PVDF	POLYESTER	POLYCARBONATE	POLYSULFONE
OPERATING TEMPERATURE RANGE	-55°C to +100°C	-55°C to +125°C	-55°C to +125°C	-55°C to +150°C
CAPACITANCE CHANGE 25°C to -55°C	-65%	- 5%	±2%	+0.5%
WITH TEMPERATURE 25°C to HI-TEMP.	+10%	+15%	±2%	-1.5%
DISSIPATION FACTOR -55°C	5.00%	1.50%	0.40%	0.40%
+25°C	1.50%	0.50%	0.15%	0.15%
AT HI-TEMP	2.00%	2.00%	0.60%	0.40%
INSULATION RESISTANCE 25°C	10,000	20,000	200,000	200,000
MEGOHM - uF AT HI-TEMP	200	20	2,000	1,000
DIELECTRIC CONSTANT, 1 KHz;25°C	10.95	3.1	2.8	3.0
DIELECTRIC ABSORPTION, 25°C; 100 VDC	3.5%	0.3%	0.1%	0.1%
RETRACE AND DRIFT (SHORT-TERM)	±1.0%	±0.5%	0.1%	0.1%

CONCLUSIONS

Polyvinylidene fluoride film (PVDF) has demonstrated properties which make it highly suitable as a capacitor dielectric. Its high dielectric constant provides a threefold increase in the volumetric efficiency of metallized film capacitors. The data presented indicate that it represents a useful addition to currently available film dielectrics. A.C. losses are slightly higher than most currently used materials, but are not prohibitive as shown by the A.C. performance of test capacitors. Applications where low temperature operation is contemplated will have to consider the sharp drop off in capacitance at temperatures below 0°C.

The performance characteristics of capacitors with PVDF film dielectric are comparable to those of the more common dielectric films in most applications. Its use in high performance, ultra stable, or low loss, applications is not recommended without a careful review of the circuit requirements and the impact of device parameters on those needs.

REFERENCES

1 Kureha Chemical Industry Co., Ltd., Bulletin Number 72-6.2000S

2 J. W. Borough, W. G. Brammer, J. Burnham, "Degradation of Polyvinylidene Fluoride Capacitors During Accelerated Tests", in Proc. Reliability Physics Symposium, 1978, pp 219-223

THE APPLICATION OF PERFLUOROCARBONS AS IMPREGNANTS FOR PLASTIC FILM CAPACITORS*

G. Howard Mauldin
Division 2153
Sandia National Laboratories
Albuquerque, NM 87185
(505) 844-4260

SUMMARY

Sandia National Laboratories has developed a liquid-impregnated, plastic film (wet) capacitor that is thought to be the most reliable and space-efficient capacitor of any type ever produced for high-voltage, pulse-discharge service.

The initial design will store five times the energy of a premium-quality, Sandia-designed dry capacitor of equivalent energy and reliability, and future designs are expected to boost this energy ratio even higher.

Credit for this dramatic improvement in electrical performance is given to the near perfect attributes of the liquid chosen as the capacitor impregnant. The impregnant, a perfluorocarbon fluid, embodies all of the attributes Sandia has identified as essential to capacitor-impregnating quality. No other single fluid approaches its combination of properties. This paper will describe the technology, a production capacitor design using this technology, and the winding technology for capacitors used at Sandia National Laboratories.

THE NEAR PERFECT IMPREGNANT

A well-known relationship in the capacitor field is that the energy storage capability of any dielectric system is a squared function of the operating field stress. A doubling of the operating stress yields a fourfold increase in energy.

The high ultimate electrical strength of plastic films has long tempted workers[1] in the energy storage capacitor field. This high ultimate strength suggests the possibility of operating at higher stresses with the attendant increase in energy density. This ultimate performance has been hard to achieve in practice because plastic films are difficult to perfectly impregnate with traditional fluids. Unless they can be perfectly impregnated or if they are left dry, trapped air pockets and other irregularities in the windings cause widely varying electrical breakdown levels. Because of this, in systems requiring high reliability the resulting capacitors must be severely derated against the average breakdown levels to assure reliable performance. This derating can be as extreme as 70 percent to 80 percent of the average performance. This results in capacitors larger than desired to ensure reliable performance.

It would appear then that in the quest for higher energy density capacitors, a search for more reliable impregnating materials would be quite productive. This has been our approach and in this we have identified what we believe to be the near perfect liquid for impregnating plastic film dielectrics.

Before discussing the details of the new capacitor technology we would like to say a few words about the search tool we use in looking for promising dielectric combinations. The main procedure used in this search we call the short-term breakdown test.

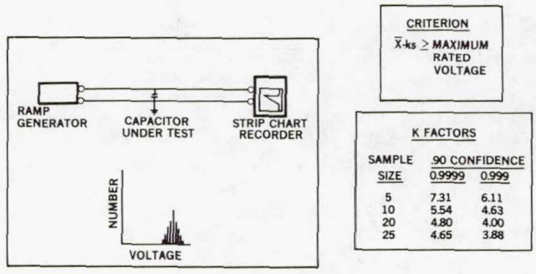

Fig. 1. The Short Term Breakdown Test

The short-term breakdown is illustrated in Figure 1. The equipment consists of a programmable power supply, a strip chart recorder, and

*This work supported by the U.S. Department of Energy.

test fixturing to connect the capacitor to this equipment as illustrated in the block diagram. The programmable power supply generates a linear ramp of voltage. The ramp rate is typically 250 V/second. The strip chart recorder is used to indicate the capacitor breakdown point on the voltage ramp and also serves as a permanent data record.

In applying this test, a quantity of samples is broken down in the above test procedure. The breakdown data is obtained and calculations of mean and standard deviation are made. A calculation of the mean minus a constant, k, times the standard deviation is made. The criterion is that this quantity must be greater than the maximum stress the dielectric system would be operated. The constant, k, is a function of sample size, reliability goals, and confidence limits as shown in Figure 1.

Some seven years ago in our continuing search for attractive film and liquid combinations, we experimented with a unique family of dielectric liquids. We believe this was the first application of these materials as capacitor impregnants. These liquids are chemically named perfluorocarbons.

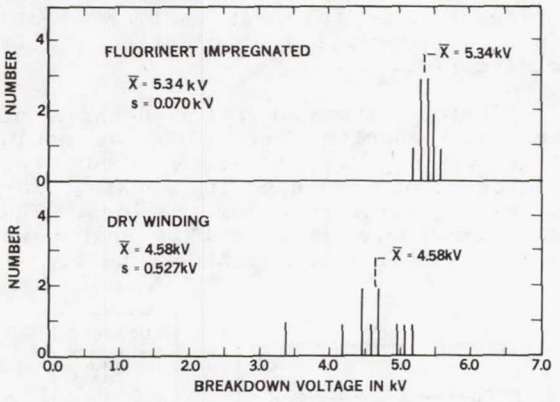

Fig. 2. A Comparison of 12 μm Plastic Films in Dry Capacitors vs. Ones Impregnated with Fluorinert*

The first indication of things to come was observed in an experiment some years ago. Figure 2 plots the comparison of short-term breakdown of 12 μm Mylar* in a dry condition versus the same material impregnated with one of the perfluorocarbons. Notice the significantly higher mean breakdown of the impregnated samples and the dramatic stabilization of the breakdown around the mean. This mean breakdown represents a stress of 444 MV/m. After duplicating these results a few times to demonstrate that it was not an experimental fluke, we did the tests necessary to plot Figure 3.

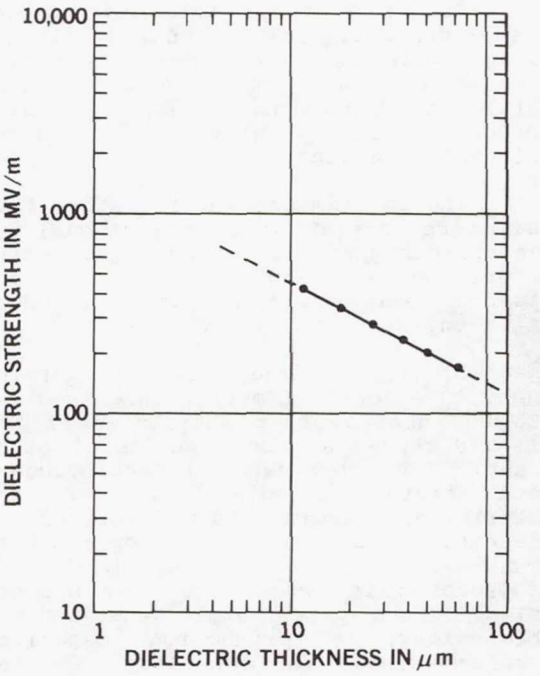

Fig. 3. Dielectric Strength vs. Thickness of Mylar Impregnated with FC-40 Fluorinert.

Figure 3 is a plot of dielectric strength versus thickness for Mylar impregnated with one of the perfluorocarbons. This curve now serves as our design guide for specific capacitors at various voltage ratings.

Credit for this dramatic improvement in electrical performance is given to the near perfect attributes of the perfluorocarbon used as the impregnant. It embodies all of the attributes Sandia has identified as essential to capacitor impregnating quality. No other single fluid approaches its combination of properties. It has a dielectric strength significantly higher than common impregnating liquids. Its surface tension is perhaps the lowest of any fluid

* Mylar is a trade name of the DuPont Company. Fluorinert is a trade name of the 3M Company.

material. This allows it to wick into and completely wet plastic film capacitor rolls without requiring such auxiliary measures as interleaved paper wicks. The impregnant is a highly effective coolant which allows it to moderate hot spots in capacitor rolls before they lead to catastrophic failure.

A PRODUCTION CAPACITOR DESIGN

Several years ago we had a need for a high-energy density capacitor. This new technology was chosen to fulfill this need. Figure 4 contains the vital statistics of the MC3344 design that has reached production status. The key factors to note in Figure 4 are the average stress of 236 MV/m on the dielectric at rated voltage and the energy density by weight of 0.1 J/g and by volume of 0.28 J/cc. New efforts underway promise to double and perhaps triple these density figures.

Figure 4 also contains an exploded view of the details of this design. The dielectric pad is made up of two layers of 12 μm Mylar wound between two 6 μm aluminum electrode foils.

CAPACITANCE	3.0 μfd.
VOLTAGE RATING	6000 V.
ENERGY	54 J
DIELECTRIC STRESS	236 MV/m
DIAMETER	57.16 mm
LENGTH	76.2 mm
VOLUME	195.3 cc
WEIGHT	535 g
ENERGY DENSITY	
WEIGHT	0.1 J/g
VOLUME	0.28 J/cc

Fig. 4. The MC3344 High Energy Density Capacitor.

The winding is an extended foil configuration. The winding criteria is somewhat unique in that it is wound to a specified tension on the film and foil in order to achieve a controlled looseness. The controlled looseness guarantees an optimum thickness of the liquid between the layers of the films and foils. We have found this to be a major determinant of discharge life. We believe this is due to the better cooling performance of the thicker liquid layers.

The winding is done on a hollow mandrel whose interior is used to house a welded stainless steel bellows. The bellows is used to compensate for the change in volume of the liquid over the wide operating temperature range (-55^{o} to $+74^{o}$C). We believe that it is essential to compensate for this liquid volume change in order to provide a void-free condition at all times in the assembly. The bellows also provides pressure on the liquid over all temperature conditions.

Another somewhat unique feature of this design is the electroding system. At the 25 kA discharge current peak required by the application the current density in the electrodes is some 1500 A/cm^2. Considerable development effort was required to achieve a system that would repeatedly withstand this condition. The system finally chosen uses silver conductive epoxy as the basic interconnect but also uses a copper screen to act as mechanical reinforcement and provide increased conductivity.

The case is formed from a stainless steel tube to which are welded end caps to complete the closure. Electron beam or laser welding is used for their superior hermetic sealing capabilities. The high-voltage bushing and ground ring are oven-brazed to the top cover. The copper fill tubes are oven-brazed to the stainless steel case. The final closure after assembly is an electron beam weld joint between the high-voltage terminal and a sleeve on the high-voltage bushing. Through this assembly process, we have achieved an all welded closure system with its superior hermetic sealing properties.

We use an individual filling process with each unit connected to a vacuum and liquid manifold through separate fill tubes. The dry assemblies are vacuum degassed until they meet a maximum outgas rate. At the same time, the liquid is being degassed in a thin film configuration and filtered. Once these intermediate steps are completed, the assembly is impregnated while still under vacuum and sealed by a mechanical pinch-off procedure. Final sealing of the pinch-off tubes is accomplished by an ultrasonic welding procedure.

WINDING TECHNOLOGY

Perhaps the major learning experience on this program was in the area of roll winding. Others[2] have reported similar experiences. We started out with what could be characterized as traditional winding technology and soon found it to be inadequate for the task. We then evolved the winding technology adequate for the requirements.

In the quest for higher and higher energy density such mechanical factors as end margin length and foil extension for outside connection became important. Mechanical wander of either of these parameters becomes important since both of them affect the active region in the roll and hence the energy density. One would like to operate at as small end margins as possible, but excessive wander requires a conservative nominal value to prevent wander from encroaching on a critical dimension. Essentially the same can be said about foil end extension with one additional factor. Excessive wander of the foil extension also makes for a difficult electroding problem. The solution to excess wander lies in the precision of the film and foil handling systems on a particular winder. In solving this problem on our machine we have gone to precision instrument bearings on all film and foil rollers. In some of the roller positions we have experienced film or foil slippage over the roller instead of continuous rolling. This has been due to inadequate contact with the rollers due to a shallow angle of engagement. Slippage rather than rolling can cause excessive wander and film wrinkling. This was solved by using two rollers at each position where an S-shaped wraparound could be obtained for greater engagement. With these improvements we have reduced wander and wrinkling to an insignificant level.

Perhaps the most critical factor has to do with the tightness of the winding. It has been so critical to our performance that we have labeled it the "tight winding syndrome." As the name implies, this is a condition involving the tightness of the winding. Figure 5 indicates its effect on discharge life performance. We define winding tightness by a parameter called space factor. Space factor is the ratio of the space between foil and film layers expressed as a percentage of the total film thickness. A large space factor indicates a loose winding and a small space factor represents a tight winding. In Figure 5, the numbers associated with each space factor curve is a tabulation of discharge life from samples representative of that type winding. The units with space factors at or above ten percent exhibit far superior discharge lives than those in the seven percent or lower range. We have solved this problem by replacing the mechanical tension (Prony brake) system with electric motor tensioning devices.

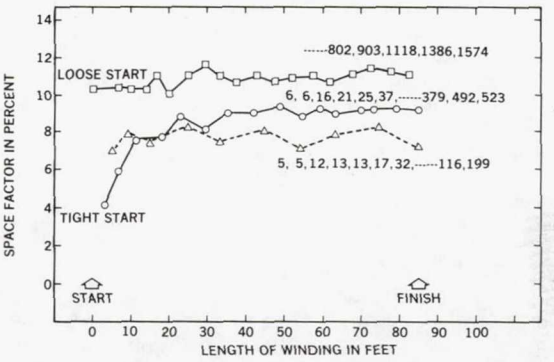

Fig. 5. The Effect of Winding Tightness on Discharge Life.

Figure 6 is a photograph of this modified winder. This is a twelve-supply spindle machine with electric motor tension control. It employs an electronic system using force transducers and meters to continuously monitor the tension being applied on the material from all twelve spindles. This machine also employs instrument grade bearings in all feed rollers and double rollers in those locations where greater roller engagement is required. With this system we have been able to wind wrinkle-free windings at tensions as low as 50 grams. The foil and film wander is held under 5 mils.

SUMMARY AND CONCLUSIONS

We have reached production status on the MC3344 having completed the first production lot. In our system we go through distinct phases to achieve production status. These are design prove-in, manufacturing feasibility, and production. Table I summarizes the data up to and including the first production lot. Significant factors to note in Table I are the very uniform Xs and sigmas as well as the calculation X - ks. The uniformity

of these parameters is maintained over different lots of film, different lots of liquid, and fabrication by different personnel. We conclude, then, that the technology is highly predictable and reliable and fabrication processes can be well controlled with standard production practices.

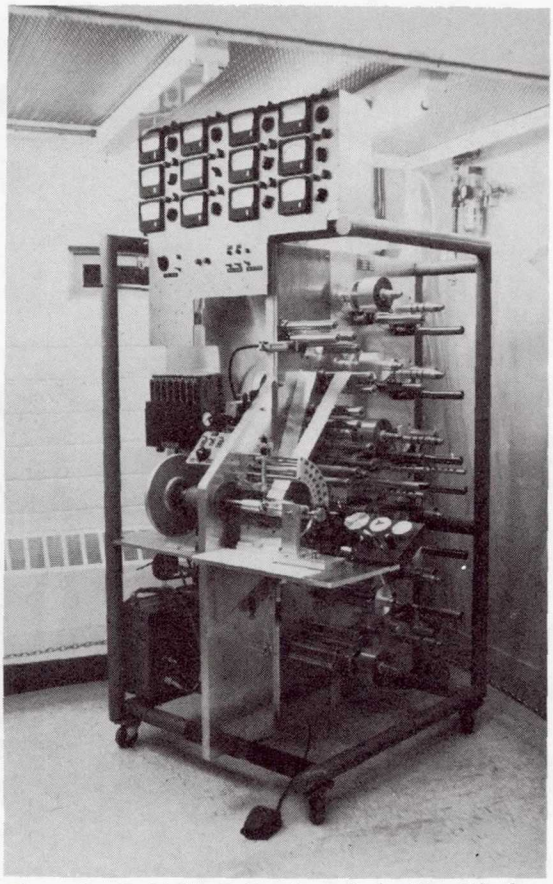

Fig. 6. Modified Twelve Spindle Winder.

ACKNOWLEDGMENT

The author would like to thank C. B. McCampbell, D. H. Weingarten, K. J. Urquhart, and M. L. Reichenbach of Sandia National Laboratories, and W. E. Packer, N. A. Sidneil, and C. I. Biver of the General Electric Neutron Devices Department for continuing support and assistance.

REFERENCES

1. R. D. Parker, "Technological Development of High Energy Density Capacitors," NASA Lewis Research Center, Cleveland, Ohio, NASA CR 124926, February 1976.

2. R. D. Parker, "Capacitors for Aircraft High Power," Air Force Aero Propulsion Laboratory/POD, Wright-Patterson AFB, Ohio, Tech Report AFAPL-TR-77-40, December 1976.

TABLE I

Summary of MC3344 History

	Short-Term Breakdown			
Phase	X	s	X - ks	Discharge Life
Design Prove-in	7.53 kV	.265 kV	6.30 kV	10 units passed 500 discharges
Manufacturing Feasibility	7.55 kV	.299 kV	6.38 kV	23 units passed 500 discharges
First Production	7.55 kV	.248 kV	6.38 kV	20 units passed 500 discharges

PERFORMANCE COMPARISON: ALUMINUM ELECTROLYTIC AND SOLID TANTALUM CAPACITORS

by
Mr. B.G. Hawthornthwaite U.C.C.
Mr. J. Piper U.C.C.
Mr. H.W. Holland U.C.C.
(803) 963-6300

SUMMARY

This paper evaluates several key electrical and environmental parameters of latest-technology Aluminum Electrolytic and Solid Tantalum capacitors in light of recent price fluctuations of tantalum metal.

Brief History of Tantalum Capacitors

Solid tantalum capacitor usage has grown at an astounding rate since this product was invented at Bell Laboratories and adopted for telecommunications use. Military and aerospace hardware designers were soon attracted to this capacitor because of its advantage in size, stability of characteristics, resistance to environmental damage and probably most important of all, long life with apparent absence of wearout behavior. These qualities later attracted industrial users in areas such as instruments and especially in large commercial computers. As production volume mounted, prices fell and solid tantalums found application in consumer devices such as automobiles and television receivers.

From 1960 the decline in solid tantalum capacitor prices continued generally over two decades. The decline was interrupted briefly in 1973-74 during the economic super-boom and then slowed (in then-current dollars) from deflation of the currency. Then, in late 1979, a gradual rise in tantalum ore price turned into a reverse avalanche. Tantalite ore (30% Ta_2O_5) sold for $6.00/pound in 1972; its price rose above $100/pound in 1980. It is fatuous to talk of productivity offsets under these conditions. Capacitor prices necessarily responded and doubled within 9 months.

It is not surprising that designers began seeking alternatives. While monolithic ceramics may substitute in very small capacitances, only aluminum electrolytics offer a reasonable consideration over significant areas of application. While we shall speak more of economics later let us now examine performance differences between solid tantalums and aluminum electrolytics.

Parametrics and Environmental Evaluation

A laboratory test program was based upon comparison between aluminums and the Kemet T390, a resin-dipped tantalum product used in many commercial applications. The initial testing of aluminums was performed on a product offered especially for automotive service. These data have been published in a sense but only through internal bulletins. Later, competing aluminum manufacturers offered products with the announced intention of competing with tantalums. Tests on samples of these latter products from three manufacturers formed the basis of this paper. These data have not heretofore been published at all. In general, results were very similar to those from the earlier data.

The complete matrix of equivalent capacitance-voltage ratings could not be assembled without inordinate delivery delays. Figure 1 shows the actual ratings tested. In all but the one instance noted, identical CV ratings were used. The test scheme, is illustrated in the flow chart of Figure 2.

While the tantalum capacitors retain a size advantage for equivalent capacitance-voltage ratings, the recent miniaturization efforts of the aluminum manufacturers has met with some success and the differences have been narrowed as seen in Figure 3. The total volume occupied by the tantalum is much less, of course, but in this analysis the tantalum was treated as a right cylinder, having the diameter equal to the maximum recorded diameter of the teardrop shape, which the tantalum slug really is.

The recorded test values are much too voluminous to be included in this paper. Many of the results are conveniently summarized in graphical form,

and these will be treated in the following illustrations.

Differences among products from the three aluminum manufacturers were frequently insignificant. Unless otherwise stated, the graphs were typical of all manufacturers. The first comparisons dealt with temperature stability, or change of parameters versus temperature. The result of the first parameter, capacitance, is seen in Figure 4 for the 10 mfd. 20 volt unit. In this figure, the aluminums were not measured below their rated -40°C. As the capacitance value increased, the effect of temperature on capacitance of the aluminums also increased. Figure 5 illustrates this effect with the 100 mfd. 10 volt rating.

In the next parameter, dissipation factor, the inherent influence of a liquid electrolyte is seen. Resistance of the electrolyte necessarily rises as the temperature decreases. Figure 6 illustrates this effect with 1 mfd 50 volt capacitors. The effect is much more pronounced as the size of the capacitor increases. Figure 7 and Figure 8 illustrate this effect for 10 mfd. 25 volt capacitors and 100 mfd. 10 volt capacitors, respectively. The effect of temperature on DC leakage is illustrated in the table of Figure 9 for two ratings near the smallest and near the largest. These data are difficult to interpret graphically, because at 105° the voltage was reduced by 33% from the rated voltage. The column headings use conventional, statistical notation of $\bar{X}$ for the arithmetic mean and S for the standard deviation of the data.

Temperature cycling did not reveal dramatic differences between tantalum and aluminum but was one of the tests where a distinct deviation among aluminum manufacturers was seen. The difference was only in DC leakage current which is illustrated in Figure 10.

Impedance and equivalent series resistance (ESR) were measured over the range from 120 hertz to 10 megahertz. Typical results for 1 mfd. 50 volt capacitors and 100 mfd. 10 volt capacitors are seen in Figures 11 and 12, respectively. Neither the aluminum nor the tantalum 1 mfd. 50 volt capacitors have completely passed through the self-resonant areas in Figure 11. The lower ESR of the tantalum throughout the range is evident, however. In Figure 12 the tantalum begins to display inductive reactance at about 2 megahertz, while the aluminum does not through 10 megahertz.

The most significant result from 100° life testing was the loss of capacitance and increase in dissipation factor of the aluminums. Results were erratic. Capacitance loss varied from less than 5% for the very smallest rating to over 90% for the largest rating. We have chosen the 10 mfd. 25 volt rating as being a fair representation of typical behavior. Results are seen in Figure 13. Dissipation factor for this same rating is seen in Figure 14. The worst-case result recorded for dissipation factor revealed an increase to over 80% DF at 1000 hours from the 100 mfd. 10 volt rating. Change in the DF of tantalums of all ratings was insignificant.

On 85° life test, changes in capacitance and dissipation factor of the aluminums was much less during the 1000 hour period, and results were less erratic between capacitance-voltage ratings. The same 10 mfd. 25 volt rating was selected as typical; results are seen for capacitance and DF in Figures 15 and 16, respectively.

The parametric changes during life test are attributed primarily to the simple loss of electrolyte during the long time at high temperature. There are published papers illustrating weight loss through the gasketed seals which are used in aluminum capacitors. (Hermetic seals would not allow venting of the hydrogen gas which evolves as a result of aluminum corrosion and electrolysis.) This effect is one of both time and temperature, so the 100° effects are greater than those at 85°.

Determination of catastrophic failure rates could not be made with the limited sample size during the 1000 hour test data available at present. These tests are continuing and a reliability comparison may be possible later. It appears certain, however, that parametric failure of aluminums, through electrolyte loss and corrosion, is simply a matter of time and temperature. It is difficult to see how these wearout mechanisms can be avoided.

The lack of wearout failure in

solid tantalums has been the subject of many papers. Solid tantalums made under controlled production processes exhibit a declining failure rate which has persisted over years of testing. The declining failure rate is contributed by a "self-healing" internal phenomenon. Any potential dielectric failure site will begin to allow passage of higher DC currents. This current must also pass through the manganese dioxide (MnO_2) layer which forms the counter-electrode of the solid tantalum capacitor. The current flow causes Joule heating. At higher temperatures, MnO_2 spontaneously converts to lower oxides such as Mn_2O_3. These oxides possess much higher resistivity than MnO_2 and the higher resistance shuts off the flow of the fault current.

Price Effects

Finally, we must consider the price effects referred to earlier. Figure 17 illustrates the prices of silver, copper and tantallite ore from 1940 through 1980. It is apparent that all three of these commodities (and many others as well) have been in an upward trend throughout this period; however, the cyclical nature of the prices should not be overlooked. There have been many times in the past when tantalite ore more than doubled. The general price level, albeit with oscillation, is seen to be relatively constant at around $6.00/pound from 1980 to 1973. During this period of time, producers of ore had absolutely no incentive to expand exploration, and a shortage gradually developed. The resultant rise in price reached a fever pitch of speculation during 1979-80 when the price finally topped-out at about $115/pound. This increased price was, of course, passed along by the tantalum powder producers to the capacitor users.

The high prices for ore provided all the incentive needed for the increased exploration, and the exploration was successful. Many smaller deposits are now economically workable when they were not previously. In addition, a major find in Australia promises to produce alone over 100 years of the world's supply at existing consumption rates.

Technology Attack

In the meantime, another attack on the high raw material price has been made by capacitor manufacturers. It is illustrated by the curve labelled "Average Powder Charge" in Figure 18, which means the number of microcoulombs obtainable from a unit weight of tantalum powder. Efforts to improve the technology have been going forward for years but, of course, were accelerated when the powder price increased so dramatically. With the technology already known, Point A on the graph could have been reached in 1980 with material grades already identified. Instead, the average powder charge decreased. This effect was another one of general shortage. Manufacturers were forced to use inefficient powder grades, simply because the supply of the more advanced powder grades were inadequate. This situation has now passed, however, and the sights can be raised again toward Point B.

Thus, the economic scare seems to have spent its force. A certain number of tantalum applications have certainly yielded to substitution by the cheaper aluminums. However, these substitutions were in areas generally of consumer grade electronic circuits where long-term reliability and stable parametric performance were not prime objectives.

CONCLUSIONS

Considering the parametric and environmental differences between tantalum and aluminum electrolytic capacitors and recent raw material and finished unit price trends, tantalum is still the best choice for applications where parametric stability and/or long-term reliability is a consideration.

FIGURE 1. ARRAY OF CAPACITANCE/VOLTAGE RATINGS TESTED
(UF/VOLTS)

GROUP	TANTALUM	ALUMINUMS		
		MFG. A	MFG. B	MFG. C
1	0.1/50	0.1/50	--	--
2	1.0/50	--	1.0/50	--
3	10/25	10/25	--	--
4	33/25	--	33/25	33/25
5	220/10	--	220/16*	220/16*
6	100/10	--	100/10	100/10

*HIGHER VOLTAGE RATING THAN THE TANTALUM.

FIGURE 2. FLOW CHART OF TEST PROGRAM

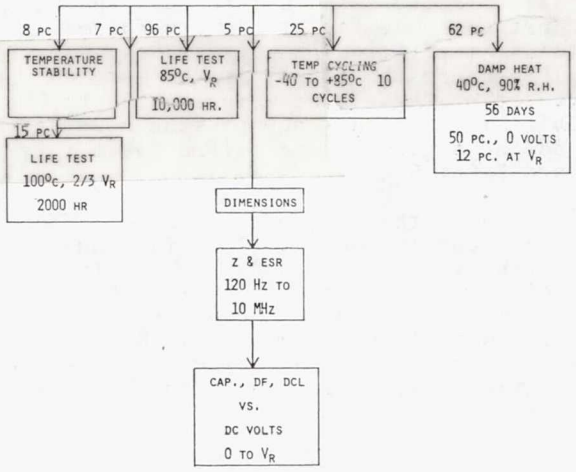

FIGURE 3. DIMENSIONS, AVERAGE OF 5 PIECES, INCHES

CV GROUP	DIAMETER		HEIGHT	
	TA	AL	TA	AL
1	0.170	0.167	0.273	0.288
2	0.190	0.202	0.339	0.447
3	0.232	0.207	0.350	0.312
4	0.307	0.321	0.448	0.491
5	0.338	0.402	0.512	0.781
6	0.291	0.320	0.429	0.498

FIGURE 4.

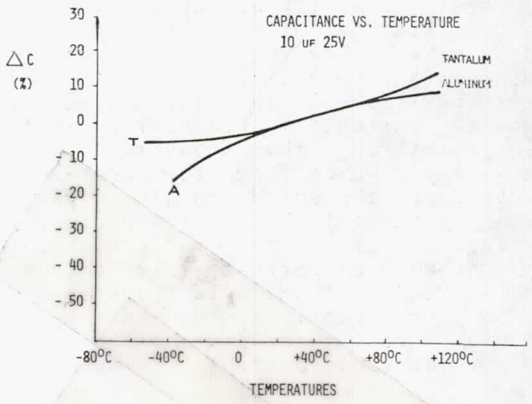

FIGURE 5.

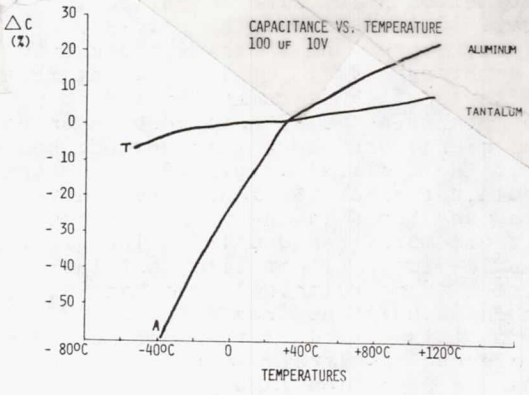

FIGURE 6.

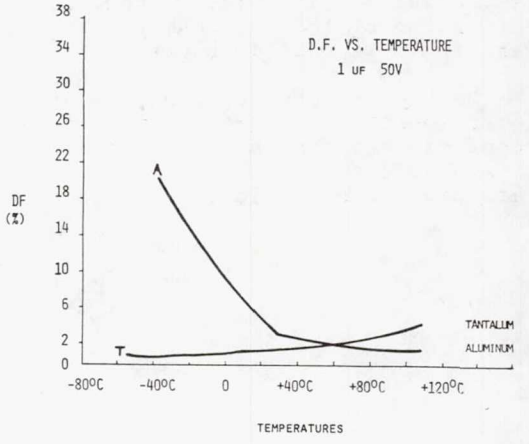

FIGURE 7.

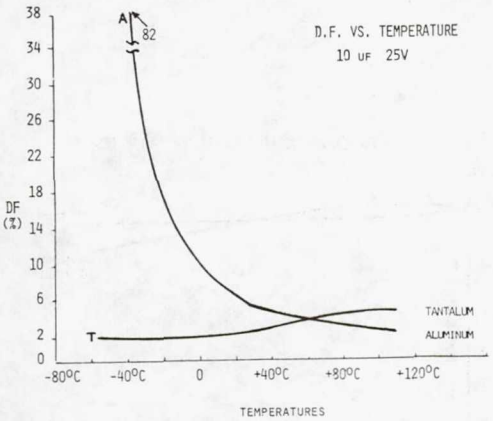

FIGURE 8.

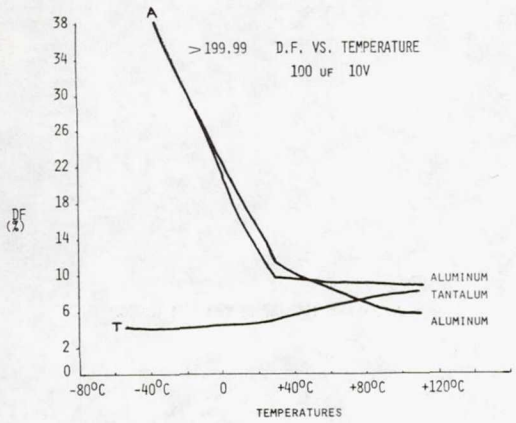

FIGURE 9. DC LEAKAGE CURRENT, UA, VS. TEMPERATURE

UF/V		25°C, V_R		85°C, V_R		105°C, 2/3 V_R	
		$\bar{X}$	S	$\bar{X}$	S	$\bar{X}$	S
1.0/50	TANTALUM	.003	.006	.029	.012	.008	.006
	ALUMINUM	.358	.196	.966	.402	.753	.276
100/10	TANTALUM	.516	.44	.952	1.26	.640	.715
	ALUMINUM	2.02	.65	6.01	.96	2.29	.610

FIGURE 10.

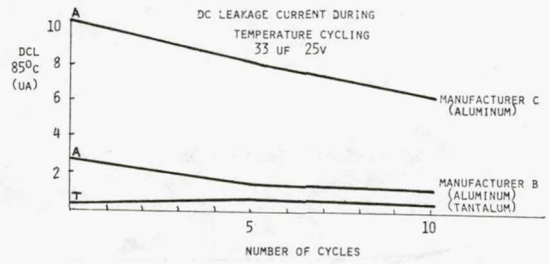

FIGURE 11.

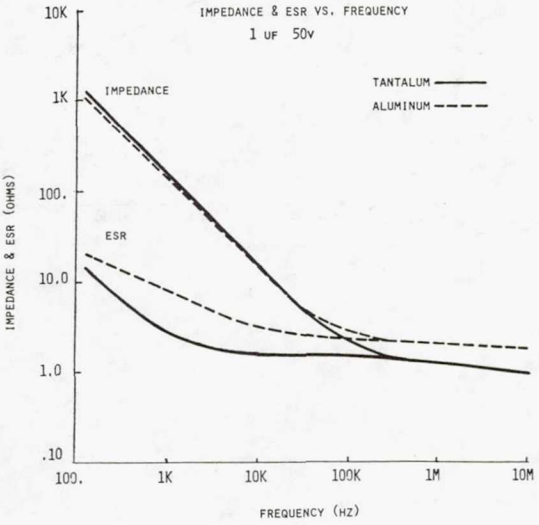

FIGURE 12.

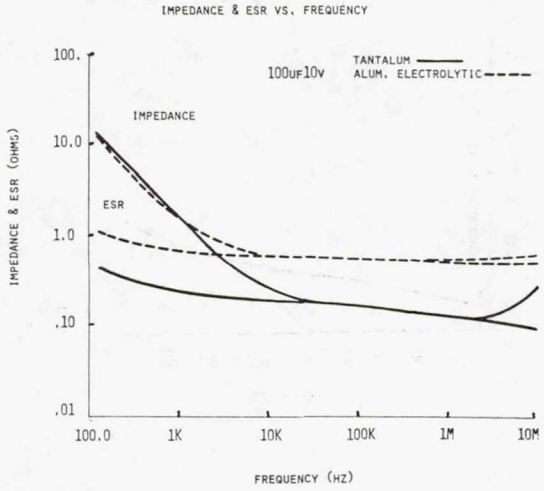

FIGURE 13.

CAPACITANCE VERSUS TIME DURING 100°C LIFE TESTING

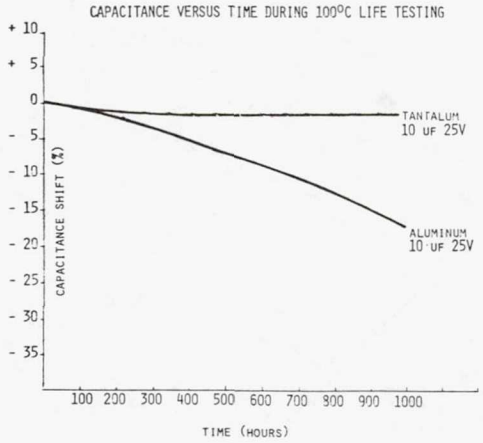

FIGURE 15.

CAPACITANCE VERSUS TIME DURING 85°C LIFE TESTING

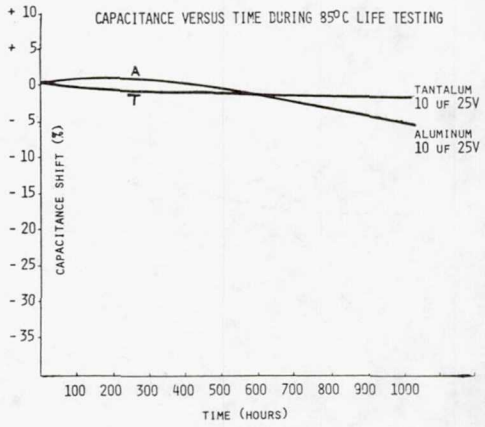

FIGURE 14.

D.F. VERSUS TIME DURING 100°C LIFE TESTING

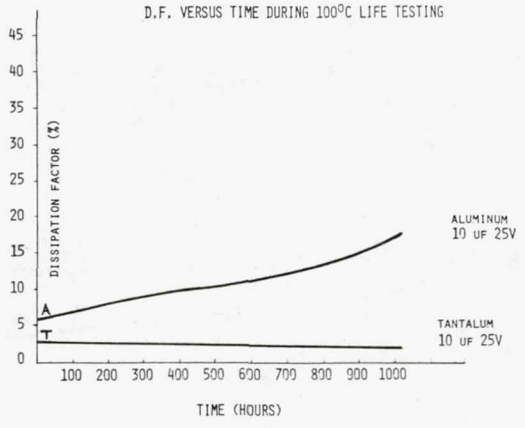

FIGURE 16.

D.F. VERSUS TIME DURING 85°C LIFE TESTING

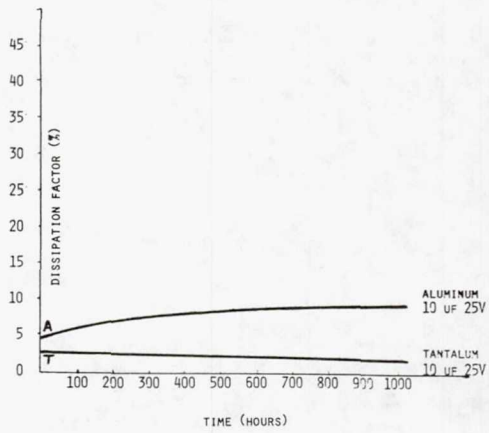

FIGURE 17.

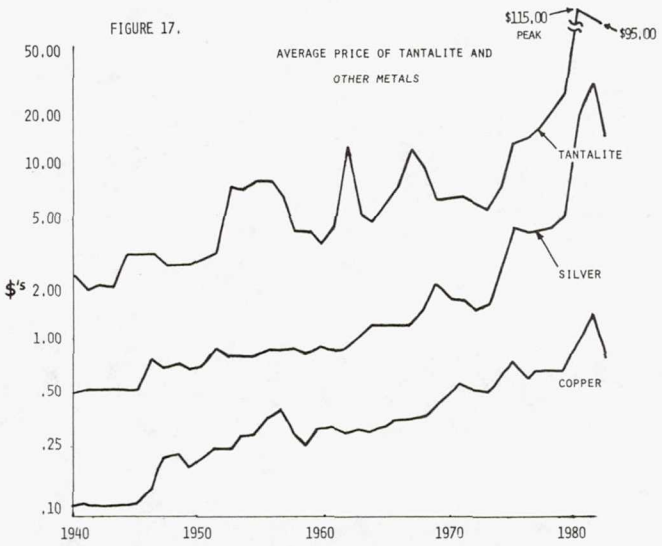

FIGURE 18.

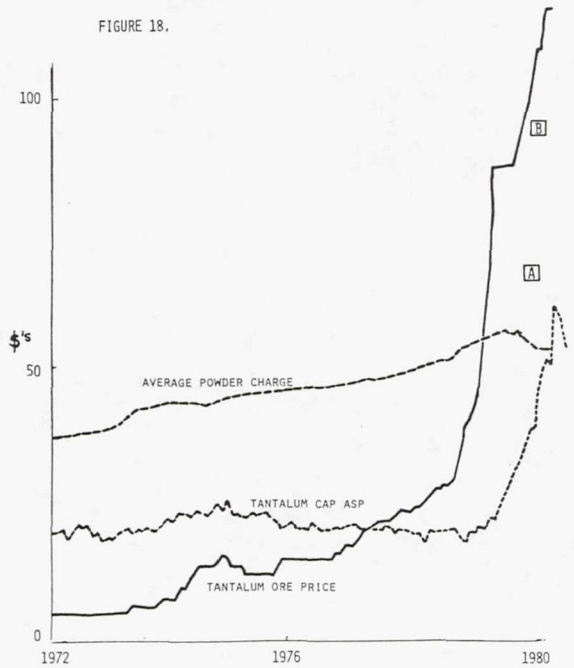

UNSTABLE INSULATION RESISTANCE IN CERAMIC CAPACITORS

Dr. A. M. Holladay, EC41
Electronics Development Division
Electronics and Control Laboratory
George C. Marshall Space Flight Center, AL 35812
(205) 453-3771

SUMMARY

In recent years low and varying values of insulation resistance (IR) have been a significant cause of failure in ceramic capacitors. This paper describes two recent experiences with this problem, and steps recommended to alleviate it.

PREVALENCE OF LOW IR PROBLEM

Of the 6.2 billion capacitors built in 1979, 71% were of the ceramic type, and over one-half of these were the "monolithic" units. It is therefore of considerable concern if any problem occurs with subject ceramic capacitors because of the wide potential impact on hardware failures. It is of even greater concern if this problem is widespread and is not understood, as is the situation with the IR instability problem discussed here.

As part of my investigation of failures of ceramic capacitors in two Shuttle black boxes caused by low and fluctuating IR, I had discussions not only with cognizant personnel at MSFC and Johnson Space Center, but also with numerous manufacturers, users, and researchers of these devices. The general impression derived from these discussions with these people in the U.S. and England is that the problem: (1) is possibly lot oriented; (2) is sporadic and widespread; (3) is not well understood; (4) has increased significantly during the 1970's as low voltage digital applications have led to capacitor design changes; and (5) has not received the serious attention that it deserves. Very little test data on IR at low voltages could be found, and even then readings were taken soon after high voltage application.

LOW IR PROBLEM ON RMS

Two specific instances of low IR problems in ceramic capacitors in Shuttle hardware have occurred in the past two years. One of these is on the electronic controls for the Remote Manipulator System (RMS) in the Shuttle bay built by Spar, Canada. The EMI filters (made by supplier "C" below) were purchased against MIL-F-15733. They use a 30-layer discoidal ceramic capacitor rated at 1.2 μF-100 volts. The dielectric is K5500, with a nominal thickness of 1.3 mils, and with a rated IR of 100 megohms minimum at 100 volts and 25°C. The device is hermetic and uses palladium electrodes. The voltage applied in the black box is in the 5-28 VDC range. At failure the IR dropped to a few kilohms. Among the failures were five capacitors from a sublot of 100 units which had never been in hardware, but had been on the shelf for about two years at room ambient. At two volts these units had an IR in the 15 kilohm region, but the value jumped suddenly to about 300 megohms when the voltage was gradually increased to 16 VDC at room ambient.

Two of the failed units from hardware were exhaustively tested at MSFC over a period of several months. To say that they were unstable with time and voltage below the five volt level is putting it mildly. Fig. 1 clearly depicts their instability. Note that the changes in IR (reciprocal of DC leakage) were quite slow and erratic. One of these units was heated to 150°C for two hours, then cooled to room ambient, and was tested for IR. The value was 300 megohms, a typical "recovery" value. All of these readings were taken on an HP Model 425A picoammeter. The conclusion is that "recovery" whether due to heat or voltage is only temporary. An unsuccessful attempt was made to correlate dissipation factor at different frequencies with IR values. Only when DC leakage is excessive can a correlation be made: both DF and capacitance increase.

The hardware problem was fixed by replacing these capacitors with a 60-layer unit from another manufacturer which had a K-1600 dielectric with a nominal thickness of 1.3 mils. We could not be certain that the stability of this new device derived from its lower K-value dielectric, from better production controls, or from other factors. We did observe in the plant of the supplier of the first device that poor, manual controls were used to maintain dielectric thickness.

LOW IR PROBLEM ON MDM

The second low IR problem occurred in the Multiplexer-Demultiplexer (MDM) made by Sperry-Phoenix for Rockwell. The MDM is used on both the Solid Rocket Booster (SRB) and the Orbiter. The SRB-MDM is environmentally sealed in dry nitrogen while the Orbiter-MDM is not. These ceramic capacitors were purchased against MIL-C-20. They are Style CCR with a minimum IR of 10^4 megohms at rated voltage and room ambient.

These capacitors are plastic encased, radial lead, rated at .01 μF-50 volts. There are generally two chips in parallel, each with 16 layers, reportedly of NPO ceramic, and with thickness ranging from 1.3 to 1.7 mils (depending on manufacturer; see Table I.). In the MDM application they operate at ±5 VDC. The low dielectric constant and the relative thickness of the dielectric make this low IR problem doubly surprising and disturbing. IR on failed units dropped to 5-90% range of correct values.

Of the five suppliers for these MDM units, A, B, C, D, and E, only one, D, has had no IR problem in this hardware, while A, B, and C have, and E has had a slight problem. Only one failure has occurred in the SRB-MDM. This was traced to a hole in the dielectric as revealed by DPA, and was apparently not moisture-bias related. All SRB-MDM capacitors came from Supplier "B". Capacitors from this same supplier have failed so extensively on the Orbiter-MDM (21 field failures, IR values 2-12 kilohms and excess factory rejects) that replacements were underway for flight MDM's. In fact, supplier "B" had replaced supplier "A" whose capacitors had so many voids, delaminations, and failures that they were purged from flight MDM's. Now the capacitors from a third supplier, "C", are showing significant failures (five recent failures at KSC) and are being replaced by units from suppliers "D" and "E". We hope that this game of musical chairs has ceased.

To help confirm the belief that moisture and bias were the immediate cause of failure in these capacitors, Sperry-Phoenix subjected capacitors from suppliers B, C, D, and E to 85°C-85% RH for several days. For supplier B there were 2/8 failures; for C, 13/80 failures; for D, 0/76; and for E, 0/16. For supplier D, 44 of the 76 units had been boiled in 5% NaCl solution for one hour prior to test, and there were still no failures--a ray of hope for the future. Test bias was 0.5 VDC.

Then, to show the effect of bias, 10 units from supplier "C" and six from "E" were tested for three weeks at 85°C-85% RH without bias. No failures occurred.

To show the effects of moisture, 9 units from "B" and 40 from "C" were tested at 85°C-5% RH and 0.5 VDC for three weeks, without failure.

To confuse these otherwise consistent results is the fact that when capacitors from suppliers B and C were heated to 125°C (slightly above the Curie point of the titanate dielectric), B units "recovered" while C units did not. However, in both cases IR increased to several hundred megohms upon application of higher voltages.

DISCUSSION AND CONCLUSIONS

As always, conclusions based on so few tests should be made cautiously. However, the following seem justified:

A. Monolithic, multilayer ceramic capacitors may exhibit low and unstable IR at low voltages, or at no voltage.

B. The major cause of this IR problem may start with thin spots in the dielectric, which are aggravated by the "aging" process. We think that the low IR in the hermetic, hi-K capacitors in the RMS likely resulted from an "aging" process in which crystal-phase transformations occurred in the titanate with time, with the unit cells in the crystal polarization domain gradually orienting themselves toward a tetragonal structure. Upon application of heat or voltage (above about 16 volts in this case) the dielectric "deages" toward a cubic structure. The heat may be from an external source, or it may come from current flow through selected thin spots in the dielectric where only one or two grains may bridge the distance between the plates. Titanate dielectrics generally deage readily at 125°C and completely at 150°C. More subtle are the effects of both low and high DCV, as seen in both the RMS and MDM capacitors that failed and that were made by suppliers A, B, and C. The most tantalizing question is: Why does IR decrease at low voltage but appear to "recover" at high voltage, only to revert to low IR later on. Haven't we all been taught that high voltage is always more stressful on a capacitor than is low voltage? Yes, but the high voltage tends to produce more catastrophic effects, of which we are generally more mindful, while the low voltage tends toward a degradation type failure, which is more subtle. Turning to Table I, the only good correlation we can find between the low IR low voltage failure and construction is the prevalence of dielectric defects. We think that this is very significant. We propose that, while heat-moisture-bias was the immediate cause of failures for suppliers B and C, the reason that suppliers D and E had no failures was probably due to a basically better dielectric. A dielectric with thin spots, voids, etc., may create a heavy fallout at the dielectric withstanding voltage test, yet marginal units pass this test. It may take months for the dipole-cells in the dielectrics to reorient themselves after these high voltage tests while either on the shelf or under low voltage. When low voltage --such as two volts-- is applied the field is strong enough to cause electrons to flow along boundaries of the relaxed grains. When the voltage is raised on the

capacitor, the IR "recovers", i.e., drastically and suddenly increases as a rule. The higher field causes at least four events. Three of these are: (1) the leakage current, though small, may represent quite high current density around these grains, and may be sufficient to change grain structure; (2) the higher field, made even higher at the thin spots, is sufficient to reorient the dipoles-cells-grains, especially if hot, so as to restrict electron flow and therefore increase IR since electrons prefer to flow along grain boundaries; and (3) the higher field exerts a considerable electrostrictive force on the plates and dielectric, further closing fissures, disrupting grain boundaries, and restricting electron flow. See Fig. 2. We doubt if burning out of metal dendrites is a major cause of "recovery".

C. Moisture/Contamination

The fourth effect of the higher field in B above is that the higher current could produce heat that would evaporate moisture and therefore increase IR. Heat alone could of course produce this same effect, and could be used to delineate between effects of moisture and of the three effects given in B. Since we do not quantitatively know the permeability to moisture of the plastic cases used by the five suppliers it is difficult to attribute precisely the low IR problem to moisture or to dielectric defects. However, these tests clearly show that failures occur on B and C units only under a combination of moisture and bias. Closely associated with these failures is the fact that DPA revealed many more dielectric defects on B and C units than on D and E units which did not fail. This would suggest that a combination of moisture, (with some necessary ionizable contamination) bias, and defects caused the IR loss, even in NPO dielectrics.

The Japanese (Sato-Ogata-Ikeo referenced paper) seem to rely on the moisture-contamination mechanism to explain the low IR. However, they did not address the "recovery" behavior of these units at all, nor the reversion to low IR once more. Their suggestion that screening at a few volts in humid air may be effective, but it does not explain anything. Nor does this approach instill confidence that the unit will ever be rid of the moisture used in the test. If the moisture-contamination-bias theory is the correct explanation of low IR, then we would need to assume that the hermetic RMS units had moisture sealed in them.

D. Lot Orientation

The date code orientation of IR failures during the 85°C-85% RH, 0.5 VDC can be judged only for Supplier C, as there were too few for Supplier B and there were no failures for D and only one bad lot for E. There were 12 date codes for Supplier C sampled in this test, and four had some failures. Two date codes had 11 of 13 unit failures. This does indicate some date code orientation for this manufacturer.

E. Screening

Another factor that may be of major significance is the strictness of screen tests. Perhaps Suppliers D and E eliminated poor capacitors by using superior dielectric withstanding voltage tests, acoustic or ultrasonic tests, or even low voltage tests, which would eliminate those capacitors with excess defects, moisture, improper metallization, and related variables.

F. "Recovery" of IR under heat or higher voltage is generally only temporary, and IR tends to a gradual reversion to lower values at low or zero voltage and room ambient.

G. The low and variable IR is a widespread problem which is not well understood.

H. Plastic encased ceramic capacitors can be made with stable IR.

I. An overriding fact is that one supplier has demonstrated that thus far his capacitors do not suffer from the low and unstable IR problem, and a second supplier has virtually eliminated the problem. Three suppliers clearly have problems. A challenge is therefore presented to these three manufacturers if they wish to meet the requirements of MIL-C-20.

RECOMMENDATIONS

To reduce/avoid low and unstable IR in multilayer ceramic capacitors in applications below 25 volts it is recommended that:

A. Voids, thin spots, and related defects in the dielectric be reduced/eliminated through better process and materials controls. Since this study shows that a defect-moisture-contamination-low voltage combination can cause low IR, and since we may not be able to control the low voltage factor, then we must control the other factors as best we can. It may not be economically feasible to maintain sufficiently low moisture and contamination to control the problem. So it seems that the more fundamental approach, and we think the necessary one, is to control to a much higher degree than has been the general practice in industry, the defects in the dielectric. Whether this is achieved by making the dielectric thicker, using low-K material, reducing voids, improving various

process parameters such as a constant monitor on thickness, or by resorting to other measures is a choice for each manufacturer to make.

B. Grain size should be small enough that there be several grains in the dielectric at any point between the plates. Low-K materials, grain growth inhibitors, thicker dielectrics, and perhaps other factors control this.

C. Presently a K of 2400 and a fired thickness of 1.3 mils minimum seem feasible and advisable.

D. The number of plates be kept to a level consistent with good yield and reliability. Currently, a single section should contain no more than about 20 plates.

E. Exposure of the capacitor element to moisture should be minimized.

F. Better screen/lot acceptance tests should be developed, including low voltage testing and possible voltage ramp testing which will detect pulses in a manner similar to ramp tests under development for polycarbonate capacitors by NASA/MSFC. Attention should be given to testing at low voltages before any high voltages are applied to the capacitors.

G. Since the best accelerated test for low IR seems to be the 85°C-85% RH-low voltage test, it is recommended, subject to further verification, that this test be used to check low or unstable IR and that this be done at one volt, at 25°C, and before and after 168 hours of stress. Occasional tests should be run on capacitors rated at 200 volts or higher to compare results on capacitors with thick and thin dielectrics.

H. An ALERT should be sent to the ceramics capacitor community on this IR problem.

I. Users of these capacitors should be careful to select suppliers who demonstrate reasonable control over IR problems at low voltage.

ACKNOWLEDGMENTS

We wish to acknowledge with appreciation the testing of these capacitors by Carl Ballard and Pete Belcher of the MSFC Electronics Development Division, and by Stan Ropiak of the Sperry-Phoenix Company.

BIBLIOGRAPHY

1. Jim McDermott, "Components", Electronic Design News, December 15, 1980, P. 44.

2. Thomas F. Brennan, "Ceramic Capacitor Insulation Resistance Failures Accelerated by Low Voltage", Proceedings of the 1978 International Reliability Physics Symposium, San Diego, CA, April 18, 1978.

3. Charles A. Harper, Editor in Chief, Handbook of Components for Electronics, McGraw-Hill Book Co., N. Y., 1977, pp 8-85 to 8-101.

4. K. Sato, Ogata and Ikeo, "Mechanism of Ceramic Capacitor Leakage Failures Due to Low DC Stress", Proceedings of the 18th International Reliability Physics Symposium, 1980.

5. Joseph L. Capitano, "Innovative Screening for Ceramic Capacitors to Remove Failure Mechanisms", Proceedings of the International Society for Testing and Failure Analysis, Los Angeles, CA, 1980.

TABLE I. CONSTRUCTION OF MDM CAPACITORS

SOME UNITS WITH TWO BLOCKS IN PARALLEL; NPO DIELECTRIC (CLASS I)

SUPPLIER	DATE CODE	NO. OF PLATES	PLATE SPACING (MILS)	CASE	VOIDS	PLATE METAL Pd	PLATE METAL Au	PLATE METAL Pt
B	7715	18	1.36	POTTED	MEDIUM	MED.	HIGH	NONE
C	7643	24	1.45	POTTED	MANY	MED.	MED.	HIGH
	7702		1.53	"	"	HIGH	NONE	MED*
	7707	28	1.55	"	"	HIGH	NONE	MED**
	7711		1.56	"	"	MED.	LOW	HIGH
	7749	31	1.75	"	"	MED.	LOW	HIGH
D	7946	40	1.45	MOLDED	VERY FEW	HIGH	NONE	NONE
	7949	30	1.38	"	" "	HIGH	NONE	NONE
E	78—			POTTED	VERY FEW	HIGH	NONE	NONE
	80—	24	1.40	"	" "	HIGH	NONE	NONE

*5/13 FAILURES **6/13 FAILURES; TOTAL 13/80

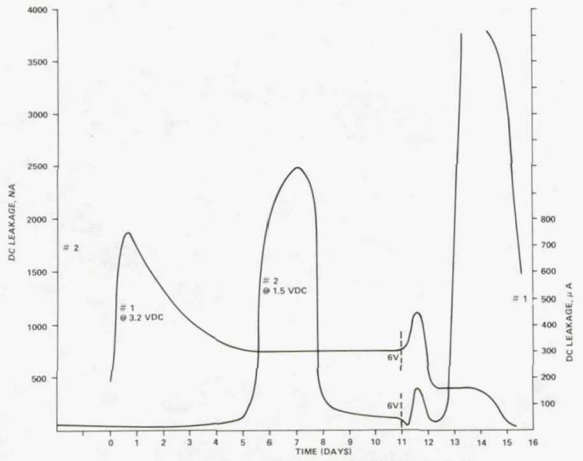

FIG. 1. VARIATIONS OF DC LEAKAGE WITH VOLTAGE AND TIME AT 25°C OF MULTILAYER HERMETICALLY SEALED CERAMIC CAPACITOR.

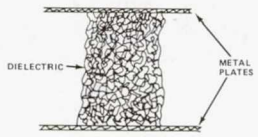

IDEAL LAYER IN THE CERAMIC CAPACITOR: MANY SMALL GRAINS; NO THIN SPOTS

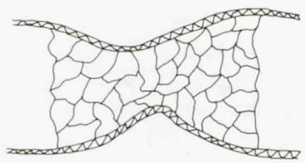

POOR LAYER, LARGE GRAINS; THIN SPOTS

FIG. 2. GOOD AND POOR CERAMIC LAYERS

INFLUENCE OF CURRENT NEEDS ON THE ADVANCEMENT OF ALUMINUM ELECTROLYTIC CAPACITORS

Joseph A. Moresi
Sprague Electric Company
Clinton, Tennessee 37716

The rapid technological growth of industrial electronics has made evident an increasing need for cost-effective, high-performance, long-life capacitors with improved reliability. With respect to miniature aluminum electrolytic capacitors, these requirements present a challenge to our industry. The challenge is to improve their electrical and temperature characteristics and parametric performances without significantly increasing their size or cost and to validate the improvements under accelerated stress conditions.

The equivalent series resistance and capacitance of most of today's low cost, small size ($\leq$10mm diameter), 85°C and 105°C aluminum capacitors may incur such changes in magnitude with time and temperature that their functional life in a critical electrical circuit or their ultimate operational life must be questioned. The parametric deterioration that can take place with such type of capacitor results in a shortened useful life. The ultimate life of a capacitor in a circuit is dependent on the sensitivities or shortcomings of the capacitor's "total design system."

The capacitor's "total design system" can be identified in terms of its elements and their critical factors. Figure 1 illustrates the electrochemical cell system of an aluminum electrolytic capacitor and depicts its elements.

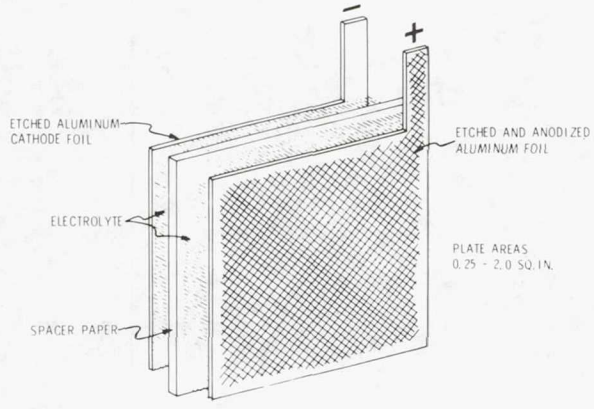

Figure 2

The critical factors that identify with the elements of the capacitor cell and their critical role in determining and governing capacitor characteristics are listed in Table 1.

	CRITICAL FACTORS		CAPACITOR CHARACTERISTICS
1.	Anode foil etch structure and anodic oxide film.	1.	Capacitance, ESR, D-C leakage current.
2.	Cathode foil etch structure and passivity of foil with electrolyte.	2.	Capacitance, voltage reversal tolerance, internal gas generation.
3.	Electrolyte System: solvent solute, conductivity, vapor pressure.	3.	ESR, anodizing efficiency, D-C leakage current, temperature characteristics, gas generation, ultimate operational and shelf life.
4.	Small plate area(s).	4.	Sensitivity to electrolyte loss and conductivity change(s).
5.	Capacitor seal.	5.	Electrolyte vapor loss rate with time and temperature.

Table 1

Present day, low-cost subminiature aluminum capacitors, in both the axial-lead and single-ended wire styles, are manufactured with elastomer or rubber seals. This construction is illustrated in Figure 2.

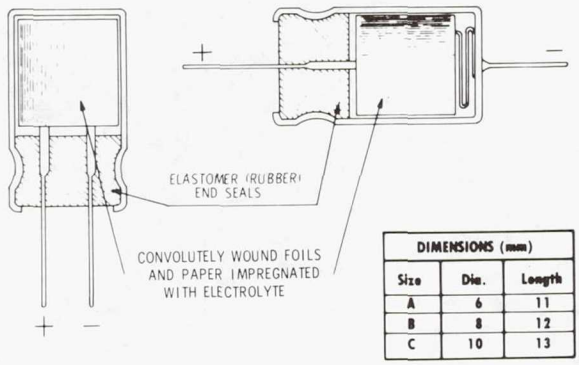

DIMENSIONS (mm)		
Size	Dia.	Length
A	6	11
B	8	12
C	10	13

Figure 1

The electrical and performance data presented are for Sprague Electric's improved Type 510D extended-temperature and extended-life miniature aluminum capacitors. Their seal design and sizes are similar to those illustrated in Figure 2.

Table 2 reports data recorded for a 10µF, 35VDC capacitor rating in a 6 X 11 mm case that exhibits stable and improved capacitor parametric performance on a long-term (3000 hr.), 125°C life test at both full and derated voltage conditions. The parametric performances for capacitance, dissipation factor or ESR, and d-c leakage current are similar and shown to be independent of the voltage applied. This is testimony that refutes the old tale that aluminum electrolytic capacitors "deform" if they are not operated at full rated voltage.

10 µF – 35 VDC
6 × 11 MM
SINGLE-ENDED

CAP. TOL. ±20%
DF (120 Hz) 0.10
DCL 1 µA

TEST TEMP: 125°C
TEST SAMPLE: 10 PCS

	0 Hours	1000 Hours	3000 Hours	ΔChange
Test Voltage: 10 VDC				
CAPACITY (µF):	9.45	9.17	8.58	−9.2 %
DF/120 Hz (%):	4.50	4.52	7.51	+3.01
DCL/2 Min. (µA):	0.22	0.011	0.023	–
Test Voltage: 25 VDC				
CAPACITY (µF):	9.60	9.34	8.79	−8.4 %
DF/120 Hz (%):	4.56	4.75	7.34	+2.78
DCL/2 Min (µA):	0.48	0.023	0.026	–
Test Voltage: 35 VDC				
CAPACITY (µF):	9.47	9.35	8.64	−8.8 %
DF/120 Hz (%):	4.62	4.91	8.49	+3.87
DCL/2 Min (µA):	0.55	0.045	0.059	–

Table 2

The performance of the 10µF, 35VDC capacitor rating is recorded again in Table 3. Parallel testing at 125° C and 105° C compare capacitance, dissipation factor, and d-c leakage current changes for both life and shelf test conditions.

10 µF – 35 VDC
6 × 11 MM
SINGLE-ENDED

CAP. TOL. ±20%
DF (120 Hz) 0.10
DCL 1.0 µA

TEST VOLTAGE: 35 VDC
TEST SAMPLE: 12 PCS

	125°C LIFE TEST			125°C SHELF TEST	
	0 HOURS	1000 HOURS	Δ CHANGE	0 HOURS	250 HOURS
CAPACITANCE (µF):	9.26	9.37	+1.2 %	9.41	9.37
DF/120 Hz (%):	3.75	4.56	+0.81	3.72	3.69
DCL/2 MIN (µA):	0.78	0.12	–	0.74	2.71
	105°C LIFE TEST			**105°C SHELF TEST**	
	0 HOURS	1000 HOURS	Δ CHANGE	0 HOURS	250 HOURS
CAPACITANCE (µF):	9.38	9.43	+0.5 %	9.30	9.29
DF/120 Hz (%):	3.71	3.90	0.19	3.79	3.14
DCL/2 MIN (µA):	0.84	0.09	–	0.67	2.40

Table 3

The life and shelf test data for a 10µf, 50VDC rating in an 8 X 12 mm case size are presented in Table 4. The 2,000-hour life test data reflect improved stability for both capacitance and DF over that shown for the 10µF, 35VDC rating in Table 3. The improved performance was attained in part from increased capacitor plate area in the larger 8 X 12 mm case and in part from a minor modification of the electrolyte.

10 µF – 50 VDC
8 × 12 MM
SINGLE-ENDED

CAP. TOL. ±20%
DF (120 Hz) 0.08
DCL 2.0 µA

TEST VOLTAGE: 50 VDC
TEST SAMPLE: 30 PCS

	125°C LIFE TEST				125° SHELF TEST	
	0 Hours	1000 Hours	2000 Hours	ΔChange	0 Hours	250 Hours
CAPACITANCE (µF):	9.74	9.81	9.73	0.02%	9.76	9.73
DF/120 Hz (%):	2.77	2.38	3.22	+0.45	2.80	1.86
DCL/2 MIN (µA):	0.61	0.07	0.06	–	0.57	2.86
	105°C LIFE TEST				**105°C SHELF TEST**	
	0 Hours	1000 Hours	2000 Hours	ΔChange	0 Hours	250 Hours
CAPACITANCE (µF):	9.76	9.91	9.89	+1.3%	9.77	9.81
DF/120 Hz (%):	2.73	1.94	2.07	−0.66	2.76	2.40
DCL/2 MIN (µA):	0.68	0.06	0.055	–	0.61	2.53

Table 4

Table 5 presents data for a 47µF, 6.3VDC rating of an earlier capacitor design. The capacitance changes of -12.9% and -8.5% after 1,000 hours of test are deemed excessive. It can be noted, however, that similar capacitance changes are incurred in the shorter term 105° C and 125° C storage tests. This is an indication, confirmed with extended testing, that an initial sharp decrease in capacitance takes place during initial exposure to high temperatures and is followed by a normal and low rate of change thereafter.

47 μF — 6.3 VDC
6 × 11 MM
SINGLE-ENDED

CAP. TOL. ±20%
DF (120 Hz) 0.15
DCL 1.0 μA

TEST VOLTAGE: 6.3 VDC
TEST SAMPLE: 12 PCS

	125°C LIFE TEST			125°C SHELF TEST	
	0 HOURS	1000 HOURS	Δ CHANGE	0 HOURS	250 HOURS
CAPACITANCE (μF):	51.4	44.8	−12.9%	51.5	46.3 (−9%)
DF/120 Hz (%):	11.1	12.6	+ 1.5	11.3	11.1
DCL/2 MIN (μA):	0.31	0.07	—	0.39	0.94
ESR/100 KHz (Ω):	1.27	1.90	+35%	1.25	1.42
	105°C LIFE TEST			105°C SHELF TEST	
	0 HOURS	1000 HOURS	Δ CHANGE	0 HOURS	250 HOURS
CAPACITANCE (μF):	51.5	47.1	−8.5%	51.4	46.8 (−9.1%)
DF/120 Hz (%):	11.5	11.9	+0.4	11.4	11.4
DCL/2 MIN (μA):	0.29	0.08	—	0.21	0.68
ESR/100 KHz (Ω):	1.31	1.67	+21.5%	1.28	1.41

Table 5

Table 6 presents data for an improved capacitor design with the notably larger 100μF, 6.3VDC rating in the same 6 X 11 mm case. A decrease in capacitance change has been attained, but it is again noted that similar capacitance changes occurred on the shorter-term 105° C and 125° C storage tests. Extended testing has again confirmed that the change in capacitance is an early initial one followed by a normal and low change rate thereafter.

100 μF — 6.3 VDC
6 × 11 MM
SINGLE-ENDED

CAP. TOL. ±20%
DF (120 Hz) 0.15
DCL 1.0 μA

TEST VOLTAGE: 6.3 VDC
TEST SAMPLE: 12 PCS

	125°C LIFE TEST			125°C SHELF TEST	
	0 HOURS	1000 HOURS	Δ CHANGE	0 HOURS	250 HOURS
CAPACITANCE (μF):	116	10.7	−7.8%	116	108 (−7%)
DF/120 Hz (%):	10.2	10.3	+ 0.1	10.7	10.5
DCL/2 MIN (μA):	0.81	0.10	—	0.91	2.11
ESR/100 KHz (Ω):	0.57	0.68	+16%	0.55	0.71
	105°C LIFE TEST			105°C SHELF TEST	
	0 HOURS	1000 HOURS	Δ CHANGE	0 HOURS	250 HOURS
CAPACITANCE (μF):	116	109	−6.0%	115	107 (−7%)
DF/120 Hz (%):	10.7	9.6	−1.1	10.3	8.8
DCL/2 MIN (μA):	0.85	0.14	—	0.97	1.57
ESR/100 KHz (Ω):	0.56	0.63	+11%	0.54	0.61

Table 6

Table 7 presents data recorded for a 100μF, 10VDC rating wherein excellent capacitance and DF stability have been achieved in an 8 x 12 mm case. This performance reflects the change to the modified electrolyte and the advantages afforded by the larger plate area in the 8 X 12 mm case.

100 μF — 10 VDC
8 × 12 MM
SINGLE-ENDED

CAP. TOL. ±20%
DF (120 Hz) 0.14
DCL 2.0 μA

TEST VOLTAGE: 10 VDC
TEST SAMPLE: 12 PCS

	125°C LIFE TEST			125°C SHELF TEST	
	0 HOURS	1000 HOURS	Δ CHANGE	0 HOURS	250 HOURS
CAPACITANCE (μF):	113	114	+0.9 %	113	113
DF/120 Hz (%):	8.12	9.60	+1.48	8.10	8.01
DCL/2 MIN (μA):	0.98	0.24	—	1.04	2.97
	105°C LIFE TEST			105°C SHELF TEST	
	0 HOURS	1000 HOURS	Δ CHANGE	0 HOURS	250 HOURS
CAPACITANCE (μF):	112	114	+1.8 %	113	112
DF/120 Hz (%):	8.10	8.11	+0.01	8.0	6.64
DCL/2 MIN (μA):	1.08	0.25	—	0.94	2.41

Table 7

Table 8 presents 2,000-hour life test data recorded for a 47μF, 35VDC rating in a 10 X 13 mm case. Its parametric performance over this time frame is excellent.

47 μF — 35 VDC
10 × 13 MM
SINGLE-ENDED

CAP. TOL. ±20%
DF (120 Hz) 0.10
DCL 3.0 μA

TEST VOLTAGE: 35 VDC
TEST SAMPLE: 12 PCS

	125°C LIFE TEST			125°C SHELF TEST	
	0 HOURS	2000 HOURS	Δ CHANGE	0 HOURS	250 HOURS
CAPACITANCE (μF):	50.4	51.2	+1.6 %		
DF/120 Hz (%):	3.85	4.7	+0.85		
DCL/2 MIN (μA):	1.12	0.31	—		
	105°C LIFE TEST			105°C SHELF TEST	
	0 HOURS	2000 HOURS	Δ CHANGE	0 HOURS	250 HOURS
CAPACITANCE (μF):	49.9	49.5	−0.8 %	49.7	49.0
DF/120 Hz (%):	3.89	4.31	+0.42	3.97	3.70
DCL/2 MIN (μA):	1.15	0.27	—	1.05	2.54

Table 8

Table 9 presents data for an axial-lead type of 250μF, 16VDC in a 10 X 25 mm case. Life test data recorded after 2,000 hours at 85 C and 105°C is compared with 1,000-hour, 125°C data. The capacitance, ESR, and DCL performances are essentially identical at each test condition.

250 μF – 16 VDC
10 × 25 MM
AXIAL LEAD

TEST VOLTAGE: 16 VDC
TEST SAMPLE: 50 PCS

85°C LIFE TEST

	0 Hours			2000 Hours		
	Cap (μF)	ESR (Ω)	DCL/1 Min (μA)	Cap (μF)	ESR (Ω)	DCL/1 Min (μA)
Avg.	282	1.1	6	277	0.73	2
Min.	267	1.0	3	260	0.62	0.7
Max.	324	1.3	12	323	0.80	3

105°C LIFE TEST

	0 Hours			2000 Hours		
	Cap (μF)	ESR (Ω)	DCL/1 Min (μA)	Cap (μF)	ESR (Ω)	DCL/1 Min (μA)
Avg.	283	1.0	6	268	0.64	2
Min.	234	0.9	2	221	0.55	1
Max.	299	1.1	11	283	0.73	3

125°C LIFE TEST

	0 Hours			1000 Hours		
	Cap (μF)	ESR (Ω)	DCL/1 Min (μA)	Cap (μF)	ESR (Ω)	DCL/1 Min (μA)
Avg.	286	1.0	7	266	0.58	2
Min.	253	0.84	4	244	0.47	1
Max.	319	1.1	12	299	0.76	4

Table 9

Figure 3 identifies typical impedance versus frequency characteristics through 100MHz for the 6 and 10 mm case sizes with capacitance ratings of 33μF, 10VDC and 3.3μF, 35VDC, and of 47μF, 35VDC.

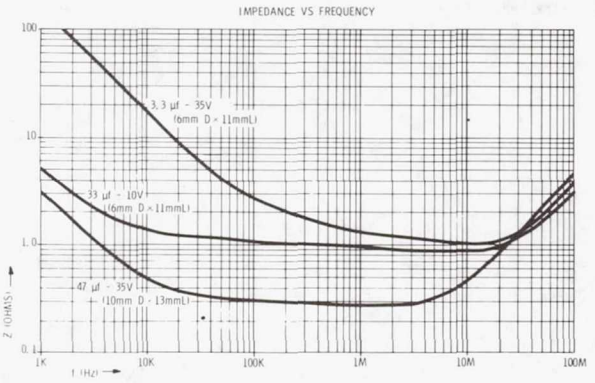

Figure 3

Table 10 identifies typical capacitor performance at temperatures of -30°C, -40°C, and -55°C for two capacitor ratings in the 6 X 11 mm case size. The changes in capacitance and impedance at each temperature are shown in reference to their 25°C value.

CAPACITANCE vs. TEMPERATURE

Temp.	1μF – 35V	10μF – 25V
25°C	–	–
–30°C	– 7%	–11%
–40°C	–10%	–16%
–55°C	–17%	–27%

IMPEDANCE (120 Hz) vs. TEMPERATURE

	1 μF – 35V		10 μF – 35V	
	Z (Ω)	Ratio	Z (Ω)	Ratio
Z (25°C)	1452	–	130	–
Z (–40°C)	1623	1.17	183	1.41
Z (–55°C)	1964	1.35	640	4.93

Table 10

Table 11 identifies the typical weight loss characteristics for Sprague Electric 6 X 11 mm case size Type 510D extended-temperature capacitor. The weight loss rate is expressed in milligrams/1,000 hours at a specific temperature. A multiplier value can be calculated that is based on the difference or the ratio of weight loss between any two given temperatures. In turn, the multiplier can be used to project or calculate hours of life at a given lower temperature condition

Historical Sprague test data for aluminum electrolytic capacitors have established that a capacitors can incur a 10% loss of its contained electrolyte weight and retain parametric characteristics that meet rigorous specified performance standards.

Table 12 identifies the weight loss characteristics for the 8 X 12 mm and 10 X 13 mm case sizes and their contained weight of electrolyte. The multiplier values listed are identical to those calculated for the 6 X 11 mm case size.

SPRAGUE 510D EXTENDED TEMPERATURE CAPACITOR
ELECTROLYTE WEIGHT LOSS IN MILLIGRAMS/1000 HOURS

Temperature	Mg/1000 Hrs 6 X 11 MM	(Referenced to 125°C) Multiplier	Calculated Life (Hours)
125°C	12.0	X 1	1000
105°C	6.0	X 2	2000
85°C	1.5	X 8	8000
55°C	0.50	X 24	24000
25/30°C	0.25	X 48	48000

Case Size	Typical Electrolyte Weight
6 X 11 MM	90 – 100 mg

EXAMPLE: 95 mg X 0.40 = 38 mg
38 mg ÷ 12 = 3.16 K Hours @ 125°C*

rojected capaci.or life for parametric characteristics that meet rigorous specified performance ndards.

Table 11

SPRAGUE 510D EXTENDED TEMPERATURE CAPACITOR
ELECTROLYTE WEIGHT LOSS IN MILLIGRAMS/1000 HOURS

Temperature	Mg/1000 Hrs 8 X 12 MM	(Referenced to 125°C) Multiplier	Mg/1000 Hrs 10 X 13 MM	(Referenced to 125°C) Multiplier
125°C	20.0	X 1	32.0	X 1
105°C	10.0	X 2	16.0	X 2
85°C	2.50	X 8	4.0	X 8
55°C	0.83	X 24	1.33	X 24
25/30°C	0.30	X 66	0.35	X 90

Case Size	Typical Electrolyte Weight
8 X 12 MM	190 – 210 mg
10 X 13 MM	280 – 320 mg

EXAMPLES: 200 mg X 0.40 = 80 mg ÷ 20 = 4.0 K Hours @ 125°C
300 mg X 0.40 = 120 mg ÷ 32 = 3.75 K Hours @ 125°C

Table 12

CONCLUSION

1. A low-cost miniature aluminum capacitor with improved reliability and proven life can be produced with present-day technology.

2. The capacitor can be specified for 125°C life and shelf test requirements and will meet established standards for their parametric performance.

3. The test data recorded thus far for these capacitors indicates that their operational life can be projected validly by extrapolation of performance and characteristic data recorded at accelerated 125°C test conditions.

SUPER MINIATURIZATION OF FILM CAPACITOR DIELECTRICS

Bernard Lavene
Electronic Concepts
Eatontown, NJ
(312) 668-8747

ABSTRACT

Results of recent production technology have led to the alignment of the stable electrical characteristics of film capacitors in the physical dimensions of ceramic and tantalum capacitors. Polycarbonate and mylar capacitors are established reliability military specifications. Graphic presentations will be shown of electrical and physical comparisons of film, ceramic and tantalum capacitors. Volumetric efficiency, weight reduction, and electrical stability are the keynotes and will be presented.

INTRODUCTION

During the past 10 years, significant advances have been made in dielectric film technology by such companies as Dupont and Mobay Chemical Corporation. These advances, in conjunction with improved converting techniques, have resulted in the availability of ultra thin capacitor films. These films are characterized by sufficient quality to enable capacitor manufacturers to produce units capable of challenging, and even exceeding, the volumetric efficiency of ceramic and tantalum capacitors.

This paper expounds upon the progress made to date by both metallizers and film capacitor manufacturers. We will discuss the most recent state-of-the-art technology and potential pitfalls in pursuing further advancements.

Film Capacitor Dielectrics

With the advent of thin capacitor film technology, films became available as thin as 1.5 to 2 microns. In conjunction with this, there arose a need for these films with a metallized coating. This was necessary since it was not practical to utilize them with conventional foil electrodes in view of their vulnerability to pinholes. Recently, metallizing companies have made significant strides in developing the capability to convert thin film without any deterioration in the basic superior electrical and physical properties. This was achieved by developing extremely low temperature chilled rollers together with mechanical masking of the safe edge. In this way, the capacitor manufacturer was provided with material which could be utilized in the manufacture of units with standard manufacturing procedures that did not reduce the integrity of the film.

In reviewing Table I, we see a comparison between base film - as directly supplied from extruders - and the specification we place on the average metallized polycarbonate capacitor. The table tells us that during the years in which metallized polycarbonate capacitors have been available, we have accepted electrical characteristics that were in the area of only 30% as good as the base film could deliver.

This situation exists among all of the metallized film capacitors regardless of dielectric type. An examination of Table II indicates a typical example of this where metallized polypropylene has approximately twice the losses of conventional polypropylene and foil.

This condition of deterioration in comparative specifications results from an aggregate of causes in the manufacturing processes such as the carbonization of the film from clearing around pinholes, the metal end spray penetrating too deeply into the safe edge, requiring additional clearing, and the overall quality of the physical winding with respect to wrinkles and other factors.

A further examination of Table I indicates that with special handling and carefully controlled manufacturing procedures, the performance characteristics of metallized film capacitors can be optimized. There is evidence that as the electrical properties of film capacitors approach the bare film properties, there is the probability of eliminating such negative characteristics as unscheduled clearing, and reduced insulation resistance in low voltage applications. These have plagued the electronic industry since the introduction of metallized film. However, the present level of electrical characteristics for parameters such as Insulation Resistance, Dissipation Factor and Dielectric Absorption has been found to be acceptable. There is a great deal of historical information and data accumulated, and these units are presently utilized on established reliability specifications such as MIL-C-55514. The low failure rate levels have supported this confidence.

Performance Comparison of Capacitor Technologies

Regardless, with this information one must be alerted to the dangers of any attempt

to further reduce the well established electrical criteria in order to achieve miniaturization.

Nonetheless, at the present acceptable levels of electrical parameters for metallized film capacitors, a comparison with the electrical performance of ceramic or tantalum devices clearly indicates the advantages of film types in most critical areas where loss factors are a concern. Table III compares key electrical performance characteristics of metallized polycarbonate capacitors to those of monolithic ceramic and a solid tantalum with dry electrolyte. However, until recently, the need for circuit miniaturization and reduced weight has compelled the design engineer to "trade-off" these superior electrical properties of film capacitors for something which would provide more space and weight efficiency.

Recently, a production technology has been developed which has resulted in the CFR12 style on MIL-C-55514. This new device is characterized by improved volumetric efficiency (see Tables IV and V) without compromising adversely any of the proven and established electrical performance standards for film capacitors. At the present time, CFR12 type capacitors do not go above the range of 0.1 mfd. However, as evidenced by Table IV, we can anticipate very shortly that when these new types of capacitors go beyond this present range we will witness volumetric efficiency greater than that of ceramic types, without trading off any of the excellent electrical properties of film dielectrics as we know them today. This style of capacitor will allow the use of metallized polycarbonate capacitors in many application areas heretofore excluded from possibility because of size and weight restrictions.

The techniques which have resulted in the creation of CFR12 can clearly be expanded to additional dielectrics such as polypropylene and polysulfone, thus optimizing such performance parameters as Temperature Coefficient (OTC-NPO) and frequency response characteristics. Additionally, subsequent research and development will clearly lead to higher capacitance values with equally efficient volumetric and weight efficiency for use in other areas of circuit design.

SUMMARY

In summation, we know that of all the various classes of capacitors available, the film types can deliver the best overall performance regarding low loss properties and temperature capability. With the advent of thinner films available plus improved know-how of capacitor manufacturing techniques, we are at the threshold of witnessing extremely small sized, light weight capacitors with excellent volumetric efficiencies comparable to ceramic and tantalum without reducing the present electrical standards for film capacitors.

The first of these types is offered as CFR12 in specification MIL-C-55514.

In the near future, we can look forward to these types being expanded upon by utilizing various combinations of film dielectrics that will yield even better performance for size and weight in addition to superior low loss characteristics along with high temperature stability.

TABLE I

	DISSIPATION FACTOR	INSULATION RESISTANCE
1. POLYCARBONATE BASE FILM PROPERTIES	.0008-.0012	10^{17} OHM-CM
2. AVERAGE SPECIFICATIONS FROM CAPACITOR MANUFACTURERS	.0030 MAX	$2.5,-5.0 \times 10^{4}$ MEGOHMS X MICROFARADS
3. OPTIMUM ATTAINABLE SPECIFICATIONS	.0010 MAX	$1.0,-5.0 \times 10^{11}$ MEGOHMS X MICROFARADS

1. MAKROFOL - MOBAY CHEMICAL CORP.

2. TYPICAL NON-HERMETICALLY SEALED CAPACITORS

TABLE II

FILM CAPACITOR COMPARISON CHART

DIELECTRIC	D.F. MAX	I.R. MEG X MFD	T.C. PPM/°C	D.A. %	STABILITY %/YR
METALLIZED POLYCARBONATE	0.30	$\geq 5 \times 10^{10}$	$\pm$ 100	.30	.25
METALLIZED POLYSULPONE	0.30	$\geq 5 \times 10^{10}$	$\pm$ 50	.25	.20
METALLIZED POLYESTER	1.00	$\geq 3 \times 10^{10}$	N/A	.50	.50
METALLIZED POPYPROPYLENE	0.10	$\geq 5 \times 10^{10}$	-200	.10	.20
POPYPROPYLENE AND FOIL	0.05	$\geq 1 \times 10^{12}$	-100	.03	.10
POLYSTYRENE AND FOIL	0.05	$\geq 1 \times 10^{12}$	-100	.01	.05

TABLE III

ELECTRICAL PROPERTIES

FILM CAPACITORS VS CERAMIC AND TANTALUM

	METALLIZED POLYCARBONATE	MONOLITHIC CERAMIC	TANTANLUM
DISSIPATION FACTOR	.003	.025	.04
INSULATION RESISTANCE OHMS X MICROFARAD	5×10^{10}	1×10^{9}	1×10^{7}
DIELECTRIC ABSORPTION %	0.1	N/A	N/A
EQUIVALENT SERIES RESISTANCE OHMS (1.0 MFD @ 1 KHZ AND 25°C)	0.5	4	6
LONG TERM STABILITY % / YEAR	0.25	± 10	± 20
PIEZOELECTRIC	NO	YES	
TEMPERATURE COEFFICIENT PPM/°C	± 100	VARIOUS	1500

TABLE IV

VOLUMETRIC EFFICIENCY COMPARISEN OF FILM CAPACITORS

VS CERAMIC AND TANTALUM

VALUES= MFD/IN^3

CAPACITANCE RANGE	CERAMIC	TANTALUM	FILM	NEW FILM
1 PF TO .10 MFD	(CKR05) 65	(CSR13) 24	(CFR05) 14	(CFR12) 65
.10 MFD TO .39 MFD	20	(CSR13) 95	(CFR05) 26	52
.39 MFD TO .50 MFD	21	(CSR13) 122	(CFR05) 25	53
.50 MFD TO 1.0 MFD	42	(CSR13) 244	(CFR05) 31	53

TABLE V

SCALE COMPARISON OF FILM CAPACITORS VS CERAMIC AND TANTALUM

CAPACITANCE RANGE	*CERAMIC*	*TANTALUM*	*NEW FILM*
1 PF TO .10 MFD	.095 x .195 x .195 	.135 x .286 	.095 x .195 x .195 
.10 MFD TO .39 MFD	.160 x .500 x .250 	.135 x .286 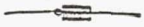	.095 x .295 x .295 
.39 MFD TO .50 MFD	.160 x .500 x .250 	.135 x .286 	.095 x .395 x .395 
.50 MFD TO 1.0 MFD	.160 x .500 x .300 	.135 x .286 	.190 x .395 x .395 

EFFECTS OF SEVERE STRESSING ON TANTALUM-CASED TANTALUM CAPACITORS

J.F. Shakar and E.H. Fairfield

Sprague Electric Company

North Adams, Mass.

SUMMARY

In an attempt to determine the ultimate capabilities of the Sprague Type 135D all tantalum capacitor, severe testing in excess of the requirements of Military Specification MIL-C-39006/ 22B has been conducted. Testing has included 175° C Life, 1000-cycle Thermal Shock, 70g Random Vibration, 3000g shock and 90°C Case-Rise Ripple Current. It is the purpose of this paper to set forth the latest available performance characteristics of the Type 135D capacitor.

EFFECTS OF SEVERE STRESSING ON TANTALUM-CASED TANTALUM CAPACITORS

Wet-slug tantalum capacitors have many characteristics which have made them desirable for military and aerospace applications, where superior performance and reliability are required. They have a very high CV product per unit volume and are substantially smaller than comparably rated capacitor types. The tantalum oxide dielectric results in low d-c leakage currents and provides stable electrical characteristics over a wide temperature range. Hermetic seals have replaced the earlier non-hermetic designs, virtually eliminating the possibility of electrolyte leakage. The primary disadvantage of the conventional silver-cased design is its inability to tolerate reverse voltages of any magnitude.

Sprague Electric Company undertook, with partial funding from the National Aeronautics and Space Administration, to develop a new type of wet-slug tantalum capacitor capable of withstanding reverse voltage. The result of this developmental program is Type 135D design.

An anodized sintered tantalum powder liner and a tantalum case combine to provide the Type 135D capacitor with reverse voltage capability.

The tantalum anode and tantalum pentoxide dielectric system of the silver-cased designs were incorporated into the Type 135D because of their excellent performance characteristics. The anode is rigidly supported between two polytetrafluoroethylene vibration spacers. The top vibration spacer is immobolized by a beaded seal, so that the capacitor will withstand high levels of shock and vibration.

The capacitor is hermetically sealed by laser welding a hermetic tantalum/ glass seal to the case. This all-welded construction makes the capacitor impervious to attack by the sulfuric acid-based electrolyte.

Tinned nickel leads are welded to the bottom of the capacitor body and to the anode tubulation to complete the construction.

The Type 135D capacitor has not only eliminated the disadvantage associated with the silver-case designs, but has improved upon many of the performance characteristics.

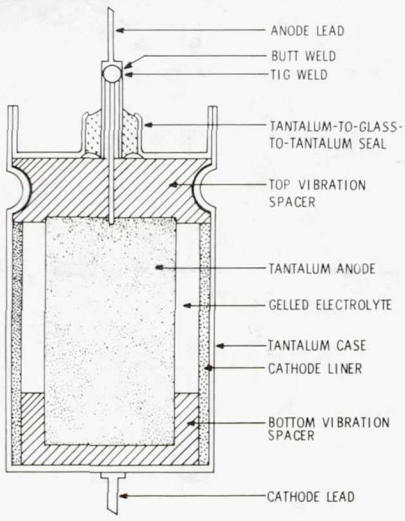

Figure 1. Cross-section of Type 135D Capacitor.

175°C Life Test

Military Specification MIL-C-39006/22B requires capacitors to meet specified criteria after 85°C and 125°C life tests. Over 29 million unit-hours of life tests on Type 135D capacitors have an "R" (0.01% failure/1000 hr.) level qualification. As an extension of this testing, ratings were selected from each of the four case sizes for a much more rigorous life test at 175°C temperature and a test voltage of 50% of the 85°C rated voltage. Test procedures conformed to Method 108 of MIL-STD-202. Electrical parameters were measured at 500-hour intervals for the 2000-hour test duration.

There are no criteria for 175°C life tests in MIL-C-39006/22B, but it is reasonable to expect greater shifts in electrical parameters than is experienced with 85°C and 125°C life tests. The capacitors performed exceptionally well and experienced no catastrophic failures. The average capacitance, dissipation factor and d-c leakage for each rating, at the initial 1000-hour and 2000-hour measurements are summarized in Table I.

The capacitance values were stable, with most capacitors changing less than ±10% from their initial measurements. The very low voltage (6 volt and 10 volt) ratings tended to decrease in capacitance while the 15 volt ratings and above showed a slight capacitance gain. Capacitance Ratio vs. Time is shown for typical low and high voltage ratings in Figure 2.

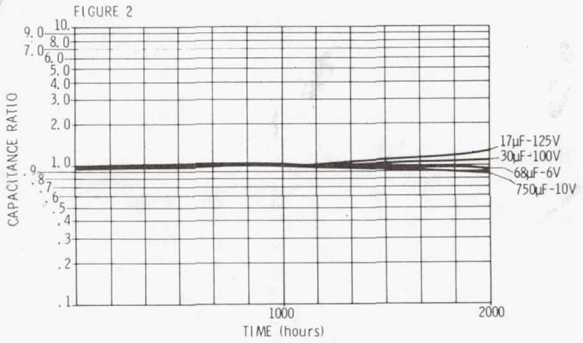

Figure 2. Capacitance Ratio vs. Time

Most capacitors showed no significant change from their initial d-c leakage measurement during the first 1000 hours of testing. At 2000 hours, leakage currents increased with greater changes observed in the lower voltage ratings. Leakage currents were still quite acceptable as shown by the average values in Table 1. Typical D-C Leakage Current Change is illustrated for each of the four case sizes in Figure 3.

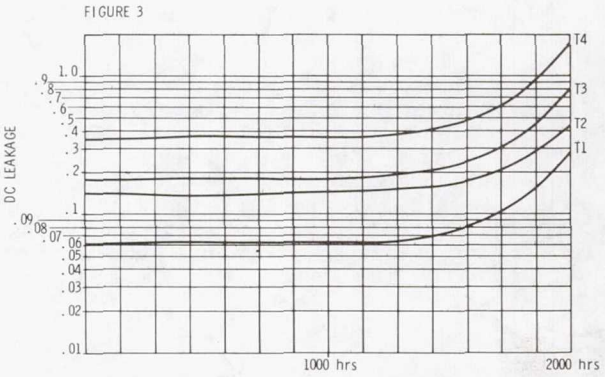

Figure 3. Typical D-C Leakage Current vs. Time

Increases in dissipation factor were observed throughout this test, with the higher voltage rating exhibiting a more rapid rate of change. This is illustrated by Figure 4. Despite these increases, the average dissipation factor for each rating still met the initial requirement of MIL-C-39006/22B after 1000 hours of testing. By 2000 hours, the average dissipation factor increased to a maximum of 200% of the initial limit, comparable in performance to the 10,000 hour, 125°C life test.

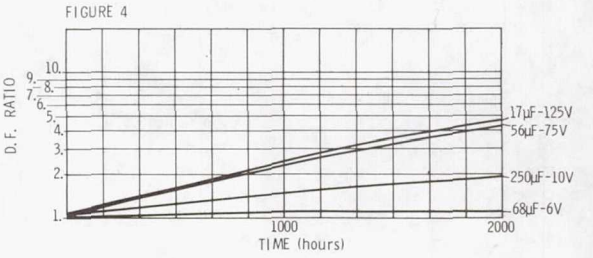

Figure 4. D.F. Ratio vs. Time

3000g Shock

Capacitors conforming to MIL-C-39006 /22B must pass a 100g shock test in accordance with Method 213 of MIL-STD-202, Condition 1. The Sprague Type 135D (CLR79) engineering bulletin NO. 3760A requires capacitors to withstand a 200g shock when tested as above, with capacitance, equivalent series resistance, and d-c leakage current still meeting the initial requirements. To more severely test the capacitors, twelve ratings were selected from the four case sizes for a 3000g shock test.

Following measurement of electrical parameters, each capacitor was mounted by its body on a mounting fixture within 30 of being parallel. The terminals were secured to stud posts, so as not to extend more than 0.375 inches from the capacitor body. The capacitors were continually monitored for intermittent shorts and opens by applying the 85° C rated voltage and making observations with an oscilloscope. Three half-sine shock pulses of 0.5 ms duration and 3000g peak value were applied in each direction along the three mutually perpendicular axes of the test specimen.

Capacitors were measured after test (see Table 2) and visually examined for evidence of mechanical damage, electrolyte leakage, or any other indication of breakdown. Results were excellent. All capacitors met the same mechanical and electrical requirements of the more benign shock test specified in MIL-C-39006/22B.

Thermal Shock (1000 Cycles)

Sixty capacitors representing six ratings were subjected to 1000 thermal cycles as described in Method 107 of MIL-STD-202. Each capacitor was conditioned for fifteen minutes at room ambient prior to measuring electrical parameters. The capacitors were placed in an inverted position and cycled from -55° C to +125° C for 1000 cycles. Minimum duration at each temperature extreme was one half hour with a five minute maximum transfer time.

MIL-C-39006/22B requires capacitors to meet the following criteria after 300 temperature cycles:

DCL-200%(max) of 25° C initial limit
ΔCap - within +5% of initial measurement
DF-115% (max) of initial measurement

The Type 135D capacitors performed exceptionally well, meeting all the above requirements after 550 cycles. Even after subjecting the capacitors to 1000 cycles (more than three times the current MIL-C-39006/22B requirement), all but two capacitors met the limits as established from the less severe 300 temperature cycle test. D-C leakage current increases (exceeding 200% of the initial 25° C limit) were measured on the two capacitors. (Data on Table 3)

Random Vibration

A random vibration test requirement has recently been added to MIL-C-39006/22 for an optional high vibration capacitor. The test is in accordance with MIL-STD-202, Method 214, Condition II, Test Condition Letter K. The test is conducted in each of three mutually perpendicular planes, one of which is parallel to the axis of the capacitor. This condition can be integrated to an overall rms value of 51g, which is the present maximum random vibration level specified by MIL-STD-202.

Table 4 shows the tabulated results for three ratings of the Type 135D capacitor after they were subjected to this 51g random vibration test for 4 hours in each of the two planes. The effect of this physical stress is observed to be rather benign. The dissipation factor and the d-c leakage current are well within internal limits and the capacitance within 1% of initial values. No discernible parameter trends were observed.

In trying to examine the upper limit of Type 135D, units were subjected to higher g levels. The 51g test conditions were used, except the power spectral density was increased to give an overall rms level of 70g. The test duration was maintained at 4 hours in each of two planes. Table 5 presents the results of the four ratings run at this level.

The units performed well, with most capacitors meeting there initial capacitance and d-c leakage current limits. Of the 24 units tested, only one could be considered a failure. In this capacitor, the tantalum wire separated from the tantalum pellet.

Four units lost their lead wires, as noted in Table 5, due to inability to secure the lead dress during mounting and are not considered failures.

Ripple Current

Subjecting capacitors to ripple current stressing, especially with frequencies up to 100 kHz, is a relatively new requirement, which has become more prevalent in the last 10 years.

Permissible ripple currents for silver-cased wet-tantalum capacitors are known to be limited by the electrochemical nature of the devices, which can cause silver dislocation.

Design of the Type 135D capacitor had elimination of silver migration as one of its major objectives. In accomplishing this, the ripple current ratings are now limited by the internal heat stresses.

When the design was released, an examination of the heat rise vs. ripple current was conducted at several points in the frequency spectrum. Upon reviewing this data a temperature rise (ΔT) of 50°C was selected for the calculation of ripple current ratings.

Using the measured power necessary to cause the 50°C heat rise and the maximum permissible ESR of the device, ripple current ratings were generated from the following equation:

$$I_{rated} = \sqrt{\frac{P_{50^\circ}}{R_{ESR}}}$$

where:

I_{rated} = ripple current in amps

P_{50° = power in watts required to cause a 50° case rise

R_{ESR} = maximum equivalent series resistance of the device at the ripple current frequency

Also, knowing the relationship of ESR with frequency, current ratings were generated for different frequencies.

Ripple life tests were performed to verify these limits. This data was used to establish the ripple current levels of MIL-C-39006/22B.

To examine higher stress levels due to ripple current, a test was conducted in which the ripple current was increased to give a ripple current temperature rise (ΔT) of 90° C. The frequency of the ripple current was 40 kHz. The units were placed in an ambient temperature of 85°C at the start of the test. The initial test was performed on two ratings for 500 hours. Another rating was tested for 2000 hours. Table 6 shows these data.

The 175° C case temperature was monitored by thermocouples welded to the case walls. The six capacitors were connected in a series-parallel bank as shown in Figure 5. The applied direct voltage was 25 VDC resulting in a peak voltage slightly less than the 50% derating factor typically used for 175°C wet-tantalum capacitor operation.

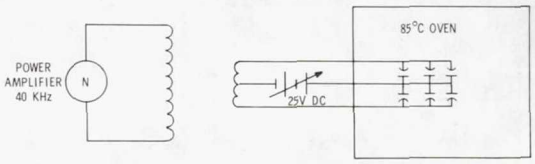

Figure 5.

The resulting data show some parameter shift. (See Table 6) Capacitance stayed within a few percent of the initial reading. The ESR stayed well within the initial limits with a slight increasing trend. The d-c leakage current fluctuated but generally stayed around initial requirements with no catastrophic failures.

TABLE 1 175°C Life Test Data

	INITIAL			1000 hrs			2000 hrs			
Rating	Cap	%DF	DCL	Cap	%DF	DCL	Cap	%DF	DCL	%ΔCap
68uF-6V	69.19	5.60	0.05	69.00	5.56	<.01	67.06	5.98	0.47	-3.08
250uF-10V	255.7	10.88	0.11	258.1	15.62	.01	252.8	21.34	1.78	-1.13
750uF-10V	786.5	19.66	0.40	743.2	24.23	.03	709.6	22.19	2.99	-9.78
15uF-15V	15.06	1 35	0.05	15.17	1.90	0.01	15.15	2.34	.20	+0.60
15uF-75V	15.34	1.19	0.07	15.66	3.20	0.07	16.26	8.31	.07	+5.00
56uF-75V	57.83	3.17	0.27	58.06	5.93	0.18	59.90	13.81	.08	+3.58
30uF-100V	31.46	2.10	0.16	31.84	4.34	0.33	31.68	12.36	0.36	+0.70
1.7uF-125V	1.72	0.40	0.09	1.75	0.69	0.12	1.78	1.37	0.21	+3.49
17uF-125V	16.82	1.36	0.14	16.98	3.16	0.22	17.32	6.22	0.85	+2.97
56-125	57.72	2.16	0.32	58.26	5.52	0.29	59.61	11.43	0.73	+3.27

TABLE 2 3000g Shock Test Data

	INITIAL			POST SHOCK			
Rating	Cap	%DF	DCL	Cap	%DF	DCL	%ΔCap
30uF-6V	30.1	3.4	.08	30.1	3.7	.04	0.00
140uF-6V	135	8.2	.38	135	9.4	.16	0.00
330uF-6V	337	13.1	.39	337	13.8	.28	0.00
1200uF-6V	1252	51.8	2.6	1256	61.2	1.8	+0.32
47uF-10V	47.1	3.9	.06	47.2	3.9	.06	+0.21
120uF-15V	118	7.1	.10	118	8.5	.13	0.00
56uF-75V	57.8	3.9	.28	57.6	4.7	.28	-0.35
86uF-100V	88.8	2.9	.62	88.7	3.2	.68	-0.11
3.6uF-125V	3.46	0.8	.05	3.46	0.8	.05	0.00
9uF-125V	8.87	1.0	.06	8.87	1.1	.03	0.00
18uF-125V	17.9	1.8	.23	17.9	2.0	.18	0.00
56-125	61.5	2.2	.83	61.5	2.7	.61	0.00

TABLE 3 THERMAL SHOCK

86μF - 100 Volt, T4

	INITIAL			550 CYCLES			1000 CYCLES		
NO.	CAP	%DF	DCL	CAP	%DF	DCL	CAP	%DF	DCL
87	90.2	2.7	<1	89.6	4.0	<1	89.6	4.2	<1
88	90.4	3.4	<1	90.0	4.0	<1	90.2	3.7	<1
89	91.1	2.8	<1	90.6	3.4	<1	90.7	3.8	1
90	91.3	2.9	<1	90.8	3.7	<1	90.9	3.4	<1
91	90.3	2.9	<1	89.8	3.7	<1	89.9	3.4	<1
92	92.5	3.4	<1	91.9	4.8	<1	92.4	3.9	<1
93	90.3	2.8	<1	89.9	3.5	<1	90.0	3.7	<1
94	93.1	2.8	<1	92.3	4.2	<1	92.6	3.7	<1
95	89.3	3.9	<1	89.0	4.5	<1	88.9	5.1	2.2
96	92.6	2.7	<1	92.0	3.9	<1	92.1	3.6	<1

Data compliments of National Aeronautics and Space Administration

TABLE 3 Thermal Shock - Con't

NO.	INITIAL CAP	INITIAL %DF	INITIAL DCL	550 CYCLES CAP	550 CYCLES %DF	550 CYCLES DCL	1000 CYCLES CAP	1000 CYCLES %DF	1000 CYCLES DCL
40µF - 30 Volt, T2									
103	40.4	2.5	<1	40.4	2.6	<1	40.5	2.6	<1
104	40.1	2.4	<1	40.0	2.4	<1	40.1	2.6	<1
105	39.4	2.9	<1	39.4	3.1	<1	39.5	3.2	<1
106	41.8	2.4	<1	41.7	2.6	<1	41.8	2.6	<1
107	40.6	2.5	<1	40.5	2.7	<1	40.6	2.6	<1
108	41.4	2.8	<1	41.3	3.0	<1	41.5	3.0	<1
109	39.8	2.5	<1	39.8	2.5	<1	39.9	2.7	<1
110	43.9	2.8	<1	43.8	3.0	<1	43.9	3.1	<1
111	40.1	2.3	<1	40.1	2.5	<1	40.2	2.5	<1
112	39.8	2.3		39.7	2.5	<1	39.8	2.7	1.8
33µF - 75 Volt, T2									
67	34.2	2.1	<1	34.2	2.1	<1	34.2	2.1	<1
68	33.7	2.1	<1	33.7	2.2	<1	33.7	2.2	<1
69	34.0	2.3	<1	33.9	2.3	<1	34.0	2.4	<1
70	34.3	2.3	<1	34.2	2.3	<1	34.3	2.4	<1
71	35.4	2.2	<1	35.4	2.7	<1	35.5	2.3	<1
72	33.8	2.2	<1	33.7	2.2	<1	33.8	2.2	<1
73	34.6	2.2	<1	34.5	2.2	<1	34.6	2.3	<1
74	36.3	2.2	1.4	36.2	2.3	<1	36.3	2.3	4.2
75	33.8	2.1	<1	33.7	2.1	<1	33.8	2.3	<1
76	33.8	2.0	<1	33.7	2.0	<1	33.8	2.0	<1
3.6µF - 125 Volt, T1									
77	3.7	0.7	<1	3.7	0.7	<1	3.7	0.7	<1
78	3.9	0.7	<1	3.9	0.7	<1	3.9	0.8	<1
79	3.8	0.7	<1	3.8	0.7	<1	3.8	0.7	<1
80	3.7	0.7	<1	3.7	0.7	<1	3.7	0.8	<1
81	3.7	0.7	<1	3.7	0.6	<1	3.7	0.7	13.7
82	3.7	0.7	<1	3.7	0.7	<1	3.7	0.7	<1
83	3.7	0.8	<1	3.7	0.8	<1	3.7	0.8	<1
84	3.7	0.7	<1	3.7	0.7	<1	3.7	0.7	<1
85	3.8	0.7	<1	3.8	0.7	<1	3.8	0.7	<1
86	3.7	0.7	<1	3.7	0.7	<1	3.7	0.7	<1
140µF - 60 Volt, T4									
125	132.1	3.8	<1	131.9	4.2	<1	132.4	4.4	<1
126	143.9	3.7	<1	143.8	3.7	<1	144.2	3.8	<1
127	140.0	3.9	<1	139.8	4.3	<1	140.2	4.5	1
128	136.3	3.8	<1	136.2	4.4	<1	136.4	4.9	<1
129	134.3	3.8	<1	134.0	5.1	<1	134.6	4.9	<1
130	135.7	4.3	<1	135.5	5.4	<1	135.8	6.1	<1
131	139.5	4.3	<1	139.4	4.6	<1	139.7	5.1	<1
132	137.2	4.5	<1	136.3	6.2	<1	136.7	7.6	<1
133	138.0	4.1	<1	137.8	4.9	<1	138.3	5.1	<1
134	138.3	3.9	<1	138.1	4.7	<1	138.5	5.1	<1
3.6µF - 125 Volt, T1									
135	882	21.7	<1	886	23.1	<1	894	23.2	<1
136	857	24.4	<1	862	24.8	<1	872	24.7	<1
137	870	27.0	<1	873	27.2	<1	882	27.8	<1
138	854	25.5	<1	854	26.1	<1	865	31.4	<1
139	863	26.9	<1	865	27.5	<1	876	27.2	<1
140	819	32.9	<1	825	33.5	<1	831	33.8	1.1
141	851	26.8	<1	819	25.9	<1	827	26.4	1.3
142	846	28.8	<1	851	29.4	<1	861	29.4	2.9
143	857	36.3	<1	861	37.9	<1	825	33.2	<1
144	821	49.1	<1	832	53.4	<1	847	49.4	1.6

Data compliments of National Aeronautics and Space Administration

TABLE 4 51G Random Vibration*

Capacitance in µF			Percent Dissipation Factor			D-C Leakage Current in µA		
Initial	Vibration		Initial	Vibration		Initial	Vibration	
Value	Radial	Axial	Value	Radial	Axial	Value	Radial	Axial
			1200 µF, 6 VOLTS D-C					
1395.6	1392.0	1391.1	46.74	52.36	50.7	0.97	1.55	0.96
1208.1	1215.5	1212.2	57.6	58.40	57.28	0.86	1.32	1.04
1270.7	1271.8	1270.2	68.2	68.89	68.20	0.85	1.00	1.02
1120.3	1130.0	1123.5	52.5	75.15	54.66	0.70	0.80	1.20
1308.6	1320.5	1313.0	57.1	60.64	59.15	0.94	1.0	1.07
955.2	959.7	956.5	51.6	51.47	51.01	0.85	0.80	1.01
1311.2	1317.7	1317.2	52.2	54.85	52.56	0.91	1.12	1.08
1388.1	1394.4	1391.7	45.4	48.50	52.13	1.06	1.38	1.04
1380.5	1387.5	1385.2	60.4	72.01	64.29	0.92	1.1	1.04
1329.5	1324.9	1325.4	59.4	73.24	71.84	1.03	1.16	1.18
			100 µF, 25 VOLTS D-C					
100.9	100.66	100.53	5.4	6.35	6.15	0.155	0.14	0.11
102.2	102.20	103.00	5.0	8.59	5.29	0.14	0.12	0.12
96.9	95.89	95.71	7.9	10.39	10.55	0.10	0.12	0.12
99.7	99.65	99.50	5.3	5.72	5.93	0.11	0.12	0.13
94.9	94.99	94.87	5.5	5.52	5.41	0.11	0.12	0.12
97.8	97.17	97.44	5.0	6.59	6.32	0.11	0.12	0.13
96.5	96.50	95.74	6.5	6.49	7.29	0.12	0.12	0.11
101.0	99.92	100.22	5.7	7.49	7.27	0.12	0.13	0.12
95.0	95.00	95.00	6.8	6.65	6.57	0.11	0.13	0.11
101.3	100.24	100.64	6.0	8.65	7.53	0.12	0.18	0.14
100.4	100.30	100.21	4.1	4.34	4.36	0.11	0.13	0.13
96.6	96.48	96.22	5.4	6.38	6.55	0.11	0.13	0.11
95.9	96.07	96.02	5.9	5.90	5.66	0.12	0.14	0.12
99.9	99.94	99.71	6.5	6.76	7.41	0.10	0.12	0.11
96.9	96.82	96.68	4.1	4.86	4.93	0.12	0.14	0.13
97.8	97.40	97.37	5.3	6.84	6.70	0.10	0.13	0.12
101.7	101.52	101.44	5.7	7.18	7.00	0.12	0.14	0.15
101.1	101.16	101.02	3.9	4.28	4.60	0.11	0.12	0.12
98.5	98.51	98.55	6.5	6.30	6.37	0.12	0.13	0.12
100.0	100.01	99.91	4.7	4.79	5.55	0.10	0.12	0.15
			22 µF, 100 VOLTS D-C					
21.32	21.37	21.22	1.93	2.04	1.75	0.15	0.75	0.45
21.93	21.87	21.84	1.57	1.61	1.50	0.14	0.26	0.20
21.38	21.38	21.33	1.99	1.20	1.50	0.13	0.35	0.34
21.77	21.74	21.69	2.0	1.40	1.47	0.14	0.22	0.16
21.60	21.49	21.47	1.89	1.34	1.23	0.12	0.22	0.16
20.71	20.63	20.65	1.81	1.49	1.44	0.13	0.22	0.16
21.78	21.66	21.63	3.49	1.54	1.61	0.12	0.22	0.16
24.49	24.44	24.41	1.98	1.79	1.93	0.22	0.25	0.19
22.45	22.36	22.39	1.79	1.27	1.32	0.14	0.24	0.18
21.19	21.26	21.14	1.78	1.61	1.43	0.12	0.35	0.24
23.68	23.63	23.68	1.39	1.45	1.42	0.22	0.26	0.19
23.04	22.98	22.98	1.23	1.34	1.43	0.18	0.26	0.20
24.38	24.31	24.28	2.03	1.60	1.55	0.23	0.30	0.22
22.99	22.91	22.87	1.82	1.47	1.57	0.20	0.27	0.20
22.72	22.62	22.64	1.81	1.46	1.50	0.14	0.22	0.15
22.79	22.72	22.74	1.69	1.27	1.55	0.13	0.22	0.15
23.85	23.90	23.76	2.49	2.33	2.07	0.12	0.36	0.30
22.42	22.34	22.39	1.53	1.70	1.57	0.64	0.53	0.46
21.22	21.09	21.05	1.98	1.55	1.65	0.11	0.21	0.14
23.18	23.14	23.11	1.2	1.55	1.60	0.18	0.25	0.18

* Data from tests conducted at Marshall Space Flight Center, NASA

TABLE 5 70G Random Vibration*

Capacitance in µF			Percent Dissipation Factor			D-C Leakage Current in µA		
Initial Value	Vibration Radial	Vibration Axial	Initial Value	Vibration Radial	Vibration Axial	Initial Value	Vibration Radial	Vibration Axial
			6.8 µF, 75 VOLT, T1 CASE					
6.10	6.12	6.12	0.94	1.07	1.68	0.11	0.46	0.38
6.36	6.35	6.32	0.73	1.12	1.06	0.08	0.32	0.30†
6.20	6.19	6.20	0.78	0.78	0.87	0.03	0.21	0.11
6.43	6.40	6.40	0.91	1.63	0.89	0.03	0.06	0.05
6.41	6.41	6.40	1.39	0.74	1.52	0.02	0.07	0.06†
6.59	6.60	6.59	0.92	1.07	0.75	0.08	0.19	0.14†
			25 µF, 50 VOLT, T2 CASE					
23.98	24.08	24.40	0.92	4.38	1.11	0.06	0.10	0.20
24.00	24.12	23.95	0.91	1.18	4.48	0.04	0.09	0.20†
24.53	24.63	25.05	1.57	4.42	1.84	0.05	0.06	0.04
23.81	25.95	23.94	0.87	1.01	4.38	0.06	0.07	0.06
25.40	25.57	25.44	2.46	0.57	4.02	0.05	0.07	0.05
23.52	23.17	23.03	1.09	0.46	2.19	0.10	0.12	0.10
			40 µF, 75 VOLT, T3 CASE					
40.44	40.20	39.92	2.05	1.89	1.96	0.12	0.35	0.27
40.83	40.11	40.62	2.53	3.04	4.18	0.12	0.25	0.18
42.68	42.69	42.91	1.70	2.37	1.53	0.18	0.76	0.60
40.01	40.83	40.61	1.97	1.80	4.68	0.48	1.8	1.8
40.51	40.81	40.47	1.81	2.00	4.68	0.10	3.0	7.0
40.62	40.47	41.04	4.54	3.05	4.61	0.13	1.14	0.94
			350 µF, 25 VOLT, T4 CASE					
339.6	340.2	339.0	9.93	16.95	12.45	0.34	0.35	0.33
342.4	344.5	347.8	9.37	12.98	12.11	0.31	0.47	0.49
344.7	46 nF	28 mF	10.72	7.67	9.76	0.32	0.06	0.10
339.6	338.8	341.7	10.71	11.99	16.58	0.32	0.34	0.38
354.9	326.9	328.4	8.76	11.59	18.18	0.33	0.36	0.35
354.9	347.5	321.9	11.06	12.98	21.29	0.30	0.31	0.33

* Data from tests conducted at Marshall Space Flight Center, NASA
† Broken leads occurred during radial vibration.

TABLE 6 90°C ΔT RIPPLE CURRENT TEST

T1 Case 8.2 µF-60V

	Intial			168 Hours			500 Hours		
	CAP	ESR	DCL	CAP	ESR	DCL	CAP	EDR	DCL
Ave.	8.247	2.4	.05	8.384	2.70	.31	8.406	2.65	.86

T4 Case 110 µF-75V

	Intial			168 Hours			500 Hours		
	CAP	ESR	DCL	CAP	ESR	DCL	CAP	EDR	DCL
Ave.	106.38	.45	.36	108.46	.57	.59	109.63	.71	.33

T2 Case 39 µF-60V

	Intial			1000 Hours			2000 Hours		
	CAP	ESR	DCL	CAP	ESR	DCL	CAP	EDR	DCL
Ave.	40.808	1.01	.13	41.288	1.02	.25	41.063	1.07	.08

BREAKDOWN VOLTAGE OF DISCRETE CAPACITORS UNDER SINGLE-PULSE CONDITIONS

Henry Domingos, Joe Scaturro, and Larry Hayes
Clarkson College
Potsdam, NY 13676
(315)268-6535

INTRODUCTION

Abnormal transient voltage impulses are often observed in electrical and electronic equipment and can represent a serious hazard to the reliable and safe operation of such equipment. These transients arise from such phenomena as lightning strokes, the electromagnetic pulse (EMP) which accompanies nuclear explosions, short circuits or other electrical accidents, switching transients, electromagnetic pickup and interference, electrostatic discharges (ESD), etc. Transients can occur surprisingly often, with astonishingly high amplitudes. For example, Martzloff and Hahn[1] report surges of 1400 to 2500 volts on ac power lines in a residential environment due to oil burner switching, and voltages of 600 to 5600 volts due to lightning induced transients. Static voltages as high as 39 kV have been reported as a result of a person walking across a carpet[2]. Transient duration ranges from a few nanoseconds for EMP and ESD pulses to several milliseconds for lightning [3-6].

The purpose of the work reported here was to investigate the susceptibility of common types of capacitors to single, high amplitude pulses, and to relate the measured breakdown voltages to the capacitor specifications, materials, and construction. There are only a limited number of references to previous work in this area[7-9]. These will be summarized here where appropriate. This type of breakdown, sometimes called intensive breakdown, should not be confused with the breakdown of capacitors under long term stresses, which is mainly of a thermal nature. This work is related, however, to work on integrated circuit MOS structures, which has been extensively reported on (see reference 10 for a review).

In the sections which follow, the experimental technique will be described in detail. The results of breakdown tests on glass, mica, plastic film, ceramic, and electrolytic capacitors will be presented, and the significance of the results will be discussed.

EXPERIMENTAL SET-UP AND TEST PROCEDURE

To measure the breakdown voltage of a capacitor, the simplest procedure is to apply a constant current step, monitor the voltage rise, and record the value of voltage at which breakdown occurs. By controlling the current, problems associated with high inrush currents can be avoided, the rate of rise of the voltage can be controlled, and possible mechanical and thermal effects can be avoided. By monitoring the current as well as the voltage, it is possible to extract additional information such as equivalent series resistance, leakage, nonlinear dielectric effects, characteristics of the breakdown event, etc.

In most of the work reported here the capacitor was charged from a high voltage source through a series resistor, with the charging voltage high enough for breakdown to occur during the linear portion of the charging curve. Under these conditions the charging current is nearly constant. By controlling the amplitude of the single, constant amplitude voltage pulse the rate of rise of the capacitor voltage could be controlled, and by adjusting the pulse width the post-breakdown damage was minimized, facilitating analysis of the failure site.

The experimental arrangement is shown in Fig. 1. The 1 ohm resistor was used to record the current waveform. The value of the other series resistor was selected to provide a time constant roughly equal to the pulse duration. The pulse generator was operated in the single-shot mode, with current and voltage waveforms recorded with a polaroid camera or on a storage scope. Typically, the pulse duration was set in the range 10-100 μs, with the amplitude adjusted so that breakdown occurred at a convenient point during the pulse. The pulse was many orders of magnitude too long for the voltage rise time to have any effect on breakdown, and orders of magnitude too short for thermal effects.

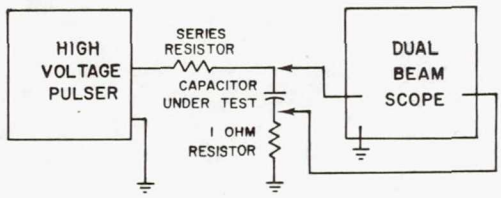

Fig. 1. Experimental set-up for testing Capacitors.

Each sample consisted of 10 capacitors. The parts were labeled, and the capacitance

value and dissipation factor at 1 kHz were recorded. For the electrolytics the leakage current was also measured. Immediately after the breakdown test these parameters were again measured. Some capacitors were also subjected to additional tests such as repeated pulses, changes in ambient temperature from -200 to +200°C, and to changes in charging current by several orders of magnitude.

For some types of capacitors it was relatively simple to perform autopsies to determine the failure site, extent of damage, and to measure plate areas, dielectric thicknesses, and other features of the construction. Where this was impractical manufacturers often generously supplied us with important data.

The waveforms associated with a typical breakdown event are illustrated in Fig. 2. When the pulse is applied the high voltage pulser and series resistor constitute a nearly-constant current source. The voltage rises almost linearly until breakdown occurs, when the current rises sharply. Damage to the capacitor occurs during the post-breakdown period, and depends on the characteristics of the external circuit as well as the energy stored in the capacitor.

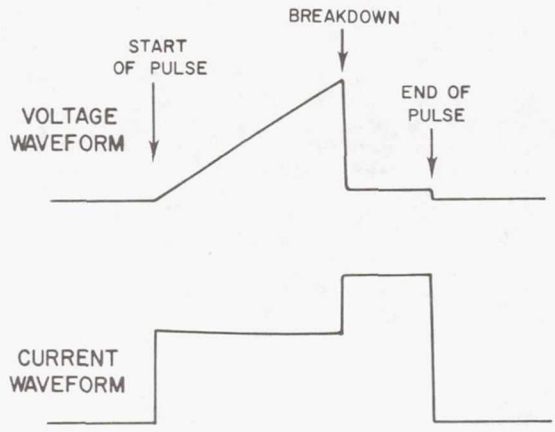

Fig. 2. Voltage and current waveforms for a typical breakdown test.

GLASS CAPACITORS

Glass capacitors are a convenient vehicle to study breakdown phenomena because the construction is fairly simple (the same material comprises both the dielectric and the package), there is only one manufacturer, and there are only a few case sizes. Glass capacitors are characterized by excellent stability, high Q, low leakage, long lifetime, and high resistance to radiation damage. They are not as widely used as less expensive types of capacitors, but find application where their superior qualities are considered necessary, such as rf circuits for military and space applications.

With the exception of the aluminum electrodes and the leads, the entire capacitor is made from 8871 glass, which is a potash lead glass with a composition 49% PbO, 42% SiO_2, 6% K_2O, 2% Na_2O, and 1% Li_2O. It has a dielectric constant of 8.4 and a power factor of 0.05 at 1 MHz. Dielectric strength is about 2,000 volts per mil (8×10^5 volts per cm) at room temperature. For a more complete listing of properties of this and other glasses the reader is referred to references 11-14.

Capacitor fabrication begins with a ribbon ranging from 1.5 to 2.8 mils thick (38 to 71 μm) and 0.12 to 0.46 inches wide (0.3 to 1.2 cm). The appropriate size is stacked with alternate layers of aluminum foil, arranged so that half the foils are extended out each side to be welded together to a lead wire. Cover glass is added, and the entire assembly sealed in vacuum at high temperature and pressure.

Glass capacitors are available in several different case styles, but those selected for testing were the common CY styles. Voltage rating is either 300 or 500 volts. The capacitance range and dimensions for each of the case styles are given in Table I.

Table I

Glass capacitor values and dimensions.

Style	Capacitance Range, pF	Thickness mm	Width mm	Length mm
CY10	0.5-300	1.98	4.37	8.74
CY15	180-1200	2.77	6.76	11.9
CY20	560-5100	3.58	10.7	18.6
CY30	3900-10000	3.58	19.1	19.5

The initial measurements of C and D were generally well within the specified limits (D < 1% and tolerances of 1, 5, or 10%). After some preliminary tests to determine the expected breakdown voltage, 10 capacitors of each type were subjected to the breakdown test. One group of 25 capacitors was also included. A histogram of the breakdown voltages for this sample is shown in Fig. 3, and a summary of all results is included in Table II.

The data in Table II show very little correlation between the rated voltage and the breakdown voltage. Yet the reasonably narrow spread in breakdown voltages within each sample indicates that the breakdown is related to some parameter of the capacitor, presumably the dielectric thickness. Each capacitor was carefully examined under a microscope using Cargille refractive index liquid. The separation between plates at the

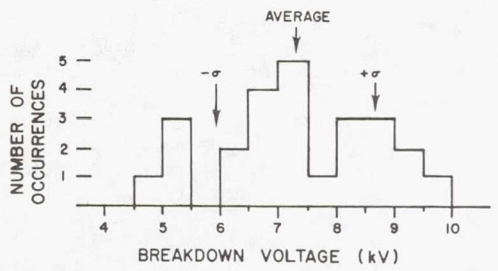

Fig. 3. Distribution of breakdown voltage for 25 glass capacitors, 22 pF, 500 volts, CY10 style.

construction are known. In fact, even the thickness of the original ribbon is not sufficient information since the plate separation and flatness are affected by the high temperature sealing process. Furthermore, the stacking pattern may call for multiple layers of dielectrics between the plates. The futility of predictions based simply on related voltage will be amply illustrated as other capacitors are discussed.

Table II shows that the variation in breakdown voltage with temperature is small. When testing is done under long-term dc or ac conditions, the dielectric strength can vary significantly with temperature. Shand[12] reports a 5% decrease in dielectric strength of glass

Table II

Breakdown voltages for glass capacitors.

Case Style	Capacitance Value (pF)	Rated Voltage	BV Min	BV Max	BV Ave	Standard Deviation in BV	Ave Dielectric Thickness (mils)	Ave Dielectric Strength (V/mil)
CY10	22±5%	500	4600	10050	7280	1410	3.15	2320
CY10	110±5%	500	3150	6850	4590	1050	1.84	2500
CY10	220±1%	300	3150	3950	3450	239	1.68	2080
CY15	220±5%	500	3100	5550	4780	699	2.66	1870
CY15	1000±5%	300	3300	4450	3810	368	1.76	2170
CY20	820±5%	500	3650	4000	3870	121	1.95	2040
CY20	4700±5%	300	2950	4100	3600	361	1.95	1930
CY30	6800±5%	300	3550	3950	3700	141	2.06	1820
CY10*	220±1%	300	3350	3600	3460	86	-	-
CY10**	220±1%	300	3150	4450	3755	405	-	-

* 5 samples at -196°C
** 10 samples at +200°C

breakdown site was measured, and the dielectric strength calculated. The average values are the entries in the last two columns of the table. Hence, it becomes clear that the dielectric thickness is the factor which determines the breakdown voltage. This is emphasized in Figs. 4 and 5, which are plots of the average breakdown voltage and average dielectric strength as functions of the average dielectric thickness. Over the somewhat limited range of dielectric thickness the average breakdown strength of all capacitors is 2063 volts/mil (8.1×10^5 volts/cm) at room temperature. Shand[12] shows that the dielectric strength of glass capacitors under dc or 60-Hz conditions varies from 2200 volts/mil to 800 volts/mil at 10 mils thickness.

These results in Table II point out that it is impossible to predict the breakdown voltage of a capacitor unless the details of the

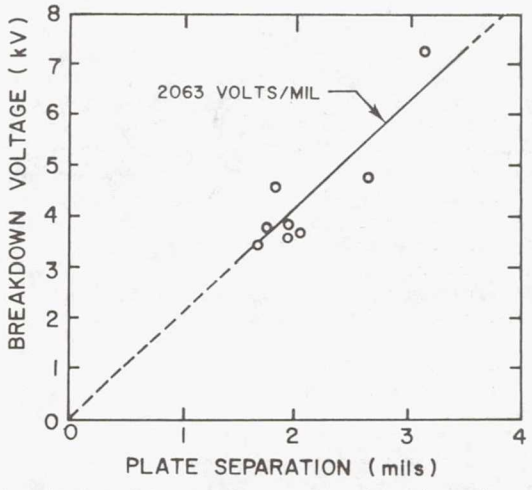

Fig. 4. Breakdown voltage as a function of dielectric thickness for glass capacitors. The plate separation is the average value measured at the breakdown site.

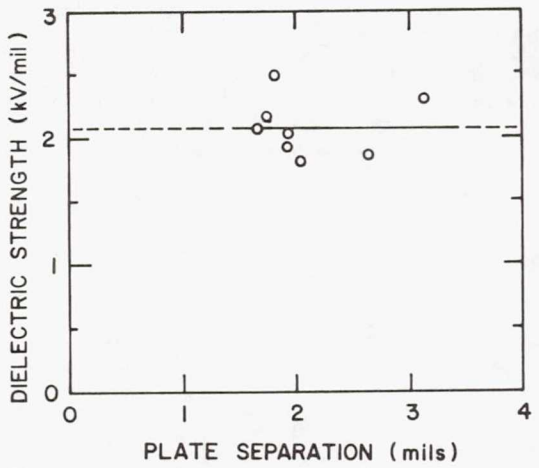

Fig. 5. Same data as Fig. 4 plotted in terms of dielectric strength.

capacitors over the range 0 to +200°C, while Saums and Pendleton[13] indicate a much larger variation in certain glasses at elevated temperatures. Vermeer[15,16] shows that the breakdown strength of several glasses is independent of temperature from -50 to + 100°C when the impulse duration was 10 μs. For longer pulses the dielectric strength decreased both with pulse duration and with temperature. This was attributed to the distortion of the field caused by migration of ions within the glass. In his work the geometry was such that edge effects were eliminated. By proper cleaning of the glass he was able to obtain good, reproducible data. The dielectric strength was independent of thickness, and about 10 times the value reported here with parallel plate capacitors.

Another important question concerns the damage to the capacitor. In glass capacitors (and in all other types as well) damage may occur to the package, and electrical measurements may reveal a short circuit (or possibly an open circuit). On the other hand, the occurrence of breakdown may be virtually undetectable except by destructive physical analysis (DPA). Since damage is incurred only after breakdown has taken place and depends on the energy available, one would surmise that damage should be more severe with large values of capacitance, since not only is there more energy stored in the capacitor, but the power delivered from the pulse generator is greater since the series resistor is smaller (to maintain breakdown during the desired pulse duration).

This is the general trend found in the post-breakdown analysis. Large capacitors were frequently short circuits. Small capacitors appeared to be undamaged. Measurements of C and D revealed virtually no change. Strangely enough, the only indicator of damage in these cases was a second breakdown test, where it was found that the new breakdown voltage was only 10-40% of its original value. In most cases however, the breakdown voltage was still well above the rated voltage for the capacitor. In the subsequent pulsing the breakdown was reduced still further. Of course, the presence of a damage site would undoubtedly have some effect on the lifetime of the part in regular use conditions.

Tasca, et al,[8] have also reported data on breakdown of glass capacitors under conditions virtually identical to the present work. For comparable sizes and ratings their results agree quite well with those in Table II.

MICA CAPACITORS

The market for mica capacitors has declined in recent years, presently accounting for 3-4% of the total U.S. market. They are used in high voltage and high frequency circuits where their high Q and good temperature, aging, and frequency characteristics offer advantages.

Capacitor plates are formed by silkscreening silver paste onto thin mica sheets. After firing, the plates are interleaved with tin-lead foils, each foil being alternately extended on opposite sides of the stack. The foils are folded over the end, then compressed tightly and clamped by the lead assembly. Capacitors are dipped repeatedly in phenolic and epoxy resins, or molded in phenolic or polyester.

Mica capacitors were not included in the testing program reported on here. However, a summary of results from work at the General Electric Company are shown in Table III[8].

A few capacitors in most case styles exhibited multiple or self-healing breakdown. When breakdown occurred the voltage dropped momentarily to a low value then rose again, and repeated. When a second pulse was applied the breakdown voltage was found to be comparable to, and usually slightly higher than, the original value. This is a phenomenon often observed in metallized film capacitors, where it is associated with vaporization of the metal in the immediate vicinity of the breakdown site. When multiple breakdown did not occur (the vast majority of cases) the breakdown during a second pulse was typically 20-60% of the original value.

The data in Table III show a trend in that lower breakdown voltages are associated with higher values of capacitance. This is emphasized in Fig. 6. This type of relationship is often observed in other types of capacitors, but not as clearly. The explanation is relatively simple. For small values of capacitance the area is impractically small when standard thicknesses of mica are used. Consequently, multiple dielectric layers are employed, increasing the area to a manageable value and

Table III

Breakdown voltages for mica capacitors[A].

Case Style	Capacitance Value (pF)	BV Min	BV Max	BV Ave	Standard Deviation	Number of Data Points
CD6[B]	83	3430	4110	3820	226	10
CD6	10	2130	8610	5260	2030	9
CD6	39	1340	5500	3730	1160	11
DM10	30	4600	5200	4810	270	7
DM10	120	3300	4730	4020	451	10
CM04	250	1870	4570	3070	957	9
CM05	5	4850	6170	5510	933	2
CM05	33	2290	6250	5010	1190	8
CM05	510	1780	4130	3520	816	7
CM06	1200	1520	2770	1790	379	9

[A]We are indebted to Dante Tasca, Hugh O'Donnell, and Samuel Stokes for permission to use their data.

[B]This capacitor was rated at 100 volts. All others were 500 volts.

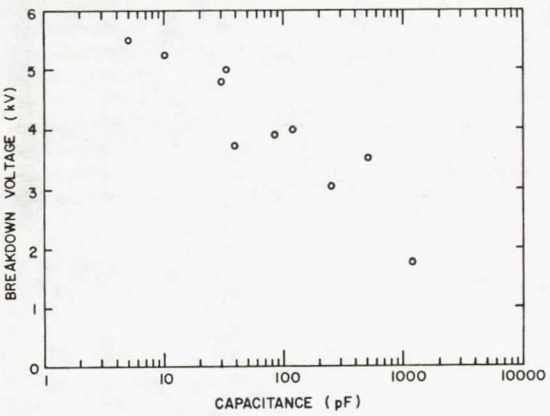

Fig. 6. Variation of breakdown voltage in mica capacitors with capacitor value.

incidentally increasing the breakdown voltage.

Presumably the breakdown voltage is directly related to the thickness of the mica dielectric, but this information was not obtained for these capacitors. Shand[12] gives values for dielectric strength of 5300 volts per mil at 1 mil thickness. These were measured at 60 Hz under oil. When edge effects are eliminated the dielectric strength is 30,000 volts per mil and is independent of thickness.

PLASTIC CAPACITORS

Plastic capacitors have largely supplanted paper capacitors for electronic applications such as coupling, bypassing, filtering, and timing. They are characterized by a wide range of available capacitance values and voltage ratings, high insulation resistance, low dissipation factor, low temperature coefficient, good stability, and high resistance to moisture. With small packages made possible by films as thin as 2 μm, they are being considered as replacements for ceramic monolithic and even electrolytic capacitors.

Polymers for use in plastic capacitors include polyester, polystyrene, polycarbonate, polyethelene, polypropylene, polyvinyl fluoride, and others. Polyester (Mylar, Kodar, etc.) is probably the most widely used film in the industry. It has high dielectric strength, low dissipation factor, low leakage, good mechanical properties, and good stability. Its main disadvantage is a large temperature coefficient. Polystyrene is also an excellent dielectric, but has an upper temperature limit of 85°C. Polycarbonate is one of the newer dielectric materials. In general, it possesses excellent electrical properties over a wide temperature range.

Plastic capacitors are either of the foil type, in which two aluminum foils separated by the plastic film are wound into a compact roll, or the metallized film type. In this case a thin layer of metal is evaporated directly onto the film. Contact is made by extending the foils, by inserting tabs during winding, or by spraying metal over the ends. Stacked film capacitors have recently been introduced. These

are made from rectangular sheets assembled like a mica or ceramic monolithic capacitor.

Data for film capacitors are listed in Tables IV and V. Several trends are apparent. In the first place, there is correlation between the rated voltage and the breakdown voltage in most cases. Secondly, as in the case of mica capacitors, the larger values generally have lower breakdown voltages. Finally, the dielectric strength is fairly uniform (except for a factor of 2, which probably indicates a double layer of film) for each type of film irrespective of film thickness and area.

healing for obvious reasons. In fact, it is claimed that a nail can be driven through a metallized film capacitor with no serious effects! For films a few micrometers thich with metal several tens of nanometers thick the energy required to clear a breakdown is 10-50 μJ. When breakdown is non self-healing, a film capacitor is normally short circuited. In most cases the breakdown site is at the edge of the foil, as one would expect from the high fringing field which exists there.

Tasca, et al[8] obtained results similar to those in Tables IV and V.

Table IV

Breakdown voltages for polyester film capacitors.

Capacitance (μF)	Rated Voltage	Construction	Average BV	Standard Deviation	Film Thickness (mils)	Average Dielectric Strength (V/mil)	Type of Breakdown*
0.01±10%	100	extended foil	1150	678	0.24	4780	SH, NSA
1.0±10%	200	extended foil	1610	662	0.32	5030	NSH
1.0±20%	100	extended foil	1630	758	0.24	6770	NSH
10±10%	100	duo metallized foil	411	119	0.14	2940	SH
10±10%	200	metallized foil	675	94	0.24	2810	SH

* SH = Self-Healing
NSH = Non Self-Healing

Table V

Breakdown voltages for polycarbonate film capacitors.

Capacitance (μF)	Rated Voltage	Construction	Average BV	Standard Deviation	Film Thickness (mils)	Average Dielectric Strength (V/mil)	Type of Breakdown*
0.01±10%	200	extended foil	1020	143	0.40	2540	SH, NSH
0.01±5%	100	extended foil	1170	532	0.24	4890	SH
0.1±10%	200	metallized foil	580	164	0.24	2420	SH
0.1±10%	100	metallized foil	300	90	0.14	2140	SH
1.0±10%	200	extended foil	828	194	0.24	2070	NSH
1.0±5%	100	extended foil	635	197	0.24	2650	NSH
4.0±5%	200	metallized foil	493	78	0.24	2050	SH
5.0±5%	100	metallized foil	252	40	0.14	1800	SH

* SH = Self-Healing
NSH = Non Self-Healing

The phenomenon of self-healing has long been associated with plastic and paper capacitors. Whether or not a breakdown site will be cleared depends on the dielectric material, its thickness, the impedance of the voltage source, the size of the capacitor, and especially, the thickness of the metal. Metallized film capacitors are the most likely to exhibit self-

CERAMIC CAPACITORS

Breakdown in both ceramic disc capacitors and ceramic multilayer capacitors has been reported by Tasca, et al[8] and in detail by Domingos, et al[9]. A summary of results from 9 is reproduced here.

Tables VI and VII list the results for ceramic discs and monolithics, respectively. Disc capacitors are made in a limited range of thicknesses and areas but with many different dielectric formulations which provide a very wide range of dielectric constants. For NPO capacitors the dielectric constant is about 20, while for Class II dielectrics it may be as high as 10,000. This was found to be the major factor in controlling the breakdown voltage.

Table VI. Average breakdown voltage for ceramic disc capacitors. (Reference 9.)

Capacitance	Rated	Measured
0.39 nF	---	5840
20	200	2725
20	600	2660
22	1000	4240
50	1000	3660
82	100	2350
56	100	4050
10	230	3060
10	200	3980
5	3000	7660

Table VII. Average breakdown voltage for ceramic multilayer capacitors. (Reference 9.)

Capacitance	Rated	Measured
100 nF	100	1450
1.5	100	2450
0.1	200	3860
100	100	1560
47	50	1020
0.016	50	4400
56	50	1080
0.22	50	2230
0.33	50	1530
0.21	50	3100
175	50	263
150	50	1160

The variation in dielectric strength is plotted in Fig. 7 for several values of thickness. The data points are averages taken from extensive records of lot testing supplied by a major manufacturer. The graph shows that by changing only the dielectric formulation it is possible to effect a 500-1 change in capacitance value while changing the breakdown voltage by a factor of 6. From this one concludes again that breakdown voltage is generally lower for larger values of capacitance.

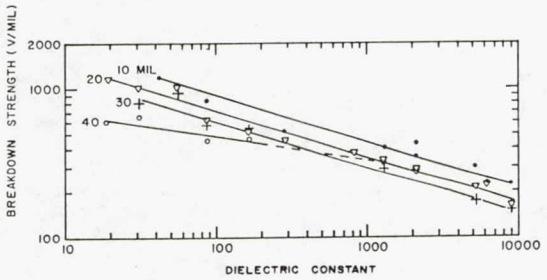

Fig. 7. Dielectric strength as a function of dielectric constant for several thicknesses of ceramic disc capacitors. (Reference 9.)

In contrast, multilayer ceramics utilize a limited range of dielectric materials, but can be made with greatly different areas by changing the plate dimensions and number of plates in a stack. This gives an opportunity to investigate the effects of area on breakdown voltage.

Fig. 8 is a plot of breakdown strength as a function of area for several different thicknesses. The dielectric constant was 1300 in all cases. The graphs were derived from lot testing data supplied by still another manufacturer. Again, it is apparent that larger values of capacitance should have lower breakdown voltages since they would have larger areas, high dielectric constants, and thinner dielectrics (although the dielectric strength is greater the breakdown voltage is less).

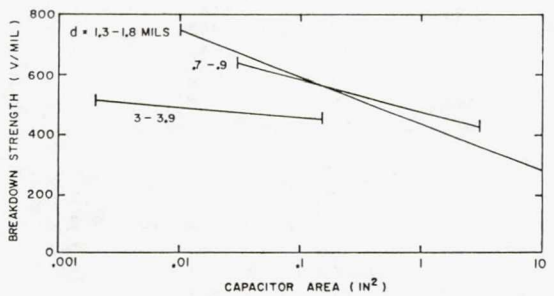

Fig. 8. Effect of capacitor area on breakdown strength for ceramic monolithic capacitors. (Reference 9.)

ELECTROLYTIC CAPACITORS

Electrolytics are distinctly different from

electrostatic capacitors in their fabrication, characteristics, applications, and even their response to high voltage transients. Electrolytics account for about 20% of unit sales in the United States, and about 40% of the dollar volume.

To interpret the results of pulse testing on electrolytic capacitors it is necessary to understand how they are made. All electrolytics are formed by anodizing a metal which then forms the positive electrode. The oxide itself is the capacitor dielectric. The thinness of this oxide (a small fraction of a micrometer) is the key to the high volumetric efficiency of electrolytics. The electrolyte, in contact with a second metal plate, serves as the cathode terminal.

Aluminum electrolytics are of the foil type, with either a wet, paste, or dry electrolyte. The anode is formed from high purity (99.3 to 99.99%) aluminum foils roughly 1 mil thick. The foils can be used as plain foils, or electrochemically etched. This increases the surface area and hence the capacitance by a factor of 8-30 times, depending on the voltage rating.

The foil is anodized to produce a layer of aluminum oxide. This process is the key to understanding the basic electrical properties of all electrolytics. Assume for the moment that the oxide is formed at constant current, say 50 mA/cm^2. The oxide thickness will increase linearly with time, as will the voltage across the oxide. An upper limit, called the scintillation voltage (about 600 volts for aluminum), is reached when the electric field causes localized momentary breakdown. In finished capacitors the scintillation voltage depends on the resistivity of the electrolyte, higher resistivity increasing the scintillation voltage, but also the equivalent series resistance. If the anodizing voltage is kept constant, the current decreases with time as the oxide grows. If at any time the voltage is changed the current will change correspondingly, but then resumes its decrease with time. When the current decreases to a specified value the oxide is considered fully formed.

The oxide thickness is about 1.2 nm/v of forming voltage. The rated voltage of the finished capacitor is typically about 60% of the forming voltage. The cathode foil of a polarized capacitor has no oxide, or perhaps a very thin oxide. If the polarity of the voltage is reversed, a large current flows from the cathode foil, through the electrolyte, and through the anode oxide layer (the mechanism which causes this rectifying property is not understood at this time). In a non-polarized unit the cathode foil is anodized in exactly the same way as the anode foil.

When a voltage less than the forming voltage is applied the current is restricted to a low value (the leakage current) by the anode oxide. If however, the voltage exceeds the forming voltage, a large current will flow causing additional oxide growth on the positive foil. In a polar capacitor the difference in behavior is due to differences in oxide thicknesses at the anode foil and cathode foil.

To complete the assembly, the two foils are wound with a paper separator into a compact roll. For the common wet foil types an electrolyte of glycol borate is common, although solutions of ethylene glycol or dimethylene formamide are occassionaly used.

Tantalum electrolytics can be of the foil type, solid, or wet slug type. The foil type is highly reliable and versatile, and is available in plain and etched foil, polar and nonpolar styles. It has both a long shelf life and use life, the principle failure mode being a gradual decrease in capacitance due to evaporation of electrolyte. The manufacture of foil types is essentially the same as aluminum electrolytics. The oxide thickness is about 1.8 nm/v of forming voltage, and shows brilliant coloration depending on the total thickness. The electrolyte is usually ethylene glycol.

Solid tantalum capacitors begin with a tantalum powder which is compressed into a cylindrical pellet around a tantalum wire. This assembly is sintered in vacuum to vaporize impurities and form a strong, porous, high conductivity body which serves as the anode. The pellet is anodized to form the dielectric layer of the capacitor. The pellet is then dipped in a manganous nitrate solution. This coating is transformed by pyrolysis into manganese dioxide, a semiconducting material which forms the first layer of the cathode. After several cycles of dipping and pyrolysis, layers of colloidal graphite and silver-loaded paint are applied. Solder attaches the pellet to the can.

Solid tantalums differ from other electrolytics in showing relatively high dielectric absorption (recovery of voltage after discharing) and certain healing effects associated with impurities in the oxide. One consequence is the practice of providing resistance in series with the capacitor of 3 ohms per applied volt to minimize the occurrence of catastrophic shorts during high current operation. Another consequence is the nature of breakdown during pulse testing, to be described shortly.

The initial manufacturing steps of wet slug capacitors are identical to those for solid tantalums. After the pellet is sintered and oxidized it is inserted into a silver case with a diluted sulfuric acid solution in gel form as

the electrolyte. It is not possible to build non-polar devices. Furthermore, the capacitor is very sensitive to reverse current flow which causes silver to be electroplated onto the anode pellet, causing permanent damage. Nevertheless, wet slug tantalums find widespread use, especially in power supply filters because of outstanding performance characteristics and the highest volumetric efficiency of any capacitor.

When a pulse of constant current is applied to an electrolytic capacitor a voltage drop is produced across the equivalent series resistance of the capacitor and across the oxide. The ESR is made up of the resistance of the foils and resistance of the electrolyte. The voltage across the oxide depends on the total charge on the capacitor plates through the familiar equation V = Q/C. Since Q is just the integral of the constant charging current, V increases linearly with time. At some point the voltage reaches the forming voltage for the oxide thickness associated with whichever plate has the positive charge. For the remainder of the pulse the voltage remains constant at this value for most types of electrolytics. The forming voltage normally is specified at a relatively low value of current, say 100 μA. If the current is increased the forming voltage, i.e., the value of voltage required to maintain this steady state conduction current, is also increased. These concepts are illustrated in Fig. 9.

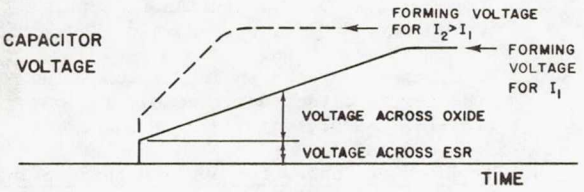

Fig. 9. Variation of voltage across an electrolytic capacitor when a constant current is applied. The limiting, or forming voltage, depends on the current value.

Forming voltage as a function of the charging current is plotted in Fig. 10 for a 25 volt, 60 μF tantalum foil capacitor. From this figure it is clear that the cathode foil also has an oxide film, which is about half as thick as the anode oxide. The capacitor has a small leakage current as long as the voltage is of the proper polarity and remains below the rated voltage. If the voltage is raised to about twice rated voltage, large currents are conducted through the oxide and the anodization process is resumed. If the anodizing were to continue the forming voltage would gradually increase. However, with the short pulses utilized in this study the change in voltage is infinitesimal.

Solid tantalum capacitors subjected to

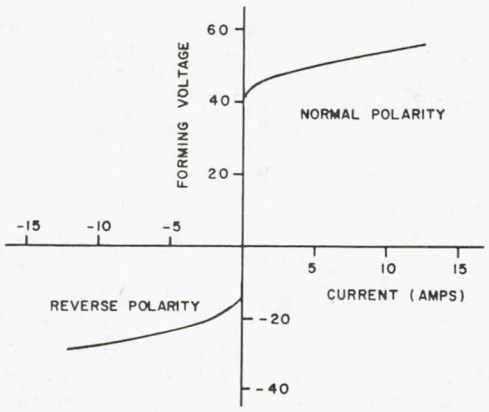

Fig. 10. Forming voltage as a function of current for a 25 volt, 60 μF tantalum foil capacitor.

pulses in the 0.1 to 10 μs range are damaged when the capacitor voltage reaches the forming voltage. The failure mode is a large increase in leakage current. Other electrolytic capacitors are able to reach and remain at the forming voltage for relatively long periods of time before any degradation in the leakage current is noted. If the charging current is increased the forming voltage is also increased. Eventually, when the forming voltage is several times its low current value, damage will occur.

Tasca, et al, measured the forming voltage of several capacitors at a current of 100 microamps per microfarad-volt. These results are listed in Table IX. Note that there is little correlation between the rated voltage and the forming voltage. This is particularly true for low capacitance, low voltage units, where the oxide layer is deliverately enhanced to avoid impractically small areas.

Table IX. Forming voltages for electrolytic capacitors measured at a current of 100 μA per μF-volt. (Reference 7.)

Capacitor Type	Capacitance (μF)	Rated Voltage	Forming Voltage
Aluminum Foil	1	3	105
	1	12	245
	1	50	130
	1	250	280
	10	12	60
	10	50	110
	100	3	15
	100	50	105
	3000	3	10
Tantalum Solid	2.2	6	90
	56	6	30
	0.33	15	150
	22	15	50

Table IX. (Cont'd)

Capacitor Type	Capacitance (μF)	Rated Voltage	Forming Voltage
Tantalum Solid	0.01	35	150
	0.1	35	205
	0.047	60	320
	0.0047	100	210
Tantalum Foil	10	10	50
	12	15	55
	200	15	35
	2	150	330
	4	150	260

To summarize the situation regarding electrolytic capacitors, there is no way to correlate the damage threshold for short pulses to capacitor value, voltage rating, or construction. The best correlation is with the low-current forming voltage. For solid tantalums the threshold voltage is approximately equal to the low-current forming voltage, while for other types it is 2 to 10 times the forming voltage.

CONCLUSIONS

For electrostatic capacitors the breakdown voltage is inherently related to the properties of the dielectric, with the important parameters being the dielectric field strength, which is related to the dielectric constant, and the dielectric thickness. These are not necessarily related to the capacitance value and the rated voltage, but generally the larger values of capacitance will have lower breakdown voltages.

Foil and wet-slug electrolytics can withstand conduction currents pulses without apparent damage (in either direction for foil types). For solid tantalums, damage occurs whenever the capacitor charges to the forming voltage.

ACKNOWLEDGEMENT

The authors would like to thank Rich Ingerson who performed the tests on plastic capacitors, and Dante Tasca, Hugh O'Donnell, and Samuel Stokes whose results were so widely used in this paper. We would also like to thank the many engineers and their companies who supplied us with samples, advice, and information.

REFERENCES

1. F. D. Martzloff and G. J. Hahn, "Surge Voltages in Residential and Industrial Power Circuits," IEEE Trans. Power Apparatus and Systems, PAS-89, pp. 1049-1056, July/Aug. 1970.

2. T. S. Speakman, "A Model for the Failure of Bipolar Silicon Integrated Circuits Subjected to Electrostatic Discharge," presented at the 12th Annual International Reliability Physics Symposium, April 1974.

3. D. L. Durgin, "An Overview of the Sources and Effects of Electrical Overstress," presented at the 1980 EOS/ESD Symposium, Sept. 1980.

4. R. J. Antinone, "Microcircuit Electrical Overstress Tolerance Testing and Qualification," presented at the 1980 EOS/ESD Symposium, Sept. 1980.

5. Transient Voltage Suppression Manual, 2nd ed., General Electric Co., Auburn, NY, 1978.

6. D. R. Kressler, "Surge Tests on Plug-in Transforms," presented at the 1980 EOS/ESD Symposium, Sept. 1980.

7. L. W. Ricketts, J. E. Bridges, and J. Miletta, EMP Radiation and Protective Techniques, Wiley and Sons, New York, 1976.

8. D. M. Tasca, H. B. O'Donnell, and S. J. Stokes, "Pulse Power and Damage Characteristics of Capacitors," Final Technical Report prepared for Air Force Weapons by General Electric Co., Dec. 1976.

9. H. Domingos, D. P. Quattro, and J. Scaturro, "Breakdown in Ceramic Capacitors Under Pulsed High-Voltage Stress," IEEE Trans. Components, Hybrids, and Manufacturing Technology, CHMT-1, pp. 423-428, Dec. 1978.

10. P. Solomon, "Breakdown in Silicon Oxide - A Review," J. Vac. Sci, Techn., 14, pp. 1122-1130, Sept./Oct. 1977.

11. Handbook of Tables for Applied Engineering Science, Chemical Rubber Co., Cleveland, 1970.

12. E. B. Shand, Glass Engineering Handbook, McGraw-Hill, New York, 1958.

13. H. L. Saums and W. W. Pendleton, Materials for Electrical Insulating and Dielectric Functions, Hayden Book Co, Rochelle Park, NJ, 1973.

14. G. W. Morey, The Properties of Glass, Reinhold, New York, 1938.

15. J. Vermeer, "The Impulse Breakdown Strength of Pyrex Glass," Physica, 20, pp. 313-326,1954.

16. J. Vermeer, "The Electric Strengths of Glasses with Different Sodium Contents," Physica, 22, pp. 1247-1253, 1956.

INTERNAL FUSE MODULES FOR SOLID TANTALUM CAPACITORS

Henrique V. DeMatos
Union Carbide Corporation
P.O. Box 5928
Greenville SC 29606
(803)963-6300

SUMMARY

Miniature fuse modules were designed for, and incorporated into, two styles of solid tantalum capacitors. One is an epoxy-molded, radial-leaded, high frequency decoupling capacitor; the other is an hermetically sealed device with axial lead wires (MIL-C-39003; CSR-style device). The fusible element, for both devices, consists of a fine bimetallic wire which reacts exothermically upon reaching a critical temperature and then disintegrates. The desirability of having fused devices is discussed, and design constraints, in particular those which minimize inductance and series resistance, while optimizing fuse actuation characteristics, are reviewed. Factors affecting the amount of energy required to actuate the fuse and reliability of actuation are identified. Construction techniques are reviewed, and parametric measurements of fused and unfused devices are compared. A device can now be produced which tolerates switching and transient surges, while protecting circuits and equipment from disruption and damage caused by short-circuit capacitor failure.

INTRODUCTION

Because of their small size, reliability and freedom from sharp resonances, solid tantalum capacitors are widely used in filtering and bypass applications. In these applications, they are frequently connected, without series resistance, across the power supply bus — first, to eliminate alternating current ripple at the output of the rectifier, and, second, locally at the circuit to prevent switching transients and other wideband, high-frequency noise from affecting circuit performance. Conventional commercial solid tantalum capacitors exhibit failure rates as low as 0.001 percent per thousand hours at 60 percent confidence level;[1] however, the increased complexity of circuit modules, higher frequency ripple currents, denser component packaging and ever higher system reliability goals are, at times, straining the reliability expected of these devices. The common failure mode in solid tantalum capacitors is a catastrophic increase in leakage current, which can, if allowed to increase uncontrolled, cause the component to become excessively hot with potential damage to the circuit module and/or nearby components. The classical method of circuit protection, an external fuse to shut down the power supply, is undesirable, because it also halts equipment operation. A fused capacitor can give several orders of magnitude increase in effective reliability, while preventing unintentional interruption in equipment operation.

This paper describes the design, construction and properties of fuse modules incorporated into solid tantalum capacitors. Minimizing inductance and resistance of the fuse modules is an important consideration to achieve low impedance and series resistance in the capacitor.

FUSE DESIGN CONSIDERATIONS

Solid tantalum capacitors are manufactured from a porous plug of sintered tantalum, which is anodized to form an oxide dielectric film over its surface. Manganese dioxide is then dispersed around and within the pores of the plug to provide a solid electrolyte and cathode. The manganese dioxide on the exterior of the plug is then metallized to provide a connection for the negative terminal. The positive terminal is a wire or strip of tantalum attached to the plug. Small defects, causing electrical leakage in the anodic film, are often healed through conversion of the manganese dioxide to more insulative lower oxides. At large leakage levels, however, thermal effects destroy the anodic film and result in catastrophic short circuit failure in the absence of current limitation in the external circuit. Thus, the failure characteristic to which the fuse module must respond is a very rapid increase in leakage current into the ampere range.

The desired sensitivity of the fuse to the rapidly increasing failure current is dependent upon circuit or system characteristics and requirements. Fuse actuation should occur before the capacitor becomes excessively hot, exhibits external damage, or otherwise affects other components when used in high density packaging applications.

The resistance and inductance of the fuse module must be minimized to optimize the high frequency response characteristics of the fused capacitor. Both are important where high frequency impedance values must be low for effective circuit performance, and the effective series resistance (ESR) is important in filtering applications where high values of ripple current are present at the capacitor terminals.

Fuse actuation current must be minimized, consistent with applications requirements; therefore, energy conservative designs are dictated. Thermal isolation of the fusible link, an exothermic link material to assure clean actuation under marginal conditions and physical strength to withstand normal handling, were some of the fuse module design considerations.

The capacitor, with fuse module attached, should be able to meet all applicable specification requirements of MIL-C-39003, including continuous 125°C performance, and ability to withstand crowbar discharge and repeated surge current and voltage cycles without loss of fuse integrity. Finally, the inclusion of the fuse module into the capacitor assembly must be accomplished with no change in the external appearance or physical size of the part.

FUSED CAPACITOR CONSTRUCTION

The above considerations were applied to the design of fuse modules for two styles of solid tantalum capacitors. One is a radial leaded, high frequency decoupling capacitor with ribbon leads; the other is an axial leaded, hermetically sealed power supply filter capacitor with wire leads. The operating characteristic and fuse actuation requirements for both the devices are presented in Table I. A previous paper[2] reports on the design and performance of a fuse module for the high frequency decoupling capacitor which is detailed in Figures 1, 2, 3 and 4. The fuse link is an exothermic wire of palladium-aluminum, made by Pyrofuse Corporation of Mount Vernon, N. Y. The wire traverses an isolating cavity to connect two conductor planes which become part of the negative lead ribbon. As the fault current increases, the wire heats, due to ohmic effects, and, when the wire reaches a temperature of about 650°C, an intermetallic compound of palladium-aluminum is formed, and the link is destroyed with a violent exotherm.[3]

TABLE I

OPERATING PARAMETERS FOR FUSED, SOLID TANTALUM CAPACITORS

Capacitor Type	Ribbon Lead, High Frequency Decoupling Capacitor, Molded	Axial Wire Lead, Power Supply Filter, Hermetically Sealed
Application	At Circuit to Supress Low Signal, High Frequency Noise and Transients	At Rectifier Output to Filter Pulsing D.C. and Eliminate Ripple From D.C. Power Supply Bus
Operating Frequency Range	To 100 MHz	To 40 KHz
Operating Current Range	<10 uA (AC or DC)	1.5A to 3.5A (AC only)
Fusing Energy	~500 mJ	~5 J
Fuse Actuation Current	~3 ampere	6A to 11A
Maximum Fuse Resistance	0.1 ohm	0.03 ohm
Maximum Fuse Inductance	0.5 nH	2 nH

Details of the fuse assembly are shown in Figure 3. An etched and drilled printed circuit board forms the insulating segment of the module. The fuse wire passes through the hole and connects to the opposing metallic lands. Lead ribbons are soldered, top and bottom to complete the assembly which is soldered to the cathode surface of the capacitor body. After a ribbon lead is welded to the anode wire or strip, the capacitor is encapsulated. Inductance was minimized by keeping connections as short as possible and maintaining close proximity between the lead ribbons.[4] Resistance was minimized by selecting an effective fuse length of 1 MM (0.04"). With shorter distances, end effects, which increase fusing current due to heat loss, are more severe; also, the likelihood of solder bridging increases. Longer distances increase the wire resistance and part ESR significantly. Fuse wire selection was made based on the data listed in Table II and to satisfy the general requirements of Table I.

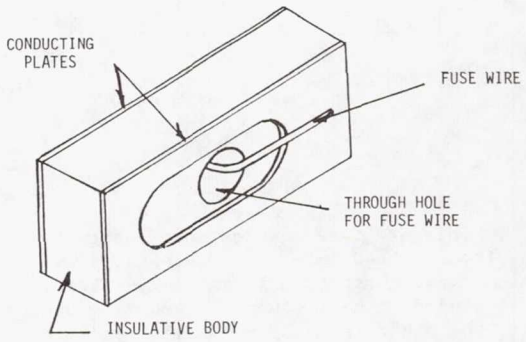

Figure 1 FUSE LINK DETAIL

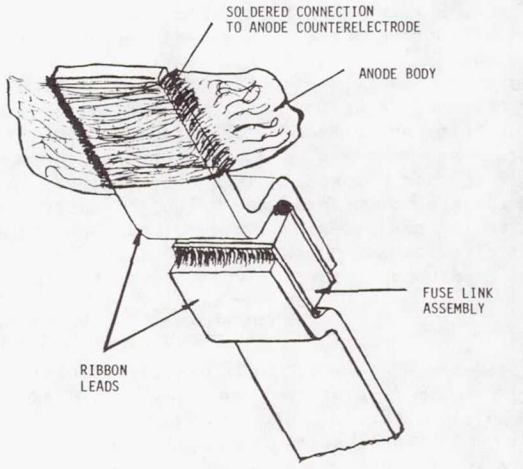

Figure 2 FUSE ATTACHMENT DETAIL

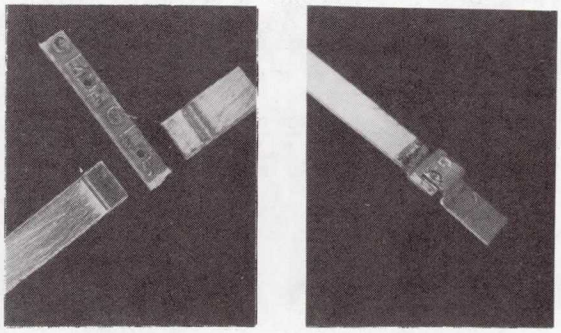

Figure 3. Fuse Assembly Detail

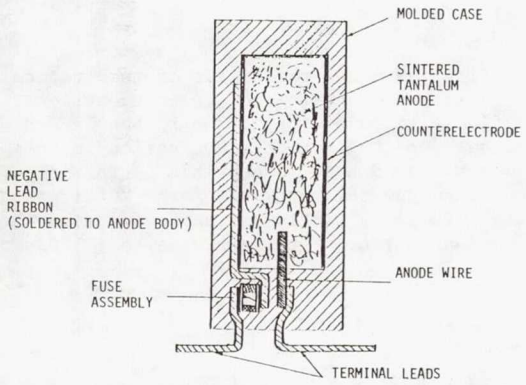

Figure 4 CAPACITOR WITH FUSE ASSEMBLY IN PLACE

TABLE II

FUSE WIRE SELECTION DATA

FUSE WIRE CHARACTERISTICS

WIRE DIA. MILS	WIRE DIA. MM	RESISTANCE IN OHMS OF 1 MM LENGTH	FUSING CURRENT AMPS*
1	0.025	0.2067	0.75
1.5	0.038	0.0917	2.00
2	0.051	0.0517	3.50
3	0.076	0.0230	5.75
4	0.102	0.0129	8.75
5	0.127	0.0083	11.25
8	0.203	0.0049	20.75

*(@ 1mm length)

Figure 5 shows the construction details of the fuse module for the hermetically sealed capacitor. The fuse module consists of two wires, insulated from each other and potted or molded

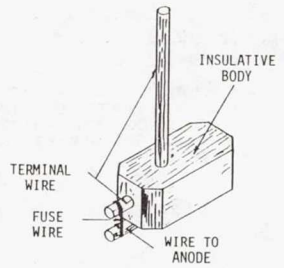

Figure 5 FUSE MODULE FOR METAL CASE UNIT

together to form a lead wire assembly. A fusible link, made of palladium-aluminum wire, is strung between the two wires, secured and soldered to them. Figure 6 shows the fuse module, connected to the anode and enclosed in the metal can. The insulated cap is used to prevent shorting of the lead wires to the case wall.

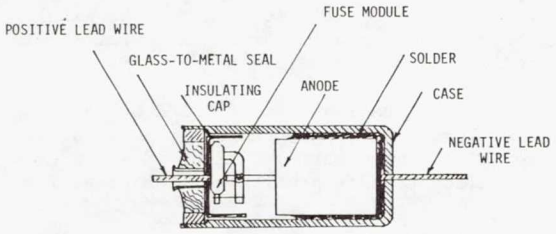

Figure 6 INTERNAL ASSEMBLY DETAIL FUSED, HERMETIC CAPACITOR

Fuse wire selection for each capacitor was based on the requirements shown in Table I. The encapsulated ribbon leaded, high frequency capacitor required fast acting, low energy fusing action, so, a wire size having a nominal actuating current of 2 amperes was selected. The hermetically sealed units would be exposed to high ripple currents (1.5 to 4.5A) and needed higher fusing currents. Wires were selected to provide actuation currents approximately three times the ripple current levels to allow for surges, heating, and other factors.

FUSED CAPACITOR CHARACTERISTICS

One rating, a 40 μF, 10 volt part, was used to evaluate the characteristics of the fused, high frequency decoupling capacitor. For the metal cased unit, two values, one at each end of the rating spectrum, were selected.

These were a 330 μF, 6 volt and a 22 μF, 50 volt device and are typical of the devices listed in MIL-C-39003/9.

The introduction of the fuse increases the impedance of the capacitor. Figure 7 shows impedance versus frequency curves for both styles.

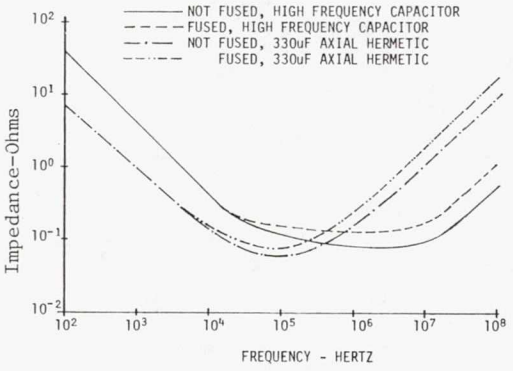

Figure 7 IMPEDANCE VS FREQUENCY FOR INDICATED CAPACITOR TYPES

The superiority of the ribbon leaded unit is obvious at the higher frequencies. The axial leaded capacitor used for the measurement was the 330 μF, 6 volt unit.

Fuse actuations were studied by inducing capacitor failure with the application of voltate in reverse polarity. Figure 8 shows the test circuit and typical actuation curve for a

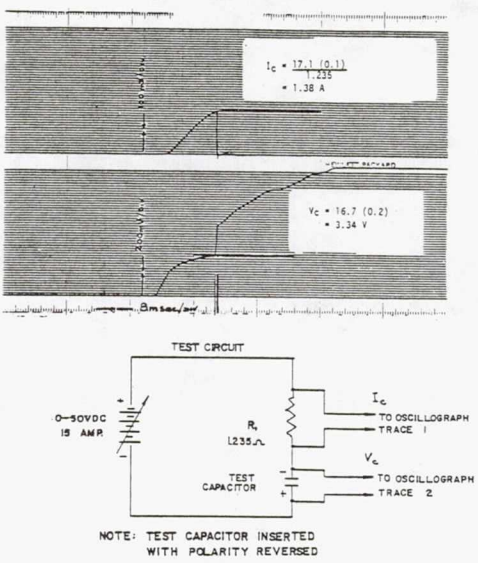

Figure 8 TYPICAL ACTUATION CURVE AND TEST CIRCUIT

40 μF, 10 volt capacitor. Table III lists fuse actuation currents for sample capacitors in both styles and ratings and illustrates typical part-to-part variations in actuation current.

TABLE III

TYPICAL FUSE ACTUATION CURRENT

	ACTUATION CURRENT IN AMPERES		
S/N	40 uF, 10 Volt High Frequency Decoupled	330 uF, 6 Volt Metal Cased Filter Cap.	22 uF, 50 Volt Metal Cased Filter Cap.
1	1.96	10.29	5.69
2	2.58	9.50	6.49
3	2.96	10.05	4.97
4	1.89	10.37	5.99
5	1.78	10.45	6.64
6	1.56	13.60	6.05
7	1.71	11.40	6.70
8	1.93	11.16	5.65
9	1.91	10.29	5.80
10	2.12	11.16	5.25
$\bar{x}$	2.04	10.83	5.92
σ	0.42	1.13	0.57

Figure 9 shows the effect of temperature on the actuation current of fused capacitors. The fine wire fuse link of the ribbon leaded unit was selected for this evaluation because it was believed more susceptible to thermal effects than the thicker wire of the metal cased units. There is little, if any, effect on the actuation current of temperatures to 175°C.

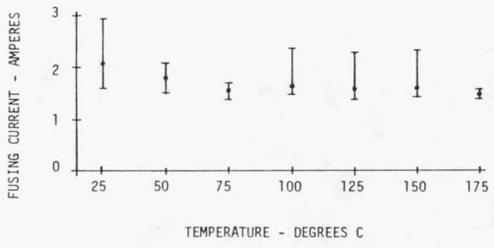

Figure 9 FUSE ACTUATION CURRENT VS TEMPERATURE

The requirements of MIL-C-39003/9 were applied to the fused, metal cased capacitor to determine the performance of the devices when exposed to the ripple current levels of the specification. Figure 10 shows no significant difference in the case temperature of fused and unfused capacitors at various ripple current levels. The nominal heat rise of the capacitors

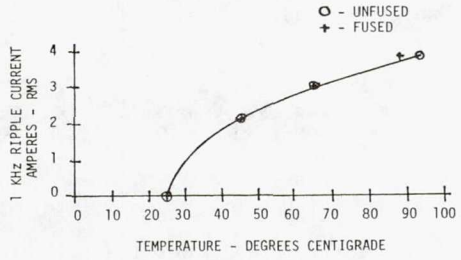

Figure 10 TEMPERATURE RISE VS RIPPLE CURRENT

tested was ∿80°C per watt dissipated. Watts dissipated are calculated as follows:

$P = I^2R$ where I = value of ripple current (1)
R = ESR at test frequency

$R = \frac{D}{\omega C}$ where D = dissipation factor at test frequency (2)
ω = 2π times test frequency
C = capacitance in farads

Performance of the fused capacitors to environmental exposures specified in MIL-C-39003, such as shock and vibration, thermal shock, surge current, humidity testing and voltage life testing, were uneventful. No new failure modes were generated by the addition of the fuse module, and all units tested satisfactorily passed the exposure testing. Humidity test data for the encapsulated devices and life test data for the metal cased unit are shown in Tables IV and V and are typical of device performance.

TABLE V

LIFE TEST PERFORMANCE DATA

22 μF; 50 VOLT

INITIAL MEASUREMENTS				POST 4000 HOUR, 85°C LIFE TEST			
AT 1 KHz		50 VDC	100 KHz	AT 1 KHz		50 VDC	100 KHz
Cap. μF	D.F. %	D.C.L. μA	ESR Ω	Cap. μF	D.F. %	D.C.L. μA	ESR Ω
32.20	3.72	1.23	0.111	32.20	3.36	0.616	0.108
32.49	3.19	0.063	0.095	32.48	2.85	0.062	0.091
31.49	3.29	0.075	0.088	31.49	3.01	0.050	0.084
32.49	3.18	0.055	0.094	32.49	2.75	0.071	0.089
33.31	3.09	0.050	0.085	33.28	2.38	0.005	0.080
31.79	3.28	0.060	0.092	31.78	2.93	0.045	0.087
33.30	3.45	0.065	0.107	33.29	3.16	0.047	0.105
31.47	4.07	0.055	0.107	31.41	3.77	0.042	0.107
32.99	2.93	0.080	0.090	32.99	2.63	0.066	0.086
31.77	3.06	0.050	0.086	31.70	2.65	0.057	0.081
32.90	2.91	2.050	0.087	32.89	2.51	1.224	0.084
33.30	3.19	0.991	0.092	33.29	2.73	0.560	0.087

TABLE IV HUMIDITY PERFORMANCE OF ENCAPSULATED UNITS

Test: Humidity Test Conditions: 85% R.H. at 85°C With Rated Voltage Applied

	INITIAL -25°C						AFTER 1000 HRS. EXPOSURE					
COND.	120 Hz	120 Hz	10VDC	2 MHz	20 MHz	100 MHz	120 Hz	120 Hz	10VDC	2 MHz	20 MHz	100 MHz
MAX.			3.0	0.2	0.4	1.5			30.0	0.4	0.8	3.0
MIN.	40.0						40.0					
PARA.	Cap.	D.F	DCL				Cap.	D.F	DCL			
UNITS	μF	%	μA				μF	%	μA			
1	42.48	1.30	0.72	0.16	0.33	1.25	44.10	1.29	1.48	0.20	0.35	1.34
2	44.98	1.33	0.59	0.16	0.34	1.33	46.82	1.53	0.496	0.17	0.34	1.32
3	41.19	1.32	0.52	0.15	0.31	1.18	42.81	1.59	0.290	0.20	0.35	1.34
4	42.26	1.20	1.82	0.18	0.26	1.24	44.00	1.57	1.57	0.23	0.39	1.35
5	44.78	1.54	0.77	0.17	0.28	1.42	46.09	1.21	0.47	0.19	0.36	1.34
6	41.80	1.66	1.06	0.16	0.30	1.33	43.49	1.19	0.799	0.23	0.37	1.37
7	42.09	1.43	0.17	0.16	0.32	1.20	43.66	1.66	0.297	0.16	0.33	1.51
8	41.60	1.32	0.29	0.17	0.34	1.25	43.00	1.49	0.218	0.19	0.30	1.36
9	40.99	1.44	0.28	0.18	0.35	1.33	42.20	1.46	0.528	0.20	0.37	1.38
10	40.67	1.36	0.61	0.15	0.35	1.45	42.05	1.78	0.206	0.22	0.34	1.51
11	44.40	1.43	1.35	0.18	0.31	1.10	46.20	1.22	1.17	0.20	0.36	1.33
12	42.97	1.51	1.45	0.18	0.29	1.18	44.43	1.28	0.940	0.22	0.33	1.45

CONCLUSIONS

Fuse modules containing exothermic fusible links are a viable means of increasing the effective, or in-circuit, reliability of solid tantalum capacitors beyond that exhibited by the capacitor element, itself. A wide range of actuation current and energy levels can be selected to suit a wide range of applications, while maintaining these levels at values small compared to those at which detrimental heating or discernible damage occurs. The fuse characteristics are relatively insensitive to environmental effects.

An ESR and inductance penalty result from incorporating the fuse; while it is small, in conventional axial leaded capacitors, it is significant in low impedance capacitor designs. These effects can be compensated for in high frequency applications by a moderate increase in the number of capacitors in the circuit modules.

REFERENCES

1 Qualified Products List, QPL-39003-48, U.S. Govt. Printing Office, 1980

2 H.V. DeMatos, "Design of an Internal Fuse for Solid Tantalum Capacitor", IEEE Trans. CHMT, Vol. CHMT-3, pp. 244-249, June 1980

3 Descriptive Data Sheet on Pyrofuse Wire, Pyrofuse Corporation, Mount Vernon, NY

4 F. W. Grover, "Inductance Calculations: Working Formulas and Tables", New York, Dover, 1962, Chapters 3 and 4

SPECIFYING CAPACITORS FOR PERFORMANCE AND RELIABILITY IN SWITCHING POWER SUPPLIES

Franklin E. Greenhalgh
CEAG Electric Corp
1324 Motor Parkway
Hauppauge, N.Y. 11787
(516) 582-4422

Over the last decade the switching power supply has grown from a laboratory curiosity to a major source of regulated energy both for military and commercial applications.

During this period component manufacturers have developed devices designed specifically for these supplies. This is especially true in the areas of semiconductors and capacitors.

I would like to discuss the various switching topologies used today and their capacitor requirements.

The three most commonly used switching circuits today are the full bridge converter, the half-bridge converter and the forward converter. Actually, all three circuits use the same pulse width concept for regulation with the major difference being how many transistors are used for power handling. The full bridge uses four transistors, the half-bridge uses two and the forward converter uses one. In practical design, forward converters are used at 300 Watts and below, half-bridges at 300 to 600 Watts and full bridges above 600 Watts.

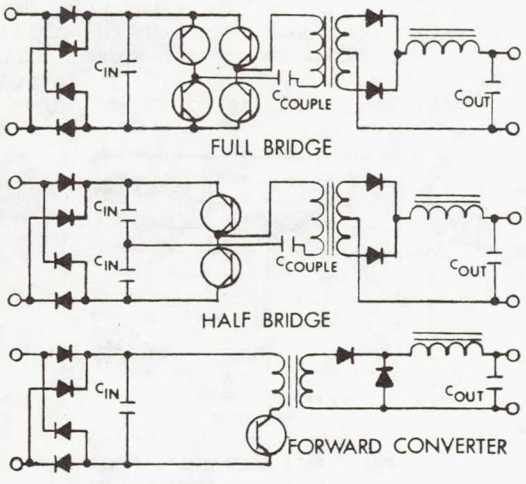

Regulation is achieved by alternately saturating diagonal pairs of transistors in the full bridge, alternately saturating transistors in the half-bridge and simply pulse modulating one transistor in the forward converter.

As shown, three capacitors are used in the power chain of the full bridge.

Input Capacitor

The input capacitor serves to filter the rectified DC at the input, it provides energy storage during line dropouts and it reduces the EMI generated by the supply. The input capacitor requirements for all three designs are similar with the half-bridge using two capacitors in series.

Ripple Reduction

The input capacitor first must reduce the rectified DC to ripple voltage levels consistent with the performance characteristics of the regulators ability (i.e., if regulator has a 1000-1 (60db) ripple reduction and 20mV P/P of fundamental is allowed on the output, P/P input ripple must be <20V). The value for C can be obtained by the formula (1).

$$C = \frac{.3\,P_{out}}{(E_{in}) \times (E_{ff}) \times (F_{req}) \times (O_{ut}R_{ipple}) \times (R_{ed}.R_{atio})} \quad (1)$$

P_{out} = Output Power

E_{in} = Low Line Input Voltage (RMS)

E_{ff} = Efficiency of Regulator

Freq = Input Frequency

Output Ripple = Max P/P Fundamental output ripple

Reduction Ratio = Regulators Ripple Reduction Ability At 2F.

Hold-Up Time

The C calculated above is the minimum capacitance required for circuit performance, however, many power supplies required a hold-up time. This is the time the power supply must maintain regulation during input dropout. Typically this number is 10ms to 100ms, with 20ms being the most common requirement. The value for C in this case can be calculated by formula (2).

$$C = \frac{2P_{out} \times T_{holdup} \times 10^{-3}}{(E_{ff}) \times (V_{op.}^2 - V_{min.}^2)} \qquad (2)$$

P_{out} = Output Power

T_{holdup} = Holdup Time In Milliseconds

E_{ff} = Expected Efficiency of Power Supply

$V_{operating}$ = Normal DC Operating Voltage

$V_{minimum}$ = Minimum DC Voltage Converter Can Regulate At

Ripple Current

Once the capacitance value is chosen it is now necessary to determine the ripple current the capacitor will see. The circuit has two waveforms which merge at the capacitors terminals. First is the charging current from the line which in most applications resembles a triangular wave shape at twice the line frequency. Second is the inverter current which is a quasi square wave at the inverter frequency.

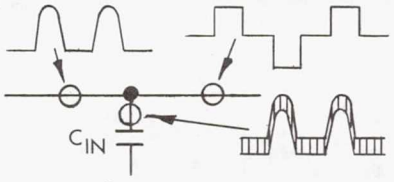

The average inverter current can be calculated by formula (3).

$$I_{INV} = \frac{P_{out}}{(E_{ff}) \times E_{dc}} \qquad (3)$$

P_{out} = Output Power

E_{ff} = Efficiency

E_{dc} = Low Line DC operating Voltage Across C.

The actual capacitor input current is a function of the capacitance, the line impedance, and the inverter current. Its calculation can be complex and in many cases it is better to measure it on the breadboard. This can be done quite easily with an RF Ammeter. Typically, the capacitor ripple current varies between 1.3 and 1.7 x inverter current and using a value of 1.5 for preliminary design is recommended.

Voltage Rating

The voltage rating of the capacitor is determined by calculating maximum DC operating voltage (1.4 X high line RMS) and the maximum surge voltage (1.4 X line transient). A derating factor should be applied to the operating voltage of the capacitor. This is not necessary for the surge voltage.

ESR and ESL

As the selection of capacitors meeting the capacitance, ripple current and voltage rating is small and in this application ESR and ESL are not critical, it is recommended that with all things being equal, select the capacitor with the lowest ESR and ESL.

The lower the ESR, the lower the EMI generated by the supply. If EMI is a problem, it is sometimes easier to parallel a small polycarbonate or mylar capacitor with the output capacitor rather than restrict the selection.

Derating

Once the parameters above have been calculated, the designer must now decide on derating requirements for reliability and performance over temperature. The capacitor derating must include capacitor tolerance and loss of capacitance with temperature.

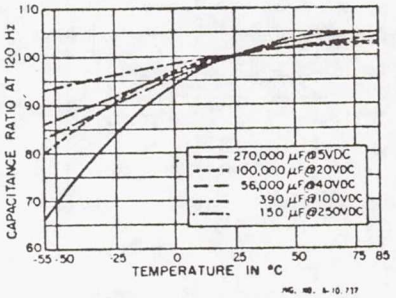

TYPICAL CURVES SHOWING CHANGE IN CAPACITANCE WITH TEMPERATURE

Ripple current either calculated or measured is generally specified at the capacitors maximum temperature rating. If the ambient temperature the capacitor is to operate is less than the specified temperature, then the ripple current rating can be increased or a failure rate reduction achieved. The actual operating temperature of the capacitor can be calculated where

$$T_{op} = T_a + \frac{I^2_{ripple} \times ESR}{K \times A}$$

T_{op} = Actual Operating Temperature Of Capacitor

T_a = Ambient Temperature

I_{ripple} = Capacitor Ripple Current

ESR = Capacitor ESR

A = Can Area

K = Thermal Resistance Of Capacitor

(K must be obtained from the manufacturer or estimated from application notes available).

Once the actual operating temperature has been determined, the failure rate can be obtained by manufacturers data (see below).

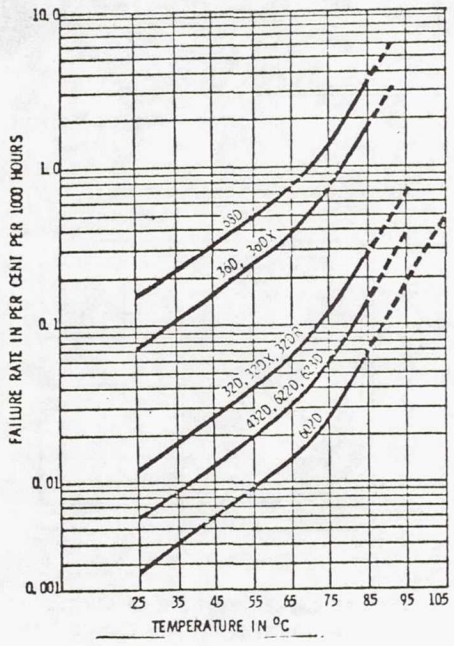

The voltage derating of the capacitor is important also in determining failure rate. Again manufacturers data is used in conjunction with calculated operating voltage to determine actual voltage rating used.

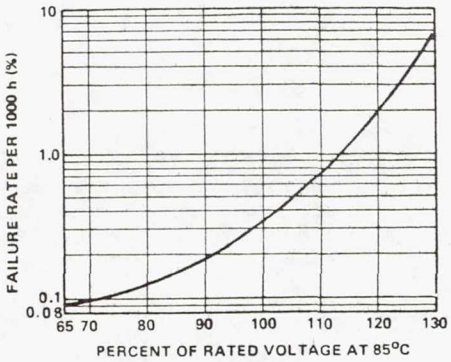

After all parameters are calculated and a search for available capacitors made, the designer generally finds that he is limited to aluminum electrolytic capacitors, and the ripple current and voltage rating will determine the selection, the capacitance available for those ratings being higher than required.

Coupling Capacitor

The coupling capacitor is chosen as follows:

Capacitance

Capacitance is determined by the amount of tilt the waveform can tolerate due either to output ripple or inverter voltage.

Typically, this value is from 1 to 20ufd.

Voltage

The operating voltage rating is determined by the circuit unbalance and is typically less than 20 Volts. The polarity however, is not known. If a transistor fails, the capacitor will see the full input voltage. Prudence generally leads to selecting a voltage rating of at least the input voltage, thus eliminating a fire hazzard in the failure mode.

Ripple Current

The ripple current of the coupling capacitor is equal to the inverter current and should be appropriately derated.

ESR

ESR and ESL should be low and will generally not affect circuit performance.

The choice of coupling capacitor type will generally be polycarbonate, mylar or paper, however, in some cases non-polar aluminum or tantalum capacitors must be used.

Output Capacitor

The selection of the output capacitor is the most critical. Its parameters affect output purity, circuit stability and reliability.

The output capacitor is used in an L-C filter to reduce the rectified carrier to a pure DC voltage.

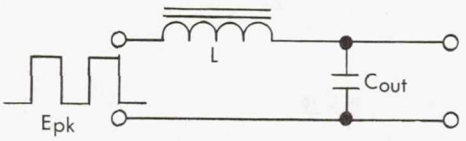

Typical ripple reduction is 1000 to 5000/1. The choice of L and C must be made considering the following:

1) ripple reduction ratio.
2) ripple current on capacitor.
3) resonant frequency of LC

The ripple reduction ratio required can be determined by the formula (4)

$$R_{ripple} R_{ed} = \frac{Z_c}{X_L}$$

where

$$Z_c = \sqrt{X_c^2 + ESR^2}$$

As Xc and ESR in this application are generally very close in value, the ESR required significantly enters into the capacitor choice.

Ripple Current

The ripple current the capacitor sees (approx) is expressed by the formula

$$I_{ripple} = \frac{.15\,E_{pk}}{LF}$$

E_{pk} = Peak Voltage At Filter Input
L = Inductance
F = Switching Frequency

The resonant frequency of the LC filter must be sufficiently high enough to allow the regulator to maintain gain over a frequency range consistent with transient response and ripple reduction requirements.

ESR

Once the capacitance and ripple current are known, then the capacitor will be selected for its ESR. The ESR rating of the capacitor is critical in the stability analysis of many switching regulators and care must be used in evaluating its change over temperature. Many power supplies depend on the ESR of the capacitor to supply a break point in the BODE plot of the supply.

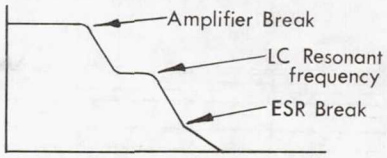

If the ESR changes greatly with temperature, the power supply will exhibit instability and oscillations which can cause capacitor failure.

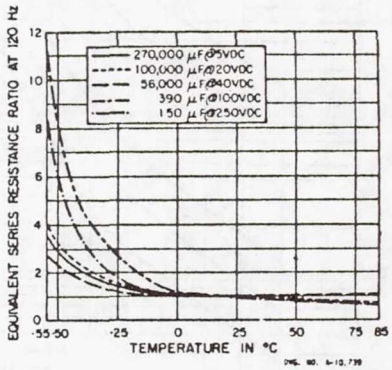

TYPICAL CURVES SHOWING CHANGE IN EQUIVALENT SERIES RESISTANCE WITH TEMPERATURE

Type

Solid tantalum or aluminum electrolytics are used in these applications. Problems can occur using capacitors from different vendors as the ESR differs from manufacturer to manufacturer.

When using aluminum, the designer must select capacitors with guaranteed ESR over the temperature range.

Flyback Regulator

Another regulator circuit commonly used is the flyback regulator.

In this circuit energy is transferred through two inductors on a common core. When the switching transistor is on the primary inductor current increases linearly proportional to E/L.

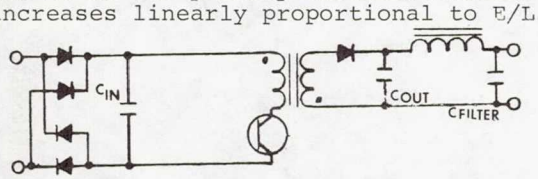

When the transistor is turned off, the secondary inductor transfers this energy to the output capacitor. The current rise is quite rapid during this time and the current peak is equal to 3 to 5 times the output current. Selection of the output capacitor in this case must include ESL characteristics.

To date no capacitor alone has sufficent ESL and generally an additional filter is used for ripple reduction.

Output ripple current is determined by the formula (5)

$$I_{ripple} = I_{pk}\sqrt{\frac{T_o}{3T}} \qquad (5)$$

Buck Regulator

The most commonly used post regulator is the "buck" regulator.

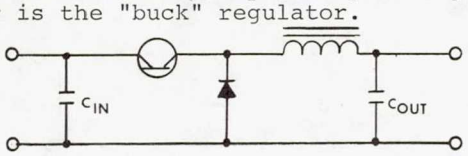

Here the transistor chops a DC voltage and an LC filter reduces the ripple. The input capacitor current may be determined by the formula (6)

$$I_{rms} = I_{out}\sqrt{\frac{T_o}{T}}$$

T_0 = On Time Of Switch

T = Total Cycle Time

"Cuk" Regulator

Another regulator gaining popularity is the "cuk" converter.

In this regulator an inductor is used in series with the input capacitor, the coupling capacitor and the output capacitor. As the ripple current is continuous on all three capacitors, this converter produces the least stress on the devices.

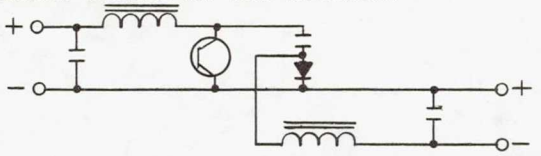

CONCLUSION

The use of capacitors in today's power supply design is no longer a simple task. The design engineer must use caution in choosing the capacitor for each application.

Manufacturer's performance specifications must be obtained to guarantee reliable operation over the complete temperature and input range. A standardization of capacitor specifications would be helpful to the design engineer.

BIBLIOGRAPHY

1) Cornell-Dubilier; Switching Regulator Capacitor Technology: Optimizing Ripple and EMI Suppression Performance.
2) Cornell-Dubilier; Ripple Current Capability of Large-Can, Computer-Grade Capacitors.
3) Sprague Electric; Capacitor Reliability In Switched-Mode Power Supply Design.
4) Sprague Electric; Permissible Ripple Current in Aluminum Electrolytic Capacitors.

MONOLITHIC CERAMIC CAPACITORS FOR HIGH RELIABILITY APPLICATIONS

E. B. Thornley
Components Engineering Department
TRW Defense and Space Systems Group
Redondo Beach, California 90278
(213) 535-0743

INTRODUCTION

Monolithic multi-layer ceramic dielectric capacitors are widely used in high reliability applications in spacecraft, launch vehicles and military equipment. Their relatively low cost, wide range of values and package styles are attractive features that result in high usage in electronic circuitry in these applications.

Established Reliability Specification MIL-C-39014 has been utilized for a number of years to define requirements for ceramic dielectric capacitors for high reliability applications. Under the test programs required by MIL-C-39014, capacitors with low failure rates have been produced by many part manufacturers.

Capacitors produced under the requirements of MIL-C-39014 are also used in very large numbers in military equipment applications where reliability requirements are less stringent than those imposed for space use.

MIL-C-39014 has several inherent shortcomings, and many users have found it necessary to perform additional test and evaluations prior to use in high reliability applications. Destructive Physical Analysis is one type of evaluation that is used in the assessment of the inherent quality of these capacitors.

A new specification, MIL-C-123, is being prepared to define requirements for high reliability ceramic capacitors. This document includes Destructive Physical Analysis (DPA) as a supplier-performed requirement along with other non-destructive tests and inspections that will provide capacitors suitable for high reliability applications.

This paper will discuss design and construction of monolithic ceramic dielectric capacitors, defects that can lead to failure, and methods for defect detection that are being incorporated in the new military specification.

DESIGN AND CONSTRUCTION

Monolithic multi-layer ceramic dielectric capacitors are fabricated by stacking thin layers of uncured ceramic sheet with previously printed electrodes, and then firing the stack to "cure" the ceramic. End metallization is applied to make contact with the electrodes and the element may then be used in "chip" form, or equipped with leads and a case for conventional installation.

The ceramic material for general purpose ceramic capacitors is essentially barium titanate with additives selected by the manufacturer to yield desired electrical properties. Other titanates are utilized for stable and low-loss capacitors. Exact formulations tend to be proprietary for competitive reasons. These materials are blended in pre-determined proportions and milled to a fine consistency.

A liquid vehicle is added to the blend and the resultant slurry is cast on a glass, stainless steel, or plastic film base to form a thin sheet. After air drying, the cast sheet is peeled from the base. At this stage, the cast sheet is pliable and can withstand handling required during further processing.

Thickness of the cast material is in the range of .001 to .005 inches, depending on the material formulation and viscosity.

Electrode patterns are applied to one surface of the cast sheet. Typically the electrode is formed by silk screening a precious metal-bearing ink pattern on the cast sheet.

These patterns are then punched out such that one edge of the electrode pattern is flush with one edge of the punched plate, while the other three edges have a margin of bare material.

A number of printed, punched plates are then stacked as illustrated in Figure 1. Alternating plates are reversed in orientation so that the flush edges of electrodes alternate at each end of the stack. The finished value of capacitance is a function of the number of stacked plates, the area of the electrode plate, the thickness of the dielectric sheet, and the dielectric constant, "K Factor" value of the ceramic. The voltage rating is proportional to the dielectric thickness.

Additional layers of blank sheet are usually added to the top and bottom of the stack to add mechanical strength and electrical insulation. The stacked element is then subjected

to a series of baking and firing operations to drive out the volatile materials in the ceramic mix and electrode ink and cause sintering of the ceramic particles. The finished element is a monolithic structure with the interspersed layers of electrode material.

After firing, the ends of the element are coated with metal-glass frit. This material is fired, making electrical connection to the electrode ends and providing a termination area for attachment of leads, or direct attachment to a suitable circuit substrate.

At this point, the capacitor is completely functional and can be electrically tested for electrical parameters.

Figure 2 illustrates the configuration of the finished capacitor element with a cut section to reveal the internal structure.

Further manufacturing operations are performed on the element to make it usable as a circuit element in a variety of applications.

The capacitor styles specified by MIL-C-39014 are cased, leaded devices in several configurations.

The capacitor manufacturer provides these configurations by solder attachment of formed leads to the end metallization areas. High temperature solders are used for these attachments to eliminate remelting when the capacitor is soldered into the circuit assembly.

Protective cases are formed around the element by transfer-molded epoxy materials to form a smooth rectangular or tubular body. Other types of finishing include simple application of epoxy dip coatings, or assembly into a pre-formed plastic container with suitable potting fills.

A current popular application of monolithic ceramic capacitors is the "chip" style, where the element is directly attached by soldering or conductive adhesives to metallized circuit substrates. For these applications, a variety of end metallization materials are available--palladium-silver, palladium-gold, and multi-layer coatings with an outer layer of solder. The metallization system chosen is related to the design of the circuit substrate and component attachment system selected by the equipment designer.

Chip style ceramic capacitors are covered by a separate document, Established Reliability Specification MIL-C-55681.

DEFECTS AND ANOMOLIES

The manufacturing process for monolithic ceramic dielectric capacitors includes a number of steps where minor deviations from specified limits or process variations can result in defects and anomolies in the finished part. Some of these can result in early failure of the capacitor in a circuit. Others are indicative of poor workmanship or non-uniformity of the production lot. The sketch in Figure 3 illustrates the types of defects that occur and can be revealed by cross-sectioning in a plane perpendicular to the electrode planes.

The defects and anomolies keyed to Figure 3 are classified as follows:

1. Void in dielectric material between opposed electrodes.

2. Void in dielectric material outside of active electrode structure.

3. Crack between opposed electrodes.

4. Crack from electrode to outside surface.

5. Delamination of adjacent layers.

6. Delamination from an electrode to opposite termination.

7. End margin too short.

8. Excessive variation of dielectric thickness.

9. Inadequately bonded end metallization.

10. Poorly attached lead.

11. Improper stacking.

12. Improper registration.

13. Inadequate side margin.

14. Varying electrode count from unit to unit within one lot.

The defects classified as voids, cracks, dielectric thickness variation and delaminations are usually the result of inadequately processed raw material, variations in the casting of the green sheet, or poor control of electrode screening, pressing, and baking/firing processes.

The remaining defects can usually be traced to poor workmanship and/or inadequately controlled punching and stacking of the elements.

DEFECTS AND ANOMOLIES AND THEIR EFFECTS ON RELIABILITY AND PERFORMANCE

In general, voids, cracks and delamination defects in ceramic dielectric capacitors can lead to severe degradation of the insulation resistance characteristic, with ultimate failure in the form of a "shorted" capacitor. These types of defects, if located within the active electrode structure, reduce the dielectric voltage withstanding capability either because the ceramic thickness is reduced or the structure fractures, allowing electrode particulate material to bridge the small clearance between the opposed electrodes.

Inadequate end margins, or delaminations to the opposed termination are potential failures either by reduction of voltage withstanding capability or further fracture along the electrode plane.

Experience has shown that even in relatively low voltage applications (i.e., much lower than rated voltage applied) dielectric defects can lead to failure in the circuit early in system life.

If these capacitors have lead attachment deficiencies, subsequent handling, lead forming, installation and environmental exposures can lead to complete loss of the lead to element connection and an "open" capacitor in the circuit.

Misregistered electrodes, and improper stacking, while not likely to affect performance, show lack of controls during processing. Non-uniform electrode patterns indicate that the lot may not be homogenous, and that elements from several lots may be mixed.

Failure analyses of these types of capacitors performed at TRW DSSG as well as by other contractors, have shown evidence of all of these types of defects.

The impact of a failure of these types of capacitors as with any other type of component part, varies in significance depending on the point in time of its occurrence.

Part failures detected in the early stages of electrical functional tests of sub-assemblies are relatively easy to correct. However, as an electronic system progresses through its manufacturing and testing sequences, part failures become increasingly more expensive to correct.

Failures occurring when several systems are being integrated into a complex spacecraft, for example, can be very costly to correct and can seriously impact the delivery schedule of the end item.

If the part failure occurs in a spacecraft after launch, corrective action is not possible at all, and a significant portion of the spacecraft function may be lost.

Even in systems that are accessible for repair, failures can be troublesome and expensive to correct.

Depending on the type of failure, it may be necessary to completely remove and replace all capacitors of the same manufacturing lot in order to minimize further failures.

TECHNIQUES TO ELIMINATE POTENTIAL FAILURES

Manufacturers and users of monolithic multi-layer ceramic capacitors have developed a number of different techniques to identify parts with internal defects that can lead to early failure. These techniques are intended to eliminate weak or defective capacitors without degrading otherwise acceptable parts.

Some of these techniques are:

- Thermal Shock - Voltage Conditioning (Burn-in),
- X-ray Inspection,
- Neutron Radiographic Inspection,
- Ultrasonic Inspection,
- Destructive Physical Analysis.

A brief discussion of each of these techniques follows.

Thermal Shock - Voltage Conditioning

This technique subjects the entire lot of capacitors to a series of successive high and low temperature exposures with minimum transfer time between temperature extremes. Following thermal shock, the lot is operated at elevated temperature with up to two times rated voltage applied. The duration of the voltage conditioning period may be 100 hours or more. Following conditioning, a measurement of electrical parameters on each capacitor is made.

The intent of this test sequence is to force failure of individual items with internal defects, without damaging otherwise good parts. It is a relatively low-cost method and is utilized in many specifications including MIL-C-39014.

The degree to which all defective or marginal capacitors are identified by this technique may be questioned. It is felt that thermal shock-voltage conditioning forces failure of grossly defective units, however, there is certainly evidence that capacitors that pass this type of test sequence can and do fail in field applications.

X-Ray Inspection

X-Ray is an effective inspection method to identify capacitors that have poorly attached leads or inadequate encapsulation. However, the ceramic capacitor element itself is opaque to X-rays and therefore, internal element defects cannot be identified with X-ray. The utility of X-ray therefore is limited to detection of lead attachment and encapsulation defects--both worthwhile objectives. This type of inspection is included in MIL-C-39014 at the highest assurance level.

Neutron Radiographic Inspection

Neutron Radiographic (N-ray) inspection is a relatively new technique that provides a non-destructive method of detection of gross internal defects, primarily delamination, of multi-layer ceramic capacitors.

The method is usually applied to fired ceramic elements prior to application of the termination material and lead attachment. This permits inspection of the total internal structure of the element.

The elements are placed between radiographic film and a gadolinium screen. The planes of the capacitor electrodes are perpendicular to the film and screen. A beam of neutrons derived from a nuclear reactor is directed through the film between the parallel electrodes.

The neutrons tend to be attenuated by the ceramic material. However, in these areas where gaps (delaminations, large voids) exist, the neutrons are less attenuated and many will strike the gadolinium screen. As the neutrons strike the screen, electrons are released and reflected back through the element and activate the sensitive radiographic film. Development of the film provides an image of the defect. Inspection of the film allows identification and removal of capacitor elements with defects.

The effectivity of N-ray is affected by a number of variables, particularly the composition of the ceramic material and its relative dielectric constant. Since these characteristics tend to vary between manufacturers, the inspection techniques need to be adjusted accordingly.

As of this point in time, N-ray has the capability to detect delamination down to .001 inch of separation in the viewing plane. The length along the active electrode detectable would include that portion that is .001 inch or more in separation.

With this capability, N-ray is a useful non-destructive inspection tool for detection of seriously delaminated elements so they can be removed from the lot.

N-ray as presently performed does not have capability to detect the smaller defects such as voids within the dielectric structure. Void type defects are known causes of capacitor breakdown and failure.

It is hoped that further refinement of the N-ray process can lead to detection of these smaller defects.

Ultrasonic Inspection

Ultrasonic inspection is another non-destructive type of inspection technique for detection of gross internal defects, primarily delamination, in multi-layer ceramic capacitors.

As with the N-ray technique, this method is applied to fired ceramic capacitor elements prior to end metallization and lead attachment.

The technique involves placing the capacitor elements on a flat surface immersed in water. The elements are oriented with the electrode planes parallel to the flat surface.

Pulses of ultrasonic energy are focused and directed through the water to impinge on the flat surface of the element. A portion of the energy is reflected by the top surface. The remaining energy is transmitted through the element and is reflected from the bottom surface. Displayed on a suitable time base, the reflected energy pulses will be separated proportional to the element thickness. If a delamination type of defect exists within the element, a reflection of part of the energy will occur at the delamination plane. This response can also be displayed and will appear between the responses represented by the top and bottom surfaces.

The effective diameter of the focused beam of energy at the element surface is approximately one millimeter (.040 inch). To totally inspect elements of larger dimensions, the beam is moved across the length of the

element several times to scan the entire surface.

The system can be mechanized to scan a large number of elements, detect the responses, and convert them to images on sensitized paper. The images will show the outline of the capacitor and the areas where delaminations exist. The elements identified in this manner can then be removed and rejected.

The effectiveness of ultrasonic inspection is considered to be similar to N-ray in that large delaminations can be identified; however, small voids are not revealed with the present state of this technique.

The utilization of this technique is considered useful in that elements with gross delamination defects can be removed from the lot prior to additional manufacturing operations.

Destructive Physical Analysis

Destructive Physical Analysis (DPA) provides a means for detailed analysis of the internal structure of multi-layer ceramic dielectric capacitors. Defects of all types discussed under the section "Defects and Anomalies" above are detectable utilizing DPA.

DPA can only be utilized on a sample of any lot of capacitors, however, it does provide a method whereby the design and inherent quality of structure can be judged, and provide information for further actions that can be taken to assess the quality of the entire lot.

DPA as conducted by TRW DSSG, consists of taking a random sample, usually five pieces, from a unique lot of ceramic capacitors. A unique lot is defined as all capacitors of a given part number, manufactured and tested as a single manufacturing lot from a single part manufacturer.

The capacitors, if of the encased, leaded types, are first subjected to terminal strength tests. Following these tests, the plastic cases are chemically removed to permit inspection of the external surfaces of the element, terminations and lead attachment.

The elements are then cast in clear plastic mounts and metallurgically cross-sectioned and polished perpendicular to the electrode planes at the approximate mid-section of the element. This provides a view like that shown in Figure 3.

Visual inspection of the cross-section at high magnification will reveal the presence of the types of defects that may exist. The samples can be compared with each other to verify a homogenous lot. The defects noted can be measured and compared to specified limits. The DPA results will then be utilized to determine what further disposition should be made of the parent lot.

At TRW DSSG, lot dispositions are based on engineering evaluation of the DPA and include:

- o Use-As-Is,
- o Return-to-Supplier,
- o Re-Screen,
- o Scrap.

A summary of DPA results at TRW DSSG is covered later in this paper.

Summary of Methods

The various methods of detection of defects in multi-layer ceramic dielectric capacitors are shown in Table I. Each method has merit and all methods have been utilized by capacitor manufacturers and users singly or collectively to aid in detection of defects prior to delivery of finished parts or utilization in electronic systems.

ESTABLISHED RELIABILITY SPECIFICATION MIL-C-39014

MIL-C-39014 and its associated detail specification sheets define qualification, acceptance inspection, and failure rate determination tests for a broad series of general purpose ceramic dielectric capacitors.

The "CKR" styles defined by this document are available from a number of sources and have been widely used in military, launch, and space systems since this specification was developed in the 1960's.

As shown in Figure 4, CKR capacitors are manufactured and then subjected to a 100-percent sequence of thermal shock, voltage conditioning and final electrical measurements. At the lowest failure rate level "S", 100-percent x-ray inspection is performed.

A limit on the number of failures allowed in a given lot is specified.

If the failure limits are met, visual, workmanship, and marking characteristics are inspected on a sampling basis. The capacitors are available for shipment following completion of the Group A test sequence.

Samples are drawn from each inspection lot for period testing to maintain product quali-

fication and accumulate life test hours for failure rate determination.

The testing program under MIL-C-39014 is reasonably stringent and does a good job of screening out most capacitors that might otherwise fail early in system use. However, two aspects of the testing program raise questions about the suitability of CKR capacitors for high reliability applications unless additional steps are taken by the manufacturer or user.

o The allowed number of failures, on a percentage basis, is based on a full week's production of all capacitors within a given style. As a broad range of values are included, an individual group of capacitors within the lot could have a high failure rate during test, but its contribution to the overall percentage could be small if other groups show a low failure rate.

o Considering the high volume of production, the number of samples taken for periodic testing is small, and not all items manufactured are truly represented in the periodic testing.

For the user who is faced with meeting stringent reliability requirements, such as in spacecraft systems, additional assurance of quality and reliability of these capacitors is required before end-item installation.

Efforts to upgrade MIL-C-39014 have been made over the years, however, implementation of some of the techniques covered in this paper have been resisted because of the potential cost impact to the non-high reliability users, who do not have the space application reliability requirements.

The bulk of the usage of CKR capacitors has been in military ground, field, avionics, and shipboard systems. In these types of applications, repair and service of the equipment is often feasible. Part failures in these types of maintainable systems, while not desirable, do not have the same impact as a similar type of failure occurring in an orbiting communications satellite or deep space probe.

To overcome some of the limitations of MIL-C-39014, the high-reliability users have taken various steps to assure themselves that their ceramic capacitors are inherently of high quality and free of defects that can cause failures in long-term applications.

A few of these steps are:

o Preparation of customer part specification documentation. User defines his own quality, screening, special inspection requirements over and above those defined in MIL-C-39014. This may include one or more of the techniques covered earlier in this paper.

o Performs in-house re-testing of capacitors under the same or more stringent conditions than specified in MIL-C-39014.

o Performs detailed analysis on samples from each lot to assess quality and acceptability - a process commonly called Destructive Physical Analysis.

Implementation of these additional steps have both a cost and schedule impact on the part user. They tend to raise the cost significantly on an item that is otherwise competitively priced as a standard CKR. Part of the cost impact is related to the relatively small quantities of individual part numbers required for the high-reliability programs.

In addition, the proliferation of "non-standard parts" represented by the customer part specifications does nothing to enhance parts standardization activities that are an important aspect of program management.

CERAMIC CAPACITORS AT TRW DSSG

TRW DSSG utilizes a broad range of monolithic multi-layer ceramic capacitors in all space programs. In the circuit population of capacitors, ceramic styles fulfill more than one half of the requirements.

The MIL-C-39014 CKR styles are the most commonly used types. However, as is the policy in most high-reliability oriented organizations, additional steps are taken prior to use to assure acceptance of only high quality, inherently reliable capacitors.

The major effort expended to obtain this assurance is Destructive Physical Analysis, discussed earlier in this paper.

Table II summarizes the DPA activities over the 1977 - 1980 time period at TRW DSSG. Out of 370 unique lots of capacitors procured over this time, 100 lots, or 27 percent, were judged "unsatisfactory" as a result of DPA. Those lots rated "satisfactory" were accepted for use without additional evaluation or testing.

Eleven of the lots were designated "use-as-is" after engineering review of the DPA results was made. The decision to use is based on the design of the capacitor, actual nature of the identified defect and history of similar items.

It was possible to negotiate a "return-to-supplier" disposition on 30 lots. Had this not been possible, many might have been rescreened, designated for non-high-reliability applications or scrapped as appropriate.

A total of 13 lots were scrapped without further evaluation. The total part quantities represented by these did not warrant expenditure of additional effort.

The remaining 49 lots were designated "rescreen". This process is basically a repeat of the thermal shock - voltage conditioning with associated electrical measurements. A low impedance, fused burn-in circuit is utilized for voltage conditioning. This is considered a very effective circuit to screen capacitors. Capacitors tested in this fashion have not failed in system use.

Table III shows the results of rescreening of the 49 lots. The 37 lots considered acceptable showed failures totaling 1.1 percent, while those 9 lots that were rejected had more than 21 percent failures.

It should be noted that 27 percent of the lots designated as "unsatisfactory" included only 17 percent of the procured parts. Review of these shows that the larger capacitance values that require more electrodes in the element, tend to show more defects than smaller capacitance values with fewer electrodes. Also, the lot quantities of large capacitance values tend to be smaller than the lower capacitance values.

However, defects have been detected in capacitors across the full range procured and rescreening has been performed on all styles.

At TRW DSSG, as well as at other organizations engaged in high-reliability programs, the total effort to perform analyses, rescreening and other tests add significantly to the cost of acquisition of MIL-C-39014 capacitors. The impact to program schedules is also of concern, however, the positive aspect of these efforts has been the minimization of failures in the electronic systems they are utilized in.

NEW HIGH RELIABILITY CERAMIC CAPACITOR SPECIFICATION

Over the past several years, various individuals and organizations have stressed the need for a new document to define and control requirements for ceramic capacitors suitable for high reliability applications.

An Ad-Hoc committee to develop these requirements was organized under the sponsorship of the Electronic Industries Association. Active participation on this committee included representatives of the ceramic capacitor manufacturers, agencies of the Department of Defense, the National Aeronautics and Space Administration and of the contractors engaged in design and manufacture of high-reliability systems.

The goal of the committee was to develop a specification that would incorporate appropriate test methods and requirements over and above those presently in MIL-C-39014 that have been shown effective in identification and elimination of defects. In addition, the definition of a series of standard parts that will cover a broad range of user requirements was included.

Figure 5 shows the sequence of inspections and controls that are imposed for the new specification which will be issued as MIL-C-123.

A key factor in the specification is the definition of a unique lot of any given capacitor rating. Each lot of capacitors of a given design and rating is formed from a single batch of raw materials, processed and tested as a single lot. Percentage of allowed defects at any inspection or test point applies only to a single lot. No averaging of data for several lots is permitted. Each lot is significantly sampled for long-term life testing, with no product shipped until the lot has satisfied all requirements.

Another interesting set of controls is the imposition of in-process requirements for 100-percent non-destructive inspection (N-ray or ultrasonic) prior to end metallization and lead attachment, sample DPA, 100-percent pre-encapsulation visual inspection and sample terminal strength tests.

These requirements provide "up-front" verification of the basic quality of the capacitors prior to completion of the manufacturing process. As discussed earlier in this paper, both the non-destructive inspection and DPA are effective methods for elimination of individual defective units, or identification of a defective lot. Imposed at this point in the process, costs of further processing and testing substandard parts are eliminated.

Following completion of manufacturing, the capacitors are subjected to "Group A Inspection", to a sequence of environmental exposures and tests similar to those in MIL-C-39014. However, during voltage conditioning, two sets of failure limits are imposed. The first limit allows a maximum of 3 to 5 percent failures (depending on capacitance value) throughout the test. The second limit of 1 part or .1 to .2 percent (depending on capacitance value) is

applied for the last 50 hours of conditioning.

This concept allows for early failures of marginal parts that may escape the in-process non-destructive test, but puts a tight limit on the later portion of the test to assure a low failure rate for delivered lots. The voltage conditioning is performed under accelerated temperature and voltage conditions, which is intended to force failures of marginal parts without damage or degradation to acceptable parts. Following completion of the 100-percent thermal shock - voltage conditioning and associated electrical measurements, visual and mechanical inspection is performed on a sample basis.

Destructive Physical Analysis is again repeated on a sample from the lot. At this point, the DPA samples are representative of a completely manufactured and tested lot. Failure to meet DPA criteria will require the entire lot to be rejected.

At the completion of the Group A inspection sequence, samples are drawn from each unique lot for the performance of environmental and physical tests under Group B and Group C inspection sequences.

The Group B sequence includes a significant sample exposed to an accelerated life test of 4000 hours duration. A performance check is made at the end of the first 1000 hours of this test. If life test failure limits are met (0 failures in 25 pieces or 1 failure in 80 pieces) the parent lot from which these samples are taken is released for shipment.

No mixing of lots is permitted in Group B so each unique lot of capacitors produced under the new specification has its own "pedigree" insofar as life testing is concerned.

Under Group C inspection, samples are accumulated over a two-month production period so as to represent all styles produced. Failures in excess of those allowed require discontinuation of shipment and corrective action to determine and eliminate the cause of the failures.

In addition to the specific controls and requirements for design, manufacturing and inspection, the new specification requires that the manufacturer prepare baseline design and manufacturing documents that are reviewed and approved by the cognizant government agency. Strict adherence to the baseline is required to maintain approval. A stringent initial qualification program is also required to obtain approval to furnish capacitors to this specification.

It is anticipated that ceramic capacitor manufacturers who intend to pursue approval will establish new techniques and equipment to meet the stringent requirements. Adherence to present standards of manufacturing MIL-C-39014 capacitors may not be adequate, as has been shown earlier in this paper. The manufacturer will be assuming new responsibilities for product quality under the new requirements.

There is no doubt that capacitors produced to meet the requirements of specification MIL-C-123 will be more costly than the CKR types. However, the additional costs to assess their inherent quality and inherent reliability by the user should be significantly reduced. Costs of additional DPA, rescreening and other special (and costly activities) by the user should significantly reduce through use of MIL-C-123 capacitors.

In addition, the detail specification sheets that define special requirements for individual parts provide an optimum range of capacitance values, voltage ratings and case styles that will satisfy the bulk of the needs for ceramic capacitors in both stable and general purpose dielectrics, cased, leaded capacitors and unencapsulated chip styles. Detail requirements for discoidal elements will also be included. These types of elements are intended for use in feed-through capacitor and electromagnetic interference filters. This will aid in the goal of reducing the number of non-standard items required for high-reliability programs.

STATUS OF DOCUMENT

As of the date of preparation of this paper, MIL-C-123 is in final editing at the Defense Electronics Supply Center. Final release is expected by mid-1981. The NASA-Marshall Space Flight Center is designated as the preparing activity.

The requirements for Destructive Physical Analysis have already been published by the Electronics Industries Association. In order to provide these requirements in a manner that would allow implementation in other part specifications and standards, the ad-hoc committee elected to prepare DPA procedures and criteria as a separate document.

This document, Standard Test Method RS-469, "Destructive Physical Analysis of High-Reliability Ceramic Monolithic Capacitors" was published in November, 1980 and is available for use wherever implementation of DPA is desirable.

CONCLUSIONS

Monolithic multi-layer ceramic dielectric capacitors, widely used in conventional military systems and high-reliability space applications are primarily the MIL-C-39014 styles. As has been shown in this paper, additional requirements are imposed on these items when the end-item usage requires additional quality and reliability assurance.

Taking advantage of techniques developed for this purpose, a new specification has been prepared to define controls and requirements that will yield high reliability ceramic capacitors. Additional testing and evaluation by users with the attendant cost and schedule impacts should be significantly reduced.

As a user of monolithic ceramic capacitors in high-reliability applications, the author encourages the consideration and utilization by others of the new MIL-C-123 styles of capacitors as they become available.

ACKNOWLEDGEMENTS

Many individuals from several industry and government organizations have actively participated in preparation of MIL-C-123 and RS-469. Acknowledgement of their contributions is appropriate. Some of these people are:

E. A. Bolton
AVX Ceramics

R. Stark
Sprague Electric Company

R. M. Regner
Union Carbide Corporation

T. J. Brown
Corning Glass Works

M. Rosenberg
San Fernando Electric

F. A. Duva
Vitramon, Inc.

S. W. Cohen
Aerospace Corporation

E. B. Thornley
TRW Defense and Space Systems Group

R. Swart
Formerly with Vitramon, Inc.

L. Hamiter
NASA/Marshall Space Flight Center

W. Heckman
Defense Electronics Supply Center

There are undoubtedly others from these organizations who have participated in this effort. The author regrets the omission of their names, but acknowledges their contributions.

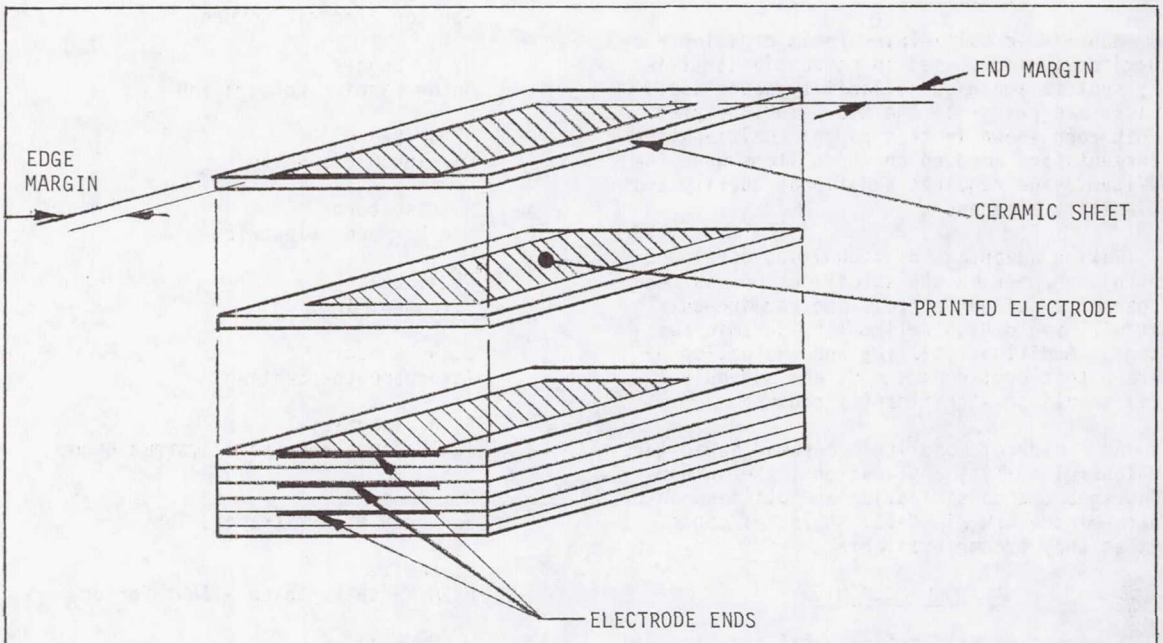

FIGURE 1. MONOLITHIC CAPACITOR STACKING ARRANGEMENT

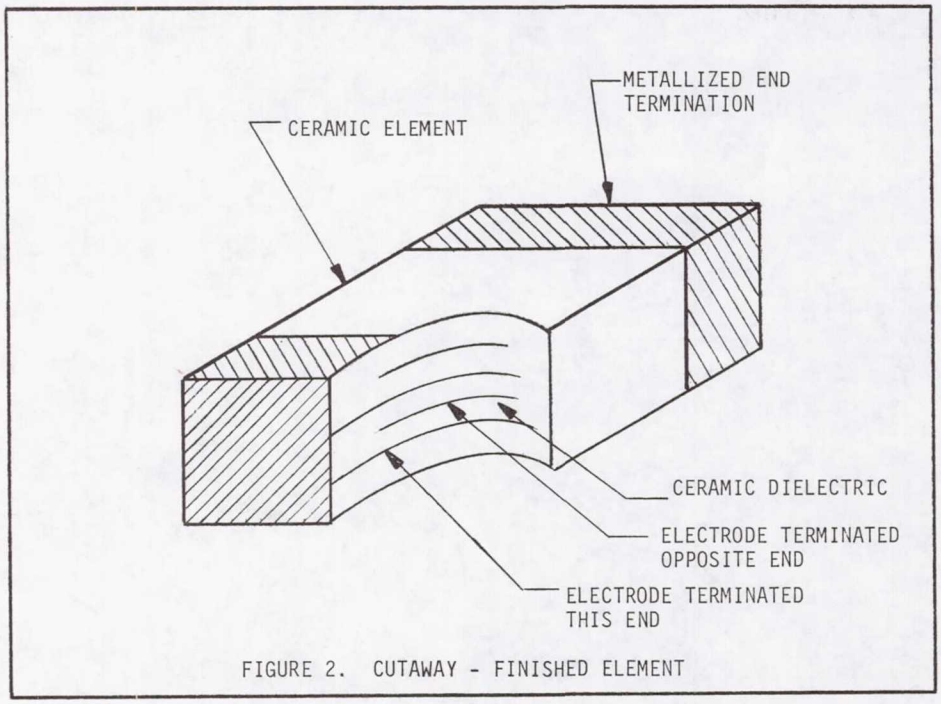

FIGURE 2. CUTAWAY - FINISHED ELEMENT

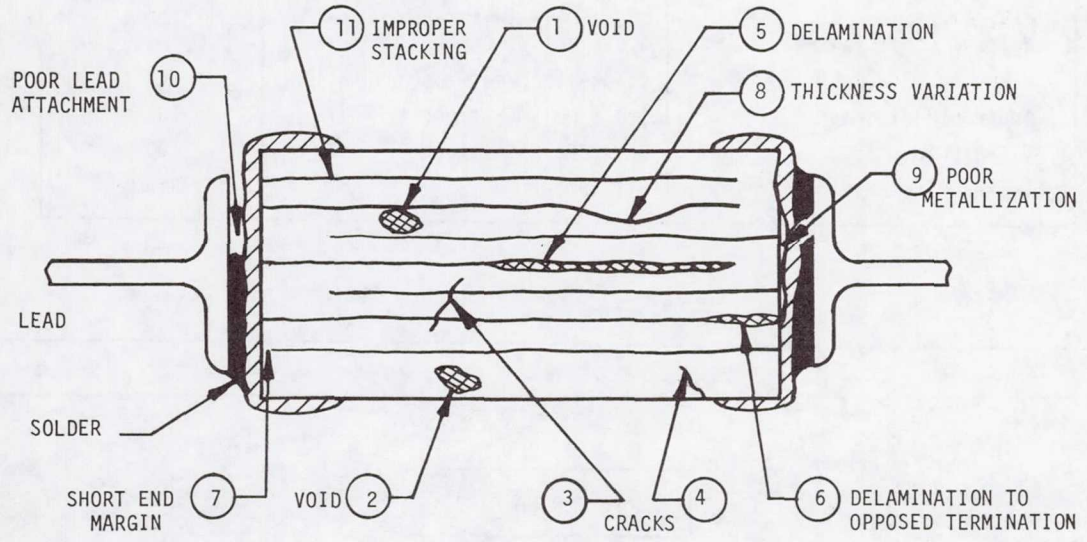

LONGITUDINAL SECTION

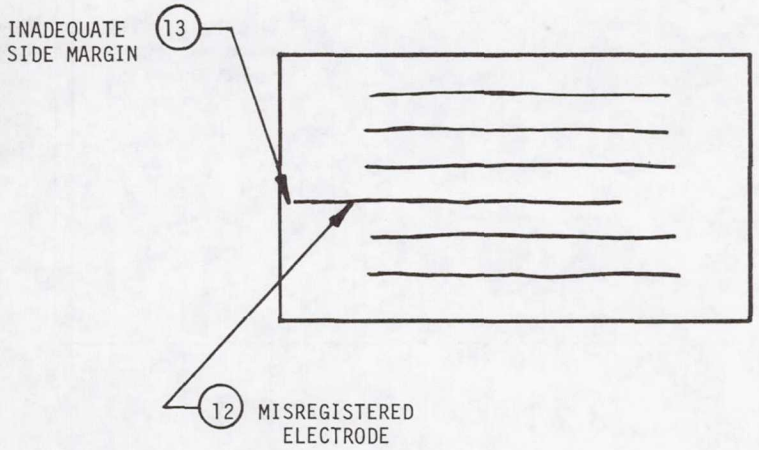

TRANSVERSE SECTION

FIGURE 3. CROSS-SECTIONED CAPACITORS

TABLE I. DEFECT DETECTION METHODS

METHOD	DEFECTS DETECTABLE	INSPECTION LEVEL
Thermal Shock - Voltage Conditioning	Gross Delaminations, Gross Voids, Cracks	100 %
X-Ray	Lead Attachment, Encapsulation	100 %
Neutron Radiographic	Gross Delaminations	100 %
Ultrasonic	Gross Delaminations	100 %
Destructive Physical Analysis	All Types	Sample

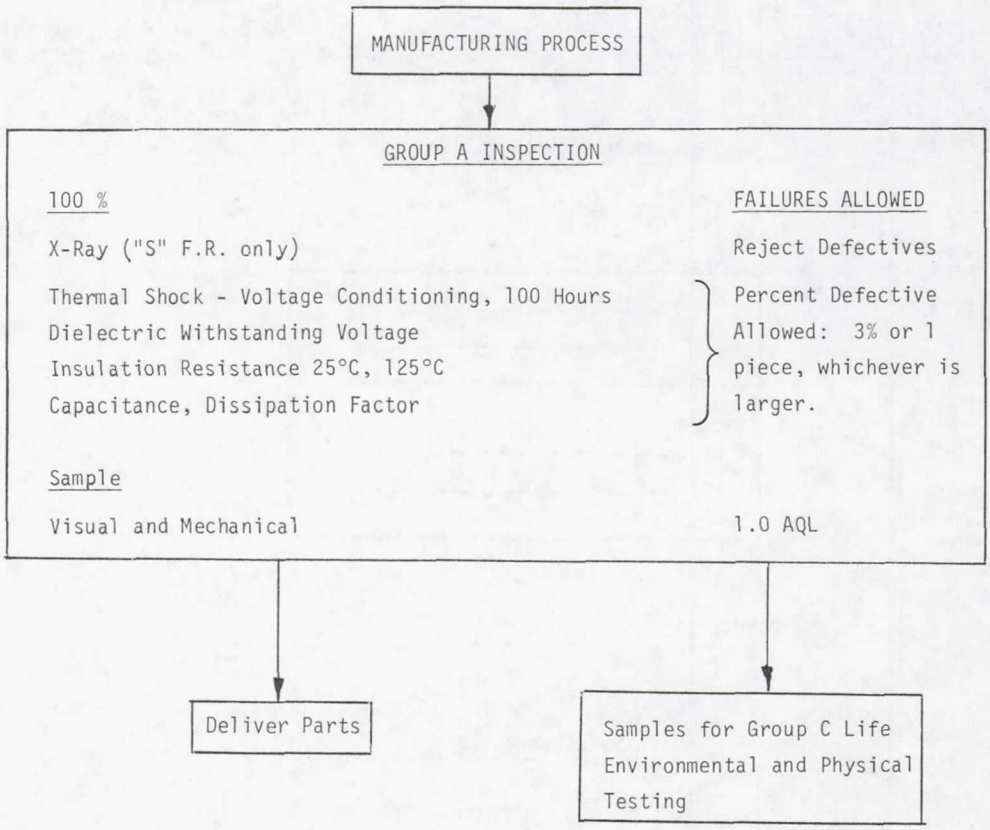

FIGURE 4. MIL-C-39014

SUMMARY OF DPA AT TRW DSSG
1977 - 1980
MIL-C-39014 CAPACITORS

TABLE II

	LOTS	PARTS
NUMBER PROCURED	370	101,664
• Satisfactory DPA	270	83,919
• Unsatisfactory DPA	100	17,745
DISPOSITION OF UNSATISFACTORY DPA:		
• Use-As-Is	11	3,614
• Return to Supplier	30	6,200
• Scrap	13	610
• Rescreen	46	7,321

RESULTS OF RESCREENING

TABLE III

	LOTS	PARTS	RESCREENING FAILURES	
			PARTS	PERCENT
NUMBER ACCEPTED	37	4992	58	1.1%
NUMBER REJECTED	9	894	190	21.2%

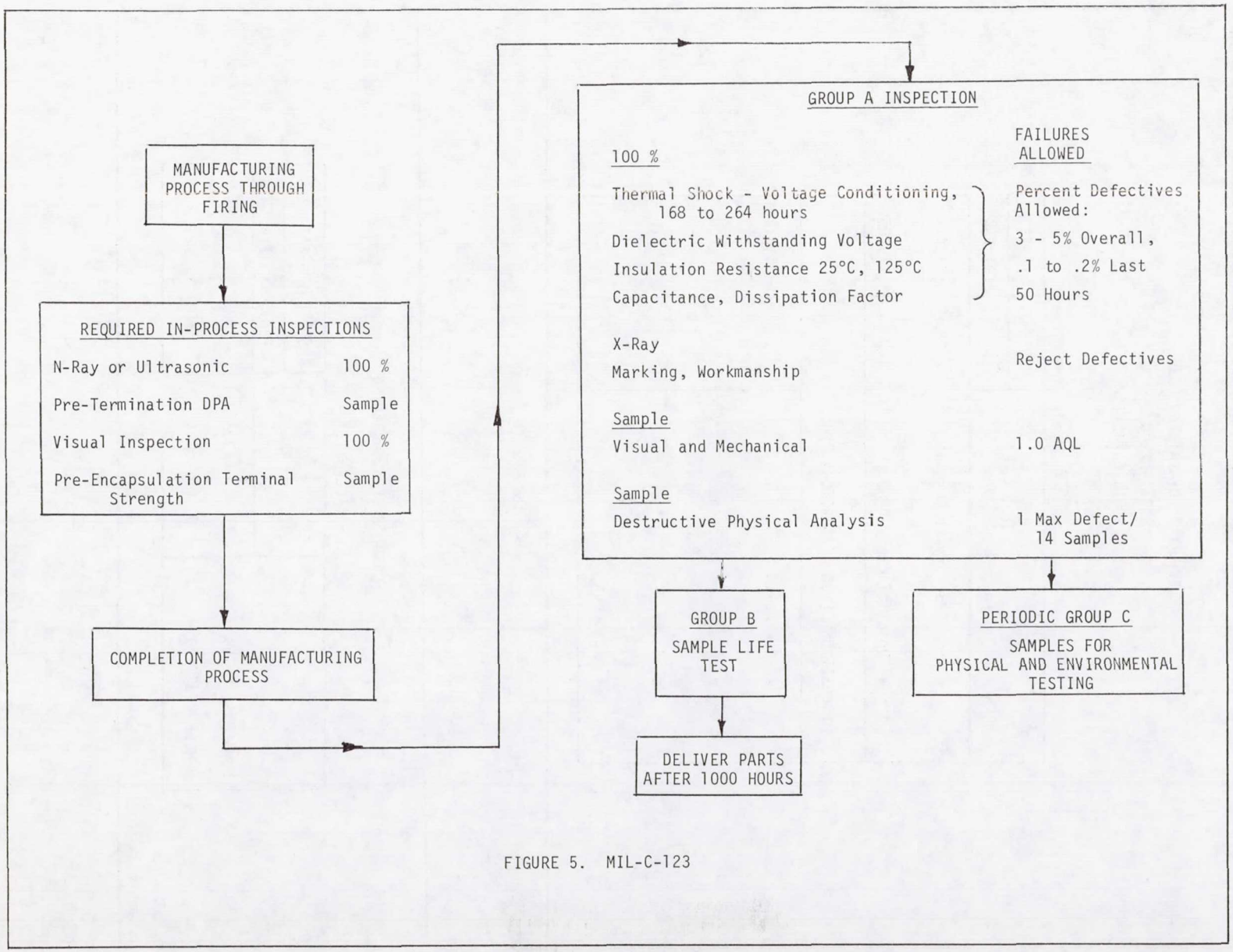

FIGURE 5. MIL-C-123

CAPACITORS, THERMAL RATING/DERATING (AC-DC OPERATION)

by J. W. Borough
Northrop Corporation Electronics Division
2302 W. 120th Street
Hawthorne, California 90250
(213) 615-3023

SUMMARY

In order to optimize equipment designs within the constraints of current Hi-Rel systems, designers need to know component performance and ratings as a function of thermal environment. For capacitors, historically this need has been satisfied by assuming a worst-case condition usually based on life tests performed in still air with no heat sink. This approach is not adequate for the requirements being experienced today.

Reductions of weight and volume are realized when a simplified thermal model of the capacitor is used in place of worst-case data. This paper describes application techniques for determining performance and ratings of cased capacitors under combined AC-DC operation as a function of the actual operating conditions. Thermal impedances between the case and external environment and between the internal "Hot Spot" and case are taken into account.

INTRODUCTION

When components such as capacitors are operated in service conditions, stresses experienced do not relate directly to the life test conditions upon which ratings are customarily based. Typically, capacitors are life tested with a fixed DC voltage applied, suspended by the leads in still or forced air at a controlled temperature. Voltage and temperature ratings based on this type of test lose significance when there is an AC voltage applied which causes some degree of self heating.

The AC life test has been used in some cases to address this problem. The most conservative method readily available for mounting, suspension in free air by the leads, has been used for CLR79[1] capacitors. This method is quite acceptable from a conservative point of view because all applications employ some heat sinking or forced air cooling.

The problem addressed in this paper appears when the attempt is made to maintain or improve performance of standard circuits with increasing constraints on size and weight of packaged systems. For example, filter capacitors across the output of DC power supplies are usually limited to rated AC ripple currents determined by free air life tests. Actual useage heat sinking provides for removal of heat at a faster rate permitting a higher ripple current for the same internal hot spot temperature. If a more realistic rating scheme, based on the heat flow characteristics of the device, were to be applied, designers could take advantage of their estimates of the thermal environment to optimize capacitor selection. An increase in ripple current per capacitor implies a reduction in the number of capacitors or an increase in performance at the same volume.

This paper presents an approach to thermal rating which takes into account the use environment.

THERMAL MODEL

The model to be employed is designed to take into account the hot spot concept in which temperature is directly related to reliability. A distributed internal heat source of magnitude equal to the power input is assumed. The hot spot temperature is assumed to increase linearly with power dissipation for any fixed mounting/cooling configuration.

There are two regions of thermal gradient which must be considered:

I. Internal, $\Delta T_I = T_{HS} - T_C$ where the internal temperature rise, ΔT_I, is defined as the difference between the hot spot temperature, T_{HS}, and the case temperature, T_C.

II. External (mounting), $\Delta T_C = T_C - T_A$ where the case temperature rise, ΔT_C, is defined as the difference between the case temperature, T_C, and the mounting surface temperature, T_A.

Specifically we assume that the temperature rise across both of these regions is proportional to the heat (power) flow through them:

Region I $\Delta T_I = \theta_I P$ (1)

Region II $\Delta T_C = \theta_M P$ (2)

where θ_I and θ_M are the respective net thermal impedances for the two regions and P is the total dissipated power.

The hot spot temperature is then written as:

$$T_{HS} = T_A + \Delta T_C + \Delta T_I \quad (3)$$

$$= T_A + P(\theta_M + \theta_I) \quad (4)$$

Equation (4) is a relationship which can be used to calculate (predict) T_{HS} for a specific application given a mounting surface temperature T_A and the dissipated power, P. This can be compared to a "rated" maximum T_{HS} to be developed through testing. θ_M and θ_I can be estimated by calculation and can be verified by infrared scan temperature measurements.

It should be noted that the case temperature and the mounting surface temperature are implicitly assumed to be uniform over their respective regions. This is reasonable since these regions normally have high thermal conductivity and do not contribute appreccіably to the temperature rise as do the intermediate regions.

APPLICAITON OF THE MODEL

In the applicaiton of equation (4) there are two parameters related to the capacitor design and consequently involved in the rating of the capacitor; these are T_{HS}(max) and θ_I. Two other parameters are related to the application and must be determined by the system designer; they are T_A and θ_M. The fifth parameter P determines the actual hot spot temperature in a given operating situation.

T_{HS}(max) may be estimated from knowledge of materials and internal construction; it would be the maximum T_{HS} consistant with a minimum reliability standard. As a starting point T_{HS}(max) should be limited to values below any melting points or other temperatures where physical changes such as crystal structure modifications take place. It should be assumed that any such critical temperatures related to structural or functional materials of the capacitor must not be exceeded. Equation (4) may be used to calculate the nominal T_{HS} for a given operating condition to determine acceptability. The absolute accuracy of this calculation will depend on the accuracy of the determination of the remaining parameters.

θ_I, the other parameter related to the capacitor, must be calculated from a detailed thermal model of the capacitor. where uncertainties arise, assumptions should bias the value of θ_I toward the high side in order to keep the estimate conservative for worst case T_{HS}. Uncertainties in θ_I can come from variations in internal geometry which are to some extent predictable based on differences in nominal capacitances and voltage ratings within the general family. More than one θ_I could be required to represent all the capacitors available in a given case size for a family. Another important consideration is the contribution of the leads to θ_I. The leads will remove heat and will lower the effective θ_I depending upon the efficienicy of the heat sinking of the leads. A conservative approach would be to ignore the leads in the model and consider only heat removal through the case.

θ_M and T_A represent the outside thermal world to the capacitor and are determined by the system design. θ_M may be calculated through considerations of material properties and geometry for the mounting interface. T_A may be calculated from known system parameters or measured on working models as part of a general thermal mapping. θ_M may be verified easily by measurements of T_C and T_A at specific operating conditions.

P must then be limited in actual service to a value which will give a conservative prediction from equation (4) of T_{HS} below (less than) the established T_{HS}(max).

Ultimately, established reliability (ER) specificaitons should relate failure rates to T_{HS} with a specified tolerance on θ_I. With heat sinking controlled for AC tests results would be much more meaningful independant of considerations for θ_I.

EXAMPLE: CLR79 TANTALUM CASED TANTALUM

The example chosen is of interest because these capacitors are being used to replace silver cased wet slug and solid tantalum capacitors where ripple currents are significant. The CLR79 type has an inherrant ripple current capability far exceeding either of the previous designs. The question immediately arises as to how much ripple current a given CLR79 can take in a given thermal environment, i.e. given (θ_M, T_A). This question can be approached by using equation (4) to establish a maximum power from which a maximum ripple current can be calculated. Since internal designs vary

among suppliers the user must be concerned with determining θ_I and T_{HS} for all styles from all manufacturers.

Internal Thermal Impedance - θ_I

Manufacturers data[2] includes standard power ratings for each case size based on a 50°C internal temperature rise (ΔT_I). The ratings relate to operation in 85°C still air. An estimate of θ_I can be obtained directly from these ratings for each case size.

CASE SIZE	SPRAGUE RATED POWER (WATTS)	CALCULATED θ_I (C°/W)
T1 (C)	1.0	50.0
T2 (F)	1.50	33.3
T3 (T)	1.75	28.6
T4 (F)	1.95	25.6

Maximum Hot Spot Temperature - $T_{HS}(max)$

An estimate of $T_{HS}(max)$ can be made by considering equation (3) as it applies to standard ripple current life test conditions for which characteristics are known. The free air temperature (T_A = 85°C) takes the place of a mounting surface temperature and the case temperature rise, ΔT_C is determined by the power dissipated across the interface between the case and ambient air. Internal temperature rise, ΔT_I, is assumed to be 50°C, the maximum permitted. Curves are given in the references[3] which yield the following values of ΔT_C at rated maximum ripple currents for two capacitor types in each of the four case sizes:

CAPACITOR TYPE	CASE SIZE	ΔT_C AT STD 40 kHz CURRENT (C°)	
3.6uF,125V	T1(C)	120	
10uF, 50V	T1(C)	125	
47uF, 50V	T2(F)	60	Mean = 67.2°C
100uF, 25V	T2(F)	66	Standard
25uF, 125V	T3(T)	65	Deviation =
56uF, 75V	T3(T)	70	6.7°C
300uF, 30V	T4(K)	63	
1200uF, 6V	T4(K)	69	

Since our estimate of $T_{HS}(max)$ is intended to be conservative we select 60°C (the lower one sigma limit) for $\Delta T_C(max)$. More extensive data would result in a better estimate. Applying equation (3) to the worst case we have:

$$T_{HS}(max) = T_A + \Delta T_C(max) + \Delta T_I(max) \quad (5)$$

$$= 85°C + 60°C + 50°C = 195°C \quad (6)$$

We have established a new rating parameter which can be derated in accordance with a rule determined by system reliability requirements. A typical rule states $T_{HS}(max)$ must be derated 30°C for nominal operating conditions and 15°C for worst case conditions. Thus:

OPERATING CONDITION	$T_{HS}(max)$
Rated	195°C
Nominal	165°C
Worst case	180°C

Typical case

Let us consider a specific capacitor say M39006/22-0216. This capacitor's characteristics[1] are 25uF, 125Vdc, T3 case, 1200 mA (rms). Manufacturer's data[2] indicates a maximum equivalent series resistance (ESR) of approximately .6 Ω at 40 kHz in the internal temperature range of 160 to 200°C (obtained by extrapolation of ESR vs temperature for the case where no power is dissipated). We assume:

T_A = 70°C, mounting surface temperature

θ_M = 20°C/watt, mounting thermal impedance. Using our estimate above for the T3 case we then apply equation (4) and

$$I = \sqrt{\frac{P}{ESR}} \quad (7)$$

where P is dissipated power, I is current, and ESR is the equivalent series resistance.

The results for the various operating conditions are:

OPERATING CONDITION	$T_{HS}(max)$ (C°)	P (WATTS)	I (Arms)
Rated	195	2.57	2.07
Derated worst case	180	2.26	1.94
Derated nominal	165	1.95	1.80

The results given compare to the standard rating of 1200 mA (rms) as follows: the new current rating based on $T_{HS}(max)$ is nominally equivalent to but slightly more conservative than the standard rating with respect to stress at the worst case operating condition. Derated currents based on derated $T_{HS}(max)$ which correspond to conservative estimates of power dissipation still exceed the free air rated current.

The results of the example are given for illustrative purposes to show the relative merits of this approach in providing the circuit designer with greater freedom of selection. This technique will permit identification and elimination of situations where over design has been necessary to provide required circuit performance and reliability.

CONCLUSIONS

There is a distinct need to specify more closely the power dissipating capabilities of capacitors for AC applications. Life test conditions should be modified so as to relate better to use conditions. The typical life test condition where capacitors are suspended in free air is difficult to relate to any use condition except to the extent that it may be considered "worst case". Known heat sinks should be used so that the internal characteristics of the capacitors could be verified more accurately. The correlation of, $T_{HS}(max)$, maximum hot spot temperature with failure rate and, θ_I, internal thermal impedance will enable system designers to make very significant improvements in space efficiency ands system performance.

REFERENCES

1. Military Specificaiton MIL-C-39006/22B; Capacitors, Fixed, Electrolytic (nonsolid Electrolyte), Tantalum.

2. Engineering Bulletin 3760A, Sprague Electric Company 1978.

3. England, Walter F., Tantalum - Cased Wet-Slug Tantalum Capacitors, Proc. 27th Electronic Components Conference, 1977.

ACCELERATED LIFE TESTING AND RELIABILITY OF HIGH K MULTILAYER CERAMIC CAPACITORS

W. J. Minford
Bell Telephone Laboratories, Incorporated
555 Union Boulevard
Allentown, Pennsylvania 18103
(215) 439-5340

INTRODUCTION

High dielectric constant ceramic multilayer capacitors are becoming more prevalent in telecommunication equipment due to their high capacitance per unit volume and the ever decreasing available circuit board space. These devices are predominantly used for power decoupling and bypass. The degradation of insulation resistance is the primary failure concern; capacitance and dissipation factor shifts are less important because the circuit application is relatively insensitive to these parameters.

This paper addresses the accelerated life testing of insulation resistance failures of high K ceramic capacitors and the estimation of reliability at use conditions. Prokopowicz and Vaskas[1] have modeled the accelerated testing of mid K ceramic multilayer capacitors at elevated temperature and voltage with the formula:

$$\frac{t_1}{t_2} = \left(\frac{V_2}{V_1}\right)^n \exp\left[E_a/k\left[\frac{1}{T_1} - \frac{1}{T_2}\right]\right] \qquad (1)$$

where t is the time to failure, V is the applied DC voltage, and T is the absolute temperature. The subscripts refer to test conditions and k is the Boltzmann constant. The voltage stress exponent, n, was reported as 2.7, and the temperature activation energy, E_a, as 0.90 eV. A voltage stress exponent of three is generally accepted for ceramic capacitors, but an activation energy of 0.3 eV or less is used to estimate temperature effects.[2,3]

Three manufacturers' 50V multilayer ceramic capacitors have been extensively evaluated with all yielding similar acceleration factors of n and E_a. The results of the product with the shortest lifetime is reported here because of the large range of stress conditions tested.

PROCEDURES

Devices

The capacitors tested were .22μf devices rated at 50 volts DC. The internal construction was evaluated from polished sections and SEM micrographs. A dielectric thickness of 36.5μm (1.4 mils) was measured and a dielectric constant of 6700 was calculated. The polished sections also revealed a high frequency of ink line delaminations.

Qualitative compositional analysis was determined with a SEM energy dispersive analyzer. The dielectric was primarily barium titanate with detectable amounts of calcium, zirconium, aluminum, and strontium also present. The electrodes were palladium and silver.

Dielectric Strength

The dielectric strength was measured at 25, 85, 125, and 170°C on samples of 25 devices. An Associated Research DC HYPOT tester was used. The voltage was increased at a rate of 10 V/sec. The device was considered a failure when the current exceeded 8 mA.

DC Resistance

The DC resistance was measured as a function of temperature using a Beckman Megohmmeter. A bias of 10 volts DC was continuously applied with readings taken after the sample was allowed to come to equilibrium at a given temperature ($\sim$10 minutes). The resistances reported were reproducible regardless of increasing or decreasing temperature.

Accelerated Life Testing

An automatic test system controlled by a Hewlett-Packard 9825A calculator was used to evaluate the accelerated life of ceramic capacitors. Each capacitor had a 24 kilohm resistor in series with the DC power supply. The voltage drop across the series resistor was measured with a voltmeter (HP 3455A) and used to calculate the resistance of the capacitor. The resistance was recorded periodically as was the time at which the device dropped below a programmed failure value.

RESULTS AND DISCUSSION

Dielectric Strength

The dielectric strength as a function of temperature is shown in Figure 1. The mean values are represented with 95 percent confidence intervals. The capacitors have a breakdown field greater than that reported for a stannate shifted barium titanate and approximately twice that reported for pure barium titanate.[4] No significant temperature dependence is observed, although the steady decline in dielectric strength above 85°C may be an indication of thermal breakdown.

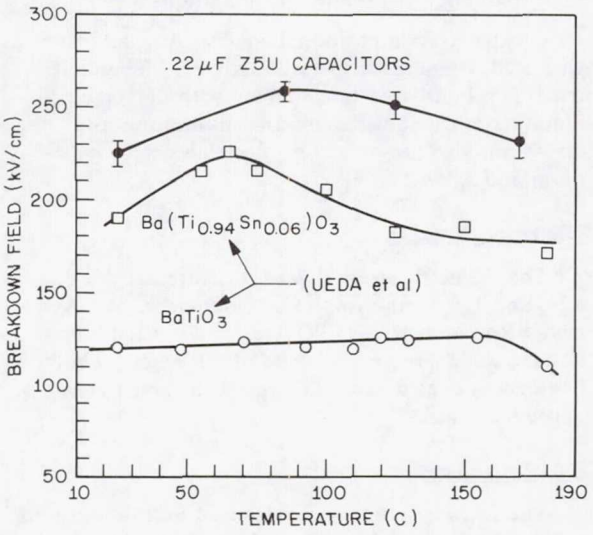

Fig. 1 Breakdown field as a function of temperature.

Due to the high dielectric strength (greater than 800 VDC) of these devices, the accelerated life testing was extended to 400 VDC with reasonable assurance that only the thermal degradation mechanism(s) predominate.

Accelerated Life Testing

Failure Criterion. The DC resistance of a sample of the capacitors, shown in Figure 2, was measured in order to establish a failure criterion that would be consistent for all test temperatures. An activation energy of 1.30 eV was calculated. This value is close to the 1.38 eV activation energy reported for the diffusion of oxygen vacancies in polycrystalline barium titanate,[5] which was proposed as the predominant conduction mechanism below 300°C.[6]

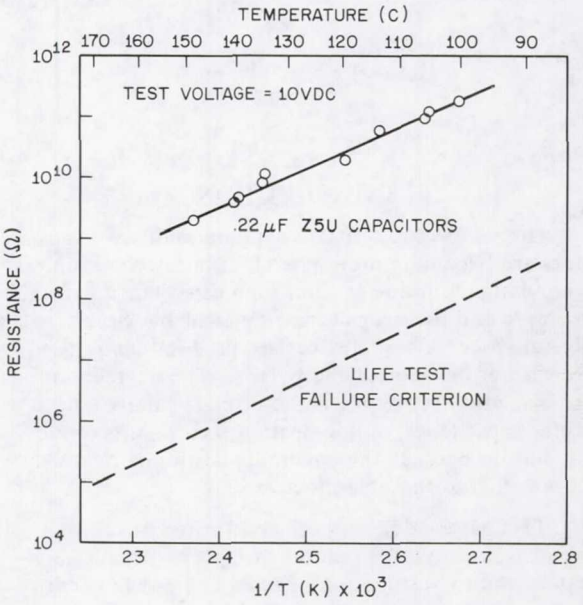

Fig. 2 Resistance as a function of reciprocal temperature at 10 volts DC. Temperature dependence of failure criterion.

The failure criterion used for the accelerated life test is shown as the dashed line in Figure 2. The device was considered a failure when the resistance at the test temperature degraded three to four orders of magnitude below its "equilibrium" value at that temperature.

Modeling. The failure times for the capacitors under all test conditions were lognormally distributed with a standard deviation approximately 0.5. As an example, Figure 3 shows the failure times of devices tested at 170°C and 75, 125, and 200 volts DC. Note the tightly distributed main population. Early failures were observed for some samples as exhibited by the devices tested at 200 volts DC. Due to the appearance of these early failures, the failure times at any stress were characterized by the median and the standard deviation estimated from the tightly distributed "main population". The results are compiled in Table I.

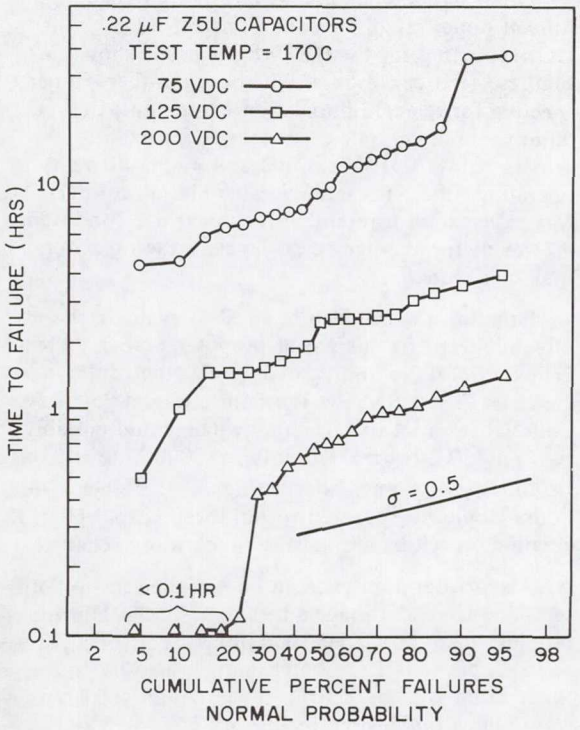

Fig. 3 Times to failure at 170°C and 75, 125, and 200 volts DC for .22μf capacitors.

TABLE I

Accelerated Life Test Results

Test Conditions			Results	
Temp (°C)	Volt (DC)	Amount Tested	Median Failure Time (Hours)	Standard Deviation
170	75	20	9.5	.596
170	125	19	2.5	.326
170	200	20	0.7	.364
150	75	20	36.5	.186
150	125	20	11.2	.199
150	200	20	3.55	.593
125	200	19	24.1	.509
110	400	19	8.2	.732
105	200	19	138.7	.858
105	400	20	13.1	.952
85	200	20	823.7	.800
85	400	19	108.7	.939

In order to model the results equation (1) was reworked as follows:

$$t_1 V_1^n \exp\left(-\frac{E_a}{kT_1}\right) = t_2 V_2^n \exp\left(-\frac{E_a}{kT_2}\right) = \text{constant} \quad (2)$$

Taking the logarithm of both sides, where A is the constant, yields:

$$\ln t = \ln A - n(\ln V) + E_a/kT \quad (3)$$

The capacitors' median lifetimes were least-squares fit to the multiple regression model, equation (3), yielding a voltage stress exponent, n, equal to 2.46 ± 0.23, an activation energy, E_a, equal to 1.19 ± 0.05 eV, and a constant, A, of (6.1 ± 4.0) x 10^{-8} with 95% confidence intervals. The 400 volt test results were not included in the modeling due to an apparent increase of the voltage stress exponent to about 3.0 from the 2.5 value which characterizes all the data of 200 volts and below.

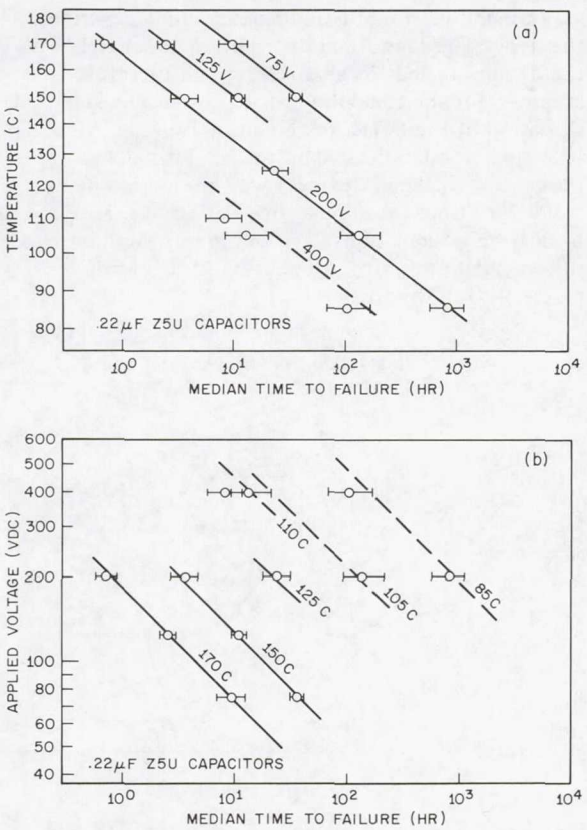

Fig. 4 Median time to failure versus temperature (a) and voltage (b).

Figure 4 shows the median time to failure data with 95 percent confidence intervals as a function of reciprocal absolute temperature (a) and logarithmic voltage (b). The solid lines are the least-squares fit. The excellent fit of the model over the entire temperature range tested, 85 to 170°C, is evident from the 200 volt data in Figure 4(a). Figure 4(b) shows that the model is adequate from 75 to 200 volts but at 400 volts the median lifetimes occur in a shorter time than expected from the remainder of the data (the dashed lines).

The activation energy estimated, 1.19 eV, is in the same range as that measured from the resistance data and that reported for oxygen vacancy diffusion.[5] But Prokopowicz and Vaskas have reported a slightly lower value for a mid-K capacitor, 0.90 eV.[1] The voltage stress exponent, 2.5, is less than the value of 3 commonly assumed.[2,3]

Reliability Estimation

The reliability of devices at any stress can be evaluated by calculating a median time to failure using equation (3) and the estimated coefficients, assuming a distribution and spread which describes the data. The lognormal distribution adequately fits the devices tested for all stresses, and therefore is assumed for the reliability calculations. The standard deviation of the devices is given in Table I. All are less than 1 (much less than the 2.5 normally observed for silicon devices) with no increasing trend with time. A standard deviation of 0.5 will be used for all calculations. An outline of the failure rate calculations using a lognormal distribution is given by Goldthwaite.[7]

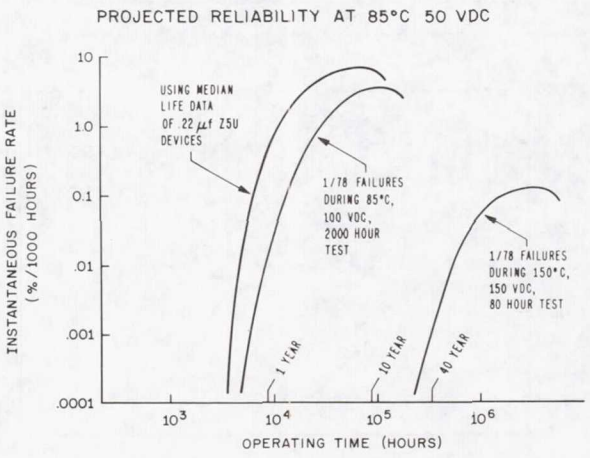

Fig. 5 Estimated instantaneous failure rate versus operating time at 85°C and 50 volts DC.

The instantaneous failure rate versus operating time at upper rated use conditions (85°C, 50 volts DC) estimated for the 0.22 μf devices is shown in Figure 5 (left curve). To put these numbers in perspective for telecommunication equipment, the failure rate of ceramic capacitors is expected to remain below .001% per 1000 hours over 40 years operating time. These devices would fail to meet this expectation if intended for upper use conditions. However, for average stress levels these capacitors may be adequate.

Equation (3) can also be used to evaluate the effectiveness of a current or proposed screening test. Using an n of 2.5 and E_a of 1.19 eV, the center curve in Figure 5 shows the failure rate at 85°C, 50 volts DC of a lot of capacitors which could possibly pass an 85°C, twice rated voltage, 2000 hour life test. Instantaneous failure rates as high as 0.5% per 1000 hours would be expected within three years. High K ceramic capacitors are usually much more reliable.

A short duration test can be designed using both temperature and voltage stress to assure a failure rate less than .001% per 1000 hours over forty years at 85°C, 50 volts DC. For example, a 150°C/three times rated voltage test run for less than 100 hours would have the desired results at 85°C, 50 VDC as shown in Figure 5 (right curve).

SUMMARY AND CONCLUSIONS

The reliability of one lot of high K multilayer ceramic capacitors was evaluated using accelerated life testing. The degradation in insulation resistance was characterized as a function of voltage (two to eight times rated) and temperature (85 to 170°C). The times to failure at a voltage-temperature stress conformed to a lognormal distribution with a standard deviation approximately 0.5.

The results were least-squares fit to the equation:

$$t = A\, V^{-n} \exp\left(\frac{E_a}{kT}\right)$$

with, n, the voltage stress exponent equal to 2.46 and, E_a, the activation energy equal to 1.19 eV. Using this model, the median time to failure at maximum rated conditions (85°C, 50 volts DC) was estimated and failure rates were calculated.

ACKNOWLEDGMENTS

I wish to thank W. A. Baker for many helpful discussions and H. Balk and J. C. Masland for their technical assistance.

REFERENCES

[1] T. I. Prokopowicz and A. R. Vaskas, "Research and Development, Intrinsic Reliability, Subminiature Ceramic Capacitors," Final Report, ECOM-90705-F, October 1969; NTIS AD-864068; 175 pp.

[2] T. Kobayashi, H. Ariyoshi, and A. Masuda, "Reliability Evaluation and Failure Analysis for Multilayer Ceramic Chip Capacitors," IEEE Trans. CHMT–1 [3], 316-324, Sept. 1978.

[3] MIL-HDBK-217B, Reliability Prediction of Electronic Equipment, Sept. 1974, pp. 2.6-1 - 2.6.4.

[4] I. Ueda, M. Takiuchi, S. Ikegamir, and H. Sato, "Dielectric Breakdown of Polycrystalline $BaTiO_3$", J. Phys. Soc., Japan *19* [8] 1267-1273 (1964).

[5] C. Schaffrin, "Oxygen Diffusion in $BaTiO_3$ Ceramic", Phys. Stat. Sol. (a) *35*, 79-88 (1976).

[6] D. D. Glower and R. C. Heckman, "Conduction-Ionic or Electronic - in $BaTiO_3$", J. Chem. Phys., *41* [3] 877-79 (1964).

[7] L. R. Goldthwaite, "Failure Rate Study for the Lognormal Lifetime Model," Proceedings Seventh National Symposium on Reliability and Quality Control in Electronics, January 1961, pp. 208-213.

A CAUSE OF THE NON-SOLDERABILITY OF CERAMIC CAPACITOR TERMINATIONS

M.J. Cozzolino, A. Kumar*, and G.J. Ewell
Hughes Aircraft Company
Culver City, CA 90230
(213) 391-0711
*SEAL, Inc.
Culver City, CA 90230
(213) 822-7474

SUMMARY

One recurrent problem faced by the users of ceramic capacitors is non-solderability; i.e., non-wetting of the base termination by the solder coating. This paper describes the results of an analysis into the cause of the non-solderability of multiple defective part lots from two capacitor manufacturers. This analysis consisted of visual, scanning electron microscopic (S.E.M.), surface, and metalographic examinations and analyses. The results of this analysis indicated that non-solderability results from areas of excess porosity in the termination which are caused by segregation of ink constituents during manufacturing. This segregation can be minimized by proper monitoring and control of process variables; where excess porosity does occur, solderability can be improved by proper precleaning of parts.

INTRODUCTION

Ceramic capacitors have been increasingly used in recent years due to their low cost and high volumetric capacitive efficiency. The first ceramic capacitors utilized air, mica, and other relatively low dielectric constant materials as the dielectric. The outbreak of of World War II and the loss of the supply of the widely used dielectric ruby mica foresaw the development of barium titanate as a substitute. A substitute with a dielectric constant a thousand times that of mica, but also with an extreme sensitivity to changes in voltage and temperature. These first capacitors were discoidal in shape with a rather thick dielectric. With improving technology, the dielectric formulation became more complex with a resulting improvement in electrical characteristic control and the dielectric became thinner with a multilayered structure. The modern multilayered chip capacitor was a natural development of this evolutionary process. This part consists of a series of stacked dielectric sheets which have been silk-screened on a single side with alternatively opposing, overlapping precious metal electrode sheets (Refer to Figure 1 for an illustration of this design). Electrical connection is made to these electrodes via a precious metal termination which is fired onto the ends of the part. These terminations, which were developed from those used as conductors on alumina substrates,

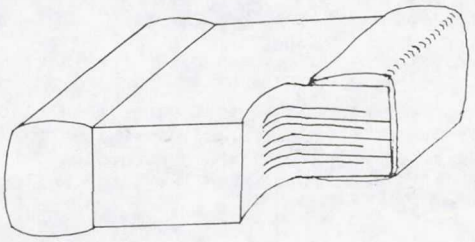

Fig. 1. Multilayered Ceramic Chip Capacitor.

consist of: one or more precious metals for electrical continuity, a glass base to mechanically and chemically interlock the dielectric to the termination, an organic binder to hold the paste together for printing, and solvents and other chemicals to maintain flow characteristics. The terminated parts are either used as they are or are further processed so that leads can be attached or parts can be directly soldered to printed wiring boards. The types of precious metals used in the termination and the processing steps utilized are characteristic of specific manufacturer's processes and the intended use of the parts. (The parts discussed in this paper are all Ag/Pd containing; for improved solder leach resistance.)

One of the recurrent ceramic capacitor problems Hughes has observed is non-solderability (non-wetting of the base termination by its solder coating). This problem has been noted to: 1) occur periodically at many manufacturers, 2) improve with multiple solder coatings, and 3) become more predominate when several days pass between the termination and solder coating processes. To date no cause had been offered for this problem. To counter this problem Hughes representatives monitored ceramic chip capacitor production at two manufacturer's facilities over a period of time. Parts with poor solderability (Refer to Figure 2) were saved an an effort was made to notice characteristics of parts which wet poorly when

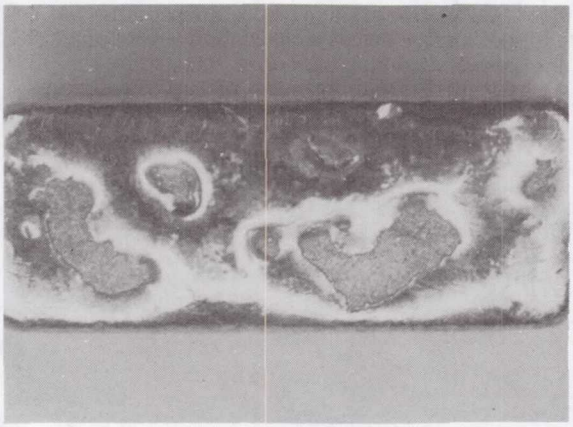

Fig. 2. Poorly wetted capacitor termination.

dipped. It was noticed that parts with rough, dark areas on their terminations (Refer to Figure 3) appeared to have poor solderability. These parts were also saved for later analysis.

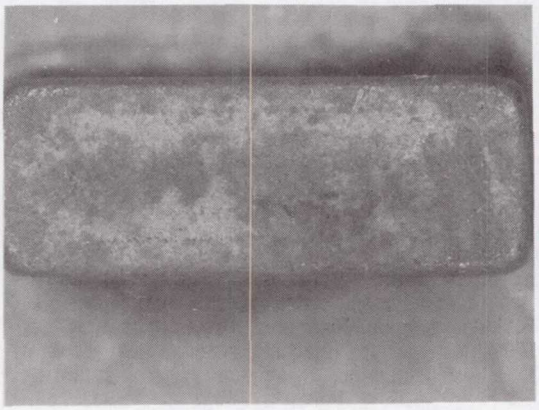

Fig. 3. Typical discolored termination later found to poorly wet.

Analysis of the subject parts was accomplished by first visual examination, followed by scanning electron microscopic (SEM) examination, energy dispersive x-ray (EDX) analysis, Ion Mass Microprobe Analysis (IMMA), and metallographic analysis of non-wetted termination cross-sections. The results of this analysis and the conclusions drawn from it are discussed in the following sections.

DISCUSSION

Description of Test Specimens

All parts evaluated were large size BX-designation ceramic chip capacitors from two manufacturer's and from a total of four part lots. Within these four lots, processing was varied so that: 1) some parts were not solder coated, 2) some had a single solder coat, 3) some had a double solder coat, 4) some were twice termination dipped and twice fired, and 5) some were twice termination dipped but fired seven times before solder dipping. In the case of each manufacturer, a single termination material was utilized. Both terminations were Ag/Pd based with a lead borosilicate-bismuth fluxed glass frit.

Results of Optical and SEM/EDX Examinations

A previously stated, the sizes and shapes of non-wetted termination areas are quite varied. This variation can clearly be seen in Figures 4 to 6 where non-wetted areas are illustrated to vary from pinhole size, to a large rounded, non-wetted islands. They do, however, appear to have details in common with each other.

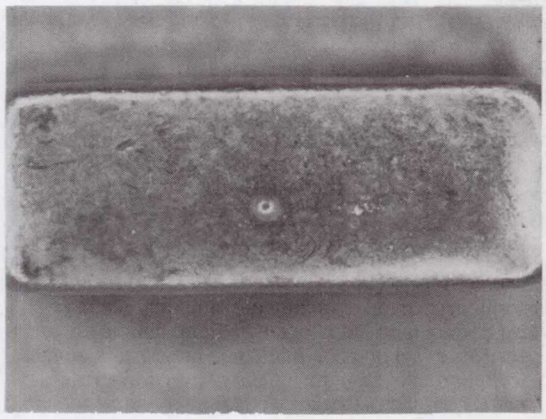

Fig. 4. Overall view of a capacitor with a single non-wetted pinhole in the solder coating. (14X)

Dewetted areas were first examined optically, then using SEM and EDX analyses. Several different non-wetted areas were examined in one manufacturers parts in detail. It was noted that some of these areas were substantially more porous than others. Traces of bismuth (Bi), titanium (Ti), and barium (Ba) were noted on all non-wetted surfaces. (Refer to Figures 7 and 8 for illustrations of these affected surfaces.)

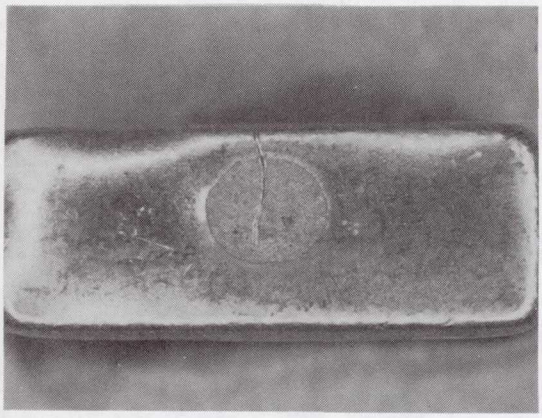

Fig. 5. Overall view of a capacitor with a large circular non-wetted area in the soldering. (14X)

Fig. 6. Overall view of a badly non-wetted capacitor termination. (14X)

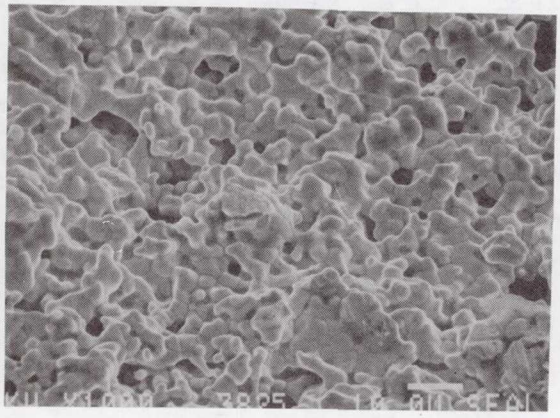

Fig. 7. SEM photomicrograph of the termination's surface structure. (1000X)

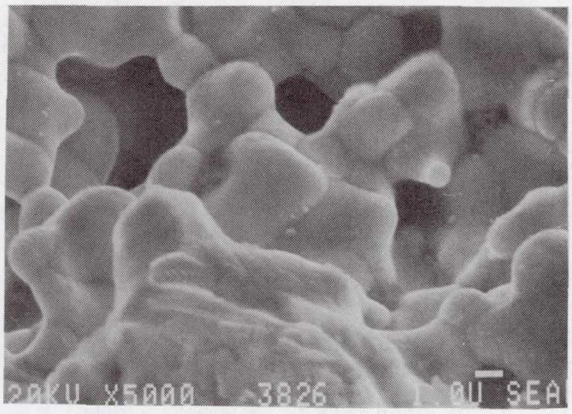

Fig. 8. Closeup SEM photomicrograph showing surface detail. (5000X)

Non-wetted areas were examined on the second manufacturers parts using the same techniques as with the first manufacturer. The common details noted on the non-wetted areas on these parts were porosity and surface bismuth. A large amount of surface contamination was noted to be randomly distributed on the exposed areas of these parts. No differences were noted between the surface appearance of non-wetted areas of single or double solder coated parts nor between the various number of termination firings. No trace of solder was noted in the non-wetted areas, however, Ba and Ti was noted on porous areas of parts which had not been solder dipped. Figures 9 to 12 illustrate the typical appearances of the porous and non-porous surfaces.

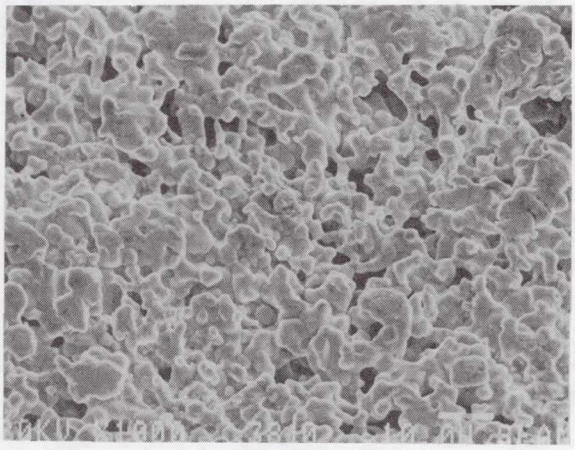

Fig. 9. Closeup view of a porous area of the termiantion. (1000X)

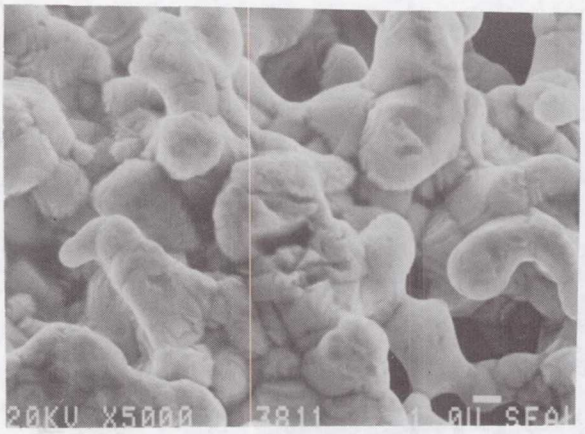

Fig. 10. Detailed view of Figure 9. (5000X)

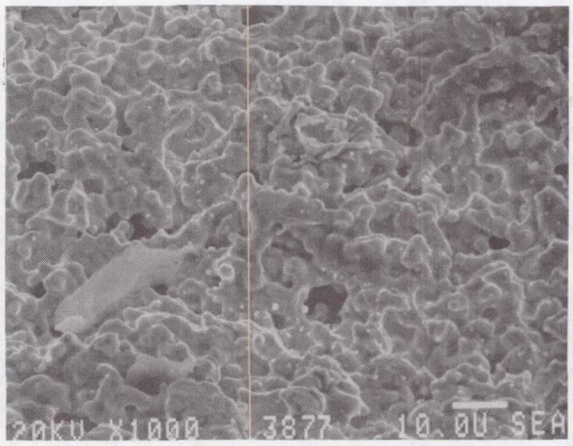

Fig. 11. Closeup view of a non-porous area of the termination. (1000X)

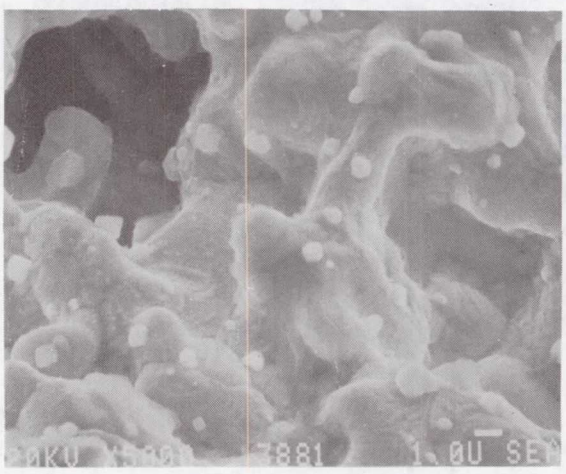

Fig. 12. Detailed view of Figure 11. (5000X)

Surface Analysis of Dewetted Areas

Surfaces were next analyzed using ion microprobe mass analysis (IMMA). Both positive and negative ions were utilized to identify specific elements at three levels (0, 200, and 500 Å) from the surface. Three of the non-wetted parts were evaluated with similar results. The following observations were made:

1) very small amount of Pb and Sn were found in the non-wetted areas of the termination,

2) bismuth was always found in the non-wetted parts,

3) barium and titanium had migrated to the surface of most non-wetted areas for one manufacturer,

4) high amounts of Na, K, and Ca were found in the non-wetted areas, possibly as halides since high chlorine and bromide peaks were also observed,

5) large amounts of hydrocarbons were detected at all levels in the non-wetted areas,

6) high oxygen levels were detected (possibly from the oxide content of the glass frit),

7) high sulfur content was observed on the surface (possibly as a result of tarnishing of the exposed silver),

8) Al and Si contents were noted at all three levels indicating that glass frit was still interspersed with the surface metal content, and,

9) no chemical differences were noted between parts with different processing.

Metalographic and SEM/EDX Analysis of Cross-Sectioned Parts

Parts from both manufacturers were cross-sectioned through non-wetted areas and examined. Areas of high porosity within the termination were found at the centers of the non-wetted areas in all cross-sectioned parts. Bismuth, barium, and titanium were revealed to segregate into 'island' areas within the termination. Also, contamination was noted within the pores, Typical cross-sections are shown in Figures 13 to 16.

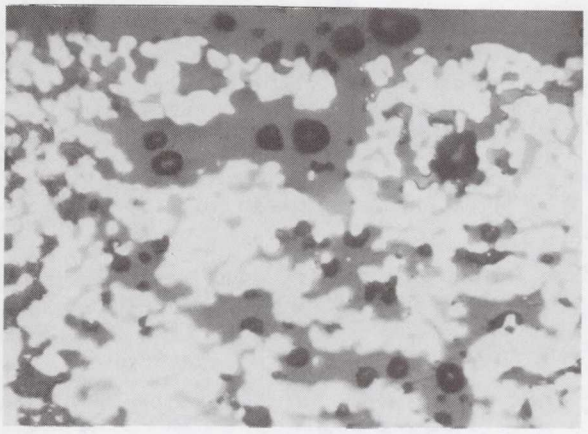

Fig. 13. Optical micrograph of a porous area in the termination. (800X)

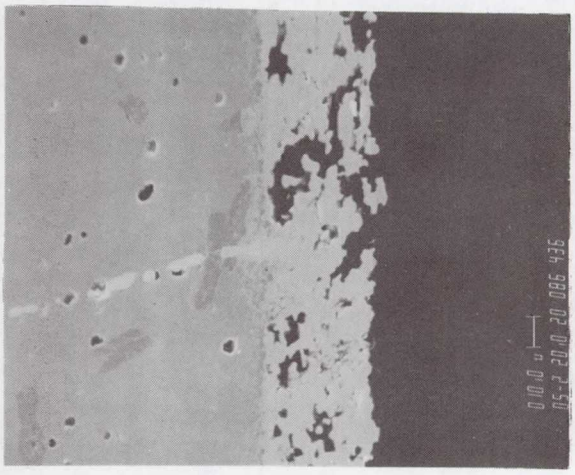

Fig. 14. Low magnification SEM view of a porous area in the termination. (800X)

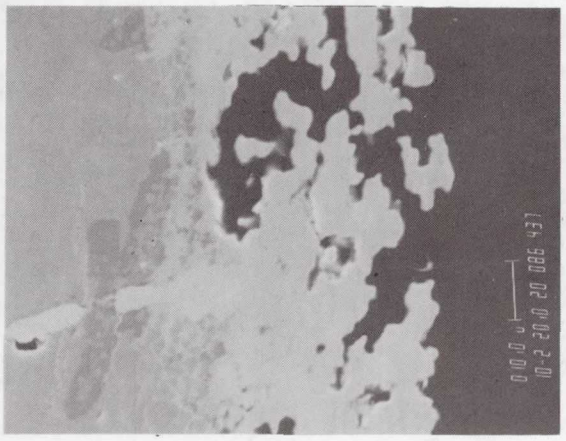

Fig. 15. Detail of Figure 14 showing dielectric glass frit interaction. (1000X)

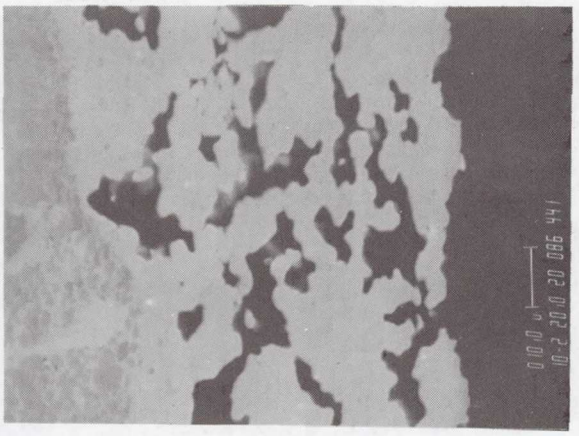

Fig. 16. Another highly porous of the termination. (1000X)

(As seen in these photographs: the light metallic areas are Ag/Pd, the dark islands within the termination were rich in bismuth and small amounts of Ba, Ti, Si, and Fe, and the pores revealed small amounts of Cl.)

DISCUSSION

All the results obtained were quite similar and independent of manufacturer, number of solder coatings, and number of times the termination has been fired. Most of the non-wetted areas were round or islands with round edges and revealed almost no solder adhesion in these areas (a very thin solder film was observed using IMMA). The porosity level in the end terminations was extremely high in the center of the non-wetted areas and unlike the wetted areas where the porosity level was low and uniform. The high porosity areas allow enrichment of the bismuth oxides (from the ink slurry) and also provide a low energy diffusion path for the barium and titanium in the ceramic. In addition, the high porosity areas would entrap surface contaminants in the pores, which may become difficult to remove. The presence of high porosity along with contaminants entrapped in the porosity and Ba, Ti, and Bi oxides render these areas non-solderable causing dewetting when dipped. The bleedout of contaminants from these high porosity areas and surface tension effects cause lack of solder wetting and make the non-wetted areas round in shape with the high porosity area in the center of the non-wetted area.

CONCLUSION

Non-solderability of ceramic chip capacitor terminations can be caused by the presence of high porosity areas in the center of the non-wetted areas. These areas entrap contamination and accumulate concentrations of bismuth and other oxides which decrease solderability.

RECOMMENDATIONS

1) Termination inks should be handled in a manner, prior to application, meant to prevent segregation of the mixture,

2) Capacitor cross-sections should be examined for uniformity of the termination's porosity, and

3) Terminations should be thoroughly cleaned prior to solder dipping. (This will minimize non-solderability when porosity does exist.)

ULTRASONIC SCANNING OF MULTILAYER CERAMIC CHIP CAPACITORS

Dr. F. N. Bradley
AVX Ceramics
P.O. Box 867
Myrtle Beach, S. C.
(803) 448-9411

SUMMARY

Ultrasonic scanning is compared to neutron radiography and scanning laser acoustic microscopy (SLAM). Data show that SLAM and ultrasonic scanning evaluations agree well. There is poor agreement between N-ray and both ultrasonic techniques because N-ray is insensitive to all but the grossest delaminations. Statistical analysis show a good correlation between ultrasonic scanning and destructive physical analysis (DPA).

INTRODUCTION

Ceramic capacitors for crital applications including satellite systems, heart pacemakers and military weapons systems must operate reliably and reproducibly for very long time periods in both transient and long term environments. These environments may be difficult to define and simulate, making it extremely difficult to correlate closely between service lifetime (MTBF) and accelerated proof testing (burn-in).

This uncertainty of correlation between burn-in and service life forces designers of critical systems to resort to rigorous inspection procedures to eliminate any questionable or flawed units. Particular attention is paid to mechanical flaws since such flaws can be discriminated more readily than regions of potential electrical failure.

Mechanical flaws certainly reduce strength and increase susceptibility to mechanical fracture or degradation. Additionally, mechanical flaws increase the probability of dielectric breakdown. Finally, mechanical flaws serve as points of entry, channels or sites for electrochemical corrosion, particularly from moisture incorporating contaminant ions (Na, Cl, S etc.).

New non-destructive testing techniques are of great interest for detection, monitoring and screening out mechanically flawed chip capacitors. Even though destructive physical analysis (DPA) is the criteria for ceramic capacitor lot quality, DPA cannot be used for sorting and it is rather crude from a statistical standpoint.(1)

The earliest form of NDT employed for ceramic capacitors was visual inspection for chips, spots, cracks, delaminations etc. While useful, such visual inspection is operator sensitive and limited to visible surface flaws. Improved resolution is obtained with penetrant techniques, especially for cracks, but this is still limited to surface flaws. X-ray radiography has not been successful because of the small size of the chips and the high absorption of the barium atoms in barium titanate.

NEUTRON RADIOGRAPHY

The availability of neutron sources overcame the limitation of X-ray radiography because of the high penetrating power of thermal neutrons. (2) Great hopes were held for neutron radiography and initial results were encouraging. Based upon these results, neutron radiography has often been specified for discrimination of internal mechanical flaws in multilayer ceramic capacitors. However, neutron radiography (N-ray) has some severe limitations despite its high penetrating power. Beyond requiring access to a nuclear reactor, the neutron beam must be closely collimated and the alignment of the chips is very critical because the chips must be set on edge. Contrast depends upon the difference in neutron absorption of the ceramic compared to the absorption of a void (delam) as shown (equation 1).

$$\ln \frac{I}{I_C} = -\frac{(1 - X) M_1 + M_2 X}{M_1} \qquad (1)$$

Where I is the intensity of the path containing a delam

I_C is the intensity of an all ceramic path

M_1 is the neutron absorption coefficient of the ceramic

M_2 is the neutron absorption coefficient of air

X is the fraction of the beam path through the delam ÷ total path length

Contrast also depends upon the relative path length in the delamination so bigger delams will show up more distinctly. The neutron absorption coefficient differs strongly for different formulations since some compositions

contain appreciable concentrations of Nd, Sm and Gd which can greatly increase neutron absorption. Excellent photographic technique and film become very important to insure reproducible and sensitive discrimination.

Neutron radiography does detect large massive delaminations but the correlation between DPA and neutron radiography is poor. Quite often major delams are missed and a number of high reliability lots judged acceptable by neutron radiography have failed DPA.

SONIC TECHNIQUES

The shortcomings of neutron radiography have resulted in intensive study of other nondestructive test methods, primarily sonic techniques. This paper will not discuss acoustic emission (which is best classified as a combination of NDT and proof test). Acoustic emission is currently being evaluated for ceramic capacitor inspection as well as for many other critical component and structural applications.

Acoustic microscopy employs a transducer operated at a high frequency (100 MHZ) which generates a cw acoustic wave transmitted through a water bath to the rear surface of the sample. The ultrasonic wave propagating through the solid elastically distorts the top surface of the ceramic chip sample. A laser beam scans the surface and the deflection is converted into an electrical signal which is mixed with the 100 MHZ exciting signal to produce a demodulated output presented on a TV screen as a C-scan display.(3)

Any delaminations within the chip sample will scatter the propagating ultrasonic beam and greatly reduce or eliminate the elastic deflection of the surface in the region shadowed by the delamination.

This acoustic microscopy technique has the advantage that it is based on scattering rather than absorption. Therefore defect discrimination is much less dependent upon the chemical composition of the ceramic and size of the delamination. The relatively small difference in acoustic impedance between the ceramic and the precious metal electrodes allows the chips to be scanned flat (direction of propagation normal to the plane of the electrodes).

ULTRASONIC SCANNING

Ultrasonic scanning was first applied to ceramic chip capacitors by Love et. al. (4). The AVX system consists of a US450 laboratory scanner with a S-80 reflectoscope supplied by Automation Industries.

Ultrasonic scanning is a pulsed system compared to the cw mode employed in acoustic microscopy. A transducer immersed in a water tank is excited at a frequency between 10 MHZ and 25 MHZ to generate a pulse about 5 x 10 (exp -7) seconds long. The transducer focuses this pulse into a convergent tight beam with a width of about 1.5 mm. Most of the ultrasonic pulse is reflected from the top surface of the ceramic but some is transmitted through the ceramic. The transmitted pulse is mainly reflected from the back surface (Figure 1) and then back to the transducer. The velocity of sound in the ceramic is about four times faster than in water, which allows the reflection from the back surface of the ceramic to be separated in time from the reflection from the glass plate.

The operation of the ultrasonic scanner depends upon two pulse gates - the "write" gate and the "alarm" gate. The write gate is set (with adjustable delay and length) from the initial pulse to open the transducer to receive the front surface and back surface reflections from the ceramic chip. The write gate is closed in time to bar the reflection from the glass plate.

When the write gate is open and the reflection from the top surface of the ceramic exceeds a set threshold, the "alarm" gate is opened. This gate is therefore delayed from the first reflected pulse. The length, amplitude level and delay of the alarm gate are adjustable and these are set to bracket the back surface reflection of the multilayer ceramic chip as shown in A-scan oscilloscope presentation of Figure 2.

Arrays of chips mounted on a flat plate are scanned mechanically by traversing the transducer mount in the y direction and incrementing along the x direction. When a mechanically good chip is scanned the back surface reflection will exceed the alarm gate threshold. A "bad" region has mechanical discontinuities (delaminations, cracks, surface chips, etc.) which scatter the back surface reflection so the returned signal does not exceed the alarm gate threshold (Figure 3).

Pulses generated when the signal in the alarm gate does not exceed threshold are amplified and transmitted to the chart stylus where they burn a hole in thermal chart paper to indicate a flawed (high scattering) region. The stylus is mechanically linked to the transducer head drive to locate the defective chips.

The mode of operation employed in scanning ceramic chips does not locate the defect in the z direction so it should not be

confused with the ultrasonic pulse echo ranging technique used for large and complex components. The threshold mode does not depend greatly upon the severity of the flaw as does neutron radiography. The magnitude of the mechanical defect is judged by the percentage of the chip area indicating excessive scattering. Figure 4 gives a guideline for grading the scanner charts with respect to accept/reject criteria.

NEUTRON RADIOGRAPHY VS. ULTRASONIC SCANNING

Apparently N-ray sorts out only the grossest of delaminations and sometimes passes severely delaminated chips. In an initial study we found 62% delaminations in an N-ray passed lot. Recently, data from a NASA study comparing N-ray, acoustic microscopy and ultrasonic scanning on a group of two hundred and fifty (250) chips (CK06 size) were kindly made available to us by Jerry Kiernan, Goddard Space Flight Center, which provided a thorough test of our assumptions. (5) The chips were graded by N-ray, acoustic microscopy and ultrasonic scanner criteria and segregated into three (3) groups which were: (1) probably delaminated; (2) possibly delaminated and (3) OK. The possibly delaminated group showed some deviation from an "ideal" or OK pattern (or film) while the probably delaminated group showed a strong degradation and failed the established criteria for acceptance (Figure 4). These results are tabulated in Table 1.

TABLE 1

Ranking of CK06 Chips

Determined by NDT Technique

Test Ranking of Chips By:	A*	B*	C*
1. Ultrasonic Scanning	98	58	84
2. Acoustic Microscopy	87	51	112
3. Neutron Radiography	12	22	216

* A = Probably Delaminated
B = Possibly Delaminated
C = OK

The agreement between acoustic microscopy (also known as SLAM) and ultrasonic scanning is good as shown in Table 2:

TABLE 2

Sorting Effectiveness

Of NDT Techniques

1. Percent (%) of U.S. "delam" group classed as SLAM "Delams"	72.4
2. Percent (%) of U.S. "OK" group classed as SLAM "OK"	82.2
3. Percent (%) of N-ray "delam" group classed as SLAM or U.S. "delam"	100.0
4. Percent (%) of N-ray OK group classed as U.S. "OK"	41.6
5. Percent (%) of N-ray OK group as SLAM "OK"	50.0
6. Percent (%) of U.S. "delam" group classed as SLAM "OK"	10.2
7. Percent (%) of SLAM "delam" group classed as U.S. "OK"	2.3

While the N-ray delam group are definitely mechanically defective by both SLAM and U.S. criteria, the N-ray "OK" group are not OK by SLAM or U.S. evaluation. This has been the AVX experience because a number of N-ray sorted lots have failed the DPA evaluation and have proven to have an unacceptably large fraction of major delaminations.

CORRELATION BETWEEN DPA AND ULTRASONIC SCANNING

Acoustic microscopy and ultrasonic scanning agree quite well considering that the evaluation is subjective and that there are "artifacts" such as warping, surface features, air bubbles etc. which cause misinterpretations, (good or acceptable chips will be rejected). More critically, there must be good agreement between DPA and these ultrasonic techniques so that chips defective by DPA criteria will not be passed by ultrasonic NDT.

DPA results at AVX have been compared with scanner data for a large number of lots (over 500)to establish the validity of ultrasonic scanning. A random sample of five (5) fired chips from each high reliability lot was sectioned, ground, polished, examined and graded according to an internal AVX criteria. Each lot was judged on the number of major delams in the five (5) piece sample (no delams, OK; one delam, marginal; two or more delams, rejected).*

Ultrasonic scanning was performed on a fifty (50) piece sample using the judging criteria shown in Figure 4. The number of ultrasonic good chips is multiplied by two to obtain the ultrasonic scan yield in percent. An exactly marginal DPA lot should give an ultrasonic yield of 80%, a rejected lot would have a U.S. yield of 60% and an OK DPA lot would have no delams and thus a U.S. yield of 100%.

An exact numerical agreement between DPA and ultrasonic scanning is unlikely for several reasons. First, ultrasonic scan artifacts tend to reduce the U.S. yield since this results in DPA acceptable chips being graded U.S. bad. Second, a major delam may not extend completely over the active region, so the sectioning may not intercept the delamination or may only slightly intersect the delamination resulting in the delam being classified as minor rather than major.

This probability of detecting a delamination is best treated as a Poisson distribution, since the delams are randomly distributed in size, shape and location.(6) The Poisson probability, P, is given by formula 2, where:

$$P = \frac{p^{r} (1 - p)^{n - r} n!}{r! \ (n - r) \ !} \qquad (2)$$

Where n is the sample size the number of defectives in the sample

r, is a positive integer including zero and no greater than n

p is the true fraction defective

As an example, if the true fraction delaminated is 0.20 (DPA marginal) the probability of detecting 0, 1, 2, 3, 4 or 5 delaminated chips in a random sample of five (5) chips is shown in Table 3.

TABLE 3

Probability of Detecting r Delaminated Chips In A Random Five (5) Piece (DPA) Sample (p = .20)

r	P	Apparent Percent Delaminated
0	32.77%	0
1	40.95%	20%
2	20.48%	40%
3	5.12%	60%
4	0.64%	80%
5	0.032%	100%

Thus, about one third of the lots would be graded DPA "OK" and one fourth of the lots would be rejected while only 40% would be correctly graded. The US yields of 378 DPA OK lots as a frequency distribution along with a fitted Poisson distribution (p = .12, n = 378) is plotted in Figure 5. The agreement is pretty good aside from some low ultrasonic yields on lots containing warped chips.

The distribution of 55 DPA marginal lots and 51 DPA rejected lots is shown in Figures 6 and 7. The average for the three DPA groups is tabulated in Table 4. Experimental standard deviations were between 15% and 20%.

TABLE 4

Ultrasonic Scanner Yield Averages for the DPA Categories

DPA Group	Assumed U.S. Yield	Experimental Average
OK	100%	88.0%
Marginal	80%	69.2%
Rejected	60%	47.4%

DISCUSSION

This data shows a strong positive correlation between DPA and ultrasonic scanning yield. Not only is the US yield average and standard deviation somewhat below the assumed US yield as expected, but the experimental difference between averages of OK, marginal and rejected lots is quite close to the assumed difference of 20%. Although no statistical correlations were run between acoustic microscopy and DPA groups, the close correlations between acoustic microscopy and ultrasonic scanning (Table 2) indicates that there would also be a strong positive correlation between acoustic microscopy patterns and major delaminations.

Using the same logic, the poor correlations between acoustic methods and neutron radiography thereby proves a poor correlation between DPA and neutron radiography. The use of neutron radiography as a non-destructive test for delaminations will at best sort out only half of the chips with major delams.

CONCLUSIONS

1. There is a close positive correlation between acoustic microscopy and ultrasonic scanning.
2. Ultrasonic scanning correlates closely to major delaminations found by DPA examination.
3. Neutron radiography is inadequate NDT technique for detection and screening of major delaminations in ceramic multilayer chip capacitors.

REFERENCES

1. Standrad test method for destructive physical analysis of ceramic capacitors, SP 1382, Electronic Industries Association, Washington, D.C. 1980.
2. H. Berger, "Neutron Radiography" Elsevier

Pub. Co. C. 1965.
3. L. W. Kessler and D. E. Yuhas, "Acoustic Microscopy - 1979" Proc. I.E.E.E., 67 (4) 526-36 (1979).
4. G. R. Love, "Non-destructive Testing of Monolithic Ceramic Capacitors", ISHM 1973 Hybrid Microelectronics conference, Union Carbide technical paper reprint.
5. G. F. Kiernan, Sperry Support Services, Goddard Space Flight Center, personal communication.
6. N. C. Barfoot, "Experimental Measurements: Precision, Error and Truth", Addison-Wesley, c. 1967 91-98.

FOOTNOTES

* Marginal and severely delaminated groups were produced by specially modified processing methods to provide samples for this comparative study of NDT techniques.

FIGURES

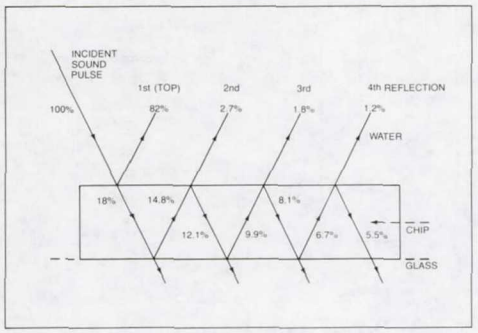

Fig. 1(a) Reflection of ultrasonic pulse from ceramic chip. (Incident pulse is actually vertical)

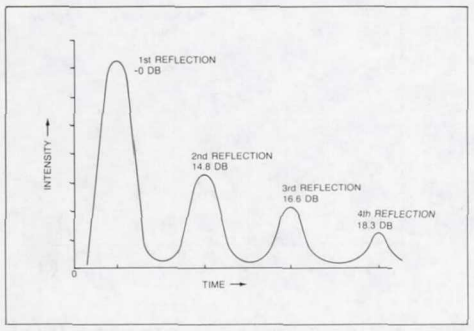

Fig. 1(b) A-scan oscilloscope trace of pulses reflected from ceramic chip.

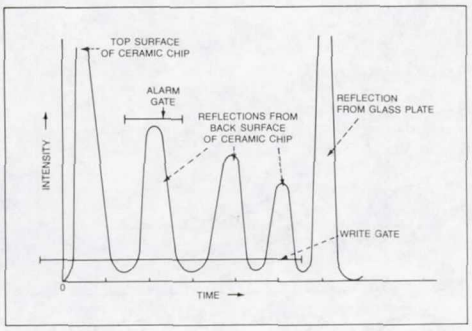

Fig. 2 A-scan oscilloscope trace of pulses reflected from edge of ceramic chip showing pulse gates.

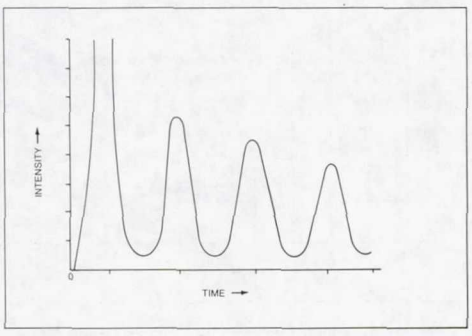

Fig. 3(a) A-scan oscilloscope trace of a good chip.

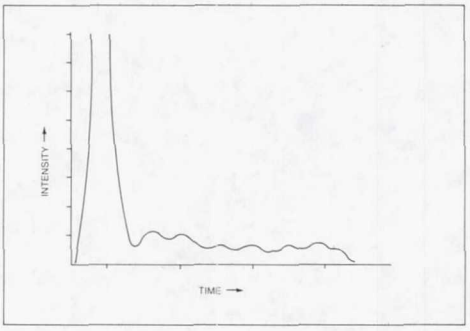

Fig. 3(b) A-scan oscilloscope trace of delaminated chip.

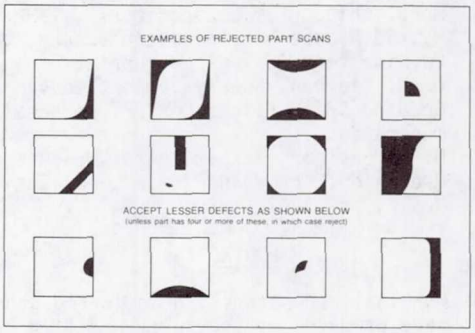

Fig. 4 Ultrasonic scan pattern rejection criteria

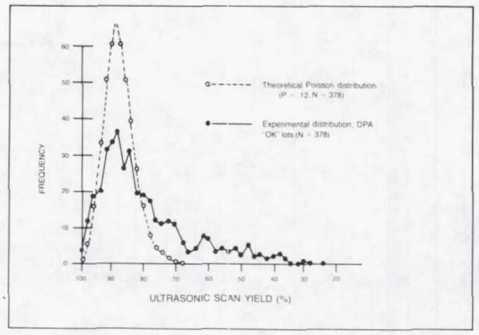

Fig. 5(a) Distribution of DPA ok high-rel lots.

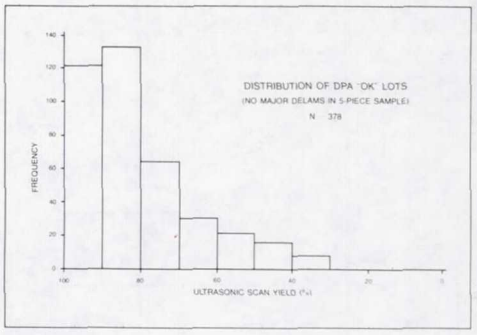

Fig. 5(b) Histogram of DPA OK lots.

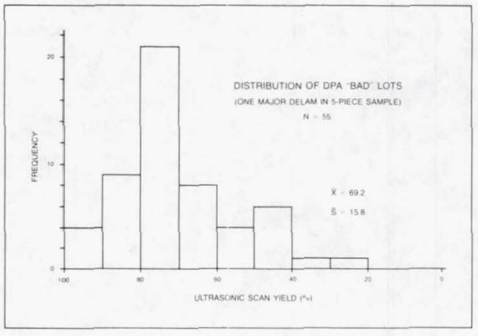

Fig. 6 Histogram of DPA marginal lots.

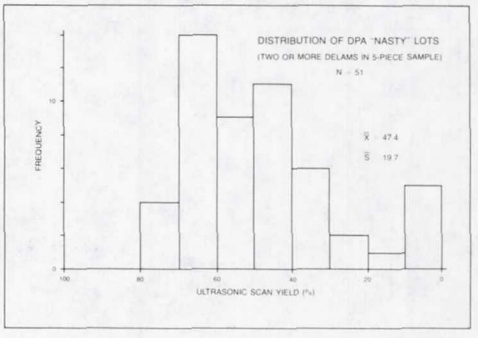

Fig. 7 Histogram of DPA rejected lots.

A COMPARISON OF SCREENING TECHNIQUES FOR CERAMIC CAPACITORS

Gerard F. Kiernan
Sperry Systems Management
Sperry Corporation
Code 310.1
Goddard Space Flight Center
Greenbelt, Maryland 20771
301-344-8830

SUMMARY

This paper is an interim report on a project to compare the effectiveness of various non-destructive screening techniques for delaminations and voids in multilayer ceramic capacitors. The techniques involved in this test program are ultrasonic scanning, neutron radiography, scanning laser acoustic microscopy, and voltage conditioning. The test capacitor, for this first phase, is a 0.47 uF, 50V capacitor, style CKR06. Eighteen of 768 devices have failed in voltage conditioning with elapsed times from 15 minutes to 1239 hours. Eleven of the failures were detected by ultrasonic scanning. Four failures were found by neutron radiography. Fourteen failures showed up in the acoustic microscopy test. Three failures in voltage conditioning were not detected by any of the techniques. Failures were confirmed by Destructive Physical Analysis (DPA). There is no direct relationship between the size of the defect and electrical failure.

INTRODUCTION

The existence of delaminations and voids in multilayer ceramic capacitors is a source of many of the reliability problems with these devices. As users look for higher values of capacitance in physically smaller capacitors, the manufacturers have responded with new and thinner dielectric materials. Manufacturers have programs to make their product as defect free as possible but everyone realizes that voids and delaminations will occur. These faults can cause degradation or catastrophic failure of devices, especially in devices with high values of capacitance where the dielectric layers are the thinnest. The capacitor manufacturers and the user community are investigating various test techniques (ultrasonic scanning, acoustic microscopy, neutron radiography) to detect voids and delamination in capacitors. The manufacturers, through the ceramic capacitor committee of the Electronic Industries Association, have cooperated with DOD and NASA to develop a new high reliability specification for multilayer ceramic capacitors. This specification will limit the amount of capacitance available in each case size and is adopting the new test techniques to detect voids and delaminations. As part of this effort, the Product Assurance Division of the Goddard Space Flight Center provided funding to its functional support contractor, Sperry Systems Management, to compare the various screening techniques so that data could be developed on their effectiveness. This information will be used to develop recommendations on accept/reject criteria for these tests in the new specifications.

TEST PLAN

The test plan consists of two phases which are identical except for the device under test.

Device Types

In the first phase, the test capacitor is a CKR06, 0.47 uF, $\pm$ 10%, 50V device. In the second phase, the capacitor will be a CKR11, 0.01 uF, $\pm$ 10%, 50V. These devices were chosen because they are high values of capacitance in their respective sizes and have thin dielectrics which are more likely to have voids and delaminations. These were chosen also to determine how the size of the part influences the effectiveness of the screening technique. The CKR06 device is approximately 60 x 235 x 220 mils while the CKR11 is approximately 60 x 60 x 150 mils.

Test Sequence

This is the plan for each phase of the test. Two lots of each device type will be purchased from two manufacturers for a total of four lots of each type. The manufacturer will serialize each chip. The serial number on each device serves two purposes. The first purpose is to trace each device through the test. The second purpose is to provide a reference point for the orientation of the device in the first three tests. The lots are subjected to the manufacturers in-house ultrasonic scanning test. The parts are mounted in the manufacturer's fixture and sent to Aerotest Operations Inc., San Ramon California for neutron radiography. The devices are shipped from Aerotest to Sonscan Inc., Bensenville,

Illinois for scanning laser acoustic microscopy tests. The devices are returned to the manufacturers for the addition of terminations and leads. The devices are not molded to simplify DPA procedures at the end of the test. All units are shipped to GSFC for initial electrical tests of capacitance, dissipation factor, insulation resistance at 25°C and 125°C, and dielectric withstanding voltage. The devices are placed in life test for 2000 hours at twice rated voltage (100V) at 125°C. Interim electrical measurements were made of insulation resistance at 125°C at 240, 500 and 1000 hours. All parameters were measured at 2000 hours. Parts were removed from test when they failed catastrophically or their insulation resistance was below 1 Megohm. Destructive Physical Analysis was performed on all failures and on 40 good units to correlate the test results.

TEST TECHNIQUES

Ultrasonic Scanning

This is a pulsed technique in which an acoustic signal in the range of 15 to 25 MHz is beamed into the device under test and the reflected signal is measured. The part under test is submerged in a water bath which provides a transmission medium for the acoustic signal. The beam is perpendicular to the plates of the device. There is a time element and amplitude element to the measurement. The time element is to determine the reflections from the front and back surfaces of the device under test and the only reflected signals of interest are those occuring between these two major reflections. This time gate allows the detector to ignore multiple reflections. If the device under test is defect free, there will be minor reflections from the ceramic-metal interfaces at the plates but these will not approach the amplitude of the reflection from the rear surface-water interface and are ignored. Any internal void or delamination will contain air and the reflected signal will be greater than that from the rear surface. An amplitude threshold is set at the level of the rear surface reflection and any internal reflection of greater amplitude is recorded. The transducer is mechanically scanned across the part and a stylus gives a trace of its path on thermal paper. When an internal reflection of sufficient magnitude is recorded, the voltage is turned on to the stylus leaving a black mark in the trace. This is how an internal defect is recorded.

Neutron Radiography

This technique is similar to x-radiography except that a beam of neutrons is used. The devices under test are arranged so that the path of the beam is parallel to the plane of the plates in the capacitor. The creation of the image is based on the penetration of the material by neutrons. If there is a void or delamination in the material, this will allow more neutrons to pass through to the detector than are passed by the surrounding solid material. The detector is standard radiographic film. Since the emulsion is not sensitive to neutrons, a sheet of gadolinium is placed between the device under test and the film. When the neutrons strike the gadolinium, they cause the secondary emission of radiation which sensitizes the film. The film is studied in the same way as a standard radiograph.

Scanning Laser Acoustic Microscopy

This is a continuous wave acoustic transmission technique. An acoustic signal is beamed into the bottom of the part under test. This acoustic wave will cause a perturbation of the top surface when it reaches it. The top surface is scanned by a laser and its reflected signal is modulated by these perturbations. The reflected signal is received by a photo-detector and used to create an image on a CRT. The microscope can be used at 30 to 100 MHz. The test on the CKR06 devices was at 30 MHz. The CKR11 parts will be tested at 30 and 100 MHz. The microscope has two imaging techniques. One is the amplitude mode. The CRT display is derived from the amplitude of the reflected laser signal. The second technique is the interference mode. The signal from the laser reflection is combined with the signal used to generate the acoustic wave to generate an interference pattern for display on the CRT. The amplitude mode seems the most suitable for detecting differences in the density of material and small voids or occlusions in a device. The interference mode is more effective for delaminations since the delamination disrupts the transmitted signal. The scans are recorded from the CRT by either a videotape recorder or 35mm photographs of the screen. The second phase of the test will attempt to determine the increase of detection sensitivity by increasing the frequency from 30 to 100 MHz.

Voltage Conditioning

The life test of the capacitors is performed in accordance with the conditions for voltage conditioning in MIL-C-39014. The capacitor burn-in system displays the elapsed time and monitors the voltage applied to the devices on test. If the applied voltage drops by 5% or more due to a device failure, the system shuts off the affected board and locates the defective unit. The part is removed and the life test restarted.

TEST RESULTS

Screening

Table I shows the number of devices by lot used in the test that were detected in the non-destructive tests as having possible defects.

Initial Electrical Failures

Since the parts received no electrical tests at the manufacturers, a number of failures were detected at initial electrical tests. Destructive physical analysis confirmed that all failures were due to manufacturing defects such as misalignments or chipped corners. Since such failures would have been detected by the manufacturer's normal in-process tests if they had been performed, these failures are considered not to be relevant to this evaluation.

Life Test Failures

Eighteen units, from three of the four lots, failed during the 2000 hour life test. Table II lists the screening results for these failed units. The table shows which tests detected anomalies in each part. Table III gives the time to failure and the cause of failure found in DPA. Table IV shows the correlation between the parts detected during screening and the DPA results.

The figures at the end of the paper show the results of the screening tests along with the results of the destructive physical analysis for three representative parts.

DPA of Good Units

Forty units (10 from each lot), that survived life test, were cross sectioned to verify the results of the screening tests. Table V shows the correlation between anomalies detected during screening and those verified during DPA.

CONCLUSIONS

Nondestructive screening tests can be used to determine the quality of a particular manufacturing lot but they will not detect every potential electrical failure.

There is no correlation between the size of faults detected during screening and electrical failure.

Acoustic techniques are preferable to neutron radiography for the detection of faults in the CKR06 size of capacitor. The Scanning Laser Acoustic Microscope, with its two modes of operation, is superior to conventional ultrasonic scanning in its ability to detect faults. The detection capability of both acoustic techniques are affected by physically deformed parts. A physical deformation could be warpage or an extra layer of ceramic material.

TABLE I. NDT RESULTS

LOT	ULTRA	N RAY	SLAM INTER.	SLAM AMP.
A	70/192	0/192	50/192	35/192
B	119/192	8/192	97/192	98/192
C	94/192	2/192	7/192	53/192
D	13/192	0/192	1/192	23/192

TABLE II. SCREENING RESULTS (FAILURES)

SN	ULTRA.	N-RAY	SLAM INTER.	SLAM AMP.
A22	-	-	x	-
A73	-	-	-	-
A80	-	-	-	x
A168	-	-	-	-
B285	x	x	x	x
B293	x	-	x	x
B297	x	-	x	x
B339	x	x	x	x
B374	x	-	x	x
B375	x	-	x	x
B379	x	x	x	x
B388	x	-	x	x
B397	x	-	x	x
B423	x	-	x	x
C16	x	-	-	-
C39	-	x	-	x
C50	-	-	-	-
C209	-	-	-	x

TABLE III. DPA RESULTS (FAILURES)

SN	Time To Fail	Cause
A22	84 hr.	Blow out
A73	1151 hr.	Void
A80	240-500 hr.	Delamination
A168	49 hr.	Blow out
B285	240-500 hr.	Delamination
B293	240-500 hr.	No defect
B297	240-500 hr.	Voids
B339	32 hr.	Delamination
B374	172 hr.	Delamination
B375	850 hr.	Void
B379	1155 hr.	Voids
B388	172 hr.	Delamination
B397	172 hr.	Delamination
B423	240-500 hr.	No defects
C16	254 hr.	Blow out
C39	15 min.	Delamination
C50	240-500 hr.	Blow out
C209	1239 hr.	Blow out

TABLE IV. LIFE TEST FAILURES

TEST	DETECT	DPA AGREE
Ultrasonic	11	8
N-ray	4	2
Slam	14	8

TABLE V. DPA (GOOD PARTS)

TEST	DETECT	DPA AGREE
Ultrasonic	23	9
N-ray	2	1
Slam	15	8

BIBLIOGRAPHY

1. N.D. Tyufyakov and A.S. Shtan, Principles of Neutron Radiography, Atomizadt Publishers, Moscow, 1975. Translated and reprinted for U.S. National Bureau of Standards and the National Science Foundation by Amerind Publishing Co., New Delhi, India, 1979.

2. L.W. Kessler and D.E. Yuhas, "Acoustic Microscopy-1979" Proceedings of the IEEE. Vol. 67, no. 4, pp. 526-536, April 1979.

3. Neutron Radiography, Aerotest Operations, San Ramon, California, Brochure.

4. G.R. Love, "Non-destructive Testing of Monolithic Ceramic Capacitors", ISHM 1973 Hybrid Microelectronics Conference, Union Carbide Corporation, Technical Paper reprint.

5. The Sonomicroscope, Sonoscan Inc., Bensenville, Illinois, Brochure.

6. Standard Test Method for Destructive Physical Analysis of Ceramic Capacitors, RS469, Electronics Industries Association, Washington, D.C., 1980.

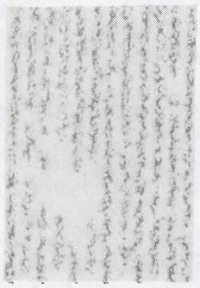

Fig. 1a. Ultrasonic Scanning View.

Fig. 1b. N-Ray view. Arrow points to delamination.

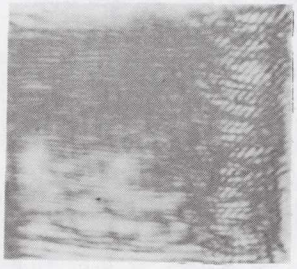

Fig. 1c. SLAM amplitude mode view.

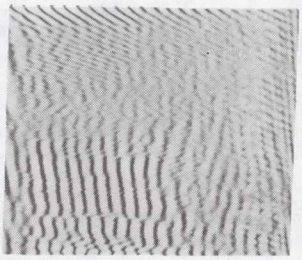

Fig. 1d. SLAM interference mode view.

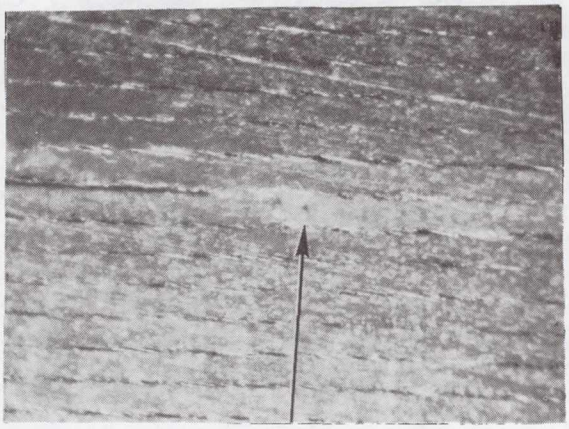

Fig. 1e. Cross section shows delamination. Arrow points to failure site.

Figure 1. SN B339

Fig. 2a. Ultrasonic Scanning View.

Fig. 2b. N-Ray view.

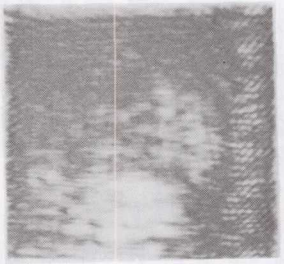

Fig. 2c. SLAM amplitude mode view.

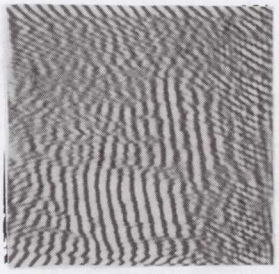

Fig. 2d. SLAM interference mode view.

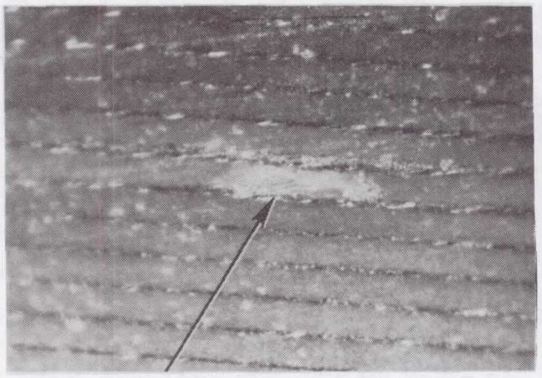

Fig. 2e. Cross section. Arrow points to defect site.

Figure 2. SN B374

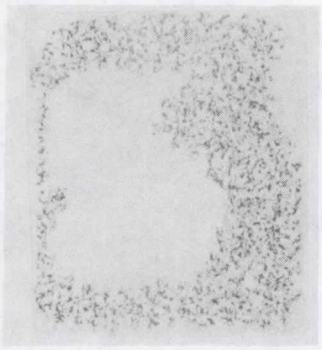

Fig. 3a. Ultrasonic Scanning View.

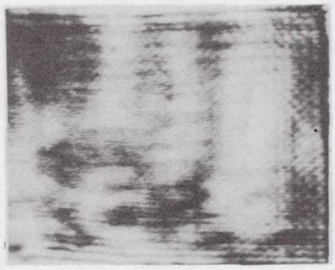

Fig. 3c. SLAM amplitude mode view.

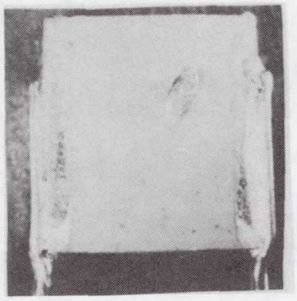

Fig. 3e. Photograph of failure.

Fig. 3b. N-Ray view.

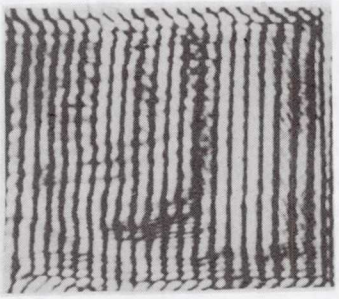

Fig. 3d. SLAM interference mode view.

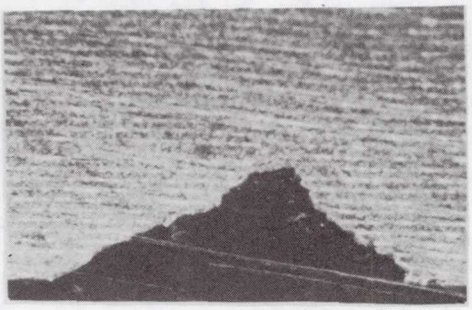

Fig. 3f. Cross section of failure.

Figure 3. SN C16

HIGH-FREQUENCY MEASUREMENT OF MULTILAYER CERAMIC CAPACITORS

Raymond E. Lafferty
Boonton Electronics
Parsippany, N.J.

John P. Maher
Sprague Electric
North Adams, MA

INTRODUCTION

Many circuit functions in high-frequency applications will suffer, either in performance or efficiency, without the use of low-loss capacitors. Until recently it was not possible to measure the loss of capacitors having high Q-factors at frequencies above about 100 MHz.

MEASUREMENT PROBLEMS

Attempts at measuring low-loss capacitors at high frequencies with admittance or impedance bridges, Q-meters, and especially with S-parameter measurements have been generally unsuccessful because of imperfect instrument components, and/or the extreme resolution needed to separate the minor (loss) parameter from the major (quadrature) parameter. The difficulty stems from a need to evaluate accurately the difference between two quantities of nearly equal value, with an uncertainty that approaches and sometimes exceeds that difference.

Measurements made with a disregard for these factors produce positive and negative results of random magnitude.

RESONANT COAXIAL TRANSMISSION-LINE

A resonant coaxial transmission-line, short-circuited at one end and open-circuited at the other, whose fundamental resonant frequency and Q-factor are known, is perturbed with a test capacitor connected either in series at the shorted end of the line, or in shunt at the open end. Measuring the Q-factor of the system with the Δf technique yields the effective series resistance (esr), capacitance, and the Q-factor of the test specimen.

This method of measurement has the advantage that there are no adjustable elements to alter circuit conditions in an unprescribed way, the only variable is the frequency which can be measured with an uncertainty of less than 1 ppm, the loss of the line as a function of frequency is quite predictable, and the Q-factor of the line can be made sufficiently high to support accurate measurements of low-loss capacitors.

The practical use of this fundamental technique is now feasible with the benefit of modern signal generators, sensitive r.f. millivoltmeters, and programmable calculators or small computers.

FREQUENCY

The measurement frequencies are a function of the length of the line and the effective capacitance of the test capacitor. The following table shows the relationship between frequency and capacitance for both series and shunt mode measurements for the Model 34A Resonant Line.

SHUNT RANGE (pF)	FREQUENCY RANGE (MHz)		SERIES RANGE (pF)	
200 to 0	25 to 130	130 to 250	> 1000 to 1.0	(1/4) λ
100 to 0	265 to 390	390 to 500	> 1000 to 1.0	(3/4)λ
30 to 0	530 to 650	650 to 750	> 1000 to 1.0	(5/4)λ
		910 to 1000	> 1000 to 1.0	(7/4)λ
		1170 to 1250	> 1000 to 1.0	(9/4)λ

METHOD OF MEASUREMENT

The measurement of a capacitor requires only the measurement of two frequencies, one on each side of the resonant response at a predetermined ratio of resonant to off-resonant voltage. These two frequencies are entered in a programmed calculator in which the fundamental resonant frequency and the Q-factor of the line have been stored, and the measurement frequency, esr, capacitance, and Q-factor of the capacitor are obtained.

The precision of the measurement is in the order of ±1%. The reproducibility (one system to another) is generally within ±10%. The accuracy of the system, without benefit of NBS standards, has been calculated as being between 7 and 20 percent, for Q-factors of 100 to 10000, respectively. The specified accuracy is,

$$\pm(5 + Q^{0.35})\ \%$$

which is approximately 50 percent greater than calculated.

MEASUREMENT SYSTEM

The components of the system consist of a stable signal generator with a digital readout of frequency of 6 or 7 digits, a sensitive r.f. millivoltmeter which is normally used on the 3 mV range, the resonant coaxial transmission-line, and a programmable calculator. The equipment, without the calculator, is in Fig. 1.

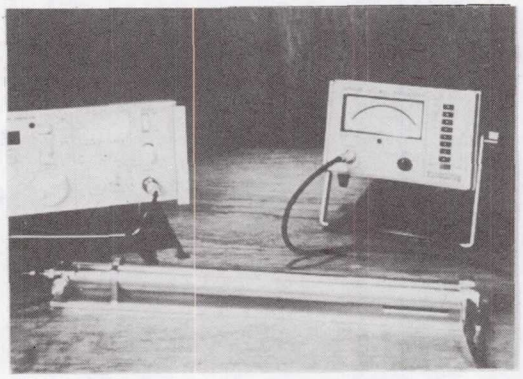

FIGURE 1.

Fig. 2 is a block diagram of the apparatus, and means of connection for both series and shunt measurements are shown in Figs. 3 and 4.

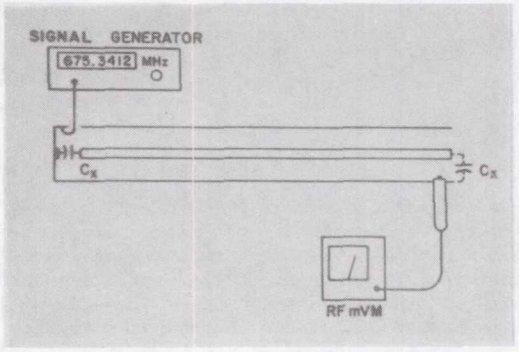

FIGURE 2.

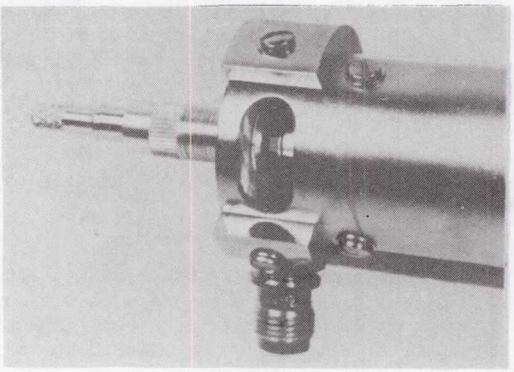

FIGURE 3.

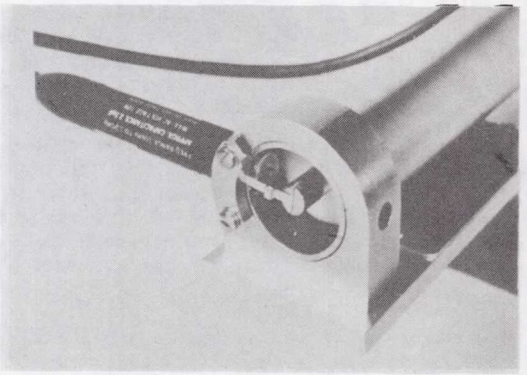

FIGURE 4.

MEASUREMENTS OF CAPACITORS

The esr of low-loss capacitors at high frequencies isgenerally the result of series resistance, and as such it is a function of the skin effect. It is normal, therefore, to expect the esr to vary as $\sqrt{f}$, and it does for many capacitors of this type. A notable exception occurs if dielectric loss is present. Dielectric loss predominates at the lower frequencies, and the esr will decrease with increasing frequency until the true series resistance becomes the principal loss, at which point the curve will reverse and the esr rises with $\sqrt{f}$.

A plot of esr vs. frequency is not always predictable. For example, minor parallel resonances can develop in certain structures and cause an inordinate rise in the esr at those frequencies.

It might be assumed that in the region where the esr is controlled by skin effect, the Q-factor is proportional to $1/f^{3\,2}$, and it is true if the region is well below the self-resonant frequency of the capacitor. The Q-factor vs. frequency of six ceramic capacitors of one manufacturer is shown in Fig. 5. The slope of the curves is close to ideal, and the spacing is such that for any given frequency the esr is the same (very nearly) for all capacitors. This is illustrated in Fig. 6 where the rectangular block encompasses the esr of all the capacitors.

Two 4.7 pF monolithic ceramic capacitors from different manufacturers were measured over a range of 220 to 1200 MHz. It is evident from Fig. 7 that B has the lower loss, as it is also apparent from Fig. 8 that B exhibits the higher Q-factors.

At this point you will question the need to give evidence of capacitor loss in two forms, i.e., esr and Q. It is unnecessary, of course, but a matter of much importance is to select the proper form. We suggest that the loss of a

capacitor be related to the esr, rather than Q. The reason is obvious when you consider what happens to the Q-factor as the test frequency passes through the self-resonant frequency of the capacitor.

The Q-factor of a capacitor may be defined sensibly as the ratio of the effective reactance of the device to its effective series resistance. The esr is unaffected by the phenom-

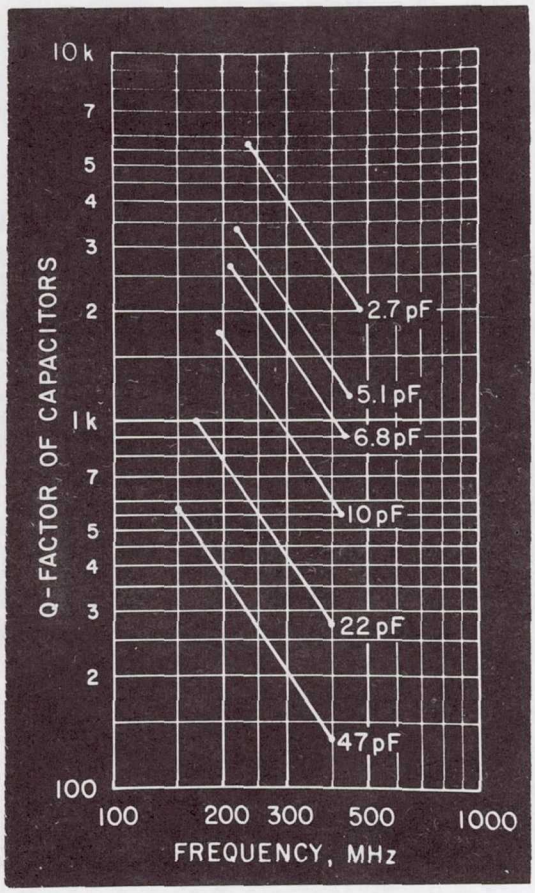

FIGURE 5.

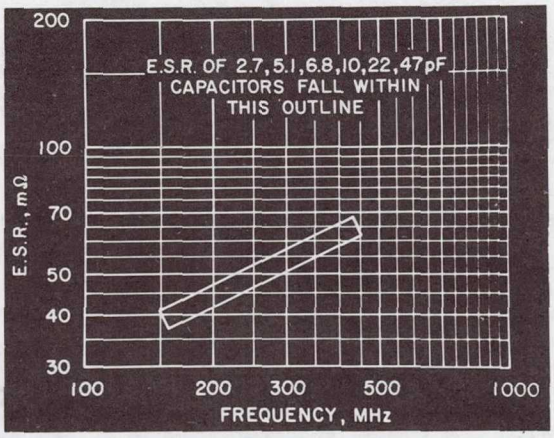

FIGURE 6.

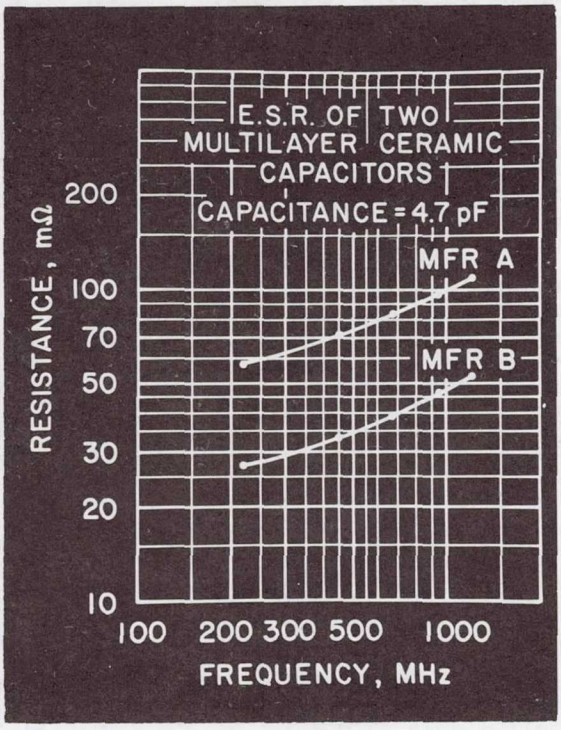

FIGURE 7.

enon of self resonance, and a plot of this parameter vs. frequency shows no deviation from a smooth curve as it passes through the neighborhood of resonance. Evidence of this is presented in Fig. 9 where the esr of four 82 pF capacitors from different manufacturers is displayed. The srf of one capacitor was 507 MHz, and 621 MHz for the other three.

The effective reactance, on the other hand, is the sum of the reactances of the capacitance and the self inductance of the device. As such it decreases to zero at resonance, as does the Q-factor. This is demonstrated in Fig. 10, where the Q-factors of these capacitors are displayed as a function of frequency. It can be seen that these curves are less than effective for characterizing capacitor loss in the vicinity of resonance.

There is no upper limit to the value of capacitance that can be measured in the series mode, and the esr of by-pass and coupling capa-

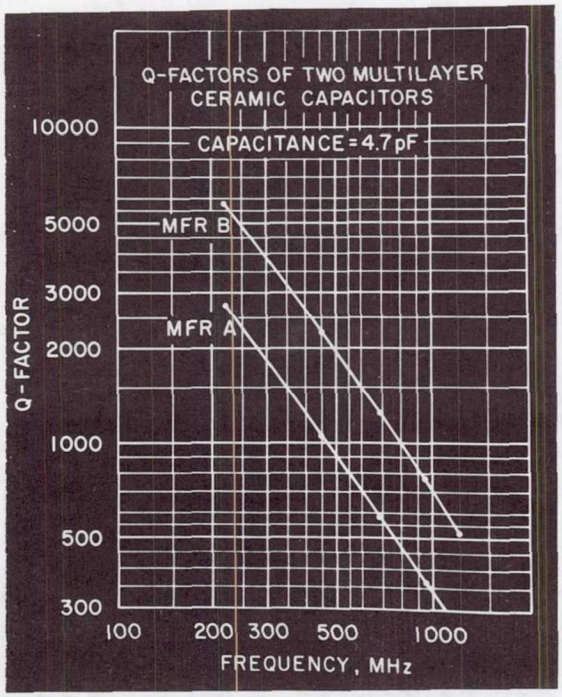

FIGURE 8.

citors is of value for high frequency applications. Leaded capacitors can be measured in the shunt mode, and large values may be evaluated in series with a previously measured smaller value.

Other components, including variable piston capacitors, will also submit to measurement in this system.

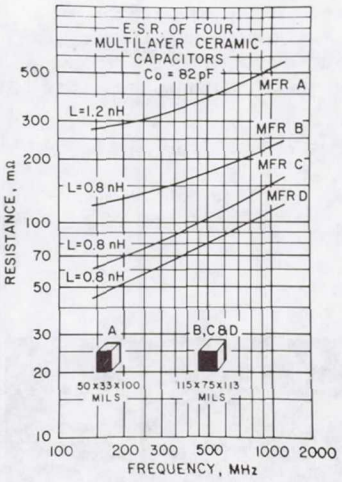

FIGURE 9.

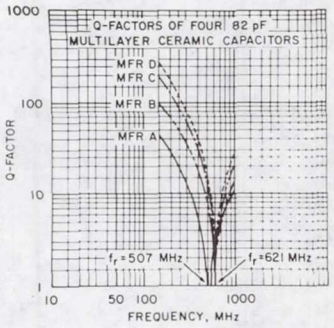

FIGURE 10.

The following equations are for the calculation of esr for series and shunt measurements.

Series: $$esr = Z_o[(\pi/4)\beta\ell \csc^2\beta\ell - 0.5 \cot\beta\ell][(1/Q_m) - (1/Q_1')] - r_f \quad (1)$$

Shunt: $$esr = Z_o[(\pi/4)\beta\ell \sec^2\beta\ell + 0.5 \tan\beta\ell][(1/Q_m) - (1/Q_1)] \quad (2)$$

Series

Z_o = characteristic impedance of line

$\beta\ell$ = line length in degrees = $(f_1/f_o')90°$

Q_m = Q-factor of system (line + test)

Q_1' = o.c. Q-factor of line at f_1

f_1 = measurement frequency

f_o' = fundamental resonant frequency of line (very nearly)*

r_f = fixture resistance at test frequency; nominally 3 to 4 mΩ

Shunt

Z_o = characteristic impedance of line

$\beta\ell$ = line length in degrees = $(f_1/f_o)90°$

Q_m = Q-factor of system (line + test)

Q_1 = s.c. Q-factor of line at f_1

f_1 = measurement frequency

f_o = fundamental resonant frequency of line

$$C = -1/\omega_1 Z_o \cot\beta\ell \quad \text{(series)}$$

$$C = 1/\omega_1 Z_o \tan\beta\ell \quad \text{(shunt)}$$

* f_o' is slightly lower than f_o to account for the discontinuity inductance of the fixture.

INVESTIGATION OF METALLIZED POLYCARBONATE FILM CAPACITOR FAILURES

Frank Ott
Jet Propulsion Laboratory
4800 Oak Grove Drive
Pasadena, CA 91109
(213) 354-4321

Manuscript was not received in time to be included in the proceedings. The author can be contacted for a copy of the paper.

ABSTRACT

Polycarbonate capacitor failures have been induced by thermal cycling and extended periods at high temperature. The temperature coefficients of the leakage paths have been measured and the results indicate that there are at least two separate types of leakage. The mechanism of the leakage paths are further complicated by what appears to be mechanical movement within the capacitor as its temperature is changed.

The failure mechanism appears to be lot related and is believed to be associated with the polycarbonate material. Chemical tests on the material of capacitors from production runs that performed well and those that did not have shown no detectable differences. Gas analyses of residual gases within the capacitors show significant differences.

A new system for pulse detecting during capacitor burn-in and during ramp testing has proven to be beneficial. Some parts that passed their conventional burn-in were subjected to an additional burn-in with pulse detection. Pulses were detected during the additional burn-in on parts that had been accepted by the conventional method of screening.

CAPACITOR DPA - DOES IT DO ANY GOOD

David C. Porter
Boeing Aerospace Company
P.O. Box 3999
Seattle, Washington 98124
(206) 773-1054

INTRODUCTION

We interpret the requirement for Destructive Physical Analysis (DPA) as one last chance on perhaps 3% of a lot to conduct a subjective analysis/ evaluation to see if you got what you paid for. The procedures are largely used on spacecraft quality parts but might have value if applied to the lowest cost parts on the market. The procedures we presently use are more applicable to the bottom of the quality scale although the accept criteria we sometimes pick can only be matched by the top quality producers.

If, DPA has a mother, it is probably the failure analysis laboratory experience in integrated circuits where in a very large percentage of cases, failures were traceable to defects which were optically visible after suitable dissection. It is not, however, immediately apparent that similar situations exist for capacitors.

This paper suggests methods of DPA which might have more usefulness if the procedures followed lines of accelerated testing. The reviews briefly present DPA procedures and discusses what value they have. It suggests a more thorough method of dissection and measurement of physical properties employing a solid tantalum as an example.

CAPACITOR LOT ACCEPTANCE TESTING ALTERNATIVE PROCEDURES

When we first heard of "DPA", it was explained that a very small sample of each lot of parts was to be sent to the failure analysis laboratory for special tests to determine if the lot was of "high quality". The first reaction to such a concept was that we would run very highly accelerated tests (perhaps combined with autopsy procedures) to assure that the resistance to stress in that lot was what one would expect of "high quality" capacitors. For this, a combination of voltage and temperature would be selected such that in a short period of time we could induce at least one failure but low enough so that we would either reject or at least re-sample if two or more failures were encountered.

Because we believed that all dielectrics wear out under the influence of an electric field at selected defect sites by subtle chemical change, we believed the most cost effective method of assuring the inherent quality of the lot would be such an accelerated test. Six years of exposure to Destructive Physical Analysis experience have not shaken this original concept. However, as much as we wanted to prepare acceptance criteria on an accelerated test basis, we were unable to do so and we are not much better equipped today than we were six years ago. There may be knowledgeable specialists who have a pretty good idea of what stress levels to expect but that information is not immediately available to us.

On ceramics, we could certainly go to 2 1/2 times rated voltage and maybe 4 times rated on some vendors product. We are uncertain about validity of accelerated testing at levels appreciably higher than that. On ceramics, if we are seriously concerned with cracks and delaminations as a failure cause, logically we would subject them to temperature shock exposures to aggravate such defects. However, we have poor information on which temperature shock conditions might aggravate defects without causing failure of fault free units.

On film capacitors, more so than on ceramics, it is obvious that the probability of a defect is very capacitance dependent. The percentage failure for a 10uF capacitor after a given stress should certainly be much larger than the percentage failures to be expected on a 0.01uF unit simply because the probability of a defect is much larger than on a smaller unit. On higher voltage units we would be concerned with the validity of acceleration if we had to enter the corona region. However, on high voltage product, the use of a corona test set with a suitable rejection criteria might be very useful. On solid tantalum units, some literature suggests very high acceleration factors with voltage yet is contradicted by guidelines such as MIL HDBK 217C which shows essentially no voltage acceleration of failure rate at all. On solid tantalum units, the buyer is basically unaware of either the formation

voltage or the re-formation voltage and accelerated testing above those levels might be invalid.

We are not equipped to recommend high voltage accelerated testing on wet tantalum units. However, substitution of a very high ripple current life test to uncover lots unusually failure inclined has considerable appeal.

Although the concept of accelerated testing had strong appeal, the fact that we could not write procedures identifying stress levels and the to be expected results caused us to revert to writing procedures which would primarily dissect and physically examine the unit. The decision to go this route was aided by the fact that those types of standardized procedures were really what the customer wanted anyway. Now let us examine those basic procedures, their motivations and the effects of such analysis on several capacitor types.

Ceramics

On ceramics, we started with three samples and elected to pot and section two; one perpendicular to the leads for delaminations, voids, evenness and adherance of coating, end margins, etc., and one parallel to the leads to inspect the quality of solder connections. The third unit was chemically stripped so the body could be inspected for cracks, signs of silver migration, and so that a pull test could be conducted on the solder joints. With one brand of parts, gross cracks were typically introduced in the body of the first sectioned sample because of potting compound pressures but that was not a significant problem; we could pot and section the third sample to accomplish the same objectives. With a second brand, our potting techniques only rarely caused cracks in the chip but on those cases where it did, an extra sample has to be acquired and the experiment repeated after stripping the body to be sure it was not lab technique causing the problem. The outer coating on the second brand was almost impossible to strip with organic solvents -- frequently taking two days and even then it has on at least one occasion pulled the outer plate requiring a repeat of the process. The only clean way we can strip the coating is in hot nitric acid and that clearly prohibits inspection for silver migration or conditions of the solder connection to the copper leads.

What do we reject for on the sectioned sample? Originally, we looked for voids over 50% of width and for delaminations 2 1/2 times the thickness of the dielectric. This was tougher than most requirements we have reviewed but generally when they were bad enough to exceed our limits they exceeded almost the loosest of requirements as well. As time has progressed, the criteria has been negotiated with the supplier which generally wound up with a relaxing of the requirements. We have recently rejected the example of Figure 1 with the basic argument that it was not built in the intended fashion, but with the secondary argument that one plate was too close to the outside. This fault probably represents a computer software error in the equipment designed to punch out the squares of ceramic. In this same time period, we accepted the example of Figure 2 even though there is a void running between plates. The criteria is for voids less than 50% of the width but a diagonal string of voids is acceptable and this extended in argument to a continuous diagonal void having a width of 50% of the dielectric.

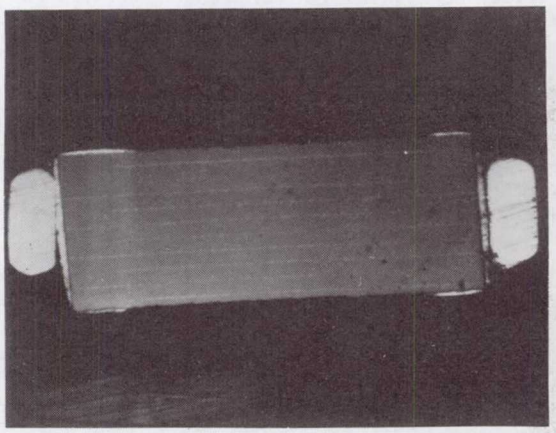

Figure 1. Rejected Ceramic Capacitor - Plates Out of Order and Too Close to Edge

POLYCARBONATE FILMS

We make two lathe cuts on the ends removing the seals and spacers and inspect the terminations. The freedom from vibration failure is considered adequate if we have to split the case lengthwise to get the winding out. We unwind the outer few layers and measure overlap and edge margins. On very small units we may unwind the whole unit after sanding away the sprayed terminations but on larger units, we consider this essentially impossible and do not check the overlap at the inside of the unit. We section one lengthwise to record the basic method of construction and have a basis of comparison with succeeding lots but unless we observe

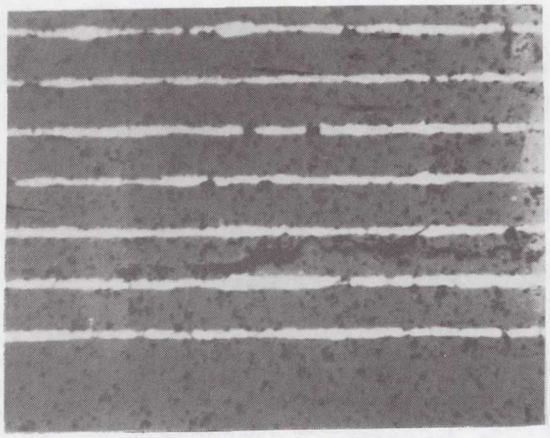

Figure 2. Accepted Ceramic Capacitor - Adjacent Plates Joined by Void No More Than 50% of Closest Distance

something drastically out of the ordinary we really have no rejection criteria at all. See Figures 3 and 4.

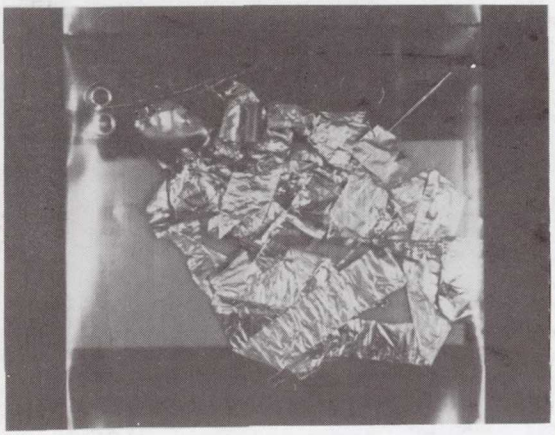

Figure 3. Disassembled Foil Capacitor

TANTALUM FOILS

The procedures are the same as for films -- two lath cuts to open the units -- unwind -- inspect the welds and look for odd discolorations. Pot and section one unit to have a record of how the basic assembly is made. We do not attempt to measure the quantity of electrolyte nor completeness of

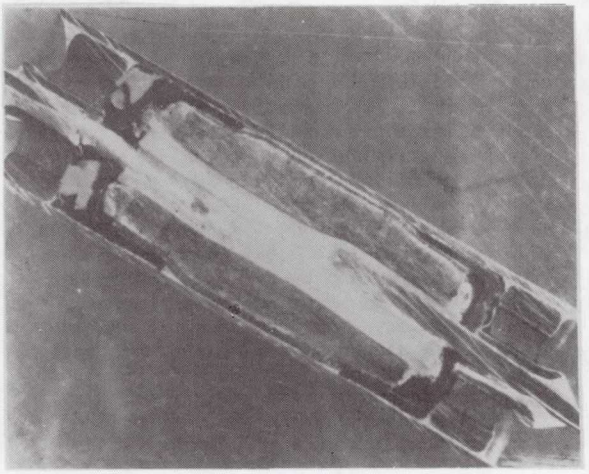

Figure 4. Sectioned Foil Capacitor

fill. It evaporates so rapidly after the case is breached that we really have no idea how completely it was filled.

SOLID TANTALUMS

We cut a window in the side near the anode and inspect for abnormalities in solder or tubulations after we have blown out the debris we introduced. We complete the opening at the top and pull on the slug measuring the force to remove it. Basically we consider it well attached if we cannot separate it from the case by pulling. We also section one unit, mostly because when we wrote the procedures we could not think of anything else to do. This gives us a general feel for the way the slug is held in the solder but actually does not do a great deal more to measure quality than a good X-ray would accomplish. We have never rejected a solid tantalum unit. We no not attempt to measure the quantity of electrolyte nor do we even routinely record the particle size and degree of sintering with a SEM.

DESTRUCTIVE EXAMINATION OF SOLID TANTALUM

Once, some sixteen years ago, we were asked to do a "design evaluation" of identical units of two different brands of solid tantalums. As a part of this effort we slowly increased (1V/sec) a current limited voltage, plotting the slope until an abrupt change in slope was observed. We interpreted this voltage as the reformation voltage. Later, after stripping all outer materials the slug was immersed in phosphoric acid and again the voltage-current curve examined until a break was observed. This was interpreted as the formation voltage. Identical samples were delivered to the chemical laboratory where,

by taking advantage of differences in solubility of the materials, physical differences, and colorimetric techniques, we were able to measure the quantities of materials present on the two brands with the results as shown in Table I.

Table I
Comparison of Two Brands of 4.7uF 35V Solid Tantalum

	Brand A	Brand B
Reformation Voltage	87V	125V
Formation Voltage	170V	160V
Wt. of Unit (Leads Removed)	.464 Grams	.637 Grams
Wt. of Carbon	.016 Grams	.047 Grams
Wt. of MnO	.022 Grams.	.056 Grams
Wt. of Slug	.362 Grams	.491 Grams

Note: Slugs were identical in size

No SEM was available when these units were examined but since then the SEM has been used to record quantitatively particle size and degree of sintering. See Figure 5.

If we wanted a top quality unit, we would want one with a heavy specific gravity slug. We would want one with a high reformation voltage. We do not know how fussy we should be about formation voltage but if we were buying units over extended periods of time, we would be interested in knowing what changes in processing had taken place and maybe an explanation for the changes. The importance of the total weight of MnO_2 is not too clear. However, consistancy in this number might indicate consistancy in the number of cycles of pyrolytic reduction of $MnNO_3$ that had been employed. Arguments have been expresssed that would suggest that the quantity of MnO_2 might have a direct relationship to the failure mode (short vs. high leakage) and it is not too hard to believe that it may have a basic relationship to the probability of surge current failure.

We have never repeated these measurements on other capacitor brands, sizes, or voltage rating. Being curious, we would like to know what the data might show but we find ourselves in the position of only getting paid for what we are asked to do. These sort of "physical" measurements have a potential role in DPA but we have not proposed them. Our customer also require that we establish the limits and reject criteria for every test. We do not have that information.

SUMMARY

In this paper, we have tried to argue that forms of accelerated testing would appear to have a good technical basis for separating good lots from bad lots of capacitors for DPA purposes especially when combined with failure analysis procedures. We have outlined briefly the technques of destructive analysis we presently employ and hope that we have conveyed a skepticism of the value of that type of effort. We have also outlined briefly a type of "physical analysis" that could be conducted using a solid tantalum as an exampled. It is suggested that such procedures might be appreciably more informative of lot to lot variations and inherent quality factors than our present procedures but there is a lack of data to justify their adoption.

This paper is really a plea to the customer for either discontinuation of DPA on capacitors as we presently practice it or adoption of procedures which have higher information value.

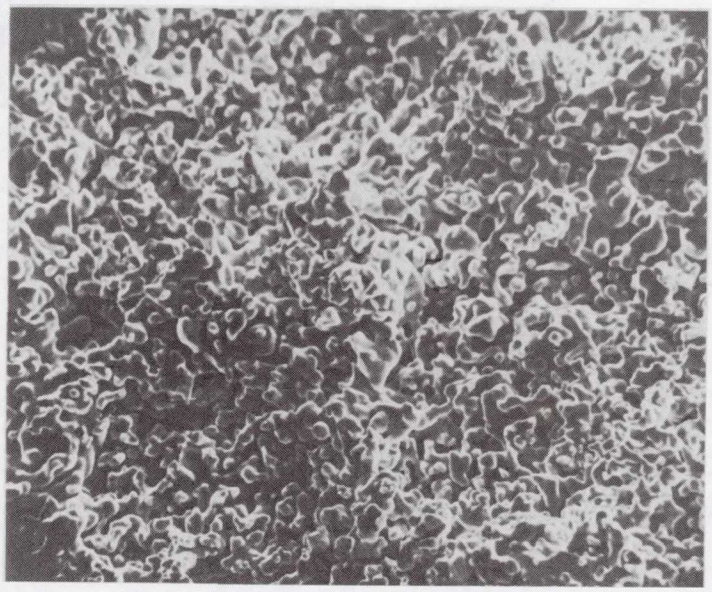

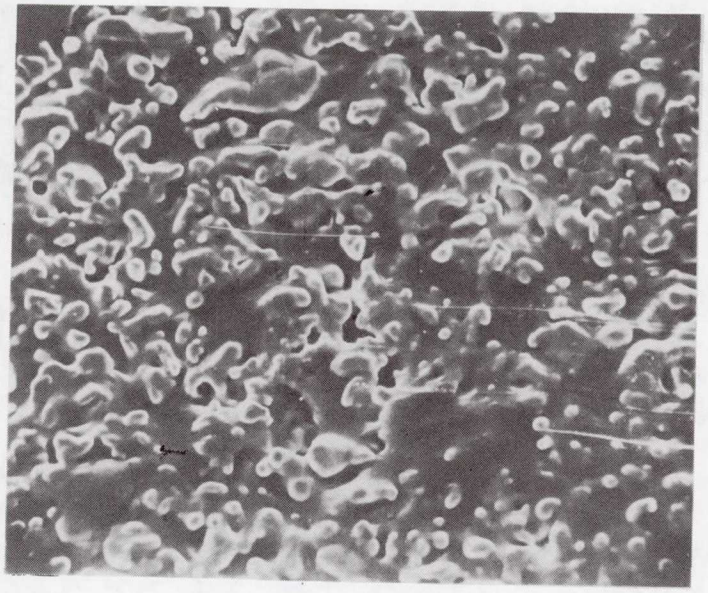

FAILURE ANALYSIS METHODS FOR CAPACITORS

BY
R. L. Hildenbrand
MARTIN MARIETTA AEROSPACE
Denver, Colorado

INTRODUCTION

It is the intent of this paper to describe the basic steps in the failure analysis of discrete capacitors used in electronic circuit boards and hybrid assemblies.

Failure Analysis of capacitors should be augmented sufficiently to provide significant recommendations to improve the component and system reliability.

Each failure, failed component, is unique and, therefore, should be treated as a single discrete failure.

An effort should be made to assure all aspects of the failure mechanism are delt with. Because this theoretical approach is not easily attained, historical data concerning the basic failure mode should be researched thoroughly to reduce the number of steps necessary to determine the actual failure cause.

Numerous varieties of capacitors are presently in use in the Aerospace Industry. To mention all is not feasible here.

The varieties discussed will be in the FIXED CAPACITOR catagory and are those most often encountered.

The varieties of capacitors will be:

Tantalum - Wet foil and wet slug
Solid electrolyte
Hybrid chip.

Ceramic - Monolithic chip encapsulated
Discoidals encapsulated.

Film - Polypropylene and metal foil
Polycarbonate metalized film.

CONSTRUCTION CHARACTERISTICS

The construction characteristics of each variety involved in the basic elements of a capacitor are dielectric, plates, terminations, encapsulants and in the case of tantalum capacitors, the electrolyte, an extension of the cathode plate. The diagram Figure 46 illustrates the most common material characteristics of the various capacitor elements. One or several of these material elements may be involved in a single failure analysis; therefore, a detailed understanding of their construction is required.

ANALYSIS CHECK LIST

To proceed with an orderly failure analysis a basic check list is quite helpful and may be developed for each of the named varieties. The analysis check list should provide at least these basic steps.

IDENTIFICATION
HISTORY
VISUAL INSPECTION
NON-DESTRUCTIVE TESTS
DISASSEMBLY
SPECIAL EXAMINATIONS
DOCUMENTATION

Identification should include the part number, manufacturer name, lot number, date code, number of parts failed, number of parts sampled, MIL-SPEC reference number, report number, etc.

History should contain the basic failure statement, the mode of failure and the circumstances involved in the failure. The specification requirement that was not met should be included in the failure statement.

It can then be determined from the history statement what tests should be performed to verify the reported failure.

Visual Inspection. The level of inspection should be sufficient to assure identification of visual anomalies. Microscope magnification values, lighting and other methods should be determined to insure identification of physical damage sites. X-ray analysis of the failed device and comparative X-ray of good devices may be useful in determining internal damage sites and other anomalies.

Potential failure sites may be determined from DPA (destructive parts analysis) data from similar parts. Typically the survey should look for external d.c. leakage sites at seals or other critical surfaces, terminal damage, case dents or cracks, evidence of overheating, charring, solder reflow or deformation, workmanship defects, etc.

Non-Destructive Tests. Initial quick look electrical tests at ambient temperature and pressure may be performed upon completion of the visual inspection. These should be simple and direct checks at the stated failure values, i.e., voltage frequency, d.c. bias, equivalent incircuit source and/or load impedance; checks for shorts, opens or leakage as required.

Seal leakage tests may also be included here, providing they do not generate alterations or loss of the failure mode. Seal tests may be deferred till after the next item if necessary.

Electrical-Mechanical Tests. Electrical parameters which the part failed should have been performed during the non-destructive verification testing. Other parameters including capacity, dissipation factor, d.c. leakage, insulation resistance, frequency response, and temperature coefficient may be measured as required to assist in determining the mode of failure.

Mechanical tests may also be necessary to verify the failure mechanism. Lead pull or bending tests, solder dewetting, metal hardness, shock, vibration, temperature burn-in, temperature cycling and/or temperature shock may be used if required to determine the mode of failure.

Disassembly. A summary review of all previous steps in the analysis should be performed to aid the analyst in determining the most suitable method to perform the disassembly.

A detailed method of dissection is required to arrive at the failure site and still maintain the failure mode as originally verified.

Method resources are:

- MIL-STD-1580 "Physical Analysis for Space Quality Parts."
- RS-469 "Standard Method for Destructive Physical Analysis of High Reliability Ceramics Monolithic Capacitors" by Electronic Industries Assoc. Standards.
- Manufacturer-Vendor recommended methods.
- Failure Analysis Research developed methods determined from DPA Samples.

Special Examinations.

Additional analysis may be required in the search for the failure cause. Special examinations may be:

Material Identification
Contamination and/or Particle I.D.
Microscopy Studies using
    Brightfield, darkfield,
    Interference contrast,
    Fluorescense microscopy,
    Infra-red microscopy,
SEM-EDX,
AUGER-SIMS,
X-ray diffraction,
Thermogravimetric-RGA,
and others.

These special examinations may be determined after completing the preliminary Analysis Check List review.

ANALYSIS METHOD GUIDELINES

Failure mechanisms and failure modes for capacitors to be covered in this paper will be presented by examining seven basic types of analysis.

- o Electrolytic wet slug encapsulated
- o Electrolytic solid encapsulated
- o Electrolytic solid hybrid
- o Ceramic chips, encapsulated
- o Ceramic discoidals, encapsulated
- o Film polypropylene metal foil
- o Film polycarbonate metal film

Sample Failure Analysis

Tantalum Wet Slug Encapsulated Part No. M39006/09-4786 Date Code 7402A. Failure history: Capacitor indicates excessive dc leakage, suspected of causing excessive current surges on the 28 VDC input to an electronic module. Capacitor was series limited by a 22 ohms 1/4 watt resistor in an encapsulated module. Analysis Procedure: Electrical measurements for d.c. leakage verified the failure. At 30 volts d.c. the leakage current measured 2 ma. Capacity was in tolerance but the dissipation factor was excessive.

X-ray analysis was performed and results are shown in Figure 1.

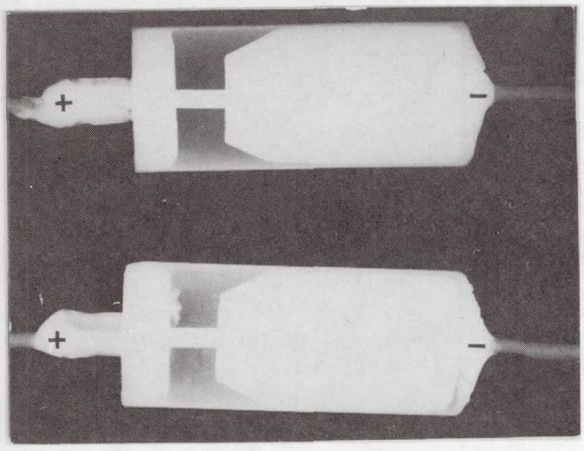

Figure 1: Capacitor X-ray M3900G/09-4786.

Illustrated in Figure 1 are two hermetically sealed wet slug tantalum capacitors. An internal cathode capsule can be seen fitted into a second outer can and hermetically sealed at the glass feed through. The lower capacitor failed the d.c. leakage test. X-ray analysis revealed an anomaly at the inner surface of the hermetic seal. The lead-in solder seal appeared intact. No evidence of electrolyte was present on the exterior of the outer seal.

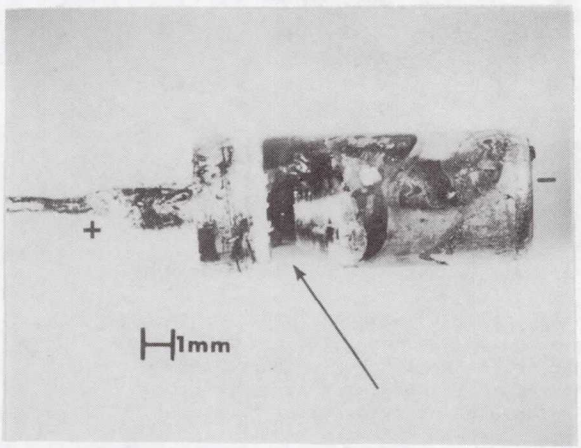

Figure 2: Capacitor with outer case removed.

Dissection was performed by removing the outer can. Grinding two sides of the cylinder allowed it to be bisected top to bottom. Using long nose pliers, the outer case was peeled off leaving the encapsulated inner capacitor.

Prior to further sectioning, a leakage test indicated the leak site was at the anode (+) header seal across the inner surface of the glass seal. No leakage was present from the anode to the inner cathode Ag can. Upon removing the epoxy encapsulant at the inner anode seal (see arrow) a black electrolyte gel was observed at the glass inner surface. Previously dissected good parts had no gel at this location.

Cause: Failure was attributed to electrolyte leakage past the inner primary seal to the outer hermetic glass feedthrough seal.

Conclusion: Apparent cause was temperature overstress above 125°C which forced the electrolyte gel through the first seal into the second outer seal area.

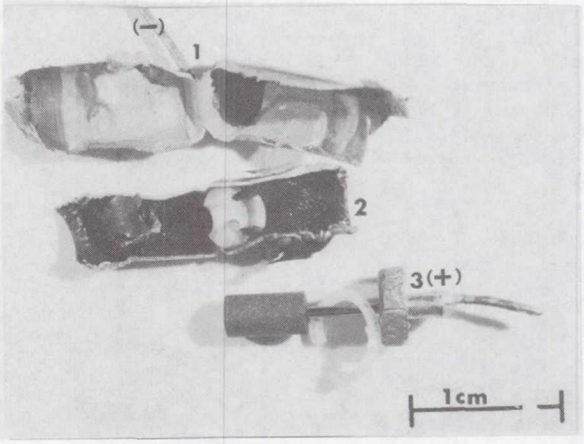

Figure 3: M39006/09-4786 "Break-down".

Subsequently, the second inner cathode can was bisected and carefully removed. The inner teflon seal was also bisected and removed. The anode slug appeared normal and displayed no evidence of breakdown.

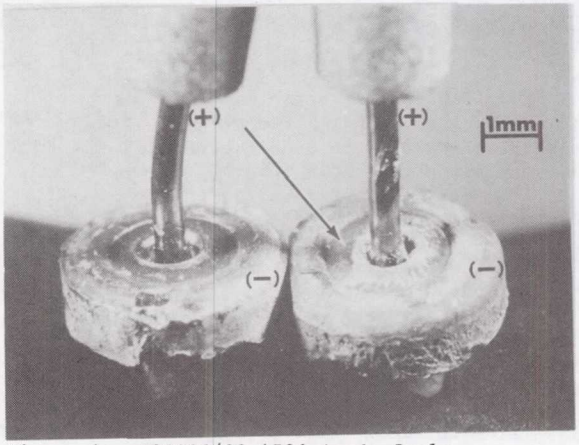

Figure 4: M39006/09-4786 Anode Seals.

Here we see the electrolized and etched surfaces where d.c. leakage occurred. The area at the arrow corresponds to the X-ray anomaly noted in Figure 1.

Because no evidence of a breakdown site was apparent on the anode slug, the failure was attributed to temperature overstress at the electronic package assembly test level.

Tantalum Solid Electrolyte, Encapsulated. Similar to MIL-C-49137 (C25) Date Code 7532.

Failure History. Capacitor exhibited excessive leakage, 9 ma. at 14 VDC. Part was removed from power supply where it was current limited by two 1/8 watt 20 ohm resisters in parallel. The two resistors had overheated and degraded. Their ambient no load resistance was 24 ohms. The capacitor leakage when removed was not sufficient to overheat the two resistors. No other defect was found in the power supply or its load. What caused the resistor to over heat?

Analysis Procedure: Visual inspection revealed extensive surface damage to the capacitor case material. The outer case was a vinyl tape filled with epoxy. See Figure 5.

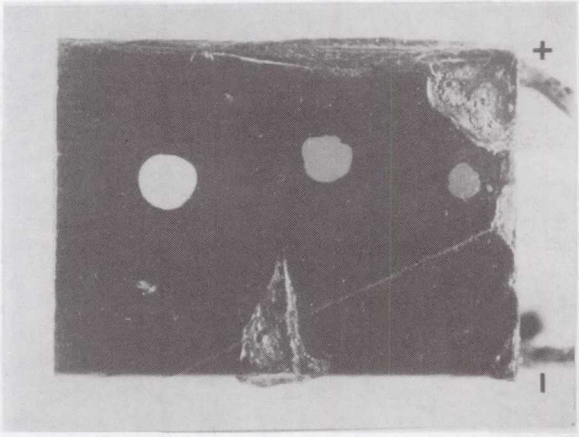

Figure 5: Capacitor C25 showing soldering iron burn marks. 10X

Electrical testing for d.c. leakage verified the reported failure mode. Dissection was begun by removing the outer tape wrap and decapsulating the epoxy. See Figure 6.

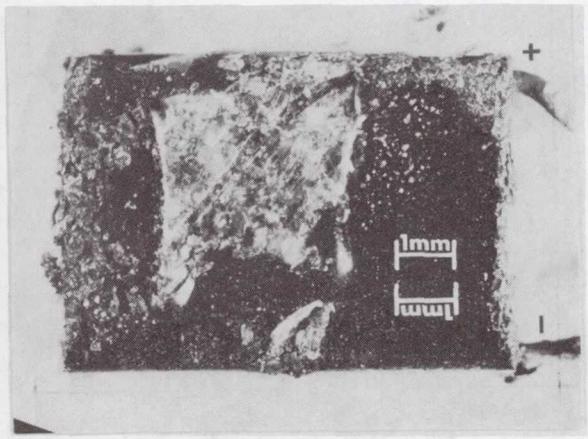

Figure 6: Capacitor after removing a portion of the Epoxy Encapsulant with a 1 hour soak in MS-111 Stripper. 10X

The cathode silver paste is showing through the inner wrap of plastic tape. Tape showed evidence of overheat and was discolored. Reference Figure 6.

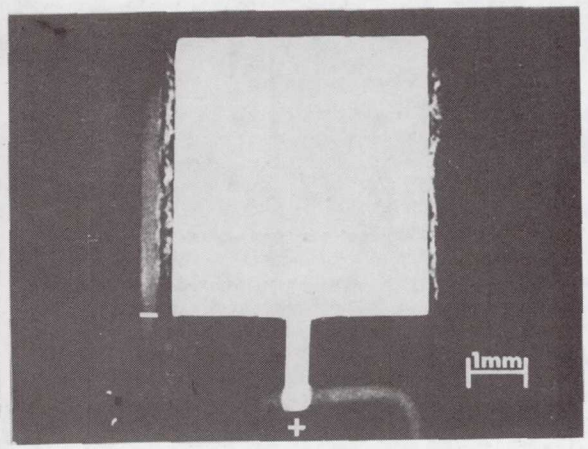

Figure 7: X-ray Macrograph showing Ta Core and the Anode and Cathode Lead positions. 10X

The irregular material on either side of the sintered core is the silver paste to manganese dioxide layer. Reference Figure 7.

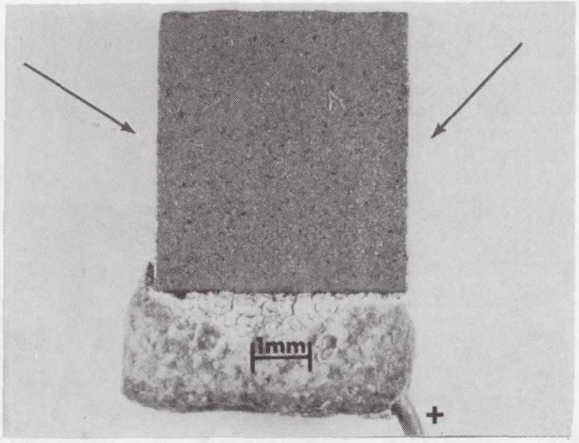

Figure 8: Ta Sintered Core after removing the Manganese Dioxide Layer of Electrolyte. 10X

Removal of the manganese dioxide layer was accomplished by soaking the part in concentrated Hydrochloric Acid for 40 hours.

After rinsing the part in deionized water, the part was ultrasonically agitated in a water bath for 30 seconds to help remove the remaining softened material. The anode was then blown dry with dry N_2 gas. Two areas indicated an insoluable reminent of material which appeared yellow-brown in color. The arrows indicate two locations with the most discoloration. Reference Figure 8.

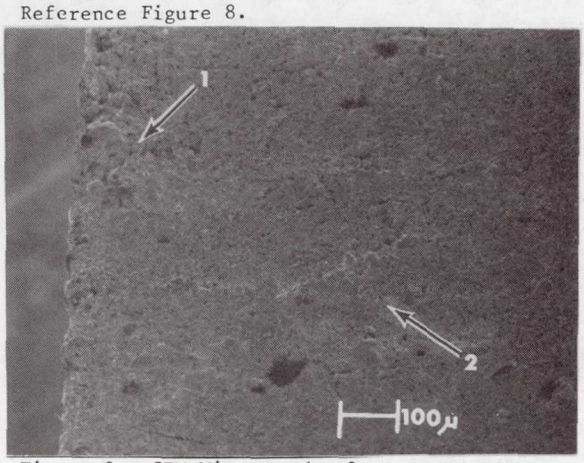

Figure 9: SEM Micrograph of an area near the point where the soldering iron appeared to have penetrated deep into the cathode edge. 100X

Area 1 and area 2 of Figure 9 are detailed below in Figures 10 and 11 and represent areas where reformation is thought to have occurred.

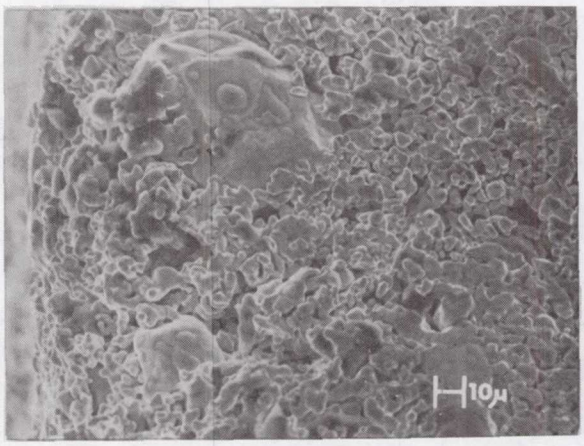

Figure 10: 500X Area 1 SEM Micrograph Showing the enlarged areas of reformation on the finely grained, sintered tantalum core material.

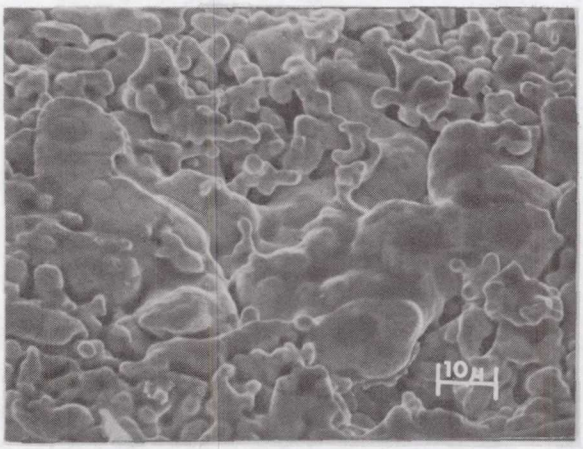

Figure 11: 1000X Area 2 SEM micrograph showing reformation sites in the overheat zone.

Because some controlled reformation is attained in the manufacturing process and does appear on other cores of similar design, it is difficult at this point of the analysis to determine if this is a definite failure site, however, it does correlate with the soldering iron damage site and the over heat zone.

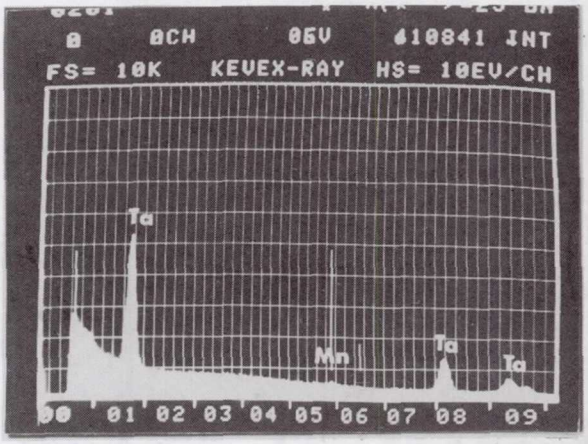

Figure 12: KEVEX-RAY spectrum analysis on one of the reformation areas. A small trace of manganese is evident at the markers. The major peaks are those of tantalum.

Cause: Excesive leakage was caused by a hot soldering iron which melted through two layers of plastic insulation and damaged the manganese dioxide layer and the TaO_5 dielectric on the sintered core.
Conclusion: The initial short destroyed the outer coating around the two thin film resistors. Current limiting provided by these resistors allowed the manganese dioxide layer to overheat sufficiently and allow reformation to occur at the failure site. A layer of manganese oxide appeared around the failure site.[1]

Tantalum Solid Electrolyte-Hybrid
Part No. CWROGHA106KR (MIL-C-55365/4)
Failure History: Part removed from circuit on alumina substrate. Part failed d.c. leakage. At 1 VDC, leakage measured 2.5 ma.

Analysis Procedure: External physical characteristics are illustrated in Figure 13 and 14. Visual examination revealed a discolored area at the anode clip as shown in Figure 15.

Electrical testing was implemented as shown in Figure 16.

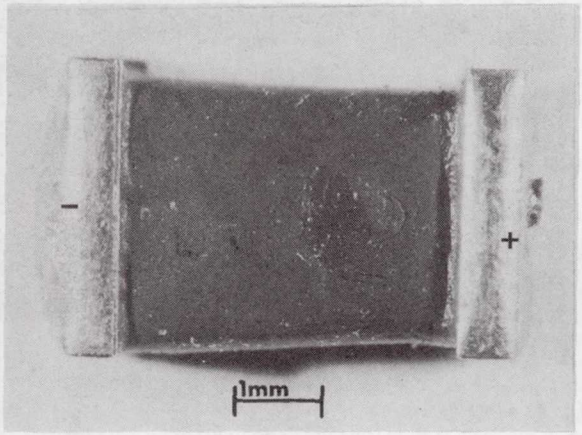

Figure 13: 15X. Top view of a CWROGHA106KR part used for comparison. Anode at right arrow indicates area where the other part failed. See Figure 15.

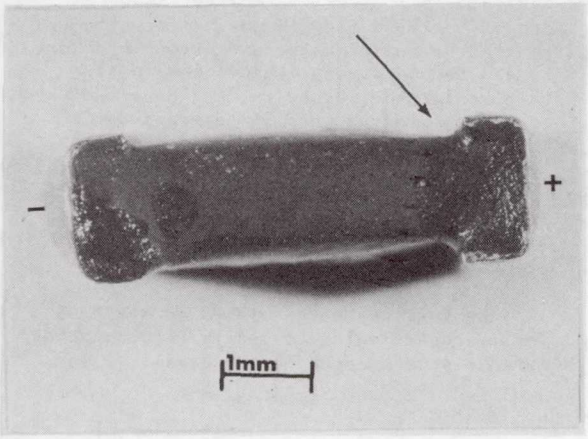

Figure 14: 15X Side view of CWROGHA106KR arrow indicates edge of clip where the other part failed. See Figure 15.

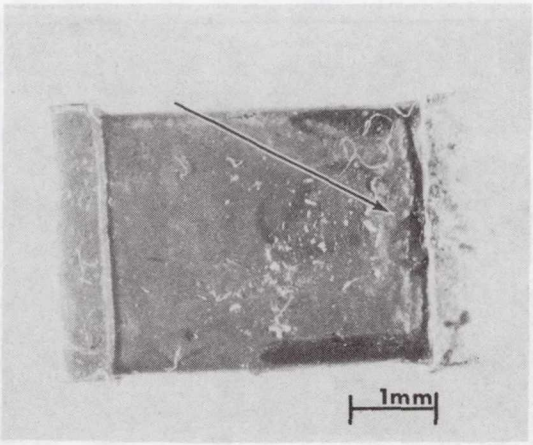

Figure 15: 15X View of failed part. Arrow indicates area where clip shorted to cathode layer of Ag underneath.

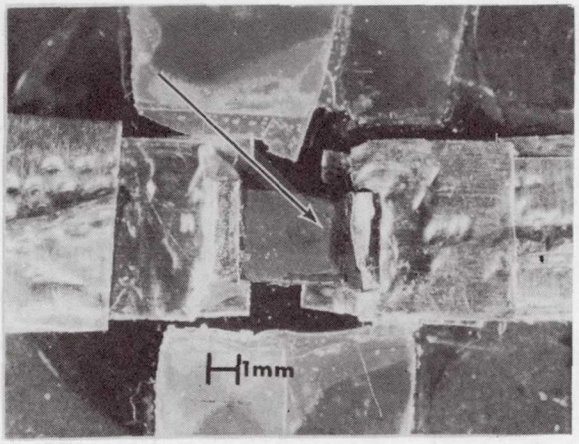

Figure 16: Test set up showing failed capacitor taped to two electrodes on a glass slide plate for continuous monitoring during the dissection analysis. 3X

The anode (+) clip was carefully lifted and bent back. D.C. leakage returned to normal. The anode clip to cathode silver epoxy layer short site is identified by the arrow. Normally, a layer of plastic insulation and epoxy isolate the metal anode clip from the underlying silver epoxy layer that covers the manganese dioxide electrolyte layer on the tantalum core.

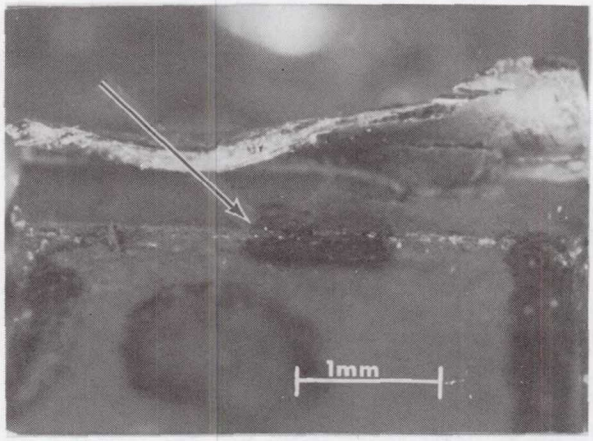

Figure 17: 30X Macrophoto showing shorted breakdown site at arrow.

Cause: Failure was attributed to a short circuit between the anode clip and the cathode silver epoxy layer below.
Conclusion: One of several possible causes may have produced the failure.

1. Mechanical stress on the top of the anode (+) clip may have pressed the clip into the Ag epoxy cathode layer.

2. Voltage (greater than 15 VDC) overstress may have punched through the thin insulation barrier under the clip.

3. The insulation barrier may have been reduced by the sharp edge of the clip, or the insulation layer was insufficient at the failure site.

A preliminary review indicated this was not a recurring item.

Encapsulated Ceramic Chip Capacitor
Part No. ST90D28-11 Date code 7411. (MIL-C-39014C)
Failure History: Capacitor failed insulation resistance measurement. Part measured 5000 ohms terminal to terminal when removed from a d.c. amplifier assembly.
Analysis Procedure: Electrical test verified the terminal to terminal resistance measured 5.55K ohms. Capacity was in tolerance, but the dissipation factor was 6.5% at 1000 Hz. Maximum D should be 2.5%.

X-ray analysis failed to reveal any defects in the case material or terminals. See Figure 18.

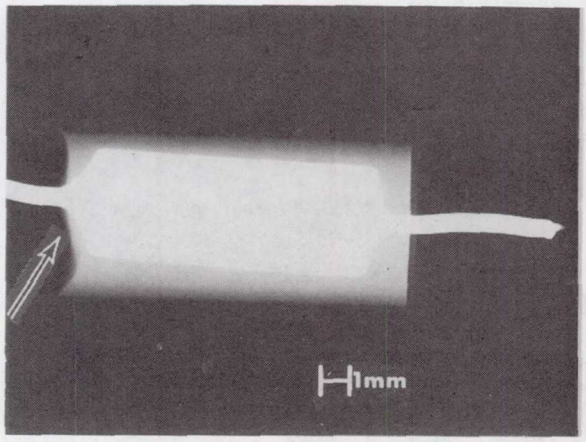

Figure 18 X-ray Macrographs of ST90D28-11

This capacitor is encapsulated in a preformed case. The encapsulating material is poured into the preform and cured. Arrow indicates the miniscus surface of the potting fill.

Decapsulation was performed by soaking the part in 1 methyl - 2 pyrrolidinone heated to 165°C for 2 hours. After rinsing in deionized water and drying with dry N_2 gas the part was retested for insulation resistance, capacity, and dissipation. All values were in tolerance. The leakage appeared to be in the encapsulant.

Visual examination of the ceramic chips in the assembly revealed exposed plates along one edge of a single chip. See Figure 19.

The part was encapsulated in MARGLASS for microsectioning to verify that no other defects were present in the ceramic chips.

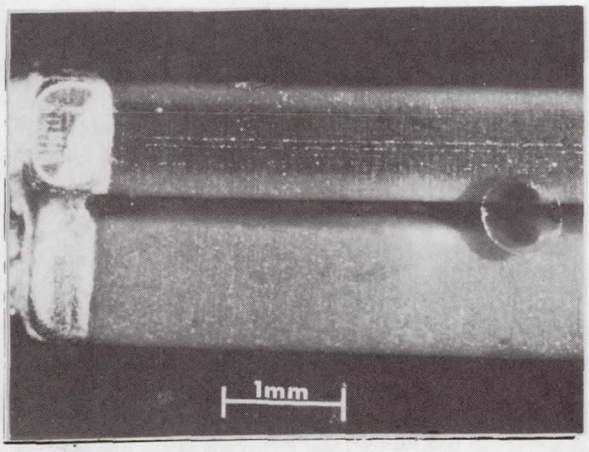

Figure 19
MARGLASS encapsulated capacitor assembly

This macrograph illustrates the exposed silver plates along the edge of one of the two ceramic chips used in this assembly.

Examination of the filtrate from the decapsulation fluid failed to reveal any ceramic chips that might have flaked off the ceramic monolithic chip during the 2-hour soak. Subsequent microsectioning slowly through the monolithic chip verified the capacitor, except for the missing margin of ceramic, was normal. No delamination sites or voids were evident.

Cause: Failure was attributed to a d.c. leakage site in the epoxy encapsulant surrounding the chip capacitor.
Conclusion: Absence of a ceramic margin allowed the capacitor plate edges to be exposed to the encapsulating material which has a lower volts per mil dielectric strength.

Ceramic Discoidals
Part no. MIL-F-15733E/01 type EMI filter.
History: A ceramic capacitor feed-through (discoidal) was removed from a battery assembly filter unit because it failed the insulation resistance test, terminal to case.

Analysis Procedure: Electrical measurements were initially performed on the type "L" filter assembly. Subsequently, after dissection, the failure to meet the 10 meg ohm insulation requirement was isolated to the discoidal capacitor assembly. Insulation resistance measured less than one meg ohm. See Figure 20.

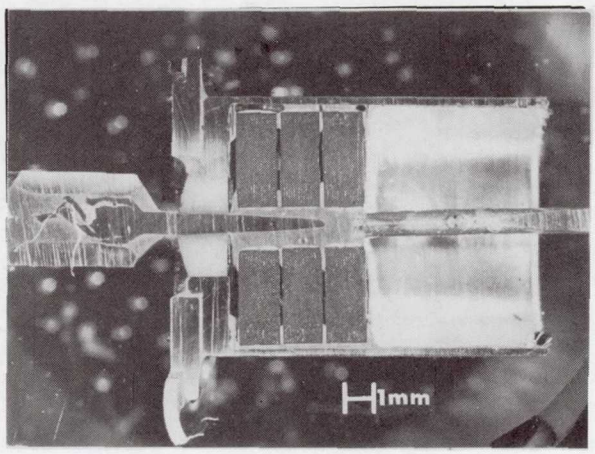

Figure 20: Typical Microsectioned Assembly.

This microsectioned three element capacitor is shown to illustrate its basic structure. The failed unit was unsoldered by heating the assembly to 480°F and carefully removing each discoidal capacitor for individual analysis. The insulation resistance failure was isolated to a single unit which was then encapsulated in MARGLASS and microsectional in a manner specified by RS-469.[2]

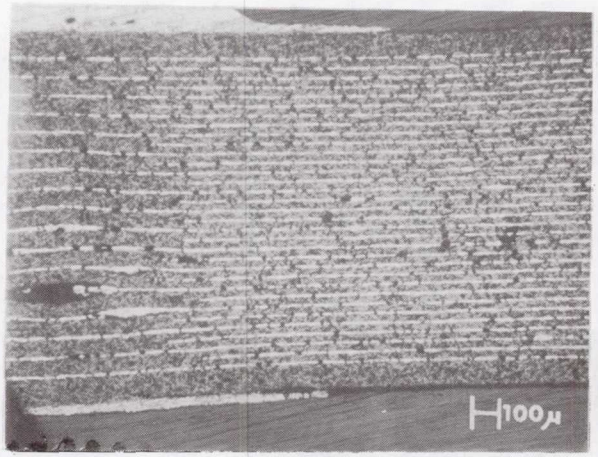

Figure 21: Microsectioned Discoidal Capacitor.

This 50X microphoto shows the location of the defect site. This high contrast photo is attained by brightfield micrography.

The location of the site was predicted before entering the actual defect site when a birefringent area was observed as shown below in Figure 22.

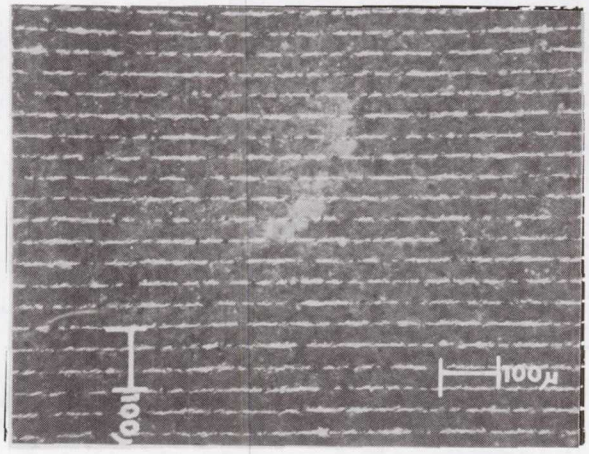

Figure 22: Microsection plane which preceded final exposure of the failure site.

This 200X microphoto shows a birefringent zone which was attained by crossing the polarizing analyzer filter with the light source filter. Areas of changing refractive index within the translucent ceramic reflect a birefringent characteristic. The large microvoid beneath this site was subsequently exposed by further lapping and polishing. Three views of the exposed defect are shown in succession to illustrate the nature of the defect site. Subsequent lapping and polishing removed the defect. The capacitor was monitored electrically between lapping steps and returned to normal insulation resistance, capacity and dissipation factor when the defect site was removed.

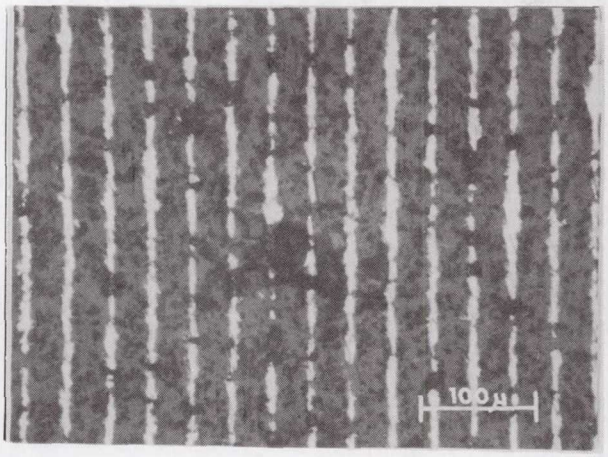

Figure 23: Brightfield image of the defect site shown here at 200X

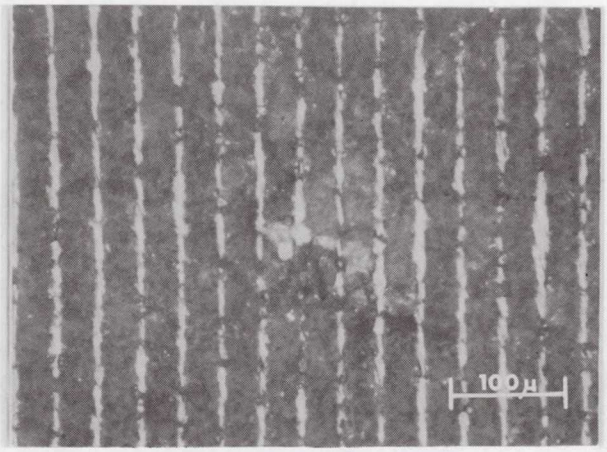

Figure 24: Slightly uncrossed polars were used to show the defect site detail at 200X.

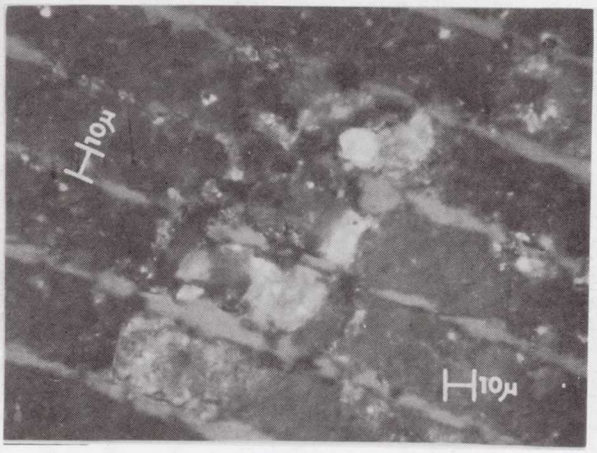

Figure 25: 500X Micrograph showing the defect site. Five layers of ceramic dielectric are involved in this microvoid.

Cause: The leakage site was isolated to a major dielectric defect which involved five layers of dielectric.
Conclusion: Screening tests were not sufficient to eliminate this defective device before installation in the assembly.

FILM, POLYPROPYLENE AND METAL FOIL

Part No. SV90D49-2 (MIL-C-83421)
Failure History: Initially one capacitor shorted at 750 hours at 100°C during a 1000 hour life test. The max. a.c. current rating for this part by specification was 4.2 amps at 40K HZ and 100°C. The capacity and voltage rating was 0.12 ufd. and 400 VDC. A sampling of parts from the same lot were submitted for further testing and evaluation.

Samples of these evaluations were submitted for dissection and analysis of the dielectric film between the plates. The samples included two Hypot failures, two newly wound parts without temperature exposure, one acceptance tested good part, one acceptance and qualification tested part and one part which had past 2400 VDC hypot test after burn-in.

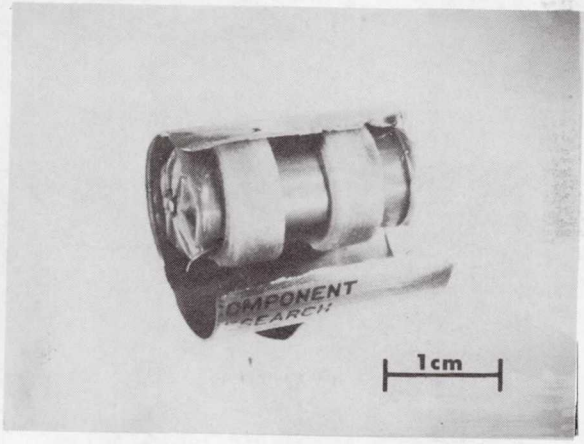

Figure 26: SV90D49-2 0.12 ufd 400 VDC Capacitor.

This assembly has been partially decapsulated by lupidary grinding on a metalurgical Polimet polishing wheel using water and Carbomet silicon carbide grinding paper-120 and 240 grit. This step removed the sealed axial lead feedthrough seals. Subsequently, the case was scribbed on each

side and bisected exposing the inner capacitor spool which was unwrapped and unspooled to expose the polypropylene film dielectric and the metal foil ribbons. The failure sites of the failed devices were exposed in the same manner.

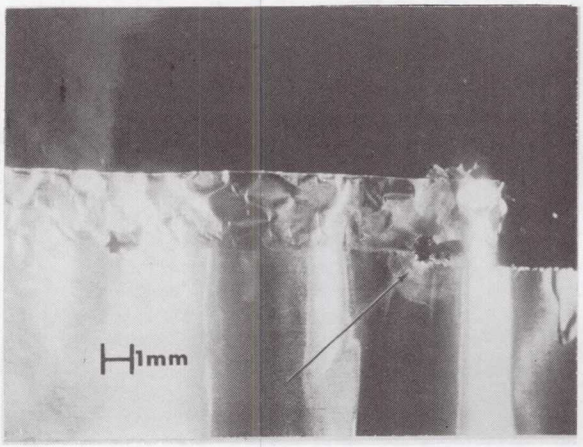

Figure 27: Failure site as seen by Stereo-Microscope at low magnification.

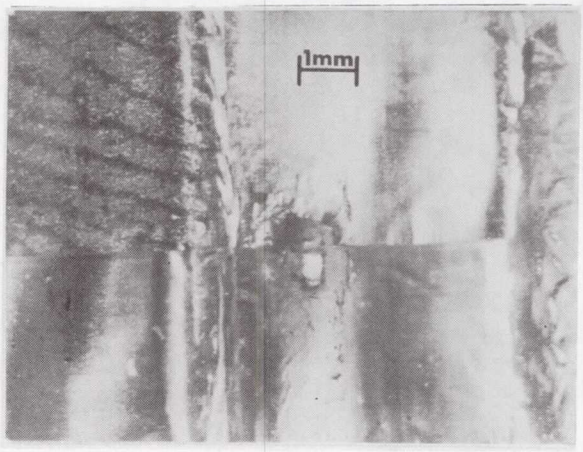

Figure 28: Failure site of another component shown here at 10X.

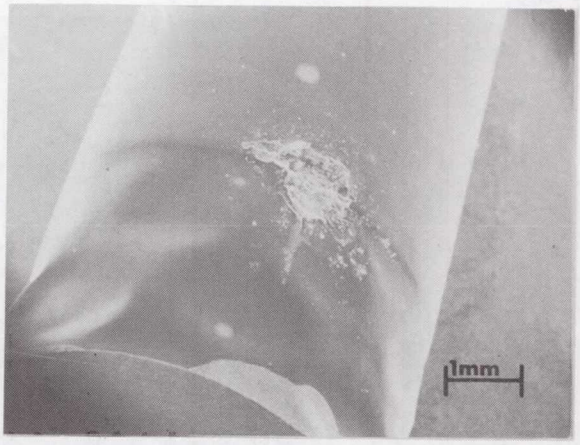

Figure 29: SEM Micrograph of the 750 hour failure shown here at 15X.

Figure 30: SEM Micrograph of same failure site at 50X.

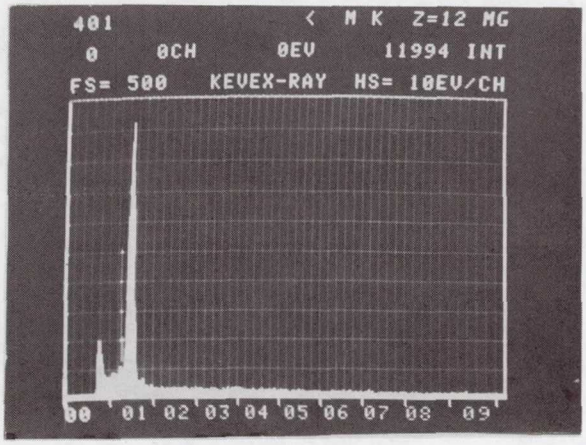

Figure 31: KEVEX-Ray typical spectrum taken at the failure site. The only element apparent was Al from the metal foil.

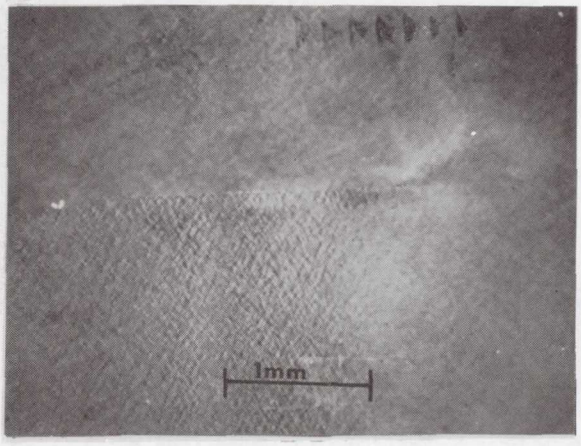

Figure 32: Slide transparency of the polypropylene shown here at 25X. The upper area is the margin beyond the foil layer.

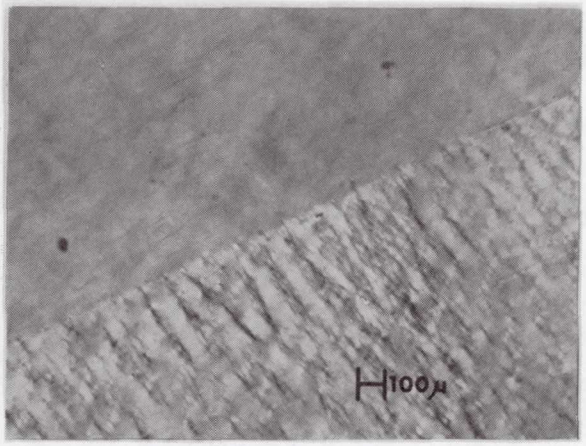

Figure 33: 50X View of the same transparency.

Note that the lower area is thinned and distorted. The linear temperature coefficient of the foil is much less than the coefficient for the polypropylene film by a ratio of approximately 1 to 4. Permanent impressions are formed during temperature exposure and temperature cycling.

The degree of degradation is apparently distributed over some probability curve determined by the individual component hot spot temperature and the film density variations present in the lot of parts tested.

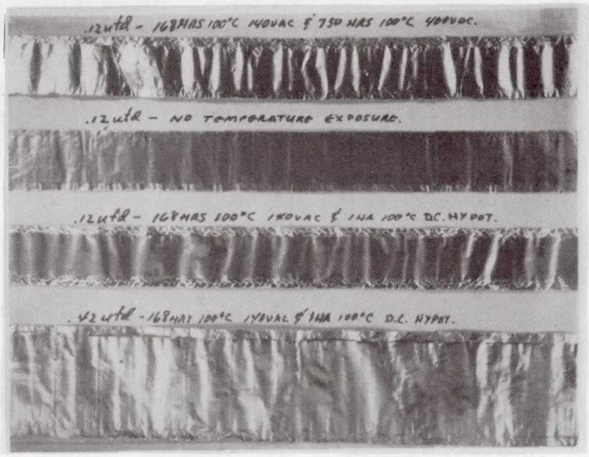

Figure 34: Foil and film ribbon samples displayed to illustrate the lack of wrinkles along the edges of ribbons not exposed to the high temperatures compared to those with high temperature exposure.

Cause: Failures were isolated to a site at the edge of the metal foil and generally toward the inner end of the spool wrap.
Conclusion: Microscopic examination of the dielectric film indicated the film was degraded by the 100°C temperature when the part was operated with 140 VAC to simulate the proper series current at 40 KHZ. Apparently the additional heating generated by the a.c. caused the dielectric film to soften. Its softing temperature is approximately 194°C. The initial specification for operation at 100°C was reduced to 85°C for subsequent lots to avoid the degradation caused by the higher temperatures.

Film, Polycarbonate, Metalized Film. Part No. SS90DM39022-1, date code 7607.
Failure History: The capacitor 0.27 ufd. 50 VDC failed open at 30°C during temperature testing.

Analysis Procedure: Electrical measurement for capacity and dissipation factor were preformed to verify the failure during temperature cycling. The capacitor was then submitted for X-ray analysis at the failure temperatures.

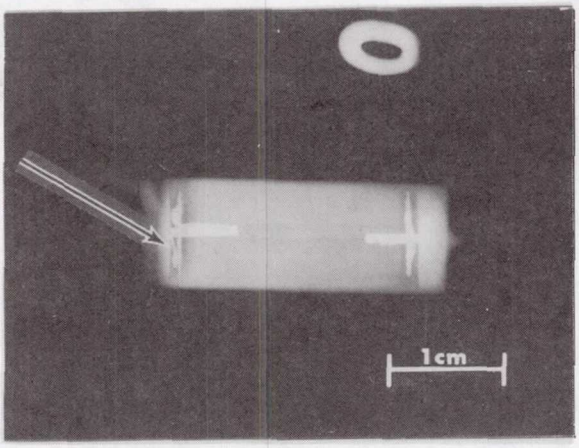

Figure 35: X-ray Macrograph of the failed capacitor SS90DM39022-1 at 30°C. 2X
Arrow at left indicates area where solder pad lifted off the babbit termination.

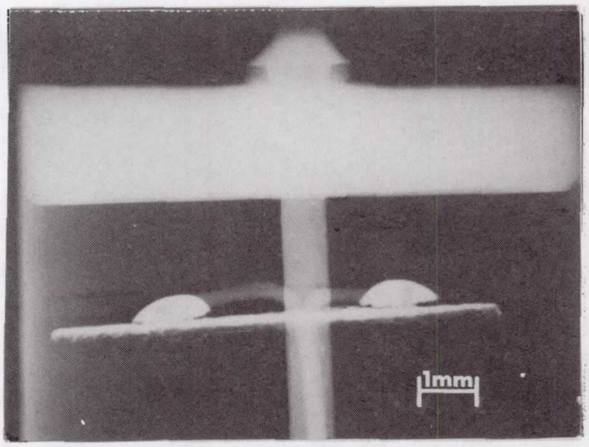

Figure 36: X-ray Macrograph detail showing solder pads lifted at 30°C. 10X

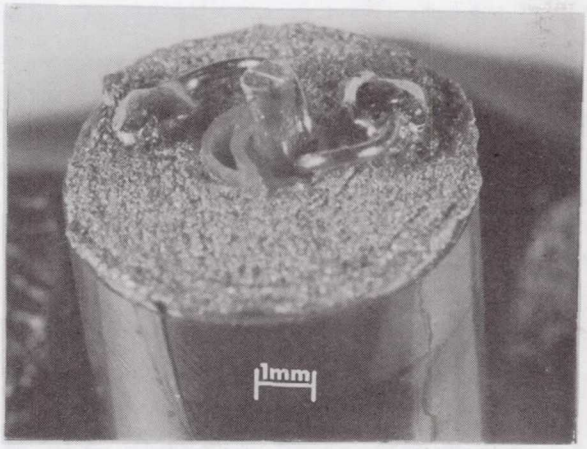

Figure 37: Macrophoto of capacitor spool after decapsulation. 10X

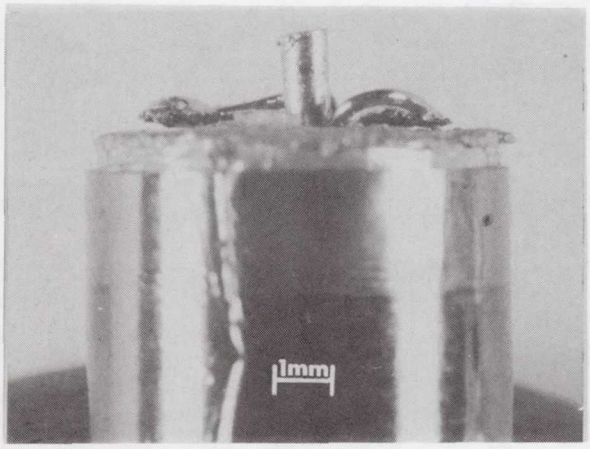

Figure 38: Macrophoto of lifted solder pads as observed after disassembly. 10X

A pull test was performed on the remaining good end of the failed capacitor. A comparative sample was made of a good part. The failed component pull strength was 150 grams compared to 709 grams for the comparative sample. The bond pull strength may have required further research but was not pursued since the temperature cycle tests were considered more significant.

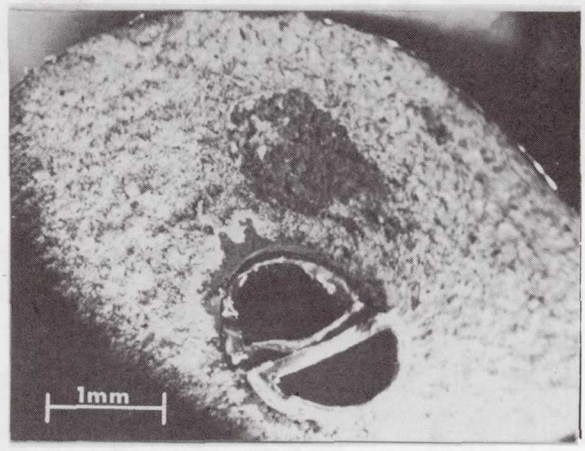

Figure 39: SEM Micrograph or fractograph of the babbit surface where one of the bond pads failed.

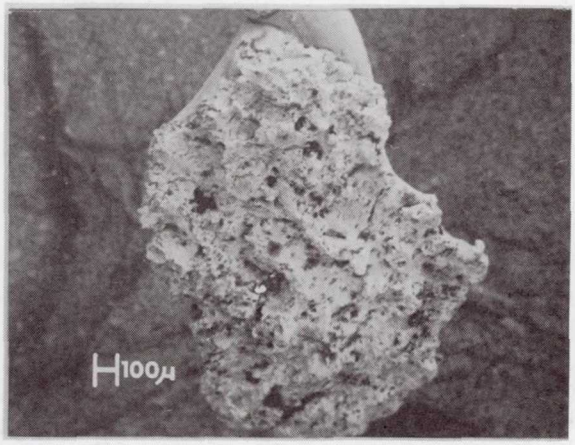

Figure 40: SEM Fractograph of one of the bond pads which failed.

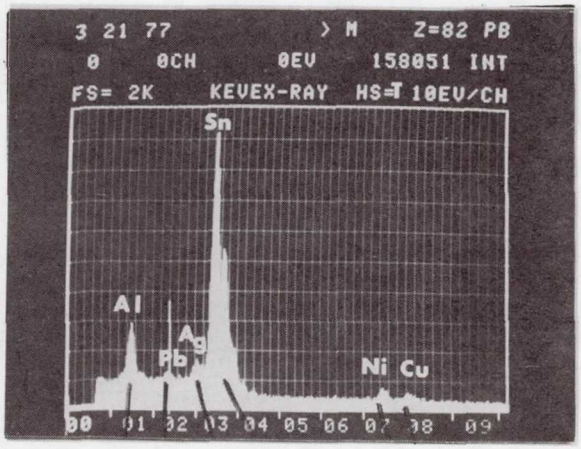

Figure 41: KEVEX-Ray Spectrum of failed bonding surface. Elements present are Al, Pb, Ag, Sn, Ni and Cu.

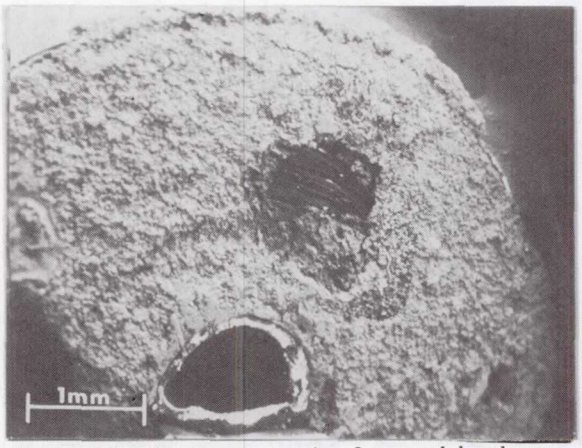

Figure 42: SEM Fractograph of a good bond. Note that the babbit pulled out of the Aluminum film leaving the ribbon exposed.

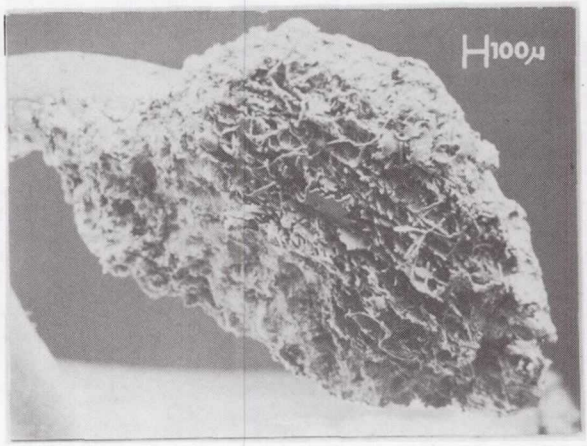

Figure 43: SEM Fractograph showing good bond pad which pulled out portions of the aluminum film.

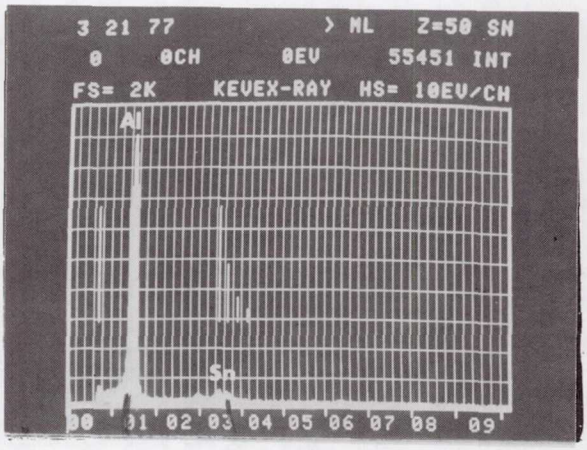

Figure 44: KEVEX-Ray Spectrum of bond pad above. Note the high Aluminum peak indicating pull out of the metalized film.

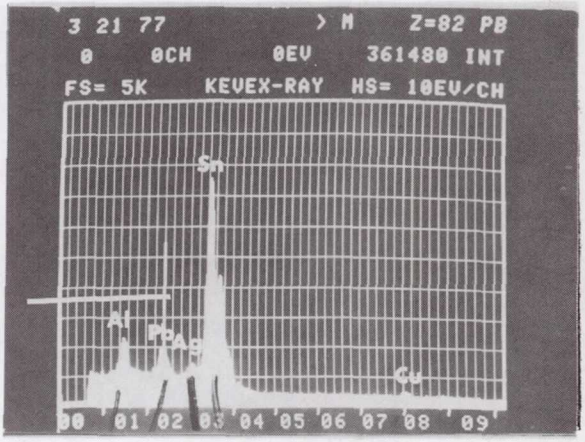

Figure 45: KEVEX-Ray Spectrum of the bond face from the good end of the failed part which pulled out at 150 grams. This surface is comparable to Figure 41.

Cause: Failure was attributed to a discontinuity at the terminal solder joint (internal) connecting the capacitor spool end to the axial lead.
Conclusion: The solder joint pulled free of its bond to the babbit (Sn, Cu, Sb) electrode on the spool end. Solder failure was attributed to improper assembly during manufacture of the part. The encapsulating

package maintained continuity by the pressure of the shock isolator pad. Subsequent temperature exposure in the electronic assembly may have weakened the pressure allowing it to open at 30°C.

The failure was verified by thermal cycling from ambient to 120°C. Fifteen parts from the same date code and 3 parts from date code 7529 were temperature cycled in groups of 6 from +125°C through ambient to -55°C. No failures were noted during the temperature cycling tests.

Failure was attributed to workmanship error during encapsulation.

SUMMARY

The mechanics involved in a typical failure analysis of a discrete part may be briefly outlined by these steps:

- o Visual Examination
- o Functional Test
- o Disassembly
- o Isolation of the Failure Site
- o Documentation

In this paper the sample failure analyses have been condensed considerably. However, the intent is that they will serve as typical examples.

The examples were extracted from actual experiences over the past ten years and represent only a few of the problems encountered in capacitors.

REFERENCES

1 Optimization of Tantalum - Manganese oxide capacitor healing, J. G. Babick, Jr. and F. M. Goll, ECC Proceedings 1972.

2 ESI-RS-469 - Standard Test Method for Destructive Physical Analysis of High Reliability Ceramic Capacitors. Electronic Industries Association, November 1980.

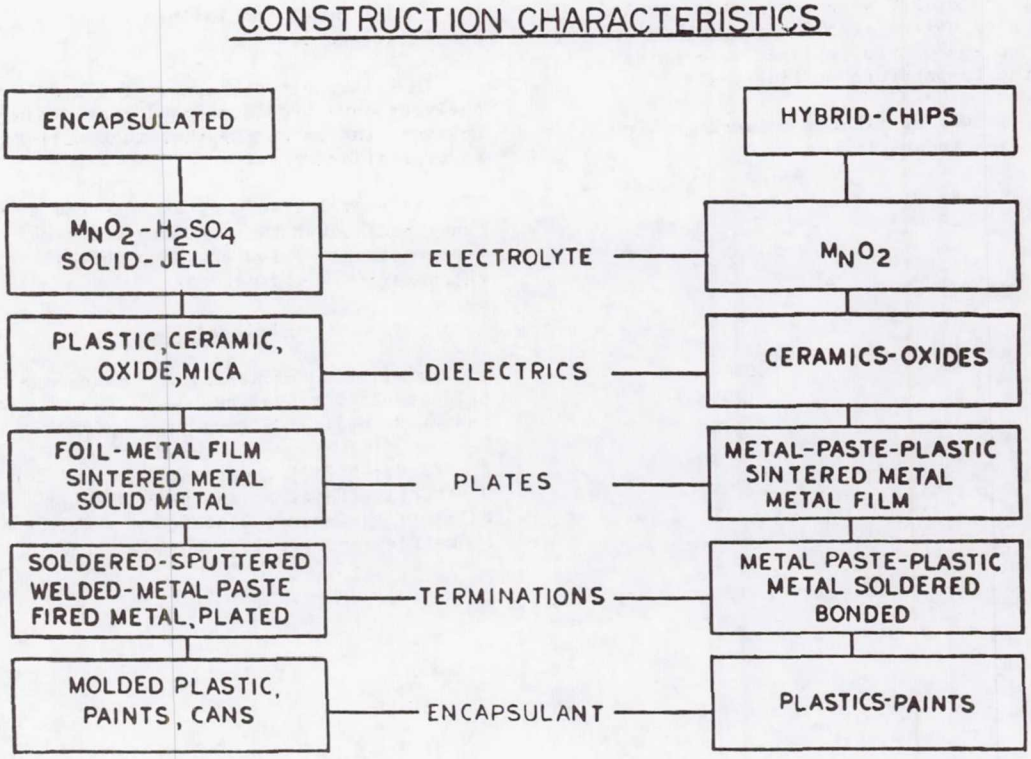

Figure 46: CONSTRUCTION CHARACTERISTICS

ATTENDEES LIST

NAME	ADDRESS	PHONE
Dick Acker	Marshall Space Flight Center Code EC11 Huntsville, AL 35812	(205) 453-2514
I. D. Akins	Goodyear Aerospace Dept. 853 Plant G Akron, OH 44315	(216) 796-2087
John Alexander	Standard Telecommunication Labs London Road, Harlow Essex, England	
Donald Anderson	Tektronix DS-78-552 P. O. Box 500 Beaverton, OR 97077	
Richard Andre	Bendix Corporation Guidance Systems Division Dept. 6401, Mail Code 2/13 Route 46 Teterboro, NJ 07608	(201) 288-2000 Ext. 1832
Robert G. Antonopolis	Aerojet ESC Mail Zone 194/8443 P. O. Box 296 Azuza, CA 91702	(213) 334-6211 Ext. 3148
Ricardo Bailey	Mattel Electronics, Inc. M.S. 128-1 5150 Rosecrann Avenue Hawthorne, CA 90250	(213) 978-6451
John Baldwin	USAMICOM DRSMI-QRT Redstone Arsenal, AL 35898	(205) 876-4438
Paul Barker	Data General Corporation M.S. D-215 4400 Computer Drive Westboro, MA 01581	(617) 366-8911 Ext. 6807
Gary Beam	Sparton Electronics Johnson Lake Road P. O. Box 788 De Leon Springs, FL 32028	(904) 985-4631
Jewell G. Belcher, Jr.	Marshall Space Flight Center Code EC43 Huntsville, AL 35812	(205) 453-4562
John Berkebile	Marshall Space Flight Center Code EC43 Huntsville, AL 35812	(205) 453-4562

Paul Berrigan	E.I. DuPont de Nemours & Co,, Inc. P. O. Box 89 Circleville, OH 43113	(614) 474-0565
E. H. Berry	Marshall Space Flight Center Code EC43 Huntsville, AL 35812	
Dr. James Biggers	Pennsylvania State University Materials Research Laboratory University Park, PA 16802	(814) 865-1638
Walt Billin	Bunker Ramd P. O. Box 5009 Westlake Village, CA 91359	(213) 889-2211
Mike Blamire	Erie Technological Products 5 Fraser Avenue Trenton, Ontario K8V 5S1	
Richard J. Blomgren	Kollsman Company Daniel Webster Highway Merrimack, NH 03054	(603) 889-2500 Ext. 2092
Ed Bolton	AVX-Ceramics P. O. Drawer K Wareham, MA 02571	
Woody Bombara	Marshall Space Flight Center Code EG02 Huntsville, AL 35812	(205) 453-5469
Jon W. Borough	Northrop Corporation Electronics Divison 2301 W. 120th Street Hawthorne, CA 90250	(213) 615-3026
E. P. Bork	IBM Corporation Dept. 106, Bldg. 708 P. O. Box 950 Poughkeepsie, NY 12602	
D. G. Boyd	USAMICOM 703 Delwood Road Huntsville, AL 35802	
Dr. F. N. Bradley	AVX Ceramics P. O. Box 867 Myrtle Beach, SC 29577	
Bill Brecht	Matsushita Industrial Company 9401 West Grand Avenue Franklin Park, IL 60101	(312) 451-1200 Ext. 3784
Charles O. Brooks	Marshall Space Flight Center Code EG01 Huntsville, AL 35812	(205) 453-1600
Bill Brown	Tansitor Electronics, Inc. P. O. Box 230 Bennington, VT 05201	(802) 442-5473
Richard Buckelew	USAMICOM DRSMI-QRT Redstone Arsenal, AL 35898	(205) 876-4438

Eugene J. Buhmann	Marshall Space Flight Center Code EC43 Huntsville, AL 35812	(205) 453-4562
Patrick J. Burkett	General Electric Electronics Parkway Building 7, Room 181, Mail Drop 25 Syracuse, NY 13221	
Jim Burka	Marshall Space Flight Center Code EH22 Huntsville, AL 35812	
Darnall Burks	Sprague Electric P. O Box 5327 Wichita Falls, TX 76307	(817) 767-8351
H. T. Cannon	MEPCO/Electra, Inc. 6071 St. Andrews Road Columbia, SC 29210	(803) 772-2500
W. P. Carrier	Mallory Capacitor Company P. O. Box 372 Indianapolis, IN 46208	(317) 636-5353
Philip M. Chase	IBM Corporation Dept. 1D6, Bldg. 708 P. O. Box 950 Poughkeepsie, NY 12602	(914) 463-8044
Robert Checkaneck	Western Electric 50 Lawrence Road Springfield, NJ 07081	(201) 467-7132
Samuel E. Church	Sprague Electric Company North Adams, MA 01247	
J. Clark	Perkin-Elmer Corporation, ASD 2771 Garey Avenue Pomona, CA 91767	(714) 593-3581 Ext. 322
Duane Clemmer	Centralab 7158 Merchant Avenue El Paso, TX 77915	(915) 779-3961
Jerry Clubb	Marshall Space Flight Center Code EF13 Huntsville, AL 35812	(205) 453-0129
Nello Coda	Erie Technological Products 645 W. 11th Street Erie, PA 16512	(814) 453-5611
Sherman W. Cohen	Aerospace Corporation M. S. A2/1013 P. O. Box 92957 Los Angeles, CA 90009	(213) 648-5257
Allen Cole	AVX-Ceramics 2179 Northlake Parkway Tucker, GA 30084	
Frank Corbin	Chrysler Corporation 102 Wynn Drive Huntsville, AL	

Ed Cornelius	SCI Systems, Inc. P. O. Box 4000 Mail Stop 23 Huntsville, AL 35802	
Michael J. Cozzolino	Hughes Aircraft Company Culver City, CA 90230	
St. John Courtenay	Marshall Space Flight Center Code EC43 Huntsville, AL 35812	(205) 453-4562
R. L. Crafton	E Systems, Inc. Garland Division P. O. Box 226118 Dallas, TX 75266	(214) 272-0515 Ext. 4633
Ansley Crouch	Tansitor Electronics, Inc. P. O. Box 230 Bennington, VT 05201	
Don Daebler	GTE Subscriber Equipment 13000 Memorial Parkway W Huntsville, AL 35803	(205) 883-3109
George Davenport	Mallory Capacitor 2615 Memorial Parkway Huntsville, AL 35801	
H. V. DeMatos	Union Carbide Corporation P. O. Box 5928 Greenville, SC 29606	
Albert J. Divigard	Colt Industries Chandler Evans, Inc. Control Systems Division Dept. 937 (Guided Projectile Controls) Charter Oak Boulevard West Hartford, CT 06101	(203) 236-0651
Dr. George Doanne	Marshall Space Flight Center Code EC21 Huntsville, AL 35812	
Henry Domingos	ECE Department Clarkson College Potsdam, NY 13676	(315) 268-6535
H. B. Drexler	Martin-Marietta/Orlando P. O. Box 5837 Orlando, FL 32855	(305) 352-2145
Frank A. Duva	Vitramon, Inc. P. O. Box 544 Bridgeport, CT 06601	(203) 268-6261
Dick Eliason	Honeywell DSD Code MN11-2443 600 2nd Street, N.E. Hopkins, MN 55343	(612) 931-6941
R. E. Ellingwood	IBM Corporation Dept. 1D5, Bldg. 708 P. O. BOx 950 Poughkeepsie, NY 12602	

Walt England	Sprague Electric North Adams, MA	
E. P. Fabbri	GTE Automatic Electric Labs 688 Industrial Drive Elmhurst, IL 60126	(312) 681-7248
Edward H. Fairfield	Sprague Electric 87 Marshall Street North Adams, MA 01247	(413) 664-4411 Ext. 2028
Bob Fanning	GTE Automatic Electric 13000 Memorial Parkway, South Huntsville, AL 35803	
Don Favorito	Lockheed Missile & Space Company Dept. 8451, Bldg. 153 P. O. Box 504 Sunnyvale, CA 94086	(408) 743-2035
Ron Fitzgerald	GTE Subscriber Equipment 13000 Memorial Parkway, South Huntsville, AL 35803	(205) 883-3109
Marie M. Fegley	CS Draper Labs 555 Technology Square Cambridge, MA 02139	
Jim Fosnaugh	Martin-Marietta/Orlando MP-246 P. O. Box 5837 Orlando, FL 32855	
Rolf A. Frantz	Bell Labs Room 8E-020 Whippany, NJ 07981	(201) 386-2020
A. Fugiel	Zenith Radio 1000 Milwaukee Avenue Glennview, IL 60025	
Kenneth Gage	Sparton Electronics 2400 East Ganson Street Jackson, MI 49202	(517) 787-8600
Ernest D. Ganz	MEPCO/Electra Company 5900 Australian Avenue West Palm Beach, FL 33407	(305) 842-3201
John Galuagni	Viclan Component 7373 Engineer Road P. O. Box 81403 San Diego, CA 92138	
Robert Gardner	GTE Subscriber Equipment 13000 Memorial Parkway West Huntsville, AL 35803	(205) 883-3109
Stanley Garlock	Lear-Siegler Instrument Division 4141 Eastern Avenue, S.E. Grand Rapids, MI 49508	(616) 241-7447
Pierre Gerondeau	Western Electric 50 Lawrence Road Springfield, NJ 07081	(201) 467-7132

Jerry Getson	IBM Corporation Mail Drop 102A365 Owego, NY 13827	(607) 751-4191
Lee Graham	USAMICOM DRSMI-QRT Redstone Arsenal, AL 35898	(205) 876-4438
Harrison D. Gray	Parts Engineering Consultants 57 Arcadia Tuscaloosa, Al 35404	(205) 556-5290
Frank Greenhalgh	CEAG Corporation 1324 Motor Parkway Hauppauge, NY 11787	(516) 582-4422
Shelby Gurley	GTE Automatic Electric 13000 Memorial Parkway, South Huntsville, AL 35803	(205) 883-3349
Richard Guyette	Corning Electronics 3900 Electronics Drive Raleigh, NC 27604	(919) 876-1100
Jim Hale	Litton G/CS M.S. 35 5500 Canoga Avenue Woodland Hills, CA 91306	(213) 887-3298
Dr. Charles A. Hall	Sandia National Laboratories Active Ceramics Division Code 2521 Albuquerque, NM 87185	(505) 844-8171
Bob Hamilton	Mine Safety Appliance Co. 100 North Braddock Avenue Pittsburg, PA 15208	(412) 273-5566
Leon C. Hamiter, Jr.	Marshall Space Flight Center Code EC43 Huntsville, AL 35812	(205) 453-4572
Bruce Hammer	ITT P. O. Box 831 Product Engineering Department Corinth, MS 38834	(601) 287-3771
John E. Hand	Cornell-Dubilier Electronics 2652 Dalrymple Street Sanford, NC 27330	(919) 775-2211
Julian Hanft	Barnes Engineering Company 30 Commerce Road Stamford, CT 06904	(203) 348-5381
Cecil L. Harvey	Sprague Electric Company Marshall Street North Adams, MA 01247	(413) 664-4411 Ext. 2772
David Hayward	Plessey Capacitors, Inc. 5534 Sterling Center Drive Westlake Village, CA 91361	

Bill Heckman	Defense Electronics Supply Center Code ECP 1507 Wilmington Pike Dayton, OH 45444	(516) 296-5255
Bob Henegan	Mallory Capacitor 2615 Memorial Parkway Huntsville, AL 35801	
Harold Hickman	Tansitor Electronics, Inc. P. O. Box 230 Bennington, VT 05201	(802) 442-5473
R. L. Hildenbrand	Martin-Marietta/Denver P. O. Box 179 Mail Stop 0540 Denver, CO 80201	(303) 977-4217
Frank Holman	General Dynamics/Convair Div. P. O. Box 80847 San Diego, CA 92138	(714) 277-8900 Ext. 3293
Dr. A. M. Holladay	Marshall Space Flight Center Code EC41 Huntsville, AL 35812	(205) 453-3770
Rich Homolya	Exide Electronics, Inc. P. O. Box 58189 Raleigh, NC 27658	(919) 872-3020
Hank Houck	Pfizer Medical Systems 9052 Old Annapolis Road Columbia, MD 21045	(301) 992-7235
E. Howard	Marshall Space Flight Center Code EC24 Huntsville, AL 35812	
M. Brandt Howard	Wyle Laboratories 7800 Governor's Drive Huntsville, AL 35807	(205) 837-4411 Ext. 366
Robert J. Huber	Scientific Atlanta 4300 N.E. Expressway Atlanta, GA 30340	(404) 449-2000 Ext. 2322
Paul Hyman	Electronic Buyers News 333 E. Short Road Manhasset, NY 11030	
Phil Imbrogno	Electronic Concepts 0 N 638 Delano Wheaton, IL 60187	(312) 668-8747
Harley K. James	DRSMI-RKP Building 7120 Redstone Arsenal, AL 35808	
Steve James	Honeywell Incorporated 600 2nd Street, N.E. Hopkins, MN 55343	(612) 931-6200

Jerry Jennings	Chrysler Corporation 102 Wynn Drive Huntsville, AL 35805	(205) 895-1886
William Johnson	ITT Telecon P. O. Box 831 Corinth, MS 38834	(601) 287-3771
Dr. Kinzy Jones	Cordis Corporation P. O. Box 525700 Miami, FL 33152	(305) 551-2829
Bob Josepher	Teledyne Electronics 649 Lawrence Drive Newbury Park, CA 91320	(805) 498-3621 Ext. 363
Robert Kapustka	Marshall Space Flight Center Code EC12 Huntsville, AL 35812	
William E. Kauffman	Callins Industries P. O. Box C Greenfield, TN 38230	(901) 235-2234
David Kellerman	Component Research Corporation 1655 26th Street Santa Monica, CA 90404	(213) 829-3615
Gerard F. Kiernan	Sperry Systems Management 310.1 NASA/GSFC Greenbelt, MD 20771	(301) 344-8830
Joseph Kimmel	Lewis Research Center M.S. 500-211 21000 Brookpark Road Cleveland, OH 44135	FTS 294-4212
Ivan Kirsch	Analogic Corporation Audubon Road Wakefield, MA 01880	(617) 246-0300
John Kirschner	Zenith Radio 1000 Milwaukee Avenue Glennview, IL 60025	(312) 291-8493
Lawrence J. Kiszka	Bell Labs 1600 Osgood Street North Andover, MA 01845	(617) 681-6457
Roy Klinger	Western Electric 50 Lawrence Road Springfield, NJ 07081	(201) 467-7132
William K. Lacy	Rockwell/Collins Mail Stop 108-274 Cedar Rapids, IA 52406	(319) 395-3734
Raymond Lafferty	Boonton Electronics P. O. Box 122 Parsippany, NJ 07054	

E. Laliberte	Hamilton Standard Mail Stop 3-2-34 Bradley Field Windsor Locks, CT 06096	FTS 644-5121 (203) 623-1621 Ext. 2921
Walt Lamphier	Union Carbide Corporation P. O. Box 5928 Greenville, SC 29606	(803) 63-6632
John Lange	Burroughs Corporation 4000 NW Coral Ridge Drive Coral Springs, FL 33065	(305) 752-7920 Ex. 458
Harry Larson	Honeywell Incorporated Code 813-5 13350 U.S. Highway 19, South Clearwater, FL 33516	(813) 531-4611 Ext. 2641
James W. Lassiter	Harry Diamond Laboratories DELHD-DE-OT 2800 Powder Mill Road Adelphi, MD 20783	(202) 394-2410
Bernard Lavene	Electronic Concepts 526 Industrial Way, West Eatontown, NJ 07724	
V. Le	IBM-ISD D.516/040-2) Highway 52 and 37th Street, N.W. Rochester, MN 55901	(507) 286-6632
John J. Lee	Xerox Corporation - A2/30 Electronic Operations 701 S. Aviation El Segundo, CA 90245	(213) 536-7665
Paul Leary	Ithaco, Inc. 735 W. Clinton Street Ithaca, NY 14850	(607) 272-7640
Mike Leppanen	Rockwell International Dept. 745-SK54 12214 Lakewood Boulevard Downey, CA 90241 (2201 Seal Beach Blvd, Seal Beach, CA 90740)	
Phil Lepore	Electronic Concepts 526 Industrial Way, West Eatontown, NJ 07724	
Robert Le Sage	Teletype Corporation 5555 Touhy Skokie, IL 60077	(312) 982-3668
Dr. S. Levinson	Centre Engineering 2820 E. College Avenue State College, PA 16801	(814) 237-0321
Legend Li	SCI Huntsville, AL	
Joe Limanowski	Mallory Capacitor 2615 Memorial Parkway Huntsville, AL 35801	

Lewis Lollar	Marshall Space Flight Center Code EC12 Huntsville, AL 35812	
Dr. Stanley A. Long	Centralab 4561 Colorado Boulevard Los Angeles, CA 90039	(213) 240-4880
R. G. Lundgren	3-M Company Film & Allied Product Division 3-M Center Building 236-GA St. Paul, MN 55101	(612) 733-4281
Ronald Lynds	Cornell-Dubilier Electronics 1605 E. Rodney Fr. Blvd. New Bedford, MA 02741	(617) 996-8561
Raymond Maffey	General Electric M/S E-2 Cincinnati, OH 45215	(513) 243-7291
Steve Magno	LTX Corporation 160 Charlemont Street Newton Highlands, MA 02161	(617) 964-4900
N. B. Mahoney	IBM Corporation Dept. 1D6, Bldg. 708 P. O. Box 950 Poughkeepsie, NY 12602	
John Makhijani	AVX Corporation 60 Cutter Mill Road Great Neck, NY 11021	(516) 829-8500
Michael Manna	Sperry Gyroscope M.S. H8 Marcus Avenue Great Neck, NY 11020	(516) 574-2220
Robert Marlow	Sprague Electric Company Route 109 Sanford, ME 04073	
Marvin Martindale	Delco Electronics 7929 S. Howell Avenue Oak Creek, WI 53154	(414) 768-2757
Tony Martinich	Delco Electronics 6767 Hollister Avenue Goleta, CA 93117	(805) 961-5067
Joel C. Masland	Bell Laboratories 555 Union Boulevard Allentown, PA 18103	(215) 439-5148
Howard Mauldin	Sandia Laboratories Albuquerque, NM 87185	(505) 844-4260
Arthur McAdams	Vitramon, Inc. P. O. Box 544 Bridgeport, CT 06601	(203) 268-6261

Jack McKinney	Jet Propulsion Laboratory T-1180 4800 Oak Grove Drive Pasadena, CA 91103	(213) 792-3553
Lawrence Medina	Hughes Aircraft Bldg. 6, M.S. D-139 Cintinela & Teale Culver City, CA 90230	
Paul F. Meier	Boeing Company M.s. HS-02 P. O. Box 58747 Houston, TX 77058	(713) 486-1315
James Magrini	Lewis Research Center M.S. 500-116 21000 Brookpark Road Cleveland, OH 44135	
E. J. Miller	Martin Marietta Corporation M.S. S0550 P. O. Box 179 Denver, CO 80201	(303) 977-3349
William Minford	Bell Labs 555 Union Boulevard Allentown, PA 18103	(215) 439-5340
J. Montenegro	Marshall Space Flight Center Code EC24 Huntsville, AL 35812	
Jewel W. Moody	Marshall Space Flight Center Code EG02 Huntsville, AL 35812	(205) 453-5602
Mohamed Moolji	Perkin-Elmer Corporation, ASD 2771 Garey Avenue Pomona, CA 91767	(714) 593-3581 Ext. 404
Dale E. Moore	Wyle Laboratories P. O. Box 1008 Huntsville, AL 35807	(205) 837-4411 Ext. 325
F. Brooks Moore	Marshall Space Flight Center Code EC01 Huntsville, AL 35812	(205) 453-1412
Joseph A. Moresi	Sprague Electric Company P. O. Box 458 Modine Road Clinton, TN 37716	(615) 457-4130 Ext. 110
John K. Morris	Marshall Space Flight Center Code EC43 Huntsville, AL 35812	(205) 453-4562
Mike Mosiello	Electronic Concepts 526 Industrial Way, West Eatontown, NJ 07724	
John Moynihan	Sprague Electric Company North Adams, MA 01247	(413) 644-4411 Ext. 2520
Clifford Newhart	Ithaco, Inc. 735 West Clinton Street Ithaca, NY 14850	(607) 272-7640

Wah Fea Ng	General Electric 41 Woodford Avenue Plainville, CT 06062	(203) 747-7647
Dick Ni Director, QA&R Engr.	U.S. Capacitor Corporation 11144 Penrose Street Sun Valley, CA 91352	(213) 767-6770
David Nicolas	Marshall Space Flight Center Code EC43 Huntsville, AL 35812	(205) 453-4562
Edward W. Nieckula	Northrop Corporation Electronics Division 2301 W. 120th Street Hawthorne, CA 90250	(213) 615-3090
Richard Nolan	Cordis Corporation P. O. Box 525700 Miami, FL 33152	(305) 551-2778
John Norris	Sprague Electric P. O. Box 458 Clinton, TN 37716	
Michael F. Nowakowski	Marshall Space Flight Center Code EC43 Huntsville, AL 35812	(205) 453-4562
Frank H. O'Neil	Tansitor Electronics, Inc. P. O. Box 230 Bennington, VT 05201	(802) 442-5473
Frank Ott	Jet Propulsion Laboratory Code 161-213 4800 Oak Grove Drive Pasadena, CA 91103	(213) 354-4321
Bruce Owings	Scientific Atlanta 4386 Park Drive Norcross, GA 30093	(404) 925-5958
William E. Packer	General Electric Company P. O. Box 11508 St. Petersburg, FL 33733	(813) 541-8178
Willie Page	ITT Product Engineering Dept. P. O. Box 831 Corinth, MS 38834	(601) 287-3771
Harold Palmquist	Intermedics, Inc. P. O. Box 617 240 Tarpon Inn Village Freeport, TX 77541	800-231-2330
Stephen L. Parker	SCI Systems, Inc. P. O. Box 4000 Huntsville, AL 35802	
Carl E. Peebles	ITT North - TSD P. O. Box 20345 Columbus, OH 43220	(614) 548-4301

David Perdue	Storage Technology Corporation M.D. CE 2270 South 88th Louisville, CO 80027	(303) 673-3698
Mike Persson	Delco Elctronics/General Motors 700 E. Firmin Kokomo, IN 46901	(317) 459-7823
Dennis L. Peters	Harris Corporation Mail Stop 16-005 P. O. Box 37 Melbourne, FL 32901	(305) 727-5840
Brian Phelan	Chandler-Evans Charter Oak Boulevard West Hartford, CT 06101	(203) 224-3287
Irwin Podbielak	Ontel Corporation 415 Crossways Park Drive Woodbury, NY 11797	(516) 364-0930
Dave Porter	Boeing Company P. O. Box 3999 M.S. 88-93 Seattle, WA 98124	(206) 773-1054
Joel Priest	Martin-Marietta P. O. Box 179 Denver, CO 80201	(303) 977-1344
Dr. Bharat Rawal	AVX Ceramics P. O. Box 867 Myrtle Beach SC 29577	(803) 448-9411 Ext. 458
George Reeder	Naval Weapons Support Center Code 6025 Crane, IN 47522	(812) 854-1338
R. M. Regner	Union Carbide Corporation P. O. Box 5928 Greenville, SC 29606	(803) 963-6389
William Reilly	Centre Engineering 2820 E. College Avenue State College, PA 16801	(814) 237-0321
Bill Robbins	C. S. Draper Labs Mail Stop 55 555 Technology Square Cambridge, MA 02139	(617) 258-4354
Don Robertson	BNR, Inc. 685A Middlefield Road Mountain View, CA 94043	(415) 969-9170 Ext. 2958
Stan Ropiak	Sperry Flight Systems P.O. Box 2111 Phoenix, AZ 85036	(602) 869-1649
Michael Rosenberg	SFE Technologies 1501 First Street San Fernando, CA 91341	(213) 365-9411

Dr. Osmu Saburi	Kyocera International, Inc. 8611 Balboa Avenue San Diego, CA 92123	(714) 279-8310
	(EMCON, Inc.) P. O. Box 81542 San Diego, CA 92138	(714) 459-4355
L. A. Schlesselman	Bendix Corporation P. O. Box 1159 Kansas City, MO 64141	(816) 977-2827
Frank Scofield	General Electric Company 110 Wynn Drive Huntsville, AL	
Bill Serjak	NRC, Inc. 45 Industrial Place Newton, MA 02164	(617) 969-7690
Edward Set	Sperry Gyroscope M/S 1A15 Marcus Avenue Great Neck, NY 11020	(516) 574-3509
David E. Sevier	Martin-Marietta Aerospace P. O. Box 179 Mail Stop SO540 Denver, CO 80901	(303) 977-3269
Mrs. Jill Shakar	Sprague Electric Marshall Street North Adams, MA 01247	(413) 664-4411 Ext. 2656
Lyle Shoot	Mallory Capacitor Company 3029 E. Washington Street Indianapolis, IN 46206	(317) 261-1482
Rolf Sieber	Teledyne Brown Engineering Cummings Research Park Huntsville, AL 35807	(205) 532-1625
Daniel G. Smith	McDonnell Douglas Astronautics Co. Dept. E261, Bldg. 106/3/C6 P. O. Box 516 St. Louis, MO 63166	(314) 232-0878
David Smith	Marshall Space Flight Center Code EC12 Huntsville, AL 35812	
Marty Spence Component Engineer	ELDEC Corporation Box 100 Lynnwood, WA 98036	(206) 743-1313
James C. Stamper	Lockheed Missile & Space Company D/62-95, B-104 P. O. Box 504 Sunnyvale, CA 94086	(408) 742-2629
Dick Stark	Sprague Electric 2815 Expressway East Wichita Falls, TX 76307	(817) 767-8351

Roy B. Steele	Delco-Remy Division General Motors Corporation Engineering Center Room 18-105 Anderson, IN 46011	(317) 646-7306
Harold Stetson	TRW Electronics Group R&D Center 401 North Broad Street Philadelphia, PA 19108	(215) 922-8900 Ext. 269
John Stevens	G.E. Ordnance Room 2654 Pittsfield, MA 01201	(413) 494-6788
Carl E. Stump	Gould/Ocean Systems Division Dept. 741 18901 Euclid Avenue Cleveland, OH 44117	(216) 486-8300 Ext. 3130
Edward F. Sutton	Harry Diamond Laboratories DELHD-DE-OT 2800 Powder Hill Road Adelphi, MD 20783	(202) 394-2410
W. Sutherland	Marshall Space Flight Center Code EC24 Huntsville, AL 35812	
Curtis Suyematsu	Hewlett-Packard P. O. Box 39 Boise, ID 83707	(208) 376-6000 Ext. 3064
Joe Sweet	Teledyne Systems Company M.S. 46 19601 Nordhoff Street Northridge, CA 91324	(213) 886-2211
Dennis Sylder	Vitramon, Inc. P. O. Box 544 Bridgeport, CT 06601	(203) 268-6261
Jerome Taubman	General Electric AESD M.D. 747 Broad Street Utica, NY 13503	(315) 797-1000 Ext. 5100
David Tenenbaum	Electronic Concepts 526 Industrial Way, West Eatontown, NJ 07724	
E. B. Thornley	TRW DSSG Mail Station R6-2591 One Space Park Redondo Beach, CA 90278	(213) 535-0743
John E. Till	Xerox Corporation B801-1R 1350 Jefferson Road Rochester, NY 14623	(716) 427-1816
Robert Tomashek	Delco Electronics 5113 West Radcliff Drive (Residence) Browndeer, WI 53223	(414) 768-2213

David Toomey	Sprague Electric Route 109 Sanford, ME 04073	(207) 324-4140
Bobby Tucker	Marshall Space Flight Center Code EC26 Huntsville, AL 35812	
Bedford Tuten	Marshall Space Flight Center Code EG02 Huntsville, AL 35812	(205) 453-5602
Gary W. Valentine	Hughes Aircraft Company Centinela & Teale Streets Building 6, M.S. C/137 Culver City, CA 90230	(213) 391-0711 Ext. 7216
N. Varnen	Hughes Aircraft P. O. Box 92919 S41/A354 Los Angeles, CA 90009	
Peter J. Venuto	Corning Electronics 3900 Electronics Drive Raleigh, NC 27604	(919) 876-1100
Felminio Villella	Marshall Space Flight Center Code EC43 Huntsville, AL 35812	(205) 453-4562
Jim Walker	General Electric Charlottesville, VA 22906	(804) 973-9574
W. T. Ward	Physio-Control Corporation 11811 Willows Road Redmon, WA 98052	(206) 881-4000
Richard Warren	Tokheim Corporation 1601 Wabash Avenue Ft. Wayne, IN 46801	(219) 423-2552
Robert F. White	SCI Systems P.O. Box 4000 Huntsville, AL 35802	(205) 872-4291
Henry Williams	Mallory Capacitor 2615 Memorial Parkway Huntsville, AL 35801	
Neil Williams	Boeing Company P. O. Box 3999 M.S. 8A-83 Seattle, WA 98124	(206) 773-3840
David Wolin	Lockheed Missile & Space Company Building 153, O/84-51 P. O. Box 504 Sunnyvale, CA 94086	(408) 742-1857
Dick Wooden	TRW 301 West O Street Ogallala, NE 69153	(308) 284-3611

Lori Yamashita	Marshall Space Flight Center Code EC45 Huntsville, AL 35812	
Marvin Yee	Motorola GED Mail Drop 2121 8201 E. McDowell P. O. Box 1417 Scottsdale, AZ 85252	(602) 949-4436
Larry Yudkowitz	Loral Electronic Systems 825 Bronx River Avenue Bronx, NY 10473	(212) 378-2300 Ext. 110
Don Yuhas	SONOSCAN, Inc. 530 E. Green Street Bensenville, IL 60106	(312) 766-7088
Robert R. Zarnosky	Hughes Aircraft Company Centinela & Teal Streets Building 316, M.S. R129 Culver City, CA 90230	(213) 391-0711 Ext. 2585
A. Ziemelif	Zenith Radio 1000 Milwaukee Avenue Glenview, IL 60025	